Preliminary Results of One-Dimensional Consolidation Testing on Bentonite Clay-Based Sealing Components Subjected to Two Pore-Fluid Chemistry Conditions

NWMO TR-2008-04

March 2008

P. Baumgartner[a], D. Priyanto[a], J.R. Baldwin[b], J.A. Blatz[b], B.H. Kjartanson[c] and H. Batenipour[c]

[a]Atomic Energy of Canada Limited, [b]University of Manitoba and [c]Lakehead University

nwmo

NUCLEAR WASTE MANAGEMENT ORGANIZATION   SOCIÉTÉ DE GESTION DES DÉCHETS NUCLÉAIRES

PRELIMINARY RESULTS OF ONE-DIMENSIONAL CONSOLIDATION TESTING ON BENTONITE CLAY-BASED SEALING COMPONENTS SUBJECTED TO TWO PORE-FLUID CHEMISTRY CONDITIONS

NWMO TR-2008-04

March 2008

P. Baumgartner[a], D. Priyanto[a], J.R. Baldwin[b], J.A. Blatz[b], B.H. Kjartanson[c] and H. Batenipour[c]
[a]Atomic Energy of Canada Limited, [b]University of Manitoba and [c]Lakehead University

ABSTRACT

Author(s): P. Baumgartner[a], D. Priyanto[a], J.R. Baldwin[b], J.A. Blatz[b], B.H. Kjartanson[c] and H. Batenipour[c]

Company: [a]Atomic Energy of Canada Limited, [b]University of Manitoba and [c]Lakehead University

Abstract

One-dimensional consolidation tests are performed to provide preliminary information on the time-dependent deformation properties of saturated highly compacted bentonite (HCB), light backfill (LBF) and dense backfill (DBF), three potential sealing-system components of the Emplacement-Room Sealing System. Testing includes an examination of the influence of pore-fluid salinity on the consolidation behaviour to assess the importance of groundwater chemistry on system performance.

This report provides the details of the tests including their results. The combined results of all three sealing-system components are compared on the common basis of the effective montmorillonite dry density (EMDD) and also compared to previously established swelling-pressure measurements. The resultant void ratios, dry densities and EMDDs tend to be related to the swelling pressures associated with distilled water and highly saline pore fluids. Fitted expressions for the one-dimensional constrained moduli (stiffness) are also presented for use in modelling. The appendices in this report present the procedures used in all of the testing, the detailed measurements taken during the tests, comparisons of the test results in light of the initial conditions and the modifications to the material-property calculations when saline solutions replace distilled water as the pore fluid.

TABLE OF CONTENTS

LIST OF TABLES

LIST OF FIGURES

1. INTRODUCTION

Multiple sealing-system components may be used in an emplacement-room sealing system (Figure 1) as part of a deep geological repository (DGR) for used nuclear fuel (Gierszewski et al. 2004). For the clay-based materials, five sealing-system components are being considered for repository sealing options in Canada, as follows:

- Highly compacted bentonite (HCB) – 100% bentonite clay either installed at high dry density by in-situ compaction or prefabricated as blocks;
- Bentonite-Sand Buffer (BSB) – a mixture of bentonite clay and silica sand, either installed at high dry density by in-situ compaction or prefabricated as blocks (shown in Figure 1 as "Compacted Buffer");
- Dense Backfill (DBF) – a mixture of lake clay, crushed host rock and bentonite clay, either installed at high dry density by in-situ compaction or prefabricated as blocks;
- Light Backfill (LBF) – a mixture of bentonite clay and silica sand, likely installed in the form of dense pellets and installed at low-to-medium dry density; and
- Gapfill (GF) – either bentonite clay, possibly fabricated in the form of dense pellets, silica sand or some combination of the two, which are likely to be installed at low-to-medium average dry density.
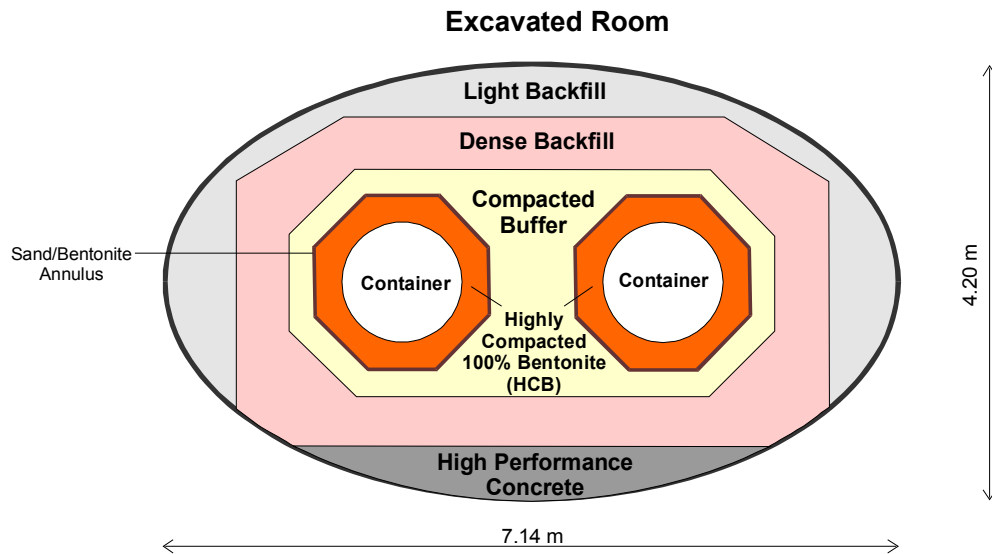
Figure 1: In-room Emplacement Cross-sectional Geometry (CTECH 2002)

Bentonite clay is composed largely of smectite-clay minerals. Montmorillonite is the preferred smectite-clay mineral because of its large swelling potential in water, particularly when the dominant exchangeable cation in the mineral structure is sodium, termed Na-montmorillonite or, generally as Na-bentonite. When the exchangeable cation sites in the mineral structure are filled with other cations such as calcium and magnesium, the swelling potential is suppressed.

Some suggested compositions and physical characteristics of candidate Na-bentonite-based sealing-system components are presented in Table 1.

Table 1: Physical Characteristics of Engineering Barriers System Components
(after Russell and Simmons 2003)

Property	HCB	BSB	GF	DBF	LBF
Composition (dry mass %)	100% bentonite	50% bentonite 50% sand	100% bentonite	5% bentonite 25% glacial lake clay 70% crushed granite	50% bentonite 50% sand
Initial Gravimetric Water Content (%)	17	18.5	2	8.5	15
As-Placed Saturation (%)	65	80	6	80	33
Dry Density (Mg/m^3)	1.61	1.69	1.40	2.12	1.24
EMDD (Mg/m^3)*	1.50	1.15	1.25	0.8	0.66

* assumes that all bentonites have a minimum 75% montmorillonite content

On water uptake of the sealing-system components, the components with high Effective Montmorillonite Dry Density[1] (EMDD) (e.g., the highly compacted bentonite (HCB) adjacent to the containers) will tend to swell (e.g., expand) more than those with lower EMDD (Dixon et al. 2002) (e.g., the bentonite-sand buffer (BSB), dense backfill (DBF), light backfill (LBF) and any gap fill (GF)). The surrounding rock is considered rigid relative to the clay-based sealing-system components and the overall volume of the room is assumed constant. This constant-room volume is a conservative assumption because minor inwards deformation is anticipated due to the thermal-mechanical response of the host rock.

Low EMDD sealing components are eventually expected to compress under the swelling loads imposed by the higher EMDD components. The interactive volumetric-deformation processes of swelling and compression for each of the sealing-system components are expected to continue until static equilibrium is attained. The volumetric changes affect both the EMDDs and corresponding mechanical stiffness or elastic modulus of each component. Note that stiffness is the inverse of compliance or compressibility. The stress-strain properties of the materials play an important role in this "compliance effect". The measurement of volumetric compressibility (m_v) and its inverse, the one-dimensional (1-D) constrained modulus of elasticity (M), for selected sealing-system-components is the subject of this report.

1.1 BACKGROUND

Scoping calculations were performed to assess the implications of compliance between the sealing-system components (Kjartanson et al. 2003). The system-averaged EMDD calculation for the HCB, GF, BSB and LBF (DBF was excluded) was based on the assumption that the

---

[1] Effective Montmorillonite Dry Density (EMDD) = (mass of bentonite *montmorillonite fraction) / (volume of voids + volume of montmorillonite minerals)

system attains static equilibrium at a uniformly distributed value (i.e., all the montmorillonite has saturated, swelled or shrunk to a final and uniform effective montmorillonite water content (EMWC) and volumetric state). The system-averaged EMDD was calculated by dividing the total mass of montmorillonite in the HCB, GF, BSB and LBF by the total volume of montmorillonite particulate plus the interparticle voids within these four sealing-system components in an emplacement room.

Results suggest that compression of the lower-EMDD BSB and LBF components and expansion of the HCB adjacent to the used-fuel containers will occur (Kjartanson et al. 2003). The expansion of the HCB would reduce its equilibrium swelling pressure and increase its hydraulic conductivity. Any unfilled gaps between precompacted blocks of sealing-system components and between each sealing-system component will further reduce swelling pressure and increase hydraulic conductivity.

The chemistry of the pore fluid strongly affects the swelling potential and hydraulic conductivity of bentonite clay with increasing salinity reducing the swelling potential and increasing hydraulic conductivity (Dixon 2000). Groundwaters at proposed repository depths of 500 to 1000 m can contain significant quantities of soluble salts. Gascoyne et al. (1987) and Mazurek (2004) have collated data on soluble salts from the crystalline rock of the Canadian Shield and the sedimentary rock in southern Ontario, respectively. Salt concentration tends to be low near surface and increases with depth. Salt concentrations also vary considerably throughout the Canadian Shield. Salinities, in terms of Total Dissolved Solids (TDS) at proposed repository depths, can vary from 8 to >100 g/L in the Shield and >200 g/L in Ordovician-age sediments. Salt speciation is often Na-Ca-Cl at shallow depth trending to Ca-Na-Cl at greater depth.

Studies of the role that the chemistry of the pore fluid plays in the behaviour of bentonite clay have largely been limited to NaCl solutions (Dixon 2000). Because of the presence of $CaCl_2$ in groundwaters, testing bentonite clay with $CaCl_2$ solutions should be started.

Numerical modelling has been initiated to ascertain the relative compliance of the emplacement-room sealing-system components after achieving full saturation and static equilibrium and to assess whether a system-averaged EMDD would develop and be uniformly distributed as suggested by Kjartanson et al. (2003). The non-linear elastic properties of the sealing-system components need to be defined based on their relationships to swelling pressure and EMDD.

1.2   SCOPE OF WORK AND ASSUMPTIONS

The work consists of a series of laboratory one-dimensional (1-D) consolidation tests to generate the material properties needed to undertake compliance modelling. The preliminary modelling results are used to define the testing protocols leading to physical conditions representative of those in a proposed DGR. Testing is divided between Atomic Energy of Canada Limited's (AECL) geotechnical laboratory at the Underground Research Laboratory (URL), the University of Manitoba's (UM) Department of Civil Engineering and Lakehead University's (LHU) Department of Civil Engineering. Each group was assigned a single material to test. AECL examined the HCB, LHU the LBF and UM the DBF.

Each test program consists of a minimum of six specimens with specified initial conditions including distilled water and $CaCl_2$ solution as the pore fluids. AECL provided the specimen materials. This report summarizes the major results of the test programs. Details of the

procedures used by the different groups, the detailed measurements taken during the tests and the specific test results in light of the initial conditions and loading/wetting paths are provided in the Appendices, including constitutive soil relationships for both distilled-water and saline pore fluids.

2. CONSOLIDATION TESTS

The following three sealing-system components are tested in the series of consolidation tests:
- HCB, composed of 100-wt% Wyoming MX80 bentonite (montmorillonite content ~75%);
- LBF, composed of 50-wt% Avonlea (Saskatchewan) bentonite (montmorillonite content ~80%) and 50-wt% silica sand; and
- DBF, composed of 75-wt% crushed granite, 18.75% crushed illite clay (Sealbond) and 6.25-wt% Avonlea bentonite (montmorillonite content ~79%). This differs from Table 1 due to the currently unavailable glacial lake clay (see Appendix B).

Each sealing-system component is tested in distilled water[2] and in a saline solution (i.e., 75-g/L to 200-g/L or 1.35- to 3.6-mol/L of $CaCl_2$ solution) to observe the effect that this electrolyte has on consolidation and swelling behaviour.

3. CONSOLIDATION RESULTS

Tables 2 and 3 provide the initial conditions for each of the consolidation tests for the fresh-water and saline-solution specimens, respectively. These tables should be referenced when reviewing the graphed results.

---

[2] Note: The term "fresh water" means distilled water throughout this document.

Table 2: Fresh-water Test Initial Conditions

Fresh-water Test Specimen	Starting Condition	Target Initial Dry Density (Mg/m^3)	Actual Initial Dry Density (Mg/m^3)
LBF2	Confined*	1.24	1.26
LBF3	20% Swell**	1.24	1.25
LBF4	Confined	1.24	1.30
LBF6	21% Swell	1.24	1.31
LBF7	Confined	1.24	1.35
LBF8	22% Swell	1.24	1.47
LBF9	Confined	1.24	1.30
HCB1	1 MPa	1.65	1.67
HCB2	1 MPa	1.65	1.67
HCB5	1 MPa	1.40	1.44
DBF1	20% Swell	2.10	2.13
DBF2	Confined	2.10	2.14
DBF5	1 MPa	2.10	2.10

*   Specimen is initially rigidly confined during the saturation period by increasing the load to prevent swelling displacement (i.e., maintain constant volume of the specimen).

** Specimens are permitted to swell up to 20% at very low load before significant load increments are applied. Actual swell values are presented. Specimens with values at or over 20% have greater free-swell capacity but swelling was terminated at or near the prescribe amount. Specimens with lesser values are at their maximums.

Table 3: Saline-Solution Test Initial Conditions*

Saline Solution Test Specimen	Mixing Solution**	Reservoir Solution	Starting Condition	Target Initial Dry Density (Mg/m^3)	Actual Initial Dry Density (Mg/m^3)
LBF11	Fresh	100 g/L	10% Swell	1.24	1.41
LBF12	Fresh	100 g/L	8% Swell	1.24	1.39
LBF13	100 g/L	100 g/L	6% Swell	1.24	1.37
LBF14	Fresh	100 g/L	Confined	1.24	1.38
LBF15	100 g/L	100 g/L	6% Swell	1.24	1.40
LBF16	Fresh	200 g/L	7% Swell	1.24	1.51
LBF19	Fresh	100 g/L	6% Swell	1.24	1.36
HCB3	75 g/L	75 g/L	1 MPa	1.65	1.61
HCB4	75 g/L	75 g/L	8 MPa	1.65	1.76
HCB6	75 g/L	75 g/L	1 MPa	1.40	1.47
DBF3	100 g/L	100 g/L	1% Swell	2.10	2.13
DBF4	100 g/L	100 g/L	Confined	2.10	2.13
DBF6	100 g/L	100 g/L	1 MPa	2.10	2.12

* See notes in Table 2.
** The mixing solution is the fluid that is mixed with the dry soil to produce compacted, unsaturated specimens. All reservoir solutions are saline ($CaCl_2$) solutions

3.1 FRESH-WATER RESULTS

3.1.1 Void Ratio Results

Figure 2 presents all the fresh-water-test results in the format of void ratio versus the applied stress (log scale). The bentonite-rich (i.e., 50-wt%-bentonite LBF and 100-wt%-bentonite HCB) sealing-system components show high void ratios as compared to the bentonite-poor DBF (i.e., 6.25-wt% bentonite). The high void ratios for the bentonite-rich components at given applied stresses are due to the high clay contents and the repulsion between the smectite-clay minerals, particularly montmorillonite (i.e., smectite clays have a proportionately greater diffuse double layer as compared to illite).

The derived compression (C_c) (i.e., the normal or virgin consolidation line) and rebound (C_s) indices for the fresh-water consolidation specimens are presented in Table 4 (see details of the indices in Appendix A). The values of C_c for bentonite-rich components are very similar and are about an order of magnitude greater than those for the bentonite-poor DBF, as expected. Note that the LBF does not rigorously follow a straight line on the void ratio vs. log-stress plot (Figure 2) but tends to follow a concave-downwards trend as the stress increases above 1000 kPa. This may indicate that a portion of the applied stress is transferring from the loading of the clay-soil skeleton to the loading of the silica-sand skeleton, thereby increasing its stiffness.
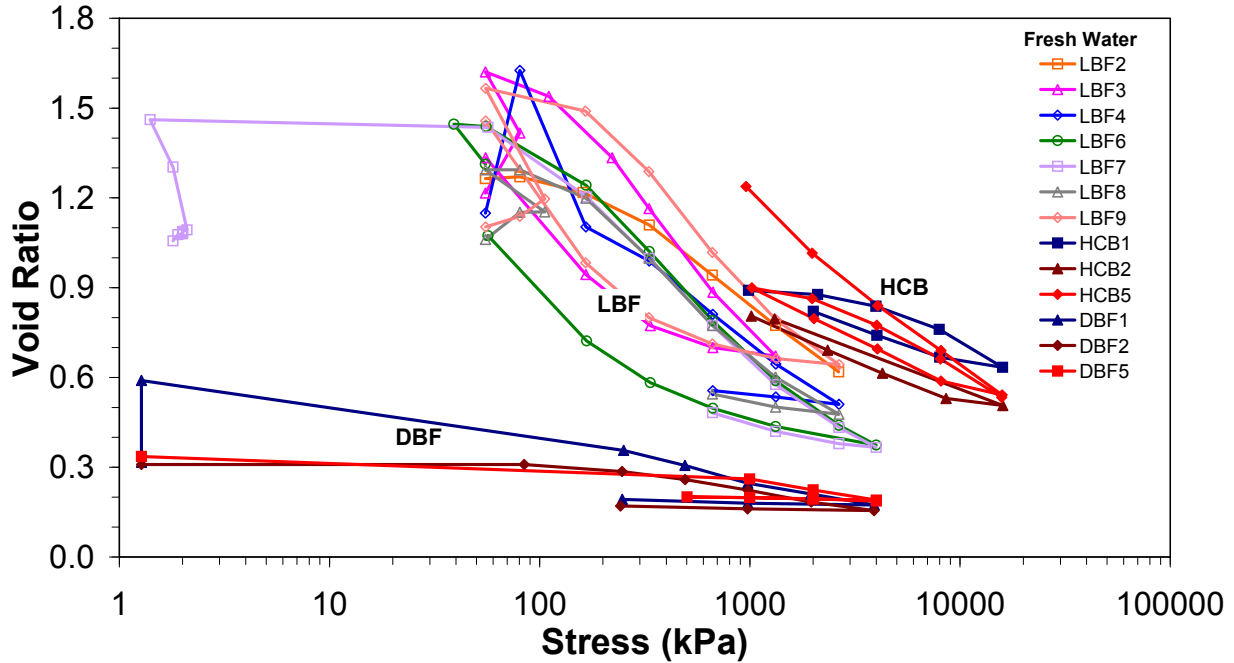
Figure 2: Void Ratio of Fresh-Water Consolidation Specimens. See Table 2 for legend details

The rebound index (C_s) (Table 4) is calculated on the basis of the first unloading step following the incremental loading stage. The traditional term "swelling index", as used in the literature to describe the non-linear-elastic unloading response of non-swelling clays, tends to be linear on a void ratio vs. log-stress plot. The bentonite-rich sealing-system components do not display this log-linear type of unloading response (Figure 2). Since the materials tested are truly swelling materials, the "swelling index" as originally intended is a misnomer and this index does not describe the non-elastic portion of this response.

The limited rebound measurements of DBF tend to be linear on the void ratio vs. log-stress plot (Figure 2). The low values for both the C_c and C_s indicate a very stiff material, most likely the result of load transmission through the crushed granite with some clay between the contacting granite particulate. Very limited swelling is apparent during the unloading stage.

Table 4: Fresh-water Compression and Rebound Indices

Fresh-water Test Specimen	Compression Index C_c	Rebound Index* C_s
LBF2	0.50	NA
LBF3	0.83	0.09
LBF4	0.53	0.08
LBF6	0.64	0.13
LBF7	0.62	0.07
LBF8	0.61	0.08
LBF9	0.73	0.07
HCB1	0.42	0.11
HCB2	NA**	0.09
HCB5	0.50	0.16
DBF1	0.05	0.007
DBF2	0.05	0.006
DBF5	0.05	0.005

* First unloading step only, increasing values on subsequent unloading
   steps indicative of a combined elastic and swelling response.
**NA – not applicable or not available.

3.1.2   Dry Density and EMDD Results

Figure 3 presents the test results with the void ratio converted to dry density for the sealing-system components. Little insight is gained by the information presented in this form.

When dry density is converted to the effective montmorillonite dry density (EMDD) as a common basis for comparison and the axes switched, then a much more consistent pattern emerges as shown in Figure 4. The compression-line portions (i.e., derived from the normal or virgin consolidation lines) of all of the consolidation tests and the rebound-portions of the HCB and LBF series of tests tend to align with each other throughout the EMDD range.

Both Dixon et al. (2002) and Karnland et al. (2003) explored the role that differing salinities of pore fluids have on the swelling pressures of bentonites. The equation used to represent the swelling-pressure (P_s) data by Dixon et al. (2002) for all bentonites in fresh water is as follows (Baumgartner 2006):

$$P_s^{fresh} = 1 \text{x} 10^{-2} e^{4.58 \text{EMDD}}$$

(1)

where P_s^{fresh} = swelling pressure with fresh-water pore fluid (MPa)
       EMDD = effective montmorillonite dry density (Mg/m^3).
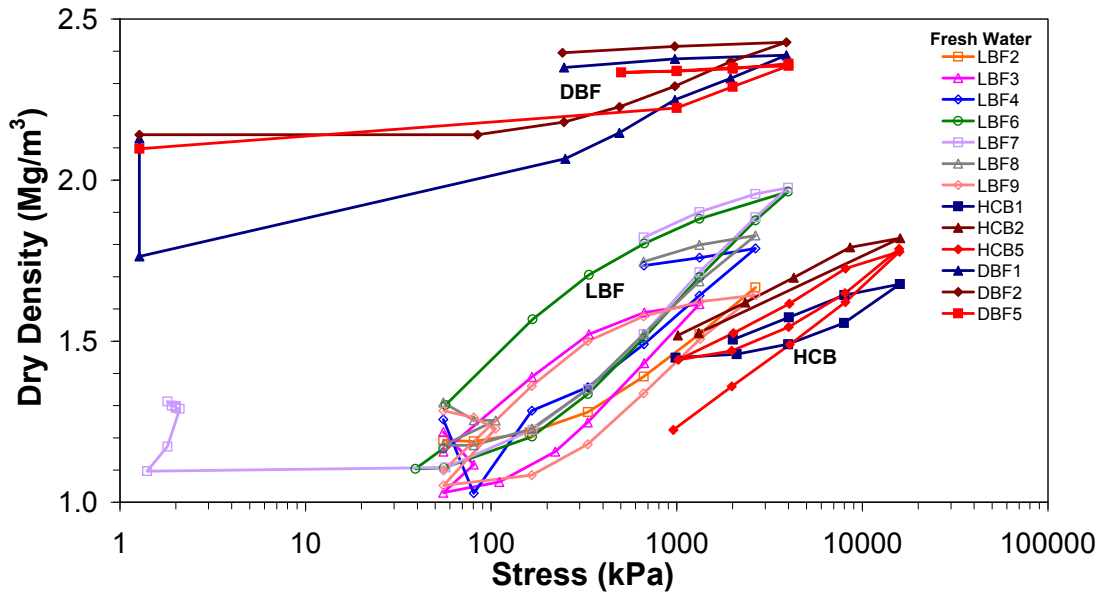
Figure 3: Dry Density of Fresh-Water Consolidation Specimens. See Table 2 for legend details.
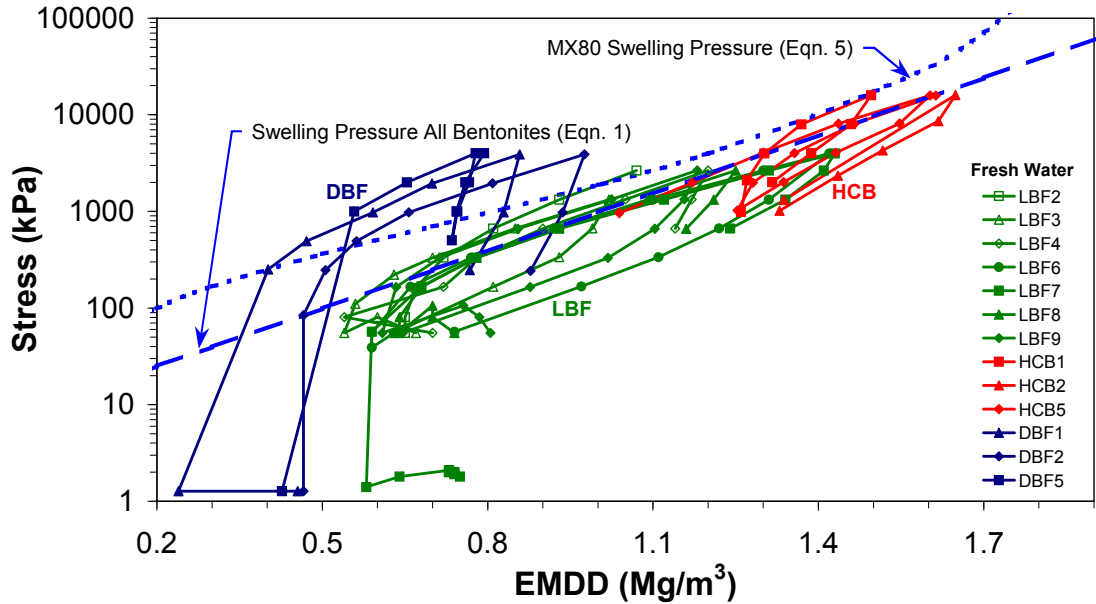
Figure 4: EMDD of Fresh-Water Consolidation Specimens. See Table 2 for legend details.

The equation used to represent the swelling-pressure (P_s) data for MX80 bentonite in fresh water is as follows (Hedin 2004):

$$P_s^{fresh} = AT\left\{ e^{\left[B \cdot \frac{\rho_s \ (\rho_{sat} - \rho_w)}{\rho_w \ (\rho_s - \rho_w)} \right]} - 1 \right\} \tag{2}$$

where A = fitting parameter (i.e., ~1.153 x 10^{-3} for MX80);
       T = temperature (K) (i.e., room temperature @ 20°C);
       B = fitting parameter (i.e., ~0.896 for MX80);
       ρ_s = density of soil solids (Mg/m^3);
       ρ_{sat} = density of saturated soil (Mg/m^3); and
       ρ_w = density of water (Mg/m^3) (i.e., ~1 Mg/m^3).

The relationship between saturated density (ρ_{sat}) and dry density (ρ_d) is:

$$\rho_d = G_s \frac{(\rho_{sat} - \rho_w)}{(G_s - 1)} \tag{3}$$

where ρ_d = density of dry soil (Mg/m^3); and
       G_s = relative density of soil solids (i.e., 2.74 for MX80 bentonite).

Thus, Equation 2 is converted from saturated density (ρ_{sat}) to dry density (ρ_d) (i.e., the top-most line in Figure 5):

$$P_s^{fresh} = AT\left\{ e^{\left[B \cdot G_s \frac{\rho_d}{(\rho_s - \rho_d)} \right]} - 1 \right\} \tag{4}$$

The relationship between EMDD and dry density is (Kjartanson et al. 2005, Baumgartner and Snider 2002):

$$EMDD = \frac{f_m \cdot f_c \cdot \rho_d}{1 - \left[\frac{(1 - f_c) \cdot \rho_d}{G_a \cdot \rho_w} \right] - \left[\frac{(1 - f_m) \cdot f_c \cdot \rho_d}{G_n \cdot \rho_w} \right]} \tag{5}$$

where f_m = mass fraction of montmorillonite in clay (e.g., >75% in MX80);
       f_c = mass fraction of clay in soil (e.g., 100% in bentonite clay);
       G_a = relative density of aggregate solids (e.g., quartz sand = 2.65); and
       G_n = relative density of non-montmorillonite clays (e.g., ~2.645).
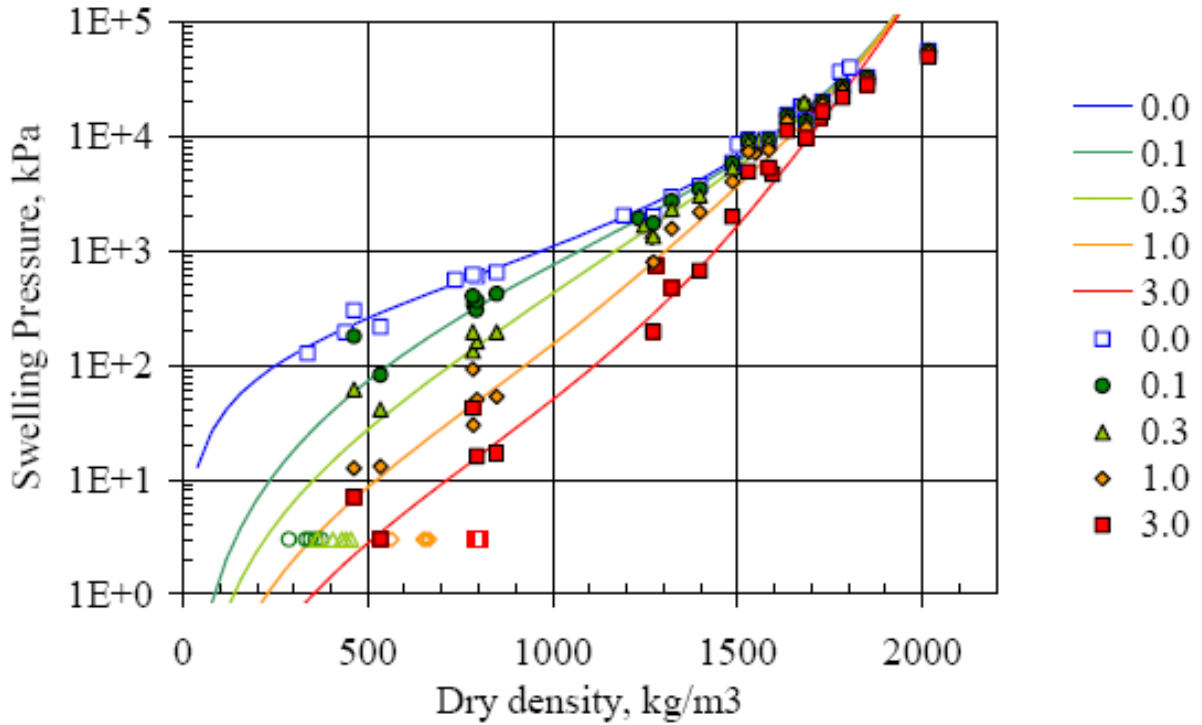
Figure 5: Swelling Pressure as a Function of Bentonite Dry Density (Karnland et al. 2003). **Legend shows external solution concentration in mole/L.**

In converting from dry density (ρ_d) to EMDD by substituting Equation 5 into Equation 4, the expression becomes extremely cumbersome:

$$P_s^{fresh} = AT\left\{e^{\left[B\cdot G_s \frac{\frac{EMDD}{f_m\cdot f_c+\frac{EMDD}{\rho_w}\left[\frac{1-f_c}{G_a}+\frac{(1-f_m)\cdot f_c}{G_n}\right]}}{\rho_s-\frac{EMDD}{f_m\cdot f_c+\frac{EMDD}{\rho_w}\left[\frac{1-f_c}{G_a}+\frac{(1-f_m)\cdot f_c}{G_n}\right]}}\right]}-1\right\}$$

(6)

Since the form of Equation 6 remains the same as Equation 4, Equation 6 is arbitrarily simplified by changing the fitting constant B to the revised fitting constant B_{EMDD} and by removing the complex denominators, as follows:

$$P_s^{fresh} = AT\left\{e^{\left[B_{EMDD} \cdot G_s \frac{EMDD}{(\rho_s - EMDD)}\right]} - 1\right\}$$ (7)

where B_{EMDD} =   fitting parameter (e.g., ~1.1655 for MX80).

The errors introduced by this arbitrary simplification (i.e., <10% over the full EMDD and salinity ranges) are smaller than the variability measured in natural materials and that of the empirical fitting process (Karnland et al. 2003). Equation 1 represents a broad range of Na-bentonite clays (i.e., Na/Ca ratios >1) in fresh water, whereas Equation 7 is limited to the high-quality Wyoming MX80 Na-bentonite (i.e., Na/Ca ratio ~1.8).

Both fresh-water swelling-pressure (P_s^{fresh}) lines (Equations 1 and 7) are also plotted in Figure 4. The slopes of the consolidation curves and those for the swelling pressures indicate that the stiffness of bentonite-based sealing-system components are dependent on their bentonite contents and dry densities (i.e., EMDDs).

The compression of LBF (Figure 4) tends to follow the swelling-pressure line proposed by Dixon et al. (2002) for the most part up to about an EMDD of 1.1 Mg/m^3, after which the specimens deviate below the line at higher EMDDs. The swelling-pressure line proposed by Dixon et al. is based on a literature survey of all bentonites and appears to be well suited for the Avonlea bentonite in the LBF. The deviation from this swelling-pressure line may be due to interference and friction caused by the silica-sand fraction (i.e., 50 wt%) in the LBF.

The HCB tends to fall on or below the two swelling-pressure lines in Figure 4. The HCB is composed of a Wyoming bentonite (i.e., MX80), which tends to generate slightly higher swelling pressure than Avonlea bentonite probably due to the differences in their exchangeable Na$^+$/Ca^{2+} cation ratios. Karnland et al. (2003) present the findings on MX80 swelling tests that are shown in Figure 4.

The loading of DBF does not fall on the swelling pressure lines (Figure 4), but are at greater stresses, indicating a greater stiffness than the bentonite-rich sealing-system components. The very high proportion of crushed granite aggregate (i.e., 75 wt% vs. 6.25 wt% bentonite in Section 2) forms the soil skeleton, generating this high stiffness. However, the trend of the compression lines tends somewhat to parallel the swelling lines. This may suggest that any bentonite between the aggregate contacts influences the compression behaviour of DBF. If this is the case, then the EMDD at the aggregate contacts must be higher than the average EMDD within the overall structure as shown in Figure 4 and cannot be accurately defined by averaged EMDD.

3.1.3   Constrained Moduli Results

Figure 6 presents the one-dimensional (1-D) constrained modulus of elasticity derived from the load increase curve for each LBF, HCB and DBF specimen. The moduli are based on the average dry density calculated from each load increment (e.g., 3 MPa over the 2 to 4 MPa increment) and plotted at the mid-point of each load increment (e.g., 3 MPa) of their respective loading stage. The 1-D constrained modulus of elasticity (M) is the inverse of the coefficient of volumetric compressibility (m_v), as follows (Bardet 1997):

$$M = \frac{1}{m_v} = \frac{(\sigma_2' - \sigma_1')(1 + e_1)}{(e_1 - e_2)} \tag{8}$$

where e_1 = void ratio at one load increment;
$\quad\quad\;\; e_2$ = void ratio at the next load increment;
$\quad\quad\;\; \sigma_1'$ = effective stress at one load increment, corresponding to e_1; and
$\quad\quad\;\; \sigma_2'$ = effective stress at the next load increment, corresponding to e_2.
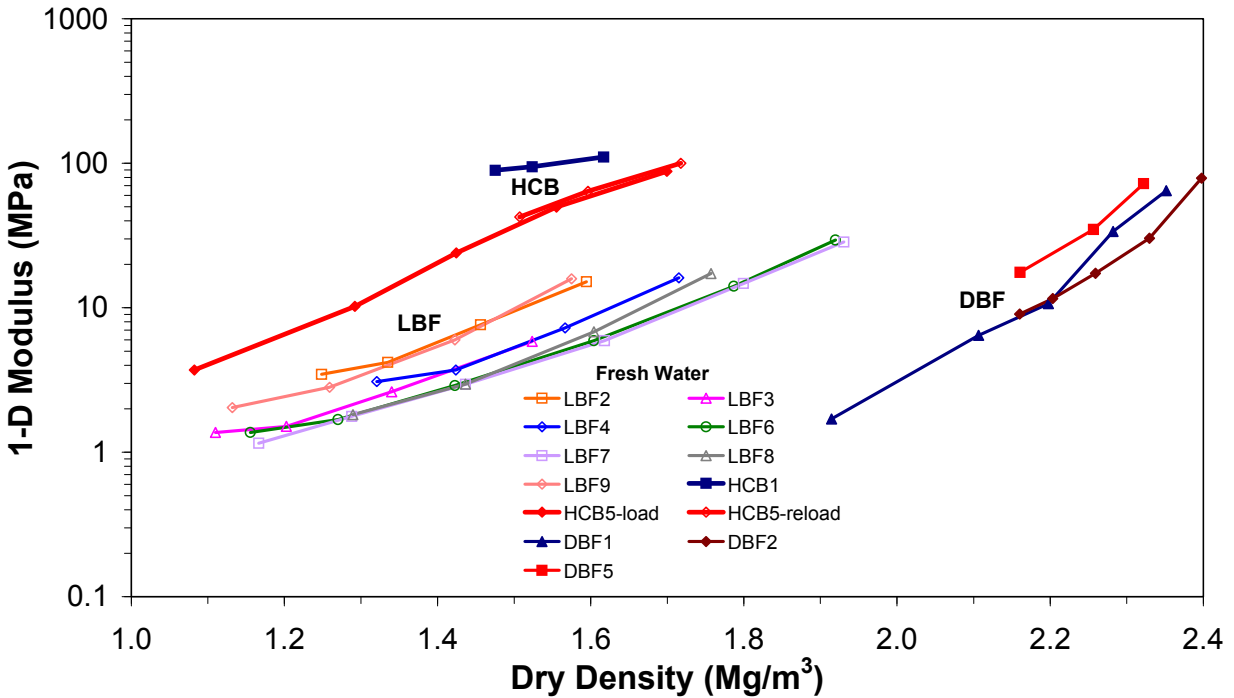
Figure 6: 1-D Constrained Moduli as a Function of Dry Density for Fresh-Water Consolidation Specimens. See Table 2 for legend details.

Dry density is calculated from void ratio by the following (Lambe and Whitman 1969):

$$\rho_d = \frac{G_s}{(1 + e)} \rho_w \tag{9}$$

where e = void ratio (unitless).

Note the parallel trends of the 1-D constrained moduli in Figure 6 suggesting a possible common basis of comparison. Figure 6 is converted to Figure 7 by replacing dry density with EMDD (Equation 5). Note that there is a continuing consistency in the parallel trends of the data. This consistency does not necessarily imply that a single curve can be fitted to all the data regardless of composition but may imply a family of curves, one for each composition.
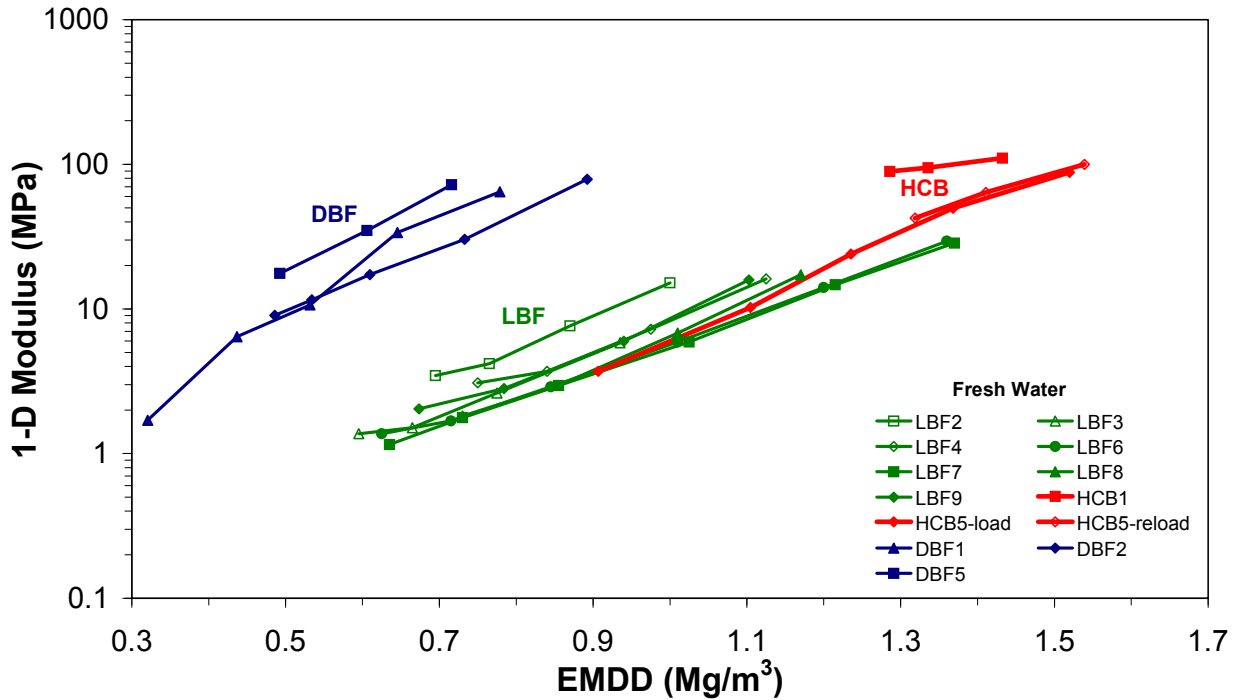
Figure 7: 1-D Constrained Moduli as a Function of EMDD for Fresh-Water Consolidation Specimens. See Table 2 for legend details.

3.1.4 Hysteresis

Bentonite-rich sealing-system components show a very strong hysteresis between the loading and unloading stages. This is best demonstrated by the HCB5 test (Figures 2 and 4) where the specimen is loaded, unloaded and then reloaded (see also Appendix A for details). The specimen was incrementally loaded to a maximum stress of 16 MPa, producing the straight compression line on the void ratio vs. log-stress plot (note: C_c is the compression index, the slope of the compression line). Unloading does not follow the expected elastic line for non-swelling clays, as shown, for example, by the unloading of the DBF specimens[3] (Figure 2 from 4000 kPa to 250 kPa) but displays considerable swelling. The unloading stage does not return to the loading stage line (or pathway), inferring that some process, such as internal friction or dilation control of clay-particle realignment, hinders this return. Subsequent loading returns the specimen to the initial loading pathway at the maximum stress (i.e., 16 MPa).

The bentonite-poor DBF displays the typical consolidation response of non-swelling clays[4] (Figure 2).

---

[3]   Note: Recent unpublished test results on DBF by students suggest that a non-elastic swelling response is observed when a further reduction in unloading stress (i.e., <50 kPa vs. the minimum of about 250 kPa in Appendix B) is carried out.

[4]   See footnote 3.

The observed load-unload plots of stress vs. EMDD for bentonite-rich components tends to parallel the swelling-pressure line (Figure 4), suggesting that EMDD-derived swelling pressure may be stress-path dependent (i.e., the slope will be unchanged but the value of swelling pressure will depend on whether the material is being loaded or unloaded). If so and if an equilibrium swelling pressure is assumed to evolve throughout a system of sealing components (e.g., Figure 1), then a uniformly distributed EMDD cannot be attained for bentonite-rich sealing-system components. The EMDD for each component is likely to be different and will vary within each component as a result of the water-uptake and thermally induced water-migration processes and the associated montmorillonite-swelling/shrinkage responses throughout the sealing system. At a conservative minimum, the equilibrium swelling pressure for each sealing-system component should be the value determined from the unloading path (Figure 4) because it is the lower value for a given EMDD.

3.2   SALINE-SOLUTION RESULTS

3.2.1   Void Ratio Results

Figure 8 presents all the saline-solution-test results in the standard format of void ratio versus applied stress.
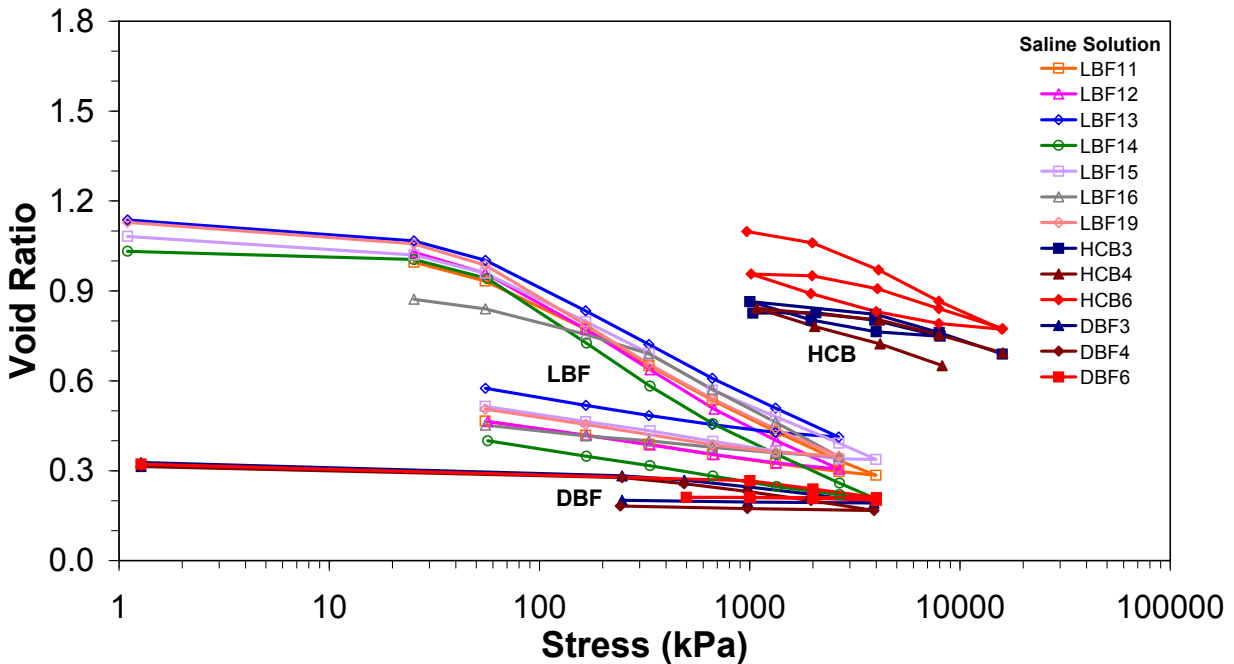
Figure 8: Void Ratio of Saline-Consolidation Specimens. See Table 3 for legend details.

The bentonite-rich sealing-system components continue to show high void ratios as compared to the bentonite-poor DBF although all void ratios in the lower stress range (i.e., <1000 kPa) are considerably reduced in the saline solution as compared to fresh water (Figure 2). The high concentration of the saline solution reduces the thickness of the diffuse double layers, thereby

reducing the repulsion between the smectite minerals. The derived compression (C_c) and rebound (C_s) indices for the saline-consolidation specimens are presented in Table 5. The values of C_c for bentonite-rich components are very similar and are about an order of magnitude greater than those for the bentonite-poor DBF. All the values of C_c for the fresh-water specimens are about 50% to 100% greater than those for saline specimens. This demonstrates that the electrolytic behaviour of the saline solution suppresses the thickness of the diffuse double layer, thereby increasing the stiffness of the saline specimens.

Table 5: Saline-Solution Compression and Rebound Indices

Saline Solution Test Specimen	Compression Index C_c	Rebound Index* C_s
LBF11	0.35	0.07
LBF12	0.40	0.07
LBF13	0.35	0.05
LBF14	0.40	0.08
LBF15	0.34	0.01
LBF16	0.38	0.04
LBF19	0.38	0.05
HCB3	0.22	0.05
HCB4	0.19	0.07
HCB6	0.34	0.06
DBF3	0.04	0.003
DBF4	0.04	0.005
DBF6	0.04	0.001

As with the fresh-water specimens, the rebound index (C_s) (Table 5) is calculated on the basis of the first unloading step following the incremental loading stage. Here too, the C_s's for the fresh-water specimens are about 25% to 50% greater than those for saline specimens, consistent with the suppression of the thickness of the diffuse double layer by the saline solution.

3.2.2 Dry Density and EMDD Results

Figures 9 and 10 present the saline test results with the void ratio converted to dry density and EMDD, respectively, for the sealing-system components, similar in fashion to Figures 3 and 4 for the fresh-water results. All the compression-line portions tend to line-up or parallel the swelling-pressure lines (after Hedin 2004 and after Dixon et al. 2002), which are also plotted in Figure 10. Note that the swelling-pressure lines are based on saline solutions composed of NaCl. Little to no swelling-pressure data are available for $CaCl_2$ solutions.
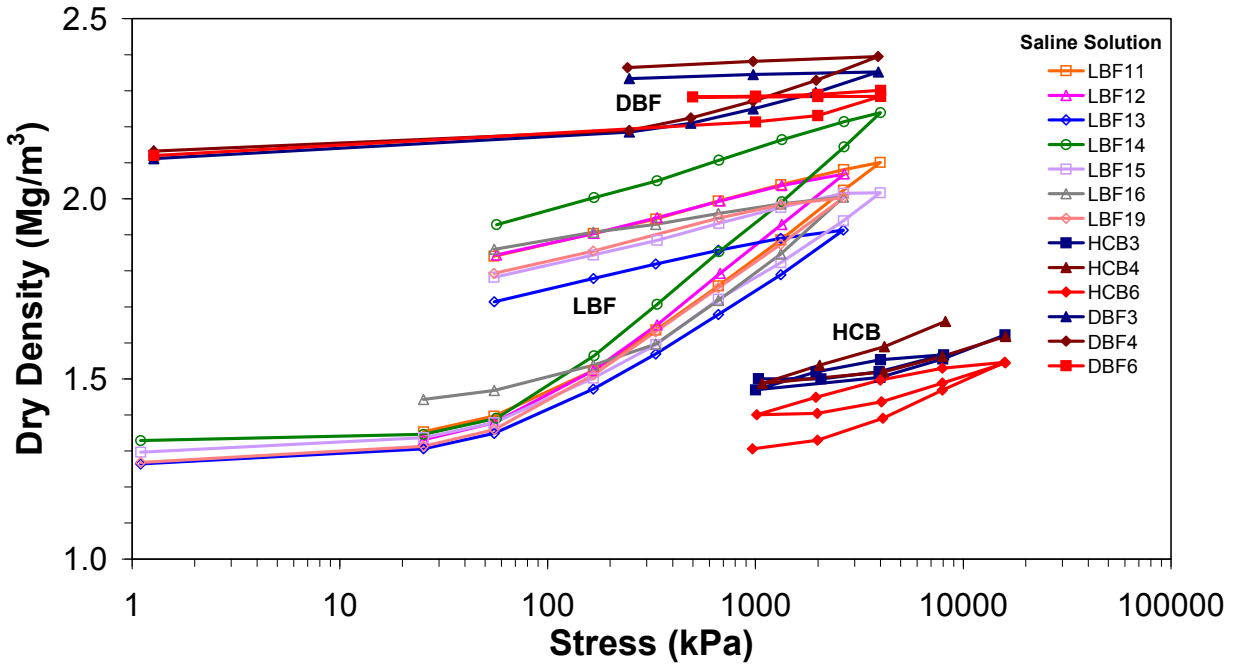
Figure 9: Dry Density of Saline-Consolidation Specimens. See Table 3 for legend details.
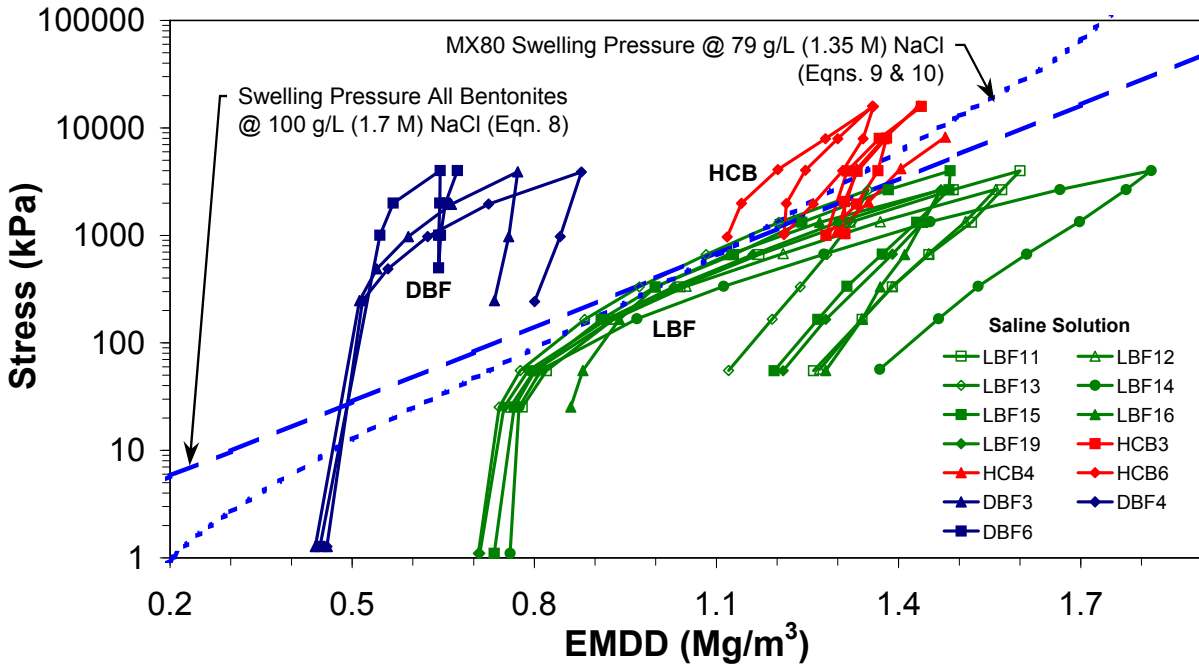
Figure 10: EMDD of Saline-Consolidation Specimens. Note: Swelling pressure lines are for NaCl solutions, unlike the $CaCl_2$-specimen solutions. See Table 3 for legend details.

The equation used to represent the swelling-pressure (P_s) at a total dissolved solids (TDS) content for a 100 g/L NaCl-solution by Dixon et al. (2002) for all bentonites in Figure 10 is as follows (Baumgartner 2006):

$$P_s = 2 \times 10^{-2} e^{5.3 EMDD} \tag{10}$$

The equation used to represent the swelling-pressure (P_s) data in NaCl solutions for MX80 bentonite (Hedin 2004, Karnland et al. 2003) in Figure 10 is as follows:

$$P_s = \left[\left(P_s^{fresh} \right)^2 + \left(2RTC\alpha_d \right)^2 \right]^{\frac{1}{2}} - 2RTC\alpha_d \tag{11}$$

where
P_s = swelling pressure in a solution (kPa);
P_s^{fresh} = swelling pressure under fresh-water conditions (e.g., Eqns. 1 or 2) (kPa);
R = molar gas constant (J/(mol·K));
T = absolute temperature (K);
C = salt concentration (mol/L); and
α_d = the calculated degree of dissociation (unitless) for the external NaCl solution of concentration C (Hedin 2004) given approximately by:

$$\alpha_d \approx 10^{\frac{-0.34\sqrt{C}}{\left(1+1.83\sqrt{C}\right)}} + 0.03C \tag{12}$$

The compression of LBF tends to parallel the swelling-pressure line (Equation 10) in Figure 10 for the most part up to about an EMDD of 1.2 Mg/m^3, after which the specimens deviate downwards at higher EMDDs. This deviation may be due to interference by the contained silica-sand fraction (i.e., 50 wt%). The HCB tends to parallel the Equation 11 swelling-pressure line proposed for MX80 swelling tests (Figure 10). The DBF is above and parallels both swelling pressure lines (Figure 10), indicating a greater stiffness than the bentonite-rich sealing-system components due to the very high proportion of crushed granite aggregate (i.e., 75 wt% vs. 6.25 wt% bentonite). This suggests that the average EMDD is not an accurate indicator of behaviour in bentonite-poor sealing-system components.

3.2.3   Constrained Moduli Results

Figure 11 presents the one-dimensional (1-D) constrained modulus of elasticity derived for each LBF, HCB and DBF specimen based on their dry density calculated at the mid-point of each load increment of their respective loading stage. Note the parallel trends of the 1-D constrained moduli in Figure 11 indicating a possible common basis of comparison.

Figure 11 is converted to Figure 12 by replacing dry density with EMDD. Note the continuing consistency in the parallel trends between the derived 1-D constrained moduli despite the differences in solution types.
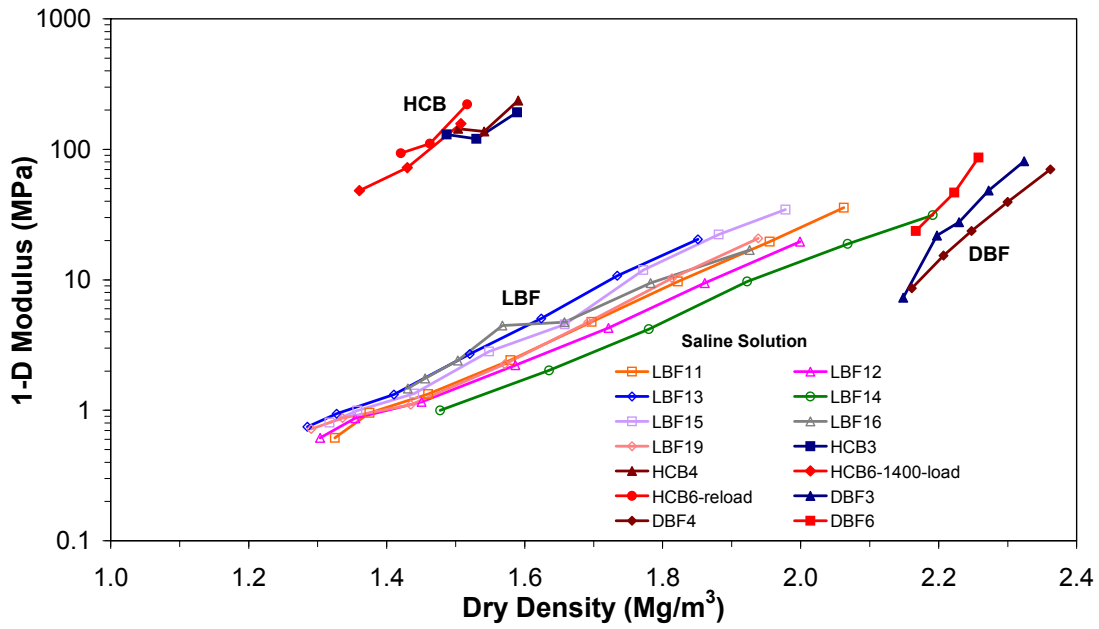
Figure 11: 1-D Constrained Moduli as a Function of Dry Density for Saline-Consolidation Specimens Based on Specimen Loading. See Table 3 for legend details.
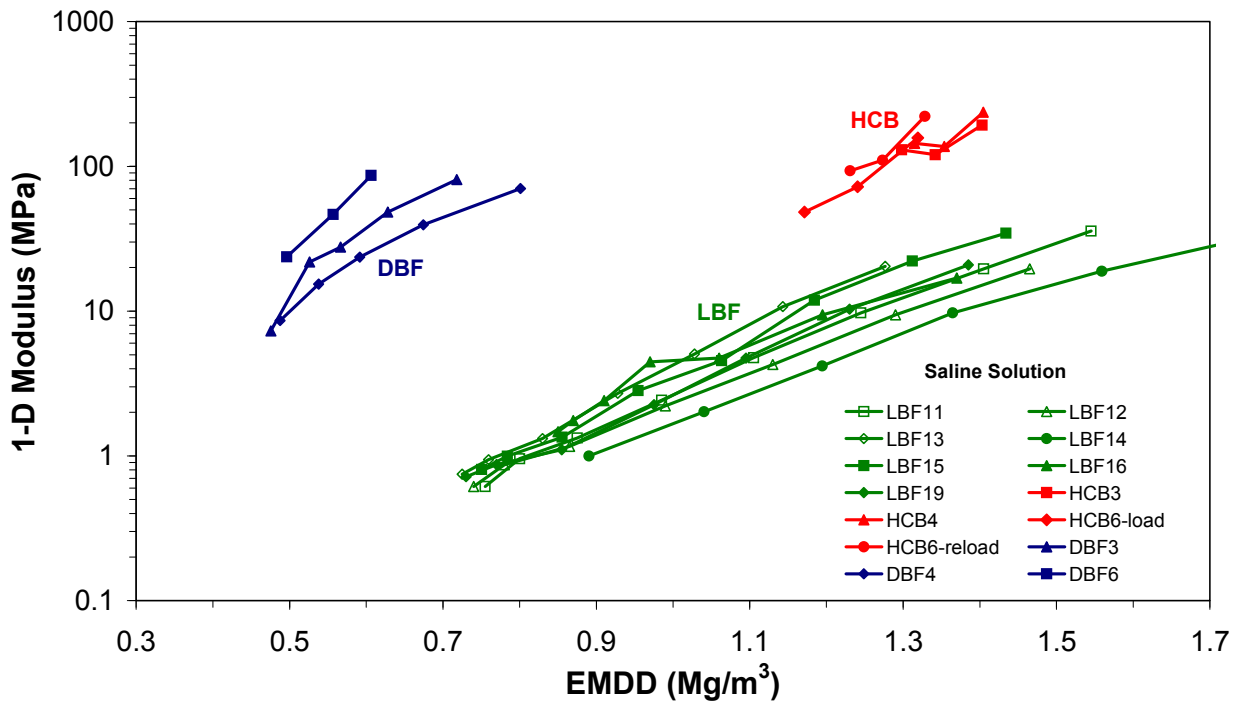
Figure 12: 1-D Constrained Moduli as a Function of EMDD for Saline-Consolidation Specimens Based on Specimen Loading. See Table 3 for legend details.

3.2.4 Hysteresis

The pore-fluid salinity affects all of the clays (e.g., bentonite and illite) by suppressing the thickness of their double layers. Bentonite-rich sealing-system components continue to show some evidence of hysteresis between the loading and unloading stages although this is greatly reduced as compared to the fresh-water specimens. This is best demonstrated by the HCB6 test (Figures 8, 9 and 10) where the specimen is loaded, unloaded and then reloaded. The unloading-stage pathway does not return to the loading-stage pathway, inferring that some process, such as internal friction or realignment of clay particles, prevents this return. Subsequent loading returns the specimen to the initial loading line at the maximum stress (i.e., 16 MPa).

The LBF has lost most of its swelling capacity (Figures 8, 9 and 10) and is tending to behave much like a non-swelling clay in that the unloading lines tend to be linear on the semi-log plots inferring a non-linear elastic response, although this conclusion may be premature without more unloading/reloading cycles and a further reduction in consolidation pressure. One difference between the LBF and HCB is the type of bentonite; the more active Wyoming bentonite has a Na/Ca ratio of about 1.8 and the less active Avonlea bentonite has a Na/Ca ratio of about 1.2, which may explain part of the difference in swelling potential. However, the unloading stage of the LBF still has more compliance than the much stiffer DBF in its unloading stage.

The observed load curves for bentonite-rich components still tend to parallel the swelling-pressure line (Figure 10). The unloading curves do not parallel the swelling-pressure line, clearly demonstrating stress-path dependency. In a saline pore-fluid environment, the equilibrium EMDD-based swelling pressure for each component will vary based on the stress path. At a conservative minimum, the equilibrium EMDD-based swelling pressure for each sealing-system component should be the value determined from the unloading path (Figure 10) because it is the lower value.

4. DISCUSSION

Sets of consolidation tests are performed on three sealing-system components to determine their preliminary hydro-mechanical behaviours. Each set of tests is performed on a different sealing-system component: two bentonite-rich components (i.e., HCB with 100 wt% Wyoming MX80 bentonite and LBF with 50 wt% Avonlea bentonite and 50 wt% silica-sand aggregate) and a bentonite-poor component (i.e., DBF with 6.25 wt% Avonlea bentonite, 18.75 wt% illite clay and 75 wt% crushed-granite aggregate). Tests are performed in both fresh-water and saline (i.e., $CaCl_2$) solutions to observe consolidation performance under differing electrolytic conditions that occur in natural groundwater systems. Differences in initial loading conditions are also performed to observe any associated stress-path effects. The details of the specific test plans, procedures and results are presented in the attached Appendices.

Consolidation results are presented in the conventional form of void ratio as a function of applied stress as well as dry density vs. stress and stress vs. EMDD. When literature-based values of swelling pressure as of function of EMDD are compared to the consolidation results, a pattern begins to emerge.

The EMDD-based consolidation results for sealing-system components in fresh-water solutions, both from specimen loading and unloading, either fall on or close to the swelling-pressure lines or are offset but parallel to the swelling-pressure lines. Although the DBF unloading curves do not parallel the swelling-pressure lines, very recent unpublished test results suggest that the unloading may not have gone to sufficiently low stress levels for this to occur.

In saline solutions, only the loading curves tend to parallel, along or offset from their corresponding salinity swelling-pressure line. The unloading curves do not. Perhaps unloading did not reach sufficiently low stress levels as discussed in the previous paragraph for the DBF in fresh-water solutions.

Castellanos et al. (2006) show, for a calcium-dominated (Ca-) bentonite, that the salt concentrations have a large effect on specimen consolidation but the salt-solution cations (e.g., Na^+ and Ca^{2+}) have little effect. Further testing of is required on sodium-dominated (Na-) bentonite with saline solutions to establish that the effect of their cations is small on medium- to high-density bentonite behaviour in the presence of electrolytes.

The behavioural comparison of bentonite in fresh-water and saline solutions generally demonstrates that electrolytes reduce the repulsion between smectite minerals (i.e., montmorillonite) caused, in part, by the reduction in the thickness of the diffuse-double layer of water around each clay particle (Mitchell 1976, Yong and Warkentin 1975). The fresh-water specimens are assumed to have the thickest diffuse-double layers of "bound" water repulsing and separating the montmorillonite particles. This would explain the observed high initial void ratios (Figure 2) at low consolidation pressures and high compression and rebound indices (C_c and C_s) (Table 4).

The saline specimens are assumed to have diffuse-double layers of reduced thickness, with a correspondingly reduced repulsion. This would explain the observed lower initial void ratios (Figure 8) and lower compression and rebound indices (C_c and C_s) (Table 5) as compared to the fresh-water specimens (Table 4).

However, the difference in void ratios for fresh-water and saline-solution specimens at specific stress increments suggest that some realignment of the montmorillonite platelets may be occurring. The void ratios for HCB (Table 6) are greater for saline-solution specimens than for fresh-water specimens at the end of each stress increment in the 1-D consolidation tests. The DBF shows only a slight increase for saline conditions but this may be within system variability. This suggests that a greater percentage of the montmorillonite platelets are aligned in a face-to-face arrangement in fresh water than in a saline solution, which appears to have a proportionately greater edge-to-face platelet structure (Figure 13). The saline electrolyte appears to promote a strong electrostatic bond for the edge-to-face structure because the void ratio remains much higher under saline conditions at the highest applied stresses without microstructure collapse (i.e., HCB at 16 MPa). The electrolyte tends to favour an edge-to-face clay-particle alignment if sufficient void space is available during sample preparation and initial saturation to permit this rearrangement from a face-to-face microstructure (Villar 2002, Wan 1996, Collins and McGown 1974). The microstructure ultimately affects the structure, stiffness and structural stability of the soil skeleton (Figure 13).

The LBF specimens consolidated in a saline solution consistently produce opposite results, lower final void ratios (and higher dry densities and EMDDs) in each stress increment than those consolidated in fresh water (Table 6). The source of this apparent discrepancy is unclear. The HCB and DBF specimens were prepared by mixing the soils with saline solution and then

they were immersed and saturated under load in a saline reservoir. Most of the LBF specimens were mixed with fresh water and then immersed and saturated under load in the saline reservoir. However, two LBF specimens were mixed with saline solution, followed by their saturation in a saline reservoir. LBF 13 and LBF 15 showed slightly greater void ratios at their maximum loads (Figure 8) than the specimens fabricated with fresh water, but this difference can be within the realm of system variability. Little difference in consolidation was apparent between the two types of mixing solutions for the LBF. Perhaps there are other factors playing a role in specimen preparation and initial loading in the unsaturated state that may account for the discrepancy in specimen response.

Future tests should be performed on specimen preparation and initial conditions as how these would affect our understanding of salinity effects on bentonite materials, both from a material science perspective and from its application in sealing-system component fabrication. Fabrication of sealing-system components using a saline solution may be detrimental to achieving low void ratios and high densities if the bentonite soil microstructure tends to an edge-to-face platelet arrangement.

Table 6: Comparison of Sealing-system Components at Specific Stress Increments

Type	Water	Stress Increment	Mean Stress (MPa)	Void Ratio @ Max. Load	Dry Density (Mg/m^3) @ Max. Load	EMDD (Mg/m^3) @ Max. Load	1-D Modulus (MPa)
HCB	Fresh	1 to 2 MPa	1.5	1.01	1.36	1.17	10
	Saline			1.06	1.33	1.14	56
	Fresh	8 to 16 MPa	12	0.55	1.77	1.59	97
	Saline			0.73	1.58	1.40	202
LBF	Fresh	0.66 to 1.33 MPa	1.0	0.66	1.63	1.05	6
	Saline			0.44	1.88	1.31	10
	Fresh	1.33 to 2.65 MPa	2.0	0.52	1.78	1.22	16
	Saline			0.34	2.01	1.48	20
	Fresh	2.65 to 4 MPa	3.3	0.37	1.97	1.43	29
	Saline			0.28	2.12	1.63	34
DBF	Fresh	0.5 to 1 MPa	6.3	0.23	2.28	0.64	23
	Saline			0.25	2.24	0.59	25
	Fresh	1 to 2 MPa	1.5	0.19	2.35	0.77	43
	Saline			0.22	2.29	0.65	45
	Fresh	2 to 4 MPa	3.0	0.17	2.39	0.87	72
	Saline			0.19	2.34	0.77	79

The fitted stiffness relationships for both fresh-water and saline-solution specimens are displayed in Figure 14 based on dry density and in Figure 15 based on EMDD. Both the HCB and DBF specimen sets show an increase in stiffness from fresh-water to saline conditions at given EMDDs. The opposite is indicated for LBF for a given EMDD, as discussed in the

previous paragraphs. Note that the maximum achievable EMDD for LBF at a given stress is greater for saline conditions than for fresh-water conditions whereas the opposite is indicated for HCB and DBF (Figures 4 and 10).
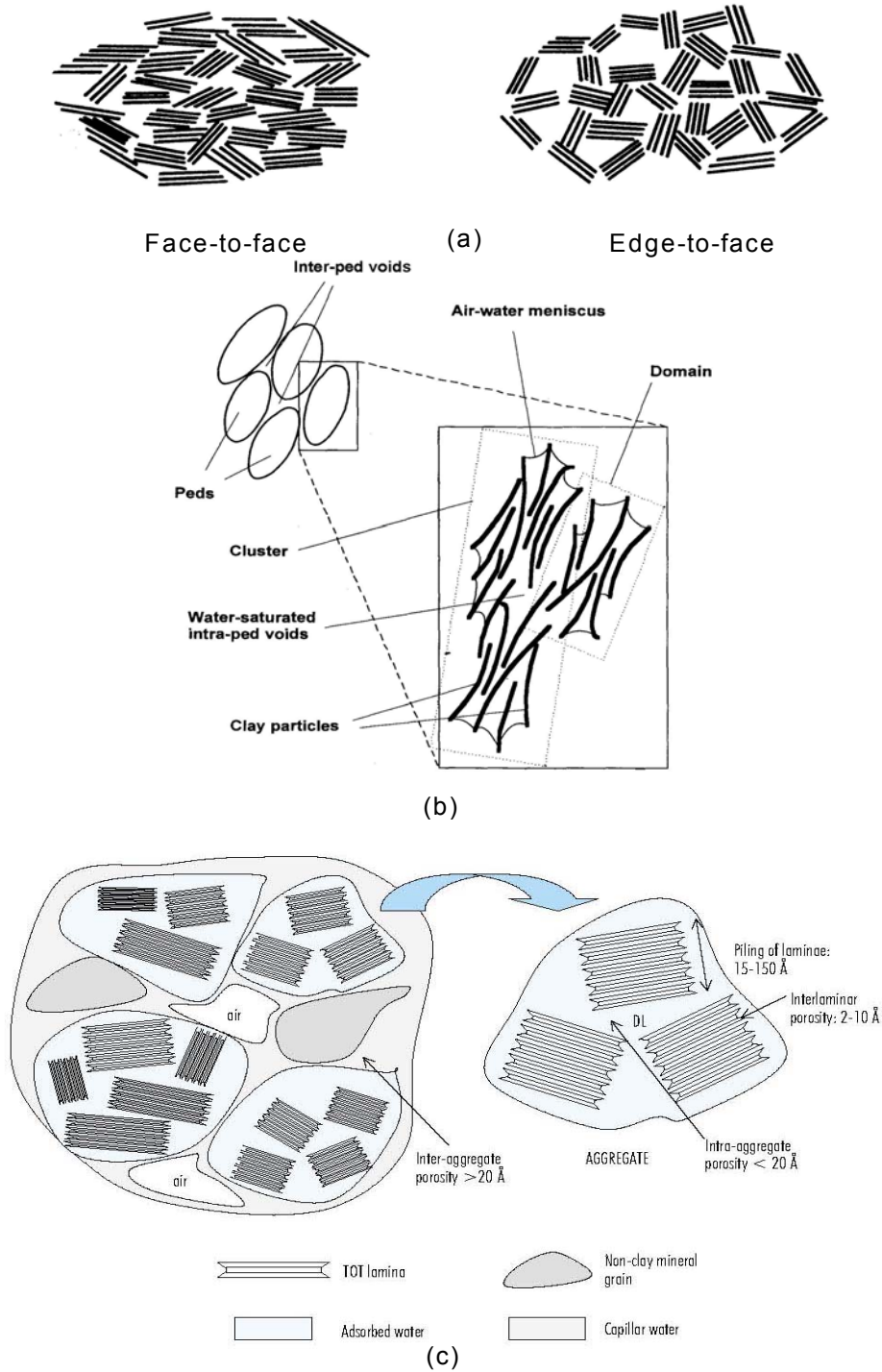
Figure 13: Simplified Representations of Complex Clay-Soil Structures (a) by Collins and McGown (1974), (b) by Wan (1996) and (c) by Villar (2002)
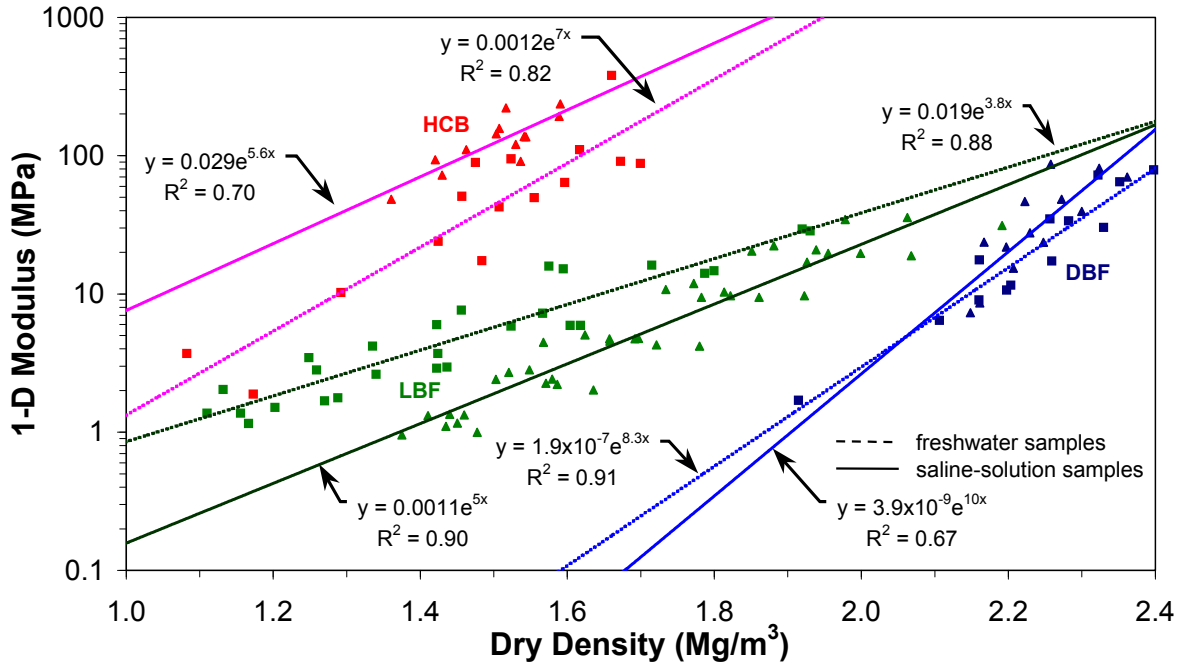
Figure 14: Fitted 1-D Constrained Moduli of Specimens Based on Dry Density
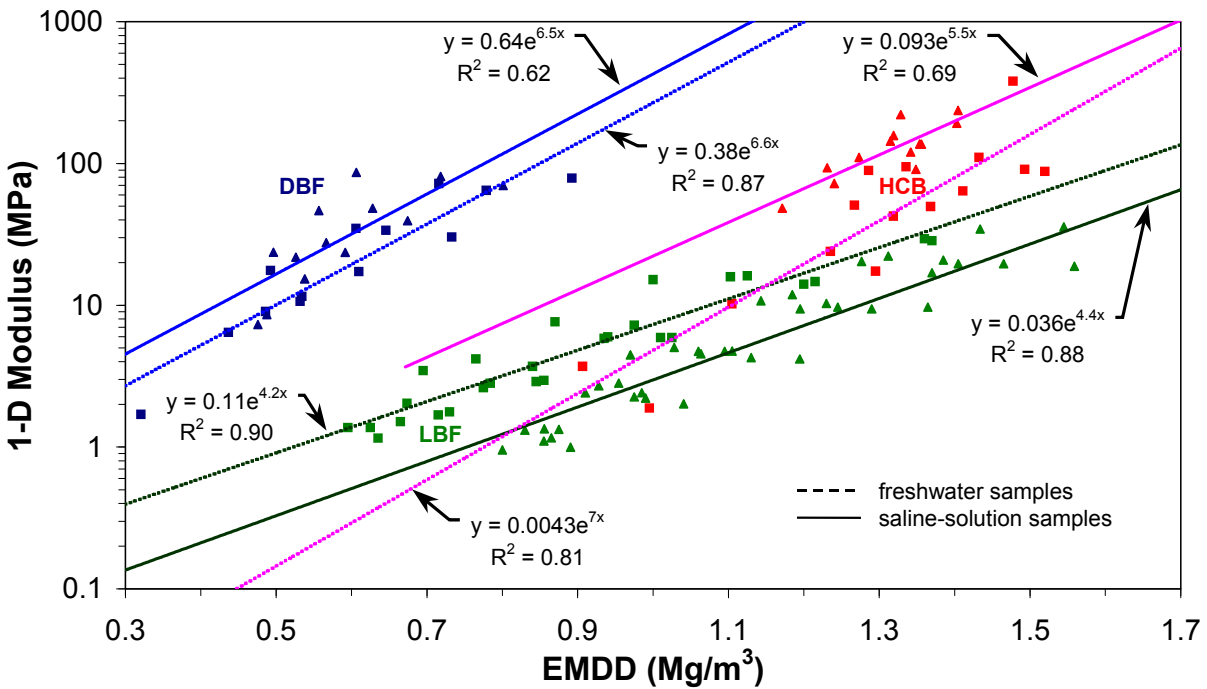
Figure 15: Fitted 1-D Constrained Moduli of Specimens Based on EMDD

Another possible difference between the testing of LBF as compared to that of DBF and HCB are in the sources of bentonite (i.e., Wyoming MX80 bentonite in HCB and Avonlea bentonite in DBF and LBF). The Wyoming bentonite tends to have a greater sodium concentration at the exchangeable cations sites in the montmorillonite than that for Avonlea bentonite (i.e., Wyoming Na/Ca ratio ~1.8 and Avonlea Na/Ca ratio ~1.2). Whether this difference in Na/Ca ratios is sufficient to affect platelet restructuring is unclear.

When bentonite-rich materials are permitted to swell under confining pressures less than the EMDD-determined swelling pressure, the swelling action appears to disrupt the soil fabric, effectively remoulding the material. For example, free swell will tend to obliterate much if not all of the preconsolidation effects by expansion of the diffuse–double layer of water (i.e., swelling) and possible clay-platelet restructuring. The unloading stage of the consolidation test following the loading stage also permits swelling under controlled loads and may also permit some clay-platelet restructuring. The effects of soil-fabric swelling are most pronounced in fresh-water solutions and tend to be least pronounced in saline solutions. Bentonite-poor sealing components tend to be less affected by unloading, possibly due to internal friction of the nonswelling clay minerals.

If the EMDD-derived swelling pressure is stress-path dependent and if an equilibrium swelling pressure is assumed to evolve throughout a system of sealing components (e.g., Figure 1), then a uniformly distributed EMDD cannot be attained for bentonite-rich sealing-system components. The equilibrium EMDD for each component is likely to be different and will vary within each component depending on the stress-path taken by the saturation and swelling processes. At a conservative minimum, the equilibrium EMDD-based swelling pressure for each sealing-system component should be the value determined from the unloading path (Figures 4 and 10) because it is the lower value.

5. CONCLUSIONS

The consolidation results demonstrate the influence of pore-fluid chemistry on the mechanical performance and swelling characteristics of sealing-system components, particularly those of bentonite-rich composition. The presence of the calcium chloride reduces the swelling potential likely due to the reduction in the thickness of the double-layer of the bound water. The reduction of both the compression and rebound indices with the corresponding increase in the 1-D constrained moduli under saline conditions shows that a stable, electrolyte-supported structure has likely formed contributing to a less compliant (i.e., stiffer) structure at relatively high void ratios as compared to fresh-water specimens although the discrepancies in the LBF sealing-system component need to be resolved. The results provide a valuable set of experimental data for numerical modelling purposes.

6. RECOMMENDATIONS

The Nuclear Waste Management Organization (NWMO) has identified Ordovician sediments as potentially suitable geologic media to host a Deep Geologic Repository for used nuclear fuel (NWMO 2005). Mazurek (2004) in his geoscientific review of the sedimentary sequence in southern Ontario indicates the presence of highly saline groundwaters (i.e., 30- to 35-g/L Ca, 40- to 60-g/L Na and 150- to 180-g/L Cl) in the Ordovician sediments, much higher salinities

than the 75-g/L $CaCl_2$ tested in these consolidation tests. Consolidation testing of bentonite-rich sealing-system components should consider these high salinity levels, both on individual NaCl and $CaCl_2$ solutions and on their mixtures to measure individual effects based on salt speciation and on their combined effect to note any unique differences.

The consolidation cells should be fabricated from more corrosion-resistant materials due to these high salinities and the long durations of each test. If swelling pressure measurements are to be made during consolidation, then consideration should be given to fabricating a servo-actuated loading system to increase load while maintaining less than 0.005 mm of displacement (i.e., a constant volume swelling test (ASTM 2003)).

One design decision for the engineering of a sealing system that should be considered is the preference for preparing the sealing materials with either fresh or saline water. Consolidation tests should include the preparation of sealing-system-component specimens with fresh water and placement of the specimens in a reservoir of saline water to measure differences in response. The roles that methods of specimen preparation have on specimen response are unclear and should be investigated. This has implications on the methods on the fabrication of sealing-system components for a repository, particularly when these components are to be applied in saline-groundwater environments.

Consolidation tests should be coupled with long-duration static testing, in terms of years, of single- and multiple-sealing materials in constant-volume pressure vessels immersed in both fresh- and saline-water reservoirs to measure long-term responses. Unlike consolidation tests, which provide short-term transient-response data, the constant-volume tests provide only end-of-test results and cannot provide any mechanistic indications as to their full transient response. The advantage of the constant-volume tests is their low cost and long-term data that includes creep effects.

REFERENCES

ASTM (ASTM International). 2003. Standard test methods for one-dimensional swell or settlement potential of cohesive soils. Standard D4546-03, ASTM International, West Conshohocken, Pennsylvania, USA.

Bardet, J.-P. 1997. Experimental Soil Mechanics. Prentice Hall Inc., Upper Saddle River, N.J.

Baumgartner, P. 2006. Generic thermal-mechanical-hydraulic (THM) data for sealing materials - Volume 1: Soil – water relationships. Ontario Power Generation, Nuclear Waste Management Division Report No: 06819-REP-01300-10122-R00.

Baumgartner, P. and G.R. Snider. 2002. Seal Evaluation and Assessment Study (SEAS): Light backfill placement trials. Atomic Energy of Canada Limited Technical Record, TR-793.

Castellanos, E., A. Gens, A. Lloret and E. Romero. 2006. Influence of water chemistry on the swelling capacity of high-density bentonite. In Unsaturated Soils 2006, Proc. 4th. Int'l. Conf. of Unsaturated Soils, 2006 Apr. 02-06, Carefree, Ariz., A.S.C.E., Reston, Virginia.

Collins, K., and A. McGown. 1974. The form and function of microfabric features in a variety of natural soils. Geotechnique, Vol. 24, No. 2, pp. 223–254.

CTECH (CTECH Radioactive Materials Management). 2002. Conceptual design for a deep geologic repository for used nuclear fuel. CTECH Report 1106/MD18085/REP/01, Nuclear Waste Management Organization, Toronto, Canada (www.nwmo.ca).

Dixon, D.A., N.A. Chandler and P. Baumgartner. 2002. The influence of groundwater salinity and interfaces on the performance of potential backfilling materials. In Trans. 6th International Workshop on Design and Construction of Final Repositories: Backfilling in Radioactive Waste Disposal. ONDRAF/NIRAS, Brussels, Belgium, 2002 March 11-13.

Dixon, D.A. 2000. Porewater salinity and the development of swelling pressure in bentonite-based buffer and backfill materials. Helsinki, Posiva Report, POSIVA 2000-04 (ISBN 951-652-090-1).

Gascoyne, M., C.C. Davison, J.D. Ross and R. Pearson. 1987. Saline groundwaters and brines in plutons in the Canadian Shield. In Saline Water and Gases in Crystalline Rocks. Editors: Fritz, P. and Frape, S.K.; Geological Association of Canada Special Paper 33, Ottawa.

Gierszewski, P., J. Avis, N. Calder, A. D'Andrea, F. Garisto, C. Kitson, T. Melnyk, K. Wei and L. Wojciechowski. 2004. Third case study – Postclosure safety assessment. Ontario Power Generation, Nuclear Waste Management Division Report 06819-REP-01200-10109-R00. Toronto, Ontario.

Hedin, A. 2004. Integrated near-field evolution model for a KBS-3 repository. SKB Report R-04-36. Swedish Nuclear Fuel and Waste Management Co., Stockholm.

Karnland O., A. Muurinen and F. Karlsson. 2003. Bentonite swelling pressure in NaCl solutions - Experimentally determined data and model calculations. Sitges Symposium on Large scale Field Tests in Granite, 2003 November 12-14, University of Catalonia, Spain.

Kjartanson, B.H., D.A. Dixon and C.L. Kohle. 2005. Placement of bentonite pellets to fill repository sealing system voids and gaps. Ontario Power Generation, Nuclear Waste Management Division, Technical Report No: 06819-REP-01200-10136-R00.

Kjartanson, B. H., D.A. Dixon, and S. Stroes-Gascoyne. 2003. Effects of container/buffer gap fill on buffer performance. Ontario Power Generation, Nuclear Waste Management Division Report 06819-REP-01200-10102-R00.

Lambe, T.W. and R.V. Whitman. 1969. Soil Mechanics. John Wiley and Sons, Inc., New York.

Mazurek, M. 2004. Long-term used nuclear fuel waste management – Geoscientific review of the sedimentary sequence in southern Ontario. Institute of Geological Sciences, Univ. of Bern, Technical Report TR 04-01, Bern, Switzerland, available from Nuclear Waste Management Organization, Toronto, Canada (www.nwmo.ca).

Mitchell, J.K. 1976. Fundamentals Of Soil Behaviour. John Wiley And Sons, Toronto.

NWMO (Nuclear Waste Management Organization). 2005. Choosing a way forward: The future management of Canada's used nuclear fuel, final study. Nuclear Waste Management Organization, Toronto, Canada (www.nwmo.ca).

Russell, S.B. and G.R. Simmons. 2003. Engineered barrier system for a deep geologic repository. Presented at the 2003 International High-Level Radioactive Waste Management Conference. 2003 March 30-April 2, Las Vegas, NV.

Villar, M.V. 2002. Thermo-hydro-mechanical characterization of a bentonite from Cabo de Gata. A study applied to the use of bentonite as sealing material in high level radioactive waste repositories. Publicasión Técnica ENRESA 01/2002, p. 258. Madrid.

Wan, A.W.L. 1996. The Use of Thermocouple Psychrometers to Measure In Situ Suctions and Water Contents in Compacted Clays. Ph.D. Thesis. Dept. of Civil and Geological Engineering, Univ. of Manitoba.

Yong, R.N. and B.P. Warkentin. 1975. Developments in Geotechnical Engineering. 5: Soil Properties and Behaviour. Elsevier, Amsterdam.

APPENDIX A: HIGHLY COMPACTED BENTONITE (HCB)

P. Baumgartner and D. Priyanto
Waste Technology Division
Atomic Energy of Canada Limited

CONTENTS

Page

A.1   HCB

Highly compacted bentonite (HCB) is a clay-based sealing-system component proposed for use in either full contact or very close proximity to the used-fuel container (Maak and Simmons 2005). HCB is composed of 100% bentonite (Russell and Simmons 2003), compacted to high dry densities. The test specimens are fabricated from 80-mesh granules of Wyoming bentonite (MX80) with an assumed minimum Na-montmorillonite content of 75%.

A.2   HCB 1-D CONSOLIDATION TESTING

A.2.1 HCB TEST OVERVIEW

All the details of the ASTM (2004) standard procedure and equipment for one-dimensional (1D) consolidation are not rigorously followed due to the highly swelling nature of the HCB and the high-load conditions to be applied on the specimens. On water uptake and saturation of the HCB, the high Effective Montmorillonite Dry Density (EMDD) in the range of 1.1 to 1.5 Mg/m^3 will generate swelling pressures in fresh water from about 1 MPa to 12 MPa, respectively, that will resist the consolidation (i.e., volumetric decrease) of the HCB specimen. Compressive stresses are required to exceed the HCB swelling pressures to define its full range of elasto-plastic behaviour.

Small-diameter oedometer cells (28.1-mm dia.) are used in this test series to permit high stresses to be applied (i.e., maximum 16 MPa). Six specimens are tested at specified conditions (Table A1). The testing includes an initially defined loading and unloading schedule for all stages of each test, which are modified based on findings from the initial series of tests. This report summarizes the procedures used in the testing, the detailed measurements taken during the tests and comparisons of the test results in light of the initial conditions.

Specimens are prepared from loose MX80 bentonite. The specimen materials are oven dried and then wetted to the prescribed water contents (Table A1) with either fresh (i.e., distilled) water or saline (i.e., 75 g/L CaCl$_2$) solution. Oedometer specimens are prepared by manually compacting a specified mass of wetted material inside the oedometer specimen ring and compacted to a specified height (i.e., ~10 mm) to achieve the specified dry density. Following specimen compaction to the target conditions, the filled specimen ring is placed in the oedometer and the specified initial consolidation conditions (i.e., load and reservoir solution) are applied as defined by the planned testing matrix (Table A1).

Two different initial conditions for the specimens are attempted, an initial constant-volume condition during water uptake and a full-swelling condition at a prescribed specimen stress (i.e., usually at 1 MPa) during water uptake. The subsequent loading and unloading steps tend to follow the incremental load and unload pattern[A1] for oedometers, with a few exceptions, as described in the loading schedules presented in the last column of Table A1.

[A1]   A typical pattern is the doubling of load with each incremental step during loading and the halving of load with each incremental step during unloading.

Table A1: 1-D Consolidation Test Matrix for HCB Specimens

Specimen No.	Mixing and Reservoir Water	Target Dry Density (kg/m^3)	Target Water Content (wt%)	Swelling on Initial Water Uptake	Load Schedule
HCB1	Distilled	1650	21.5%	100% at 1 MPa	Load to 1, 2, 4, 8 & 16 MPa Unload to 8, 4 & 2 MPa
HCB2	Distilled	1650	21.5%	Attempt Rigid Confinement with no LVDT displacement beginning at 1 MPa	Load to 1 & 16 MPa Unload to 8, 4, 2 & 1 MPa
HCB3	75 g/L CaCl$_2$	1650	21.5%	100% at 1 MPa	Load to 1, 2, 4 & 8 MPa Unload to 4, 2 & 1 MPa Load to 4, 8 & 16 MPa
HCB4	75 g/L CaCl$_2$	1650	21.5%	100% at 8 MPa	Load to 8 MPa Unload to 4, 2 & 1 MPa Load to 4, 8 & 16 MPa
HCB5	Distilled	1400	31%	100% at 1 MPa	Load to 1, 2, 4, 8 & 16 MPa Unload to 8, 4, 2 & 1 MPa Load to 2, 4, 8 & 16 MPa
HCB6	75 g/L CaCl$_2$	1400	31%	100% at 1 MPa	Load to 1, 2, 4, 8 & 16 MPa Unload to 8, 4, 2 & 1 MPa Load to 2, 4, 8 & 16 MPa

A.2.2 HCB TEST EQUIPMENT

AECL's standard dead-weight oedometers are unable to supply the necessary high loads to generate specimen stresses exceeding the specimen swelling pressures. Two compression frames are used in this test series with attached hydraulic rams (e.g., a 222 kN spring-return ram and a 445 kN double-acting ram) to produce the required high loads. Each hydraulic ram is actuated by a high-pressure nitrogen-gas cylinder acting on a gas-over-oil accumulator (Figure A1). Reduced diameter oedometer rings are constructed for the high-stress testing and small-diameter filter stones are used. All components of the oedometer cells are fabricated from stainless steel to reduce the amount of corrosion, particularly from the saline solution.

Displacements are measured with calibrated linear variable differential transformers (LVDTs). Loads are measured with calibrated strain-gauge load cells (i.e., 17.8-kN capacity). All instruments are connected to a data logger and logger scan rates are set at 5 minutes for the first 24 hours of a load/unload increment and every hour thereafter until the load/unload increment is deemed complete.
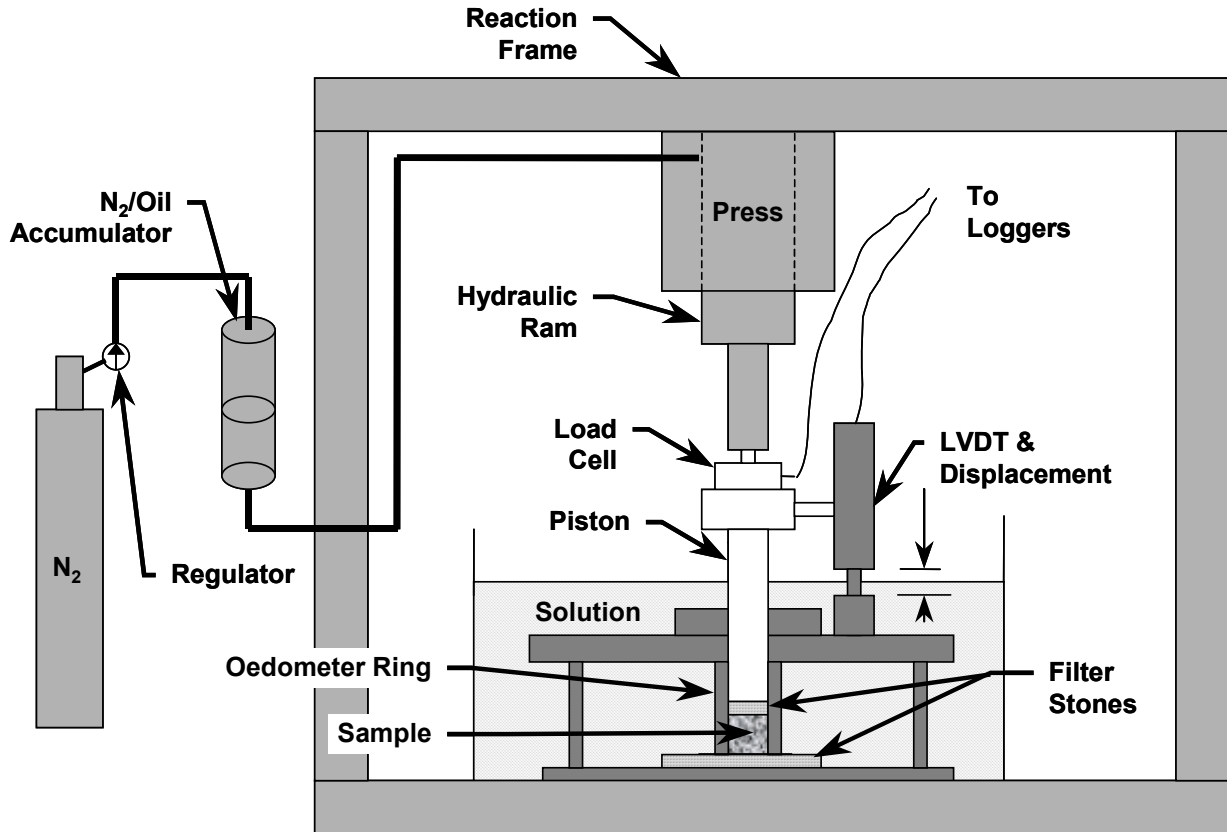
Figure A1: Schematic of Compression Frame, Loading System and Measurement System

A reference LVDT is installed on a non-displacing portion of each frame to compensate for any changes in laboratory temperatures on the LVDT installed in the oedometer cell. The laboratory seasonal temperature ranged between 19°C and 24°C, producing a maximum measured dimensional variance of 0.011 mm, or about a 0.1% variation for a 10-mm-thick specimen. This small variation is considered insignificant and no thermal compensation is included in any calculations.

A.3   HCB TEST PROCEDURE

A.3.1   SPECIMEN PREPARATION

The first four HCB specimens are compacted to a dry density of ~1650 kg/m^3 at an initial water content of ~21.5% (i.e., a bulk density of ~2000 kg/m^3) resulting in an initial degree of saturation of ~90%. The last two HCB specimens are compacted to a dry density of ~1400 kg/m^3 at an initial water content of ~31% (i.e., a bulk density of ~1840 kg/m^3) resulting in an initial degree of saturation of ~91%. Specimens are compacted in one, 10-mm high lift in the oedometer ring with a hydraulic press. The compaction piston has a mark scribed on its outer surface, which permits the technologist to observe when the specimen has reached its required height and, therefore, its initial density.

Filter papers and filter stones are installed on top and bottom of the specimen and specimen assembly is installed in the oedometer. An initial load of 1 MPa is applied to settle the specimen assembly and solution (i.e., water or saline solution) is added to the reservoir. Plastic shrouding encloses the assembly and reservoir to minimize evaporation. The reservoir solution in the oedometer is identical to that of the mixing solution. Upon assembling the oedometers, tests either begin under constant-strain or free-swell conditions according the testing matrix.

A.3.2 SPECIMEN LOADING

The specimen load is adjusted with the regulator on the nitrogen (N_2) bottle (Figure A1). Test results show that a fair amount of secondary compression/swelling occurs following the primary compression/swelling of the specimen. The decision to change load is somewhat subjective and is based on a number of factors including; the stability of the creep (secondary compression/swelling) rate, a change in the void ratio of less than 0.001 mm over a two or three day period and the potential for stick-slip phenomena associated with the loading and displacement-monitoring systems. Nominally, primary compression/swelling is complete within two or three days for a saturated specimen as shown in the displacement/log time plots.

The decision when to change the loads was somewhat subjective, observing a number of factors including the stability of the secondary-consolidation creep. Consideration must also be given to the potential for stick-slip phenomena associated with the loading system and displacement-monitoring systems.

Achieving saturation of the swelling specimen under the initial load, usually at 1 MPa, takes a long time. Experience from the initial saturation and swelling behaviours of the first four specimens indicates that the first load increments appear to be prematurely ended. The initial dry densities of the last two specimens are reduced (i.e., 1400 kg/m^3) to reduce the amount of saturation and swelling time and they still require greater than 30 days to stabilize.

A.4   HCB TEST RESULTS

The results of the HCB consolidation tests are presented as individual test results and comparisons between tests based on pore-fluid solutions. Figure A2 provides an example loading sequence (i.e., HCB6).

A.4.1. INDIVIDUAL TEST RESULTS

A.4.1.1 HCB1

Test results from the HCB1 specimen (i.e., target initial dry density 1650 kg/m^3, gravimetric water content 21.5%, degree of saturation 89%, fresh water) are plotted in Figures A3 and A4 showing the time-dependent displacements occurring in each load step and the stress-dependent void ratio at the end of each load step, respectively.

The curve for the first load increment (i.e., #1 at 1 MPa) in Figures A3a and A3b shows an initial compression, as do all subsequent specimens, due to the suddenly applied load followed by swelling as the specimen draws in water to achieve full saturation. Theoretically, the specimen should be fully saturated by the end of the load increment and for all subsequent load increments.

The primary compression/swelling phase of each load increment, except increment #1, requires 2 to 3 days of measurement. Secondary compression/swelling typically requires 1 to 2 weeks (or ~10,000 to 20,000 minutes) from the start of the load increment to establish a stable creep rate. Swelling due to unloading tends to require more time than does compression loading, probably due to differences in hydraulic forces for drawing in water than with those for squeezing water out.
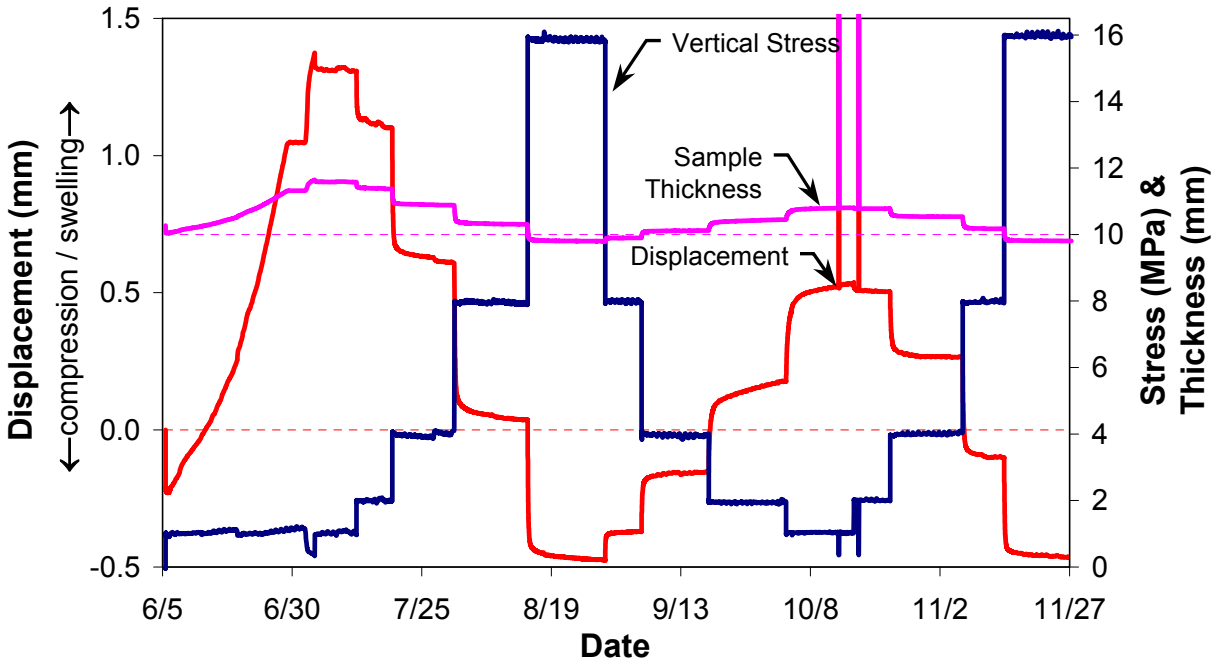
Figure A2: An Example Specimen Loading Sequence (HCB6)

The coefficients of consolidation for each load increment from Figures A3a and A3b are provided in Table A2. Two graphical methods are used: one where displacement is plotted as a function of the square root of time (sqrt time) and the other as a function of the logarithm of time (log time). The values derived from each graphical method are similar, providing confidence that the end of the primary-compression phase is reasonably determined. What cannot be resolved in the consolidation test is whether or not the secondary compression/swelling is independent of or simultaneous with primary compression/swelling.

The compression (C_c) and rebound (C_s) indices are calculated from the slopes of the void-ratio curves (i.e., Figure A4). The indices are dimensionless and $C_c > C_s$. These indices are typically established from standard consolidation tests and are used to assess the constrained compressibility for normally and overconsolidated soil conditions. The values of C_c and C_s are 0.42 and 0.11, respectively.

The term rebound is used rather than the more conventional term of swelling that is used in the literature. Rebound tends to continue in a relatively linear fashion along the rebound line (C_s) for more conventional non-swelling soils as load decreases, an expression of the non-linear

elastic behaviour of these soils and should not be termed as the swelling index. As observed in Figure A4, rebound strongly deviates from the rebound line for this strongly swelling soil showing both an initial non-linear elastic response followed by a combined elastic and swelling response.

The specimen thickness at the end of test was very difficult to measure. The ends of the specimen against the filter paper/porous stones were extremely soft due to swelling, although the duration of the final unloading step at a vertical stress of 2 MPa was ~11 days. This suggests that more time is needed to permit completion of swelling.

Table A3 presents the data for plotting Figure A4 as well as the derived dry densities and EMDDs at the end of each load increment. As noted in Sections A1.1.1 and A2.1.1, EMDDs are calculated on the basis that the Wyoming bentonite (MX80) has an assumed minimum Na-montmorillonite content of 75%.
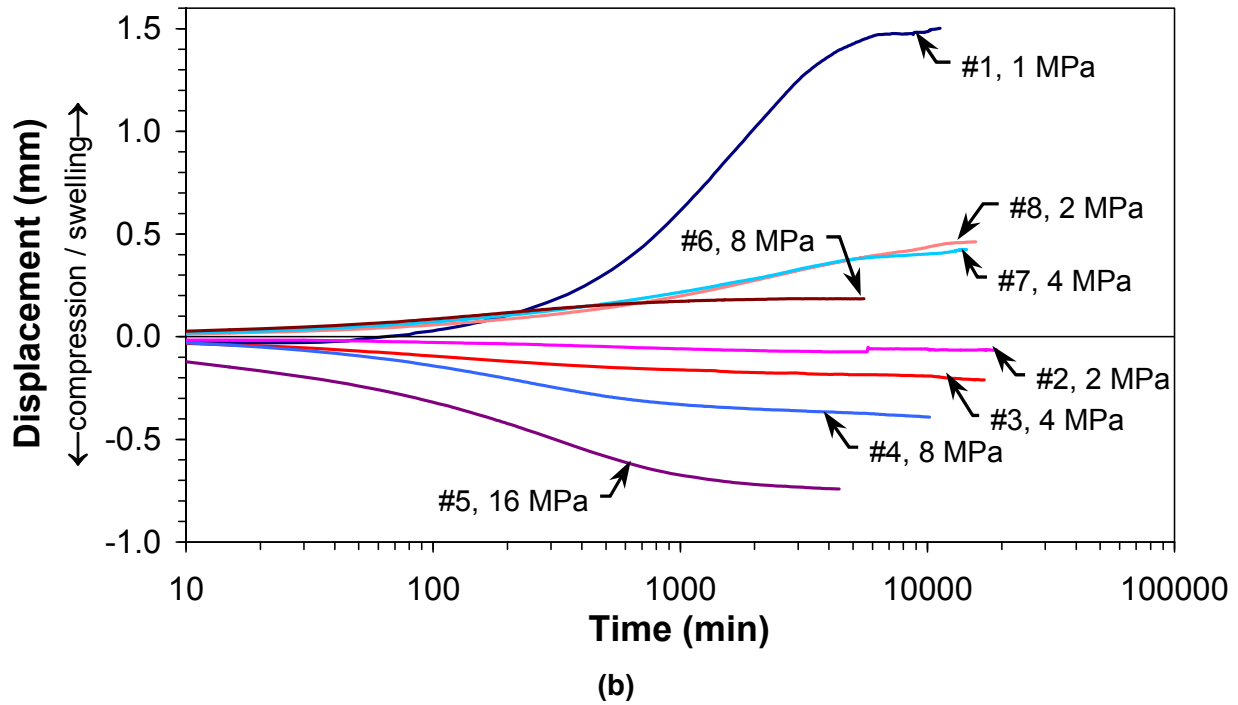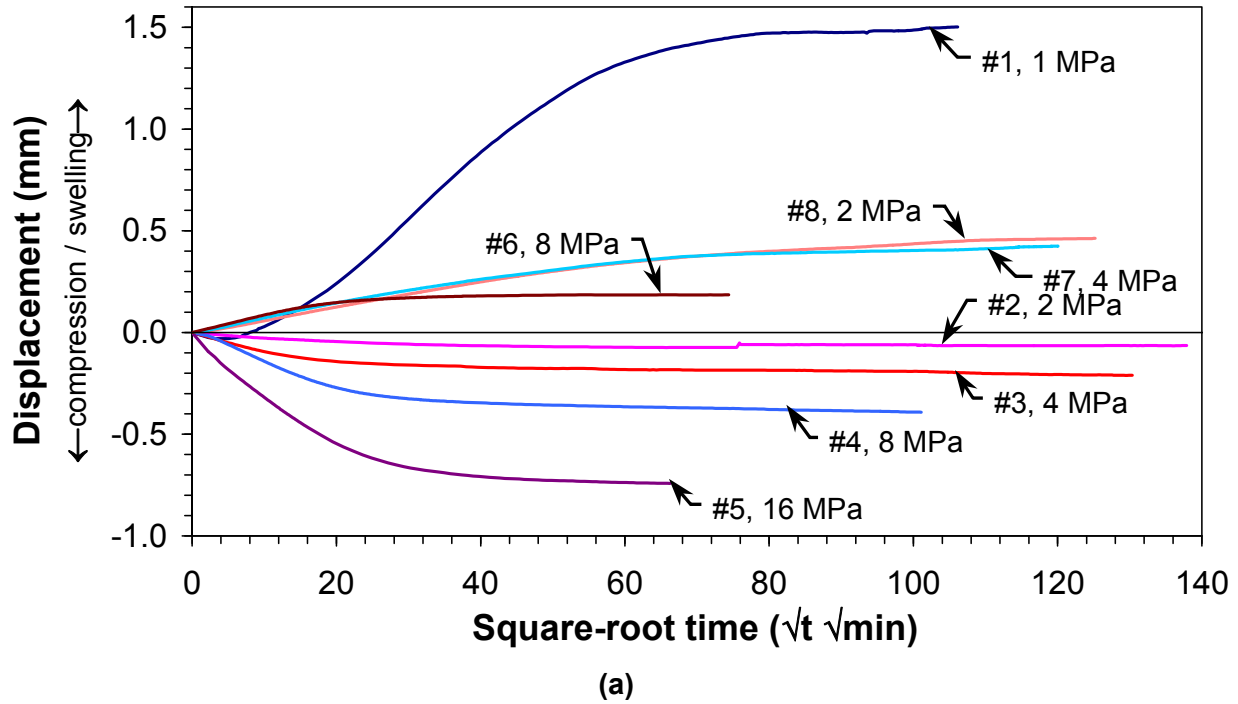
Figure A3: Time-dependent Displacements of Specimen HCB1 under Applied Specimen Stresses (both in square-root time (a) and log time (b)). Note: The sequential load-increment number is noted by the # symbol, followed by the stress induced by the load increment.
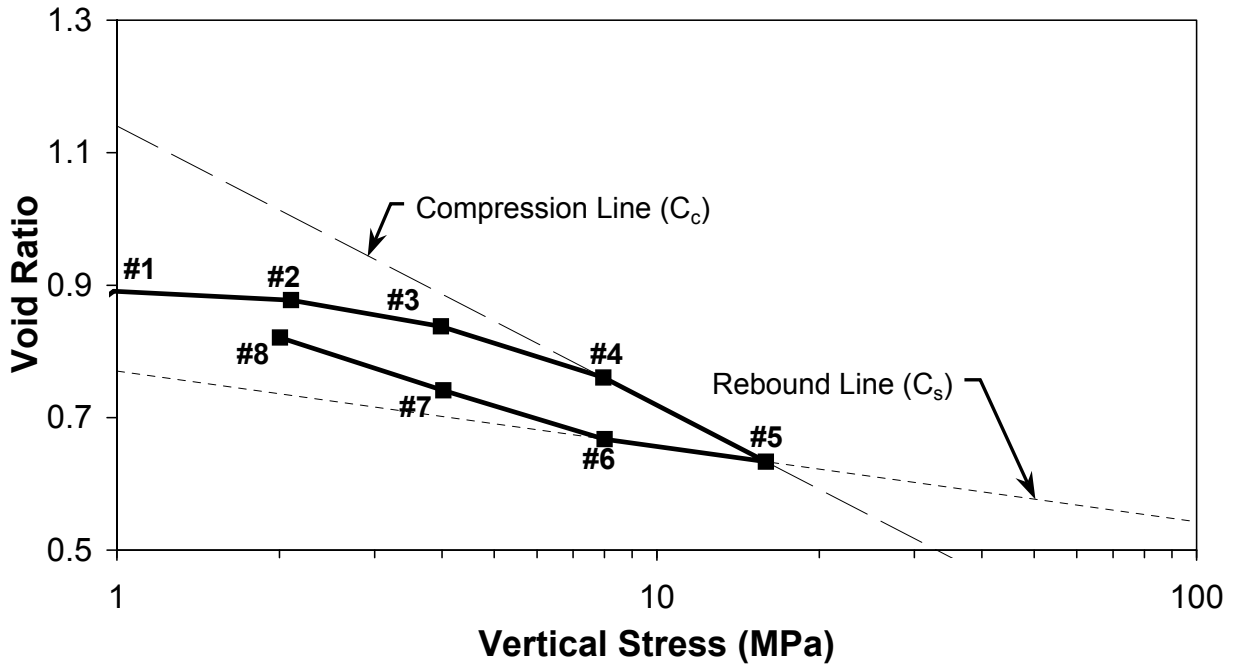
Figure A4: Derived Void Ratio of Specimen HCB1 at the End of Each Loading/Unloading Increment. Note: The sequential load-increment number is noted by the # symbol as in Figures A3a and A3b.

Table A2: HCB1 Coefficients of Consolidation

Load Increment	Vertical Stress (MPa)	Coefficient of Consolidation (mm²/min)			
		Compression		Swelling	
		Sqrt Time	Log Time	Sqrt Time	Log Time
#1	1	0.005	0.005		
#2	2	0.015	0.015		
#3	4	0.076	0.072		
#4	8	0.042	0.035		
#5	16	0.040	0.029		
#6	8			0.049	0.059
#7	4			0.004	0.004
#8	2			0.003	0.003

Table A3: HCB1 Derived Data

Load increment	Vertical Stress (MPa)	Vertical Strain (%)	Void Ratio	Dry Density (Mg/m^3)	EMDD (Mg/m^3)
start	0.38	0%	0.644	1.667	1.484
1	0.99	-15%	0.891	1.449	1.260
2	2.10	-14%	0.877	1.460	1.270
3	3.98	-12%	0.838	1.491	1.302
4	7.97	-7%	0.761	1.556	1.369
5	15.93	1%	0.634	1.677	1.495
6	8.01	-1%	0.668	1.643	1.459
7	4.02	-6%	0.741	1.574	1.387
8	2.00	-11%	0.821	1.505	1.316

Table A4 presents the derived one-dimensional constrained moduli (M) over each load increment. The one-dimensional constrained modulus of elasticity (M) is as follows (Bardet 1997):

$$M = \frac{(\sigma_2' - \sigma_1')(1 + e_1)}{(e_1 - e_2)} \qquad (A1)$$

where e_1 = void ratio at one load increment;
e_2 = void ratio at the next load increment;
σ_1' = effective stress at one load increment, corresponding to e_1; and
σ_2' = effective stress at the next load increment, corresponding to e_2.

Table A4: HCB1 One-Dimensional Constrained Moduli of Elasticity

Vertical Stress Increment (MPa)		Void Ratio Increment		1-D Constrained Modulus M (MPa)
0.99 →	2.10	0.891 →	0.877	155
2.10 →	3.98	0.877 →	0.838	89
3.98 →	7.97	0.838 →	0.761	95
7.97 →	15.93	0.761 →	0.634	111
15.93 →	8.01	0.634 →	0.668	381
8.01 →	4.02	0.668 →	0.741	91
4.02 →	2.00	0.741 →	0.821	44

A.4.1.2HCB2

Test results from the HCB2 specimen (i.e., target initial dry density 1650 kg/m^3, gravimetric water content 21.5%, degree of saturation 91%, fresh water) are plotted in Figures A5 and A6 showing the time-dependent displacements occurring in each load step and the stress-dependent void ratio at the end of each load step, respectively.
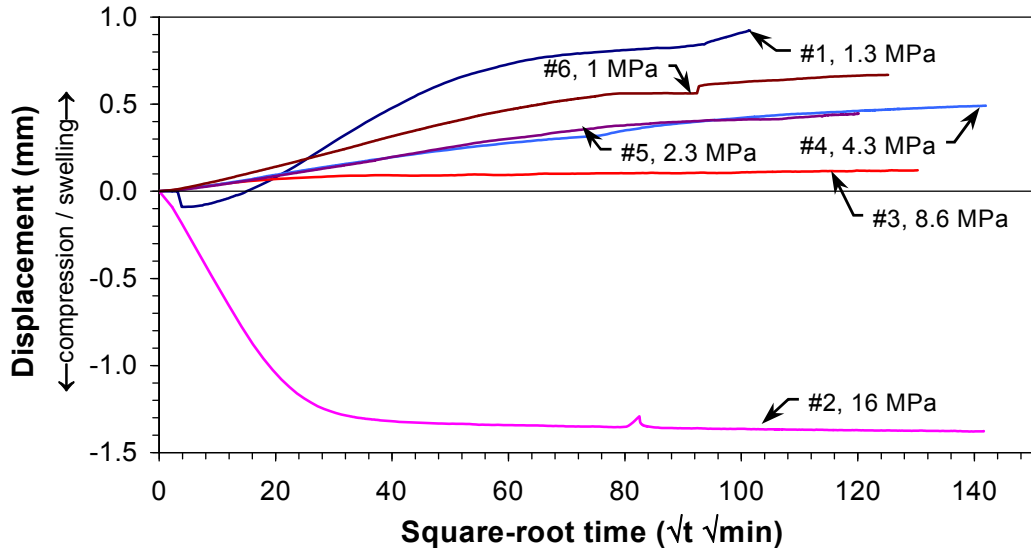
(a)
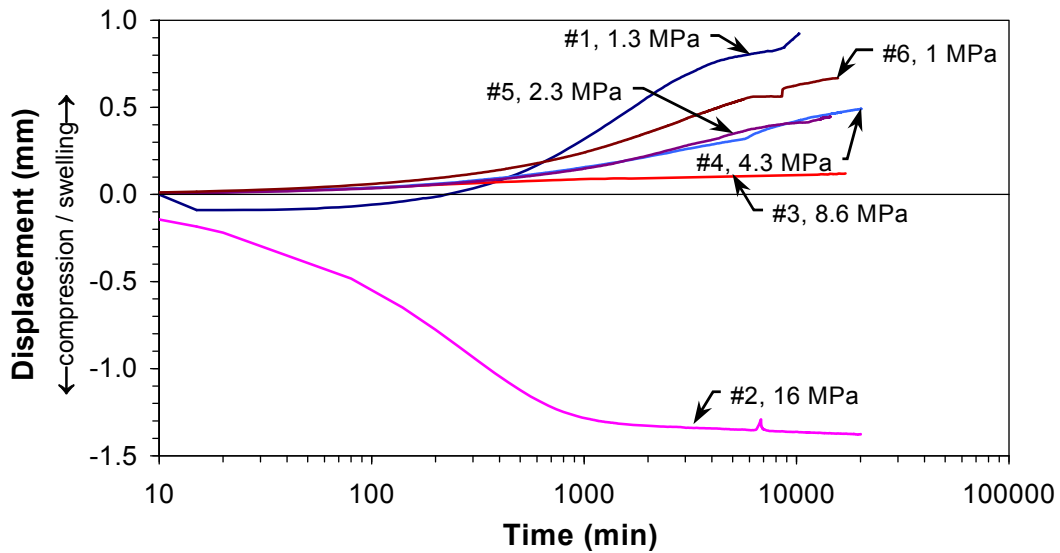
(b)

Figure A5: Time-dependent Displacements of Specimen HCB2 under Applied Specimen Stresses (both in square-root time (a) and log time (b)). Note: The sequential load-increment number is noted by the # symbol, followed by the stress induced by the load increment.
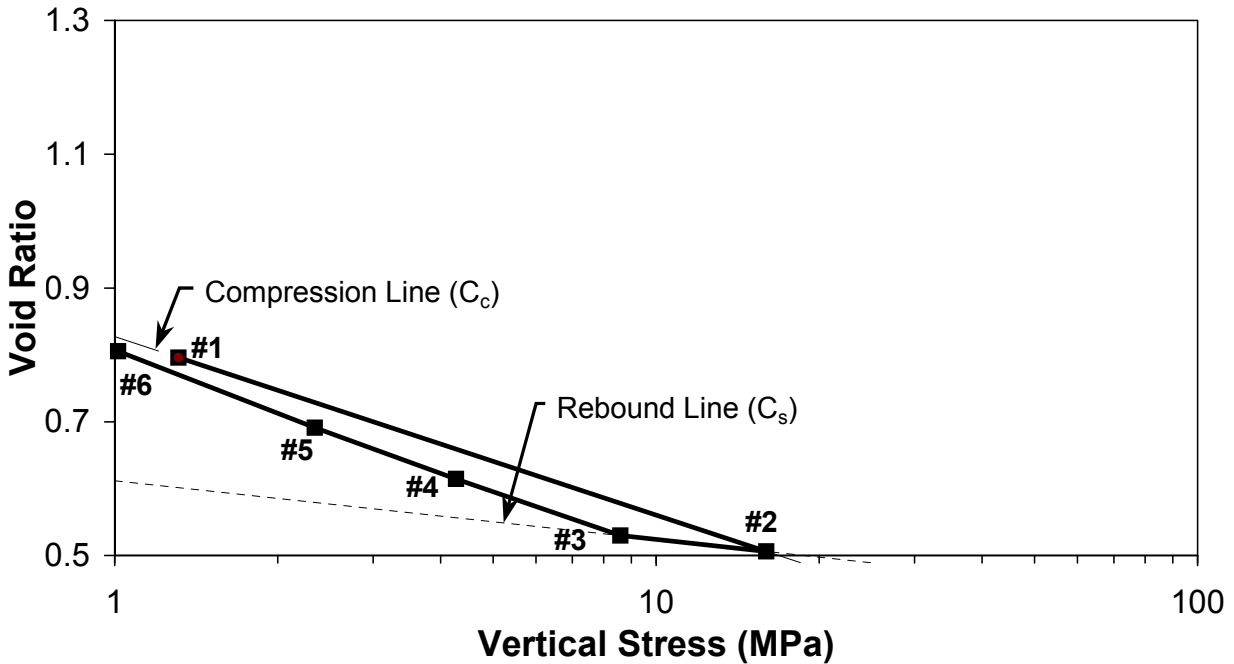
Figure A6: Derived Void Ratio of Specimen HCB2 at the End of Each Loading/Unloading Increment. Note: The sequential load-increment number is noted by the # symbol as in Figures A5a and A5b.

An attempt was made to lock the hydraulic ram to a fixed position by shutting the hydraulic valve on the feed line so that pressure increase could be monitored as the specimen swelled, beginning at a vertical stress of 1 MPa. This was unsuccessful due to leakage in the hydraulic system that could not be completely sealed and specimen strain occurred (i.e., the strain exceeded the maximum ASTM (2003) allowable requirement of <0.005 mm).

The first load increment was terminated at a specimen stress of 1.3 MPa and the second load increment was raised to 16 MPa in one step. The coefficient of consolidation for the second increment at 16 MPa (Table A5) is similar to that for HCB1 at 16 MPa (i.e., load increment #5 in Table A2) but the compression index C_c of 0.27 (Figure A6) is less than that of HCB1 of 0.42. The reduced compression index indicates that any preconsolidation pressure effects are bypassed and the true normal consolidation line is not determined. This suggests that the one-dimensional (1-D) constrained moduli should not be derived from this loading-line segment. The rebound index (C_s) is 0.09. This is very similar to that of HCB1 at 0.11.

Table A6 presents the data for plotting Figure A6 as well as the derived dry densities and EMDDs at the end of each load increment. Table A7 presents the derived one-dimensional constrained moduli (M) over each load increment.

Table A5: HCB2 Coefficients of Consolidation

Load Increment	Vertical Stress (MPa)	Coefficient of Consolidation (mm²/min)			
		Compression		Swelling	
		Sqrt Time	Log Time	Sqrt Time	Log Time
#1	1.3	0.006	0.006		
#2	16	0.040	0.033		
#3	8.6			0.034	0.022
#4	4.3			0.002	0.004
#5	2.3			0.003	0.003
#6	1			0.003	0.003

Table A6: HCB2 Derived Data

Load increment	Vertical Stress (MPa)	Vertical Strain (%)	Void Ratio	Dry Density (Mg/m³)	EMDD (Mg/m³)
start	0.98	0%	0.644	1.667	1.484
1	1.31	-9%	0.796	1.526	1.338
2	15.98	8%	0.506	1.819	1.648
3	8.59	7%	0.530	1.791	1.618
4	4.27	2%	0.614	1.697	1.517
5	2.34	-3%	0.691	1.620	1.435
6	1.02	-10%	0.805	1.518	1.329

Table A7: HCB2 One-Dimensional Constrained Moduli of Elasticity

Vertical Stress Increment (MPa)	Void Ratio Increment	1-D Constrained Modulus M (MPa)
1.31 → 15.98	0.796 → 0.506	NA*
15.98 → 8.59	0.506 → 0.530	470
8.59 → 4.27	0.530 → 0.614	78
4.27 → 2.34	0.614 → 0.691	41
2.34 → 1.02	0.691 → 0.805	20

*   NA – not applicable

A.4.1.3HCB3

HCB3 is the first specimen prepared and tested with a $CaCl_2$ solution. The total dissolved solids (TDS) content is about 75 g/L. Test results from the HCB3 specimen (i.e., target initial dry density 1650 kg/m^3, gravimetric water content 23.7%, degree of saturation 83%, saline water) are plotted in Figures A7 and A8 showing the time-dependent displacements occurring in each load step and the stress-dependent void ratio at the end of each load step, respectively.

The first load increment was the swelling/saturation phase at a specimen stress of ~1 MPa[A2], which showed both a primary stage followed by a secondary creep stage, most likely swelling (Figures A7a and A7b). Although creep was continuing after 2 weeks of loading, the second load increment was applied to a specimen stress of 2 MPa, which showed little to no displacement. This suggests that about 2 MPa is the swelling pressure for HCB with a dry density of ~1500 kg/m^3 (i.e., EMDD of ~1310 kg/m^3) in a highly saline environment. Establishing the coefficient of consolidation proved difficult for the small displacements observed (Table A8).

Subsequent load steps (i.e., #3 and #4) increase the vertical stress to 4 MPa and then 8 MPa. The specimen is then unloaded in increments (i.e., #5, #6 and #7) to the starting specimen stress of 1 MPa (Figure A8). The void ratio at the end of load increment #7 is slightly greater (i.e., less dense) than that of #1 at a specimen stress of 1 MPa, probably an indication that the specimen at load #1 had not reached full saturation and its associated swelling extent at that load.

Reloading to stresses of 4 and 8 MPa (i.e., steps #8 and #9 in Figure A8) shows a return to the compression line (C_c) at a slightly lower density. The stress is increased to 16 MPa and the compression line continues to be linear on a semi-log plot indicating normal consolidation. The compression index (C_c) is 0.22 and the rebound index (C_s) is 0.05, approximately half that for the fresh-water specimens, indicating that the HCB is stiffer in saline water.

Table A9 presents the data for plotting Figure A8 as well as the derived dry densities and EMDDs at the end of each load increment. Table A10 presents the derived one-dimensional constrained moduli (M) over each load increment.

[A2] Figure A8 shows the start and end of the first (#1) load increment where the applied stresses are slightly greater than 1 MPa. This minor deviance is due to the difficulty in controlling the air-over-hydraulic loading system at relatively low pressures.
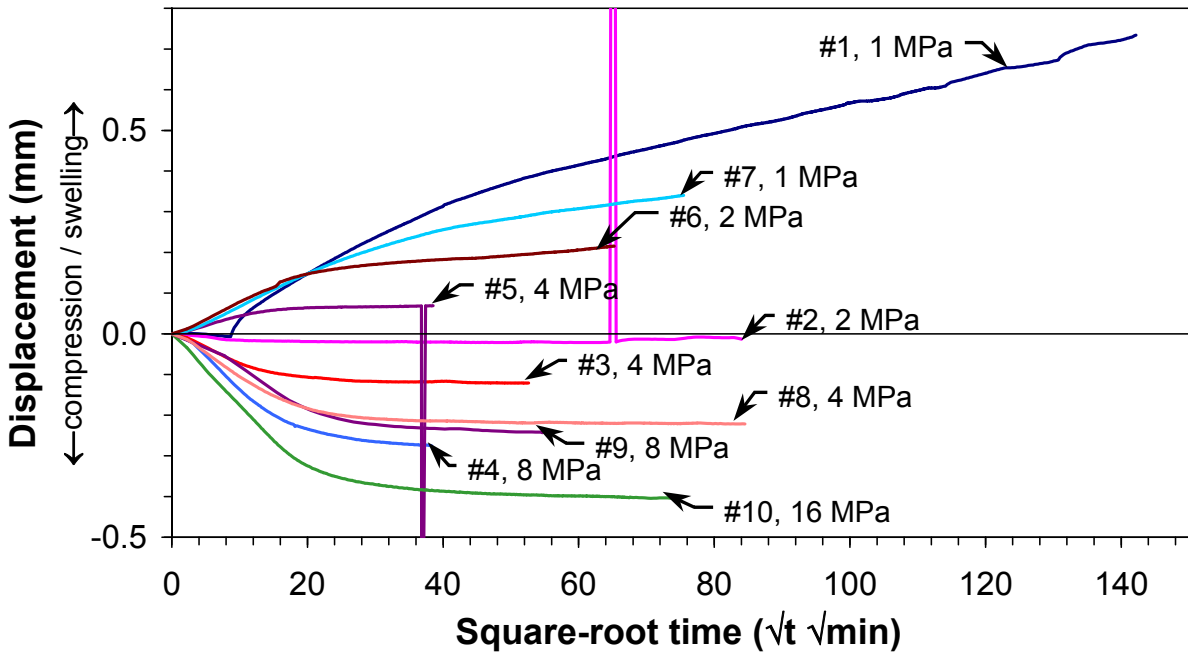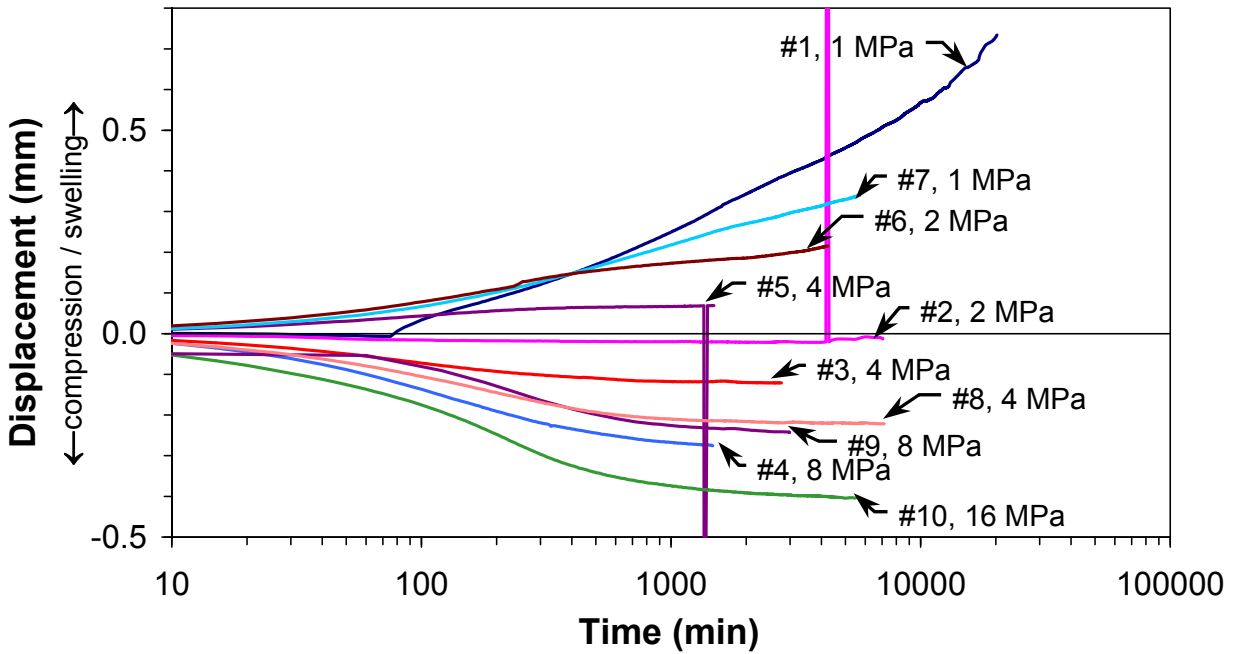
Figure A7: Time-dependent Displacements of Specimen HCB3 under Applied Specimen Stresses (both in square-root time (a) and log time (b)). Note: The sequential load-increment number is noted by the # symbol, followed by the stress induced by the load increment.
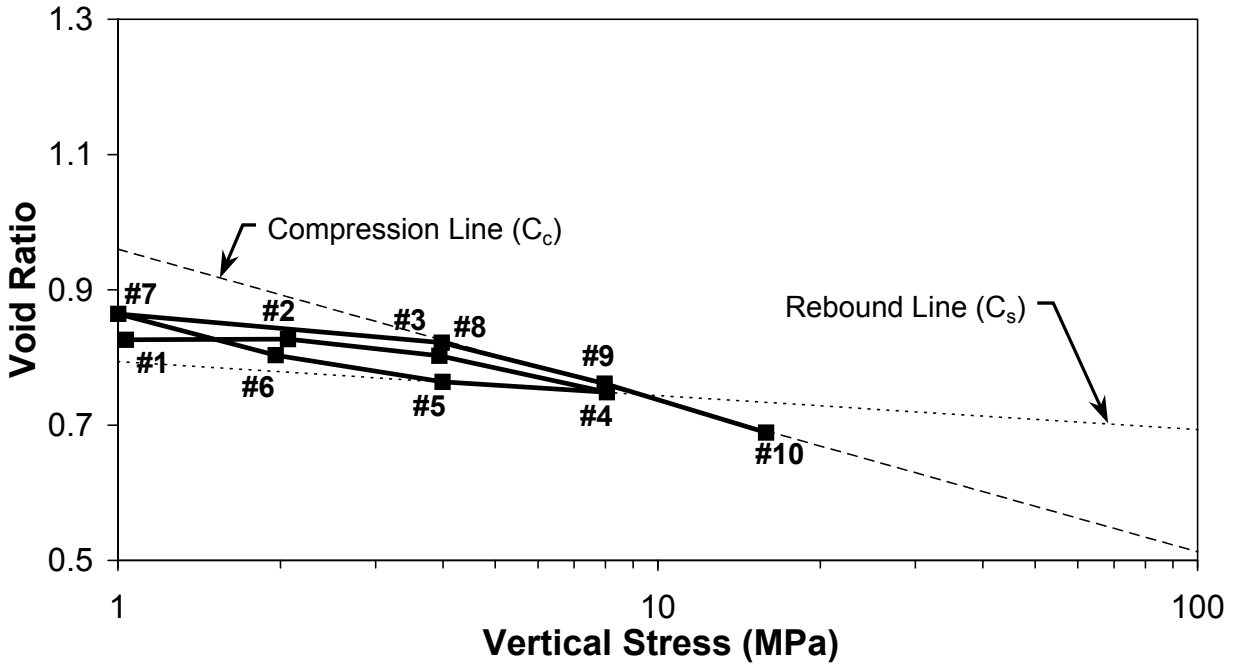
Figure A8: Derived Void Ratio of Specimen HCB3 at the End of Each Loading/Unloading Increment. Note: The sequential load-increment number is noted by the # symbol as in Figures A7a and A7b.

Table A8: HCB3 Coefficients of Consolidation

| Load Increment | Vertical Stress (MPa) | Coefficient of Consolidation (mm^2/min) | | | |
| | | Compression | | Swelling | |
		Sqrt Time	Log Time	Sqrt Time	Log Time
#1	1	0.003	0.003		
#2	2	0.222	0.490		
#3	4	0.098	0.081		
#4	8	0.068	0.056		
#5	4			0.101	0.087
#6	2			0.039	0.043
#7	1			0.013	0.012
#8	4	0.057	0.044		
#9	8	0.037	0.037		
#10	16	0.043	0.040		

Table A9: HCB3 Derived Data

Load increment	Vertical Stress (MPa)	Vertical Strain (%)	Void Ratio	Dry Density (Mg/m^3)	EMDD (Mg/m^3)
start	1.02	0%	0.701	1.611	1.425
1	1.03	-7%	0.826	1.501	1.312
2	2.07	-7%	0.827	1.500	1.311
3	3.94	-6%	0.803	1.520	1.332
4	8.05	-3%	0.749	1.567	1.380
5	3.99	-4%	0.764	1.553	1.366
6	1.96	-6%	0.803	1.520	1.331
7	1.00	-10%	0.864	1.470	1.280
8	3.98	-7%	0.822	1.504	1.315
9	7.97	-4%	0.761	1.556	1.368
10	15.88	1%	0.689	1.622	1.438

Table A10: HCB3 One-Dimensional Constrained Moduli of Elasticity

Vertical Stress Increment (MPa)	Void Ratio Increment	1-D Constrained Modulus M (MPa)
1.03 → 2.07	0.826 → 0.827	NA
2.07 → 3.94	0.827 → 0.803	140
3.94 → 8.05	0.803 → 0.749	137
8.05 → 3.99	0.749 → 0.764	463
3.99 → 1.96	0.764 → 0.803	91
1.96 → 1.00	0.803 → 0.864	28
1.00 → 3.98	0.864 → 0.822	130
3.98 → 7.97	0.822 → 0.761	120
7.97 → 15.88	0.761 → 0.689	192

*   NA – not applicable

A.4.1.4 HCB4

HCB4 is the second specimen prepared and tested with a CaCl$_2$ solution. The total dissolved solids (TDS) content is about 75 g/L. Test results from the HCB4 specimen (i.e., target initial dry density 1650 kg/m^3, gravimetric water content 23.7%, degree of saturation 99%, saline water) are plotted in Figures A9 and A10 showing the time-dependent displacements occurring in each load step and the stress-dependent void ratio at the end of each load step, respectively.
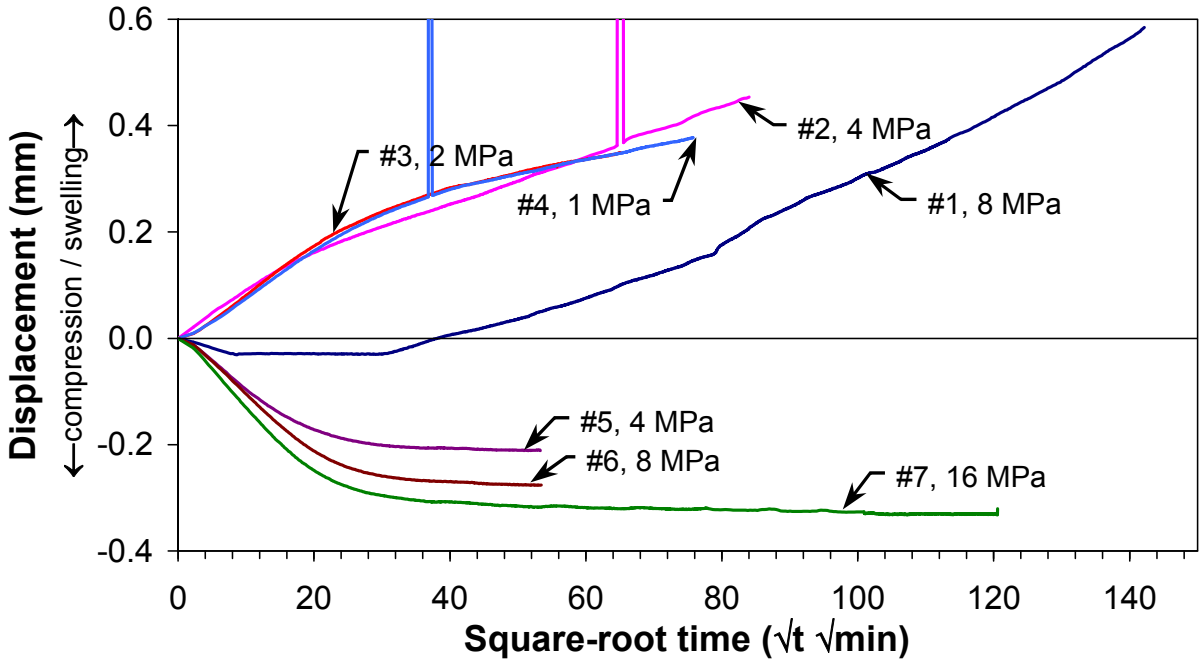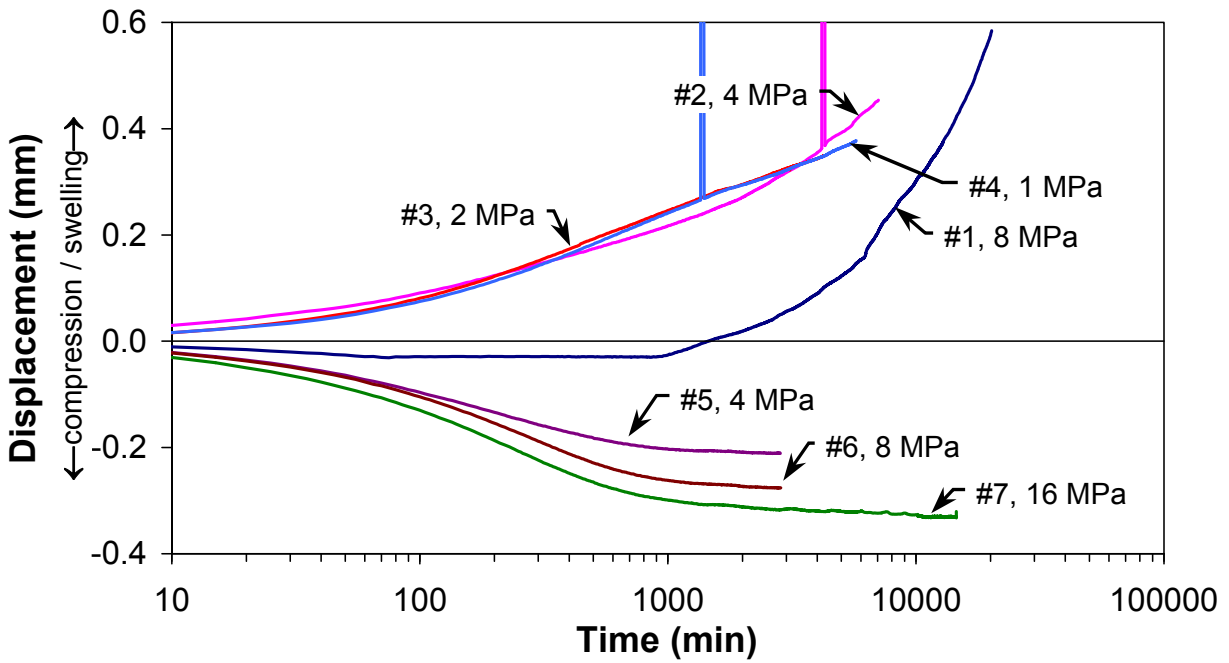
Figure A9: Time-dependent Displacements of Specimen HCB4 under Applied Specimen Stresses (both in square-root time (a) and log time (b)). Note: The sequential load-increment number is noted by the # symbol, followed by the stress induced by the load increment.
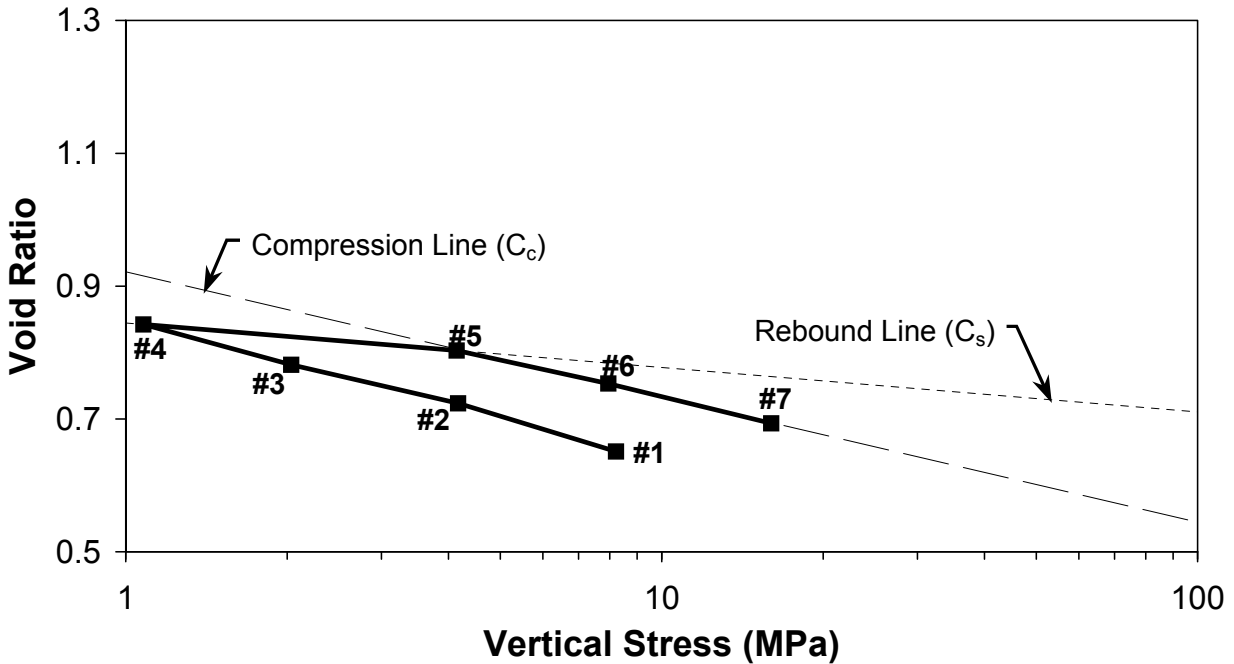
Figure A10: Derived Void Ratio of Specimen HCB4 at the End of Each Loading/Unloading Increment. Note: The sequential load-increment number is noted by the # symbol as in Figures A9a and A9b.

The first load increment (#1) is the swelling/saturation phase at a specimen stress of 8 MPa, which shows both a primary stage followed by a secondary swelling stage (Figures A9a and A9b). Although creep is continuing after two weeks of loading, the second load increment (#2) is applied to a specimen stress of 4 MPa, which shows continued swelling over a period of five days followed by #3 at 2 MPa over 3 days and #4 at 1 MPa over four days. These short durations are based on the expectancy of higher hydraulic conductivity for the specimen in saline solution and a decreased swelling pressure, which should result in significantly shorter time for each load increment. The apparent hydraulic conductivities for the specimen appear similar to or are up to one order of magnitude higher than those for the fresh-water specimens. Clearly, the time allowed for each unloading step is insufficient from a creep (swelling).

The subsequent loading steps (i.e., #5, #6 and #7) at specimen stresses of 4, 8 and 16 MPa show rapid creep stabilization in as little time as two days (Figures A9a and A9b). Loading to specimen stresses of 4 and 8 MPa shows a return to the compression line (C_c) at a slightly lower density (Figure A10). The compression line is extended to 16 MPa and is linear on a semi-log plot indicating normal consolidation. The compression index (C_c) is 0.19, similar to that of HCB3 (i.e., C_c = 0.22). No rebound index (C_s) can be directly determined from this test. The section of the consolidation curve before the preconsolidation pressure for overconsolidated soils (i.e., increment #4 to #5) often tends to parallel the rebound line. This produces an estimated C_s of 0.07, similar to that of HCB3 (i.e., C_s = 0.05). Table A11 shows the coefficients of consolidation.

Table A11: HCB4 Coefficients of Consolidation

Load Increment	Vertical Stress (MPa)	Coefficient of Consolidation (mm²/min)			
		Compression		Swelling	
		Sqrt Time	Log Time	Sqrt Time	Log Time
#1	8	0.0001	0.0002		
#2	4			0.0007	0.0005
#3	2			0.0010	0.0014
#4	1			0.0009	0.0015
#5	4	0.0038	0.0031		
#6	8	0.0027	0.0025		
#7	16	0.0031	0.0026		

Table A12 presents the data for plotting Figure A10 as well as the derived dry densities and EMDDs at the end of each load increment. Table A13 presents the derived one-dimensional constrained moduli (M) over each load increment.

Table A12: HCB4 Derived Data

Load increment	Vertical Stress (MPa)	Vertical Strain (%)	Void Ratio	Dry Density (Mg/m³)	EMDD (Mg/m³)
start	8.06	0%	0.560	1.757	1.580
1	8.22	-6%	0.651	1.660	1.477
2	4.17	-10%	0.724	1.590	1.404
3	2.04	-14%	0.782	1.538	1.350
4	1.08	-18%	0.842	1.487	1.298
5	4.14	-16%	0.803	1.520	1.331
6	7.95	-12%	0.753	1.563	1.376
7	16.00	-9%	0.693	1.618	1.433

Table A13: HCB4 One-Dimensional Constrained Moduli of Elasticity

Vertical Stress Increment (MPa)	Void Ratio Increment	1-D Constrained Modulus M (MPa)
8.22 → 4.17	0.651 → 0.724	92
4.17 → 2.04	0.724 → 0.782	64
2.04 → 1.08	0.782 → 0.842	28
1.08 → 4.14	0.842 → 0.803	144
4.14 → 7.95	0.803 → 0.753	137
7.95 → 16.00	0.753 → 0.693	237

A.4.1.5 HCB5

HCB5 is a specimen prepared and tested with fresh water and a reduced dry density. The reduced dry density is used in an attempt to reduce the duration of the saturation/swelling time for the first load increment at a specimen stress of 1 MPa. Test results from the HCB5 specimen (i.e., target initial dry density 1400 kg/m^3, gravimetric water content 31.2%, degree of saturation 91%, fresh water) are plotted in Figures A11 and A12 showing the time-dependent displacements occurring in each load step and the stress-dependent void ratio at the end of each load step, respectively.

The first load increment (#1) is the swelling/saturation phase at a specimen stress of 1 MPa. Ram pressure was lost when the nitrogen cylinder discharged due to a leak over a weekend. This resulted in about 60 hours of unloaded swelling. Subsequent reloading of the specimen to a pressure of 1 MPa over seven days did not return the specimen to its preleak displacement, which had appeared stable prior to leaking. This resulted in an apparent net increase in specimen thickness of ~1.5 mm during this disturbed-load increment (Figures A11a and A11b). This suggests that the free swell permits clay-particle realignment beyond that permitted by the initial applied load and is unrecoverable at this load. The total duration of load increment #1 was ~37 days, including the seven days of reloading after reapplying the load.

The second load increment (#2) applies a specimen stress of 2 MPa. As shown in Figures A11a and A11b, the compressive displacement is greater than those of all subsequent compressive loads (i.e., at stresses of 4, 8 and 16 MPa), suggesting that some or most of the soil-fabric restructuring generated from free swell may have collapsed at the applied stress of 2 MPa. This recovery can also be observed in Figure A12 if the construction of the compression line (C_c) is plotted through load increments #3 through #5, where load increment #2 approaches the resultant compression line. A full unload-reload cycle (i.e., increments #6 though #9 and #10 through #13) was produced and the final void ratio for increment #13 closely matches that for increment #5, indicating that the lost pressure in the first load-increment (#1) does not appear to have adversely affected the test results at high vertical stresses.

All load increments are in the range of one to two weeks except for the 37 days of the first load-increment (#1) (Figures A11a and A11b). The decision when to change the loads was somewhat subjective, as noted in Section A3.2, by observing a number of factors including the

stability of the secondary-consolidation creep. Consideration must also be given to the potential for stick-slip phenomena associated with the loading system and displacement-monitoring systems.

The compression index (C_c) is 0.50, similar to that of HCB1 (i.e., C_c = 0.42) and the rebound index (C_s) is 0.16, also similar to that of HCB1 (i.e., C_s = 0.11). Table A14 shows the coefficients of consolidation and demonstrates high consistency in the two data interpretation methods.

Table A15 presents the data for plotting Figure A12 as well as the derived dry densities and EMDDs at the end of each load increment. Table A16 presents the derived one-dimensional constrained moduli (M) over each load increment.
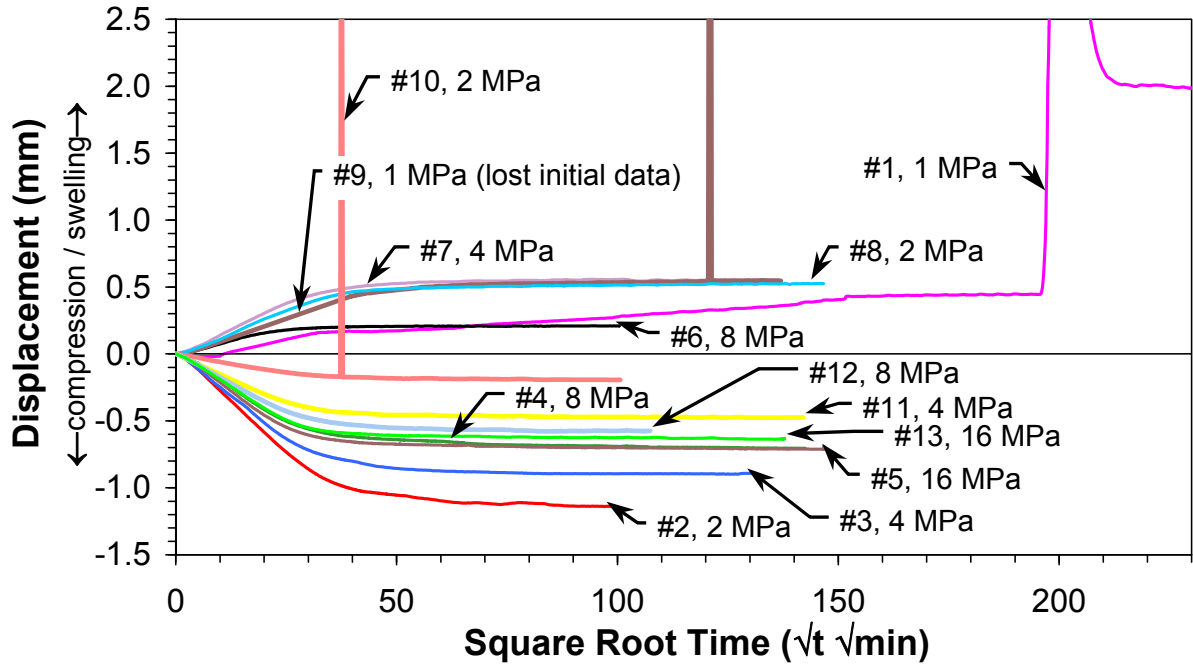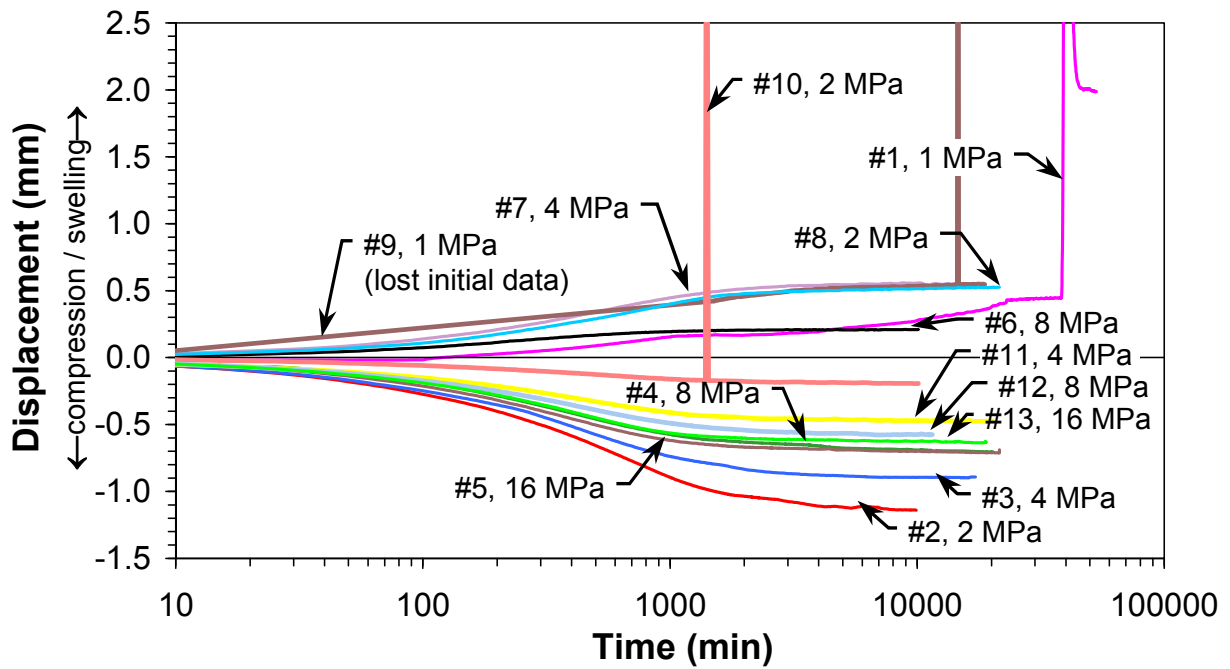
Figure A11: Time-dependent Displacements of Specimen HCB5 under Applied Specimen Stresses (both in square-root time (a) and log time (b)). Note: The sequential load-increment number is noted by the # symbol, followed by the stress induced by the load increment.
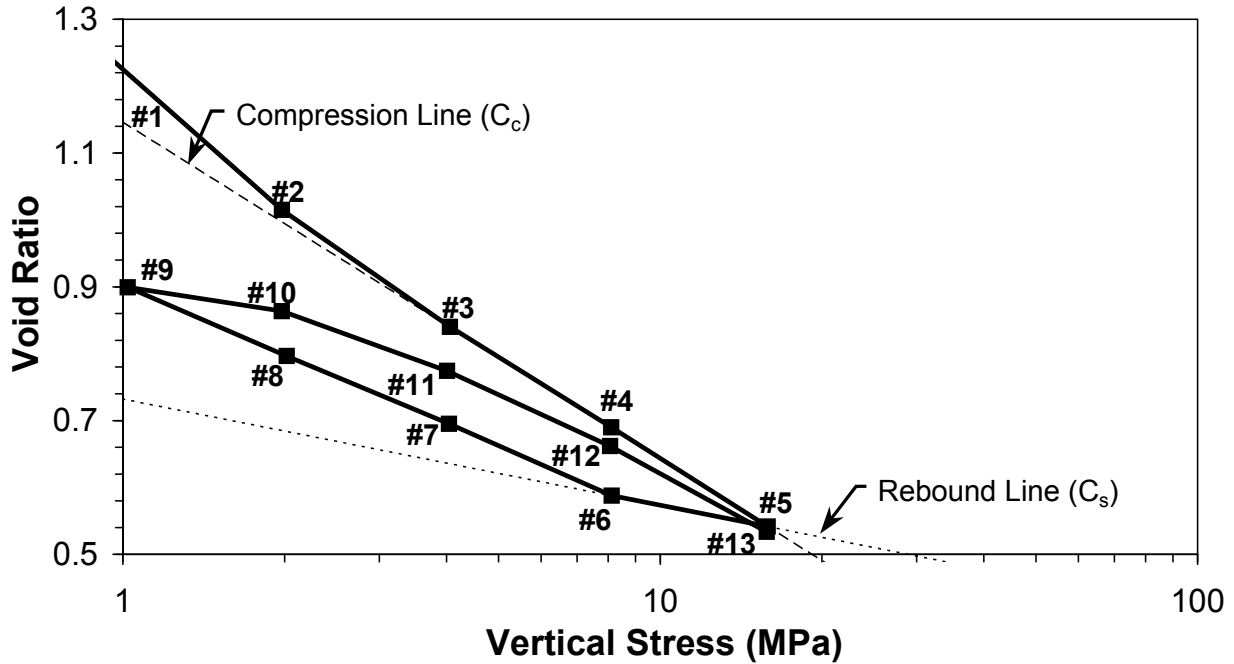
Figure A12: Derived Void Ratio of Specimen HCB5 at the End of Each Loading/Unloading Increment. Note: The sequential load-increment number is noted by the # symbol as in Figures A11a and A11b.

Table A14: HCB5 Coefficients of Consolidation

Load Increment	Vertical Stress (MPa)	Coefficient of Consolidation (mm^2/min)			
		Compression		Swelling	
		Sqrt Time	Log Time	Sqrt Time	Log Time
#1	1	0.017	0.016		
#2	2	0.017	0.015		
#3	4	0.020	0.018		
#4	8	0.026	0.025		
#5	16	0.027	0.024		
#6	8			0.036	0.031
#7	4			0.017	0.015
#8	2			0.016	0.013
#9	1			0.008	0.012
#10	2	0.033	0.019		
#11	4	0.022	0.020		
#12	8	0.022	0.022		
#13	16	0.024	0.025		

Table A15: HCB5 Derived Data

Load increment	Vertical Stress (MPa)	Vertical Strain (%)	Void Ratio	Dry Density (Mg/m^3)	EMDD (Mg/m^3)
start	1.03	0%	0.898	1.444	1.254
1	0.96	-18%	1.238	1.224	1.039
2	1.98	-6%	1.015	1.360	1.171
3	4.06	3%	0.840	1.489	1.300
4	8.11	11%	0.690	1.621	1.436
5	15.85	19%	0.542	1.777	1.603
6	8.12	16%	0.588	1.726	1.547
7	4.04	11%	0.695	1.616	1.431
8	2.02	5%	0.796	1.525	1.337
9	1.02	0%	0.899	1.443	1.253
10	1.98	2%	0.864	1.470	1.281
11	4.01	7%	0.774	1.544	1.357
12	8.07	12%	0.662	1.649	1.465
13	15.78	19%	0.534	1.787	1.613

Table A16: HCB5 One-Dimensional Constrained Moduli of Elasticity

Vertical Stress Increment (MPa)	Void Ratio Increment	1-D Constrained Modulus M (MPa)
0.96 → 1.98	1.238 → 1.015	10
1.98 → 4.06	1.015 → 0.840	24
4.06 → 8.11	0.840 → 0.690	50
8.11 → 15.85	0.690 → 0.542	88
15.85 → 8.12	0.542 → 0.588	258
8.12 → 4.04	0.588 → 0.695	60
4.04 → 2.02	0.695 → 0.796	34
2.02 → 1.02	0.796 → 0.899	17
1.02 → 1.98	0.899 → 0.864	51
1.98 → 4.01	0.864 → 0.774	42
4.01 → 8.07	0.774 → 0.662	64
8.07 → 15.78	0.662 → 0.534	100

A.4.1.6HCB6

HCB6 is a specimen prepared and tested with a saline solution with a TDS of about
75 g/L CaCl$_2$ and a reduced dry density. The reduced dry density is used in an attempt to
reduce the duration of the saturation/swelling time as for specimen HCB5. Test results from the
HCB6 specimen (i.e., target initial dry density 1400 kg/m^3, gravimetric water content 31.2%,
degree of saturation 91%, saline solution) are plotted in Figures A13 and A14 showing the time-
dependent displacements occurring in each load step and the stress-dependent void ratio at the
end of each load step, respectively.
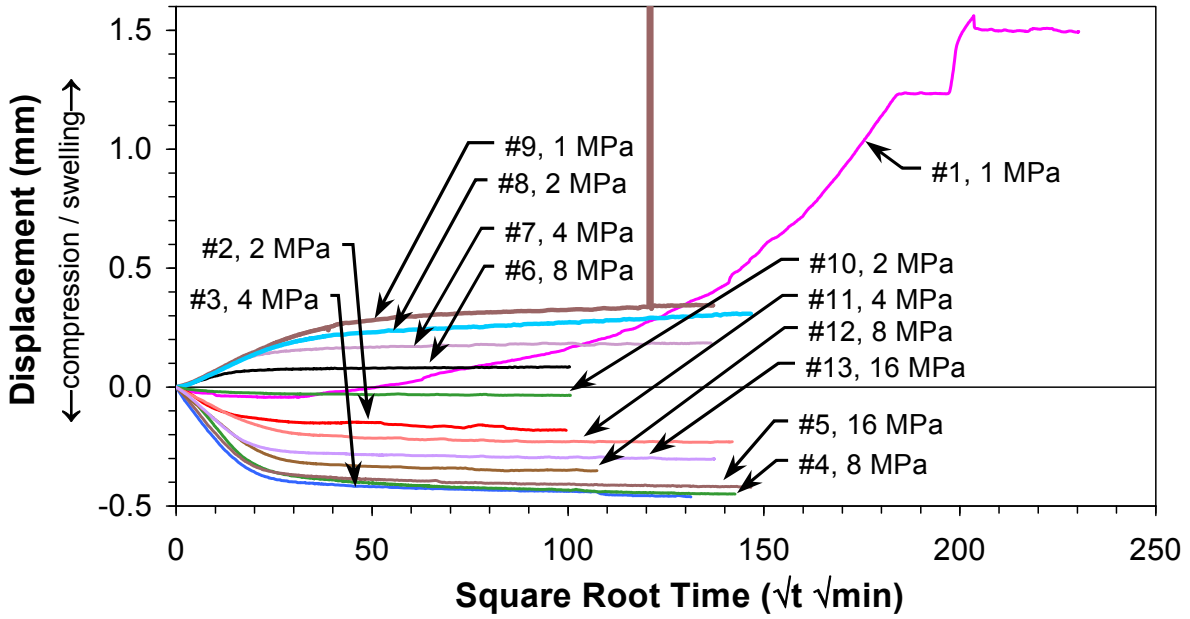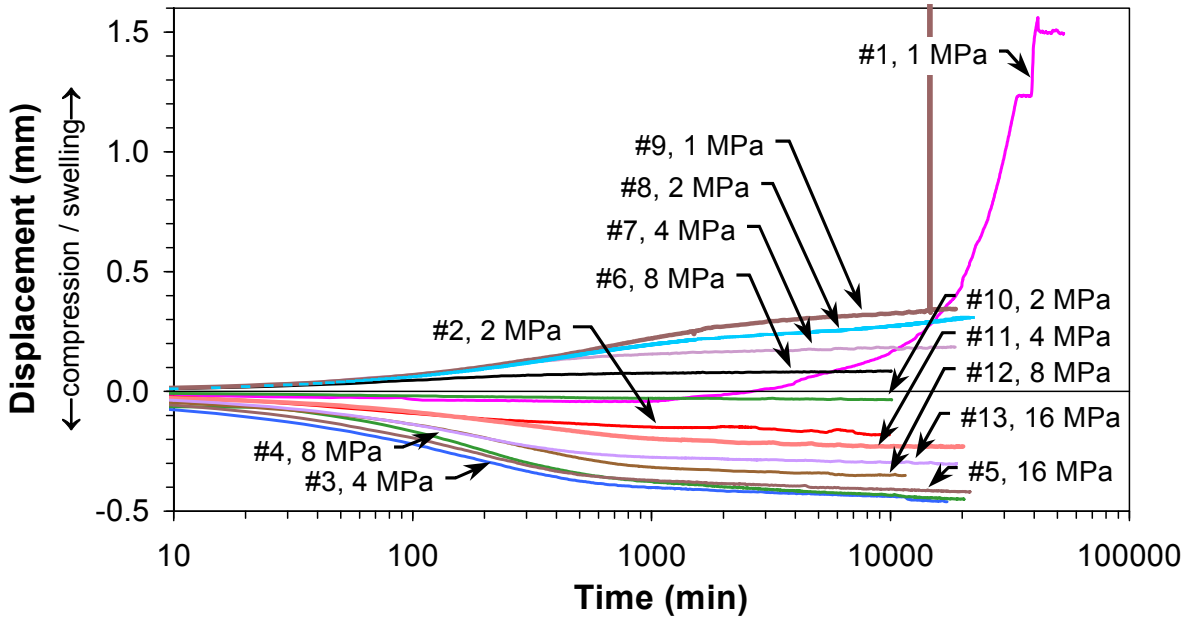
Figure A13: Time-dependent Displacements of Specimen HCB6 under Applied Specimen Stresses (both in square-root time (a) and log time (b)). Note: The sequential load-increment number is noted by the # symbol, followed by the stress induced by the load increment.
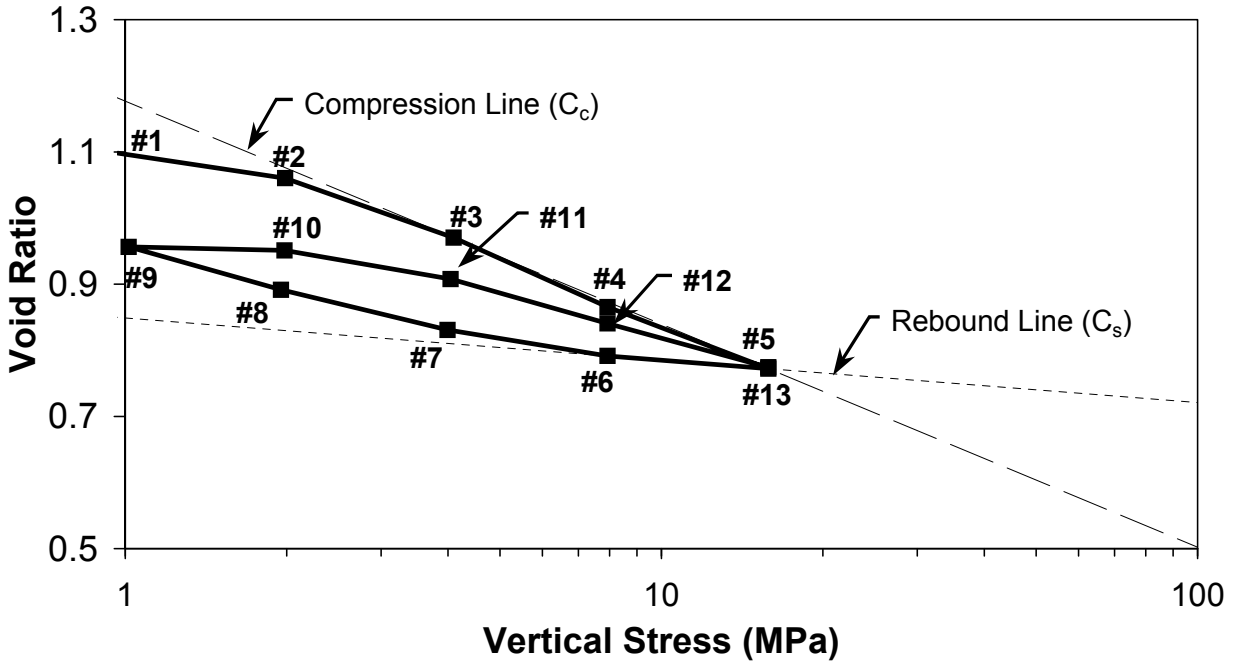
Figure A14: Derived Void Ratio of Specimen HCB6 at the End of Each Loading/Unloading Increment. Note: The sequential load-increment number is noted by the # symbol as in Figures A13a and A13b.

The first load increment (#1) is the swelling/saturation phase at a specimen stress of 1 MPa. Ram pressure was lost when the nitrogen cylinder discharged due to a leak over a weekend. Although both HCB5 and HCB6 were on a common pressure source, the hydraulic ram for HCB5 has a ram-return spring whereas that for HCB6 is a double-acting ram, which has no spring. The load-cell pressure of HCB6 gradually decreased to 0.33 MPa but not to zero (see Figure A2 from July 02 to 04). Subsequent reloading of the specimen to pressure of 1 MPa over seven days did not return the specimen to its preleak displacement, which had appeared stable prior to leaking. This resulted in a net increase in specimen thickness of ~0.26 mm during this disturbed-load increment (Figures A13a and A13b) as compared to the net increase of ~1.5 mm under free swell for specimen HCB5 during this same disturbed-load increment (Figures A11a and A11b). Part of the difference in displacement between HCB5 and HCB6 is the reduced swelling pressure of smectite clay in a saline solution (HCB6) as compared to that in fresh water (HCB5). Some clay-particle realignment probably occurred at the stresses less than the initial applied load and is irrecoverable at this load.

The second load increment (#2) is applied to a specimen stress of 2 MPa. As shown in Figure A14, the void ratio for #2 approaches the compression line (C_c) and all subsequent compressive loads (i.e., at stresses of 4, 8 and 16 MPa) fall on this line at far higher void ratios than experienced with the other saline-solution specimens (i.e., HCB3 and HCB4). Two explanations are possible in this difference of void ratios between specimen HCB6 vs. that of specimens HCB3 and HCB4. Specimens HCB3 and HCB4 may not have had sufficient time to fully swell to higher void ratios. Alternatively, the reduced initial dry density (i.e., <1400 kg/m^3) and the swelling caused by the disturbance in the first-load increment (i.e., 0.33 MPa) may have generated a different soil-fabric structure (i.e., the arrangement of particles, particle groups and

pore spaces as affected by the electrolytic-nature of the pore fluid) than that of the higher initial dry density specimens (HCB3 and HCB4).

The subsequent full unload-reload cycle (i.e., increments #6 though #9 and #10 through #13 in Figure A14) continued to produce high void ratios. This suggests that, if a different soil-fabric structure exists, then the additional loads could not collapse this apparently very stable soil-fabric structure. The void ratio at the specimen stress of 16 MPa (i.e., increment #5) matches closely to that at the end of the test (i.e., increment #13), also indicating that no subsequent structural changes occurred.

All load increments are in the range of one to two weeks except for the 37 days of the first load-increment (#1) (Figures A13a and A13b), identical to HCB5. The compression index (C_c) is 0.34, as compared to those of HCB3 and HCB4 (i.e., C_c = 0.22 and 0.19, respectively), and the rebound index (C_s) is 0.06, as compared to that of HCB3 and HCB4 (i.e., C_s = 0.05 and ~0.07, respectively). Table A17 shows the coefficients of consolidation and demonstrates high consistency in the two data interpretation methods.

Table A17: HCB6 Coefficients of Consolidation

Load Increment	Vertical Stress (MPa)	Coefficient of Consolidation (mm^2/min)			
		Compression		Swelling	
		Sqrt Time	Log Time	Sqrt Time	Log Time
#1	1	NA	NA		
#2	2	0.134	0.127		
#3	4	0.061	0.048		
#4	8	0.049	0.047		
#5	16	0.060	0.047		
#6	8			0.081	0.081
#7	4			0.044	0.041
#8	2			0.020	0.021
#9	1			0.014	0.012
#10	2	0.026	0.031		
#11	4	0.036	0.030		
#12	8	0.036	0.036		
#13	16	0.053	0.043		

*NA – not available

Table A18 presents the data for plotting Figure A14 as well as the derived dry densities and EMDDs at the end of each load increment. Table A19 presents the derived one-dimensional constrained moduli (M) over each load increment.

A.5   DISCUSSION

A.5.1 FRESH-WATER SPECIMENS

The 'as prepared' dry densities and loading schedules for the three fresh-water specimens are quite different (Figure A15). Yet, these different conditions produced a similar response in that the compression indices (i.e., C_c between 0.42 to 0.50 (Table A20)) appear to approach a common slope (i.e., normal consolidation at the higher stress values (e.g., 6 to 16 MPa), demonstrating a log-linear behaviour that is common to most clay soils. At 16 MPa, the void ratios are somewhat similar (i.e., ranging between 0.51 and 0.63), despite their very different initial conditions, with the low initial dry density HCB5 between the two outliers at higher initial dry densities (i.e., HCB1 and HCB2). Part of this difference in the range of void ratios at 16 MPa may be due to the differences in durations of the specific load increments and in the difficulties experienced with the loss of pressure and free swell during the first load increment of specimen HCB5.

Table A18: HCB6 Derived Data

Load increment	Vertical Stress (MPa)	Vertical Strain (%)	Void Ratio	Dry Density (Mg/m^3)	EMDD (Mg/m^3)
start	1.01	0%	0.859	1.474	1.285
1	0.97	-13%	1.098	1.306	1.118
2	1.99	-11%	1.060	1.330	1.141
3	4.10	-6%	0.970	1.391	1.201
4	7.94	-0%	0.865	1.469	1.280
5	15.82	5%	0.772	1.546	1.359
6	7.94	4%	0.791	1.530	1.342
7	3.99	2%	0.831	1.497	1.308
8	1.95	-2%	0.891	1.449	1.259
9	1.02	-5%	0.956	1.401	1.211
10	1.98	-5%	0.951	1.405	1.215
11	4.04	-3%	0.908	1.436	1.247
12	7.94	1%	0.840	1.489	1.300
13	15.94	5%	0.774	1.544	1.357

Table A19: HCB6 One-Dimensional Constrained Moduli of Elasticity

Vertical Stress Increment (MPa)			Void Ratio Increment			1-D Constrained Modulus M (MPa)
0.97	→	1.99	1.098	→	1.060	56
1.99	→	4.10	1.060	→	0.970	48
4.10	→	7.94	0.970	→	0.865	72
7.94	→	15.82	0.865	→	0.772	157
15.82	→	7.94	0.772	→	0.791	729
7.94	→	3.99	0.791	→	0.831	179
3.99	→	1.95	0.831	→	0.891	62
1.95	→	1.02	0.891	→	0.956	27
1.02	→	1.98	0.956	→	0.951	352
1.98	→	4.04	0.951	→	0.908	93
4.04	→	7.94	0.908	→	0.840	110
7.94	→	15.94	0.840	→	0.774	219
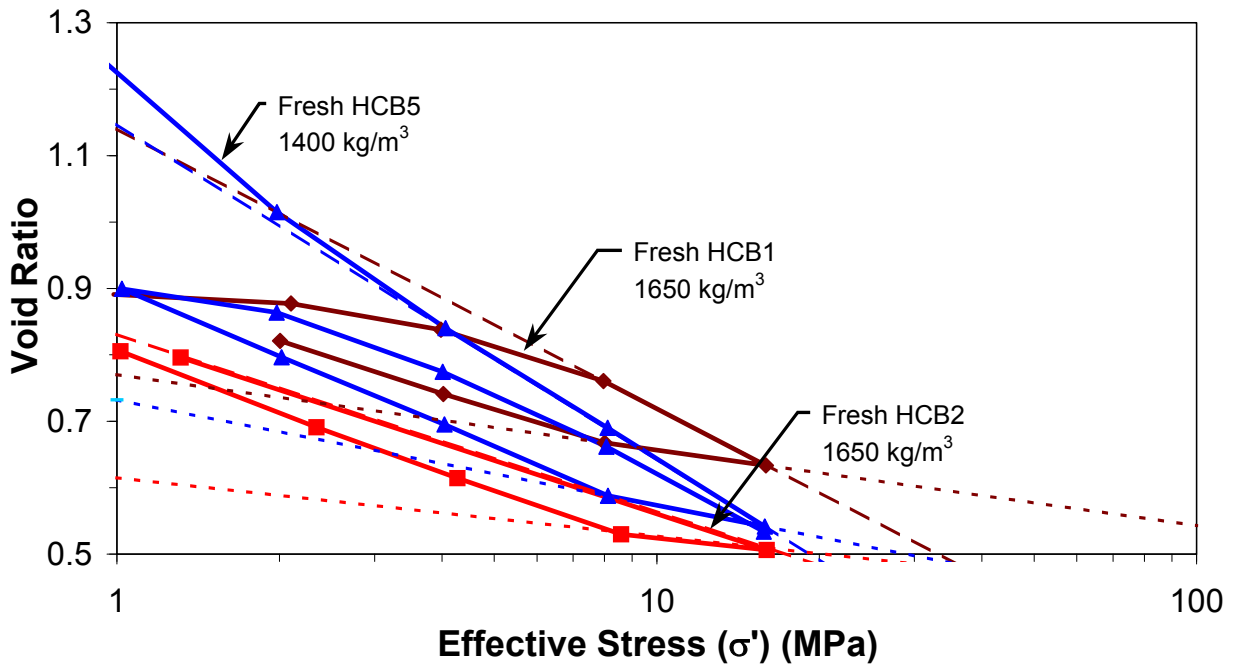
Figure A15: Void Ratio of Fresh-Water Consolidation Specimens. Notes: The initial dry densities of the specimens are noted in the labels. The compression lines (long dashes) and rebound lines (short dashes) are also plotted.

Table A20: Compression and Rebound Indices

Test Specimen	Compression Index C_c	Rebound Index* C_s
Fresh Water		
HCB1	0.42	0.11
HCB2	NA**	0.09
HCB5	0.50	0.16
75 g/L CaCl$_2$		
HCB3	0.22	0.05
HCB4	0.19	0.07
HCB6	0.34	0.06

* First unloading step only, increasing values on subsequent unloading steps indicative of a combined elastic and swelling response.

** NA – not applicable.

The rebound indices (i.e., C_s ranging between 0.09 and 0.16 (Table A20)) determined by the first unloading step from 16 MPa) are also very similar (Figure A15) despite the very different starting conditions, suggesting an initial non-linear elastic response solely associated with intergranular rebound during this initial unloading step. Subsequent unloading results continue to demonstrate a log-linear behaviour, which suggests a response that is a combination of both non-linear elasticity and swelling, returning the specimen to similar void ratios (e.g., ranging between 0.8 and 0.9) at a stress approaching 1 MPa. Again, part of this difference in the range of void ratios may be due to the differences in durations of the specific load increments and in the difficulties experienced with the loss of pressure and free swell during the first load increment of specimen HCB5.

HCB5 experienced a total loss of confining stress over a two-day period during the first load increment. Prior to the loss in loading-system pressure, the displacements appeared to stabilize (Figure A11). The starting void ratio (e) for the specimen was 0.898 (dry density (ρ_d) = 1444 kg/m^3) and reached an apparent stable void ratio (e = 0.949, ρ_d = 1410 kg/m^3) before the loss of system pressure. The final void ratio was 1.238 (ρ_d = 1224 kg/m^3) at the end of the load increment following one week of reloading to a specimen stress of 1 MPa, which was insufficient to recompress the specimen to the pre-leak void ratio. This suggests that the two-days of free swell allowed the specimen to restructure itself, possibly by the repulsion interactions between the diffuse double layers (Mitchell 1976, Yong and Warkentin 1975) surrounding the montmorillonite particles and possibly by modifications to any edge-to-plate particle orientations in clay soils (Villar 2002, Wan 1996, Mitchell 1976) (Figure A16).

If the loss of pressure had not occurred, then the specimen could have had a void ratio similar to the pre-pressure-loss value (e = 0.949, ρ_d = 1410 kg/m^3) and could have responded

somewhat similar to the low-stress portion of the HCB1 curve (Figure A15) until the normal consolidation line was reached.

Subsequent loading of HCB5 to a specimen stress of 2 MPa recovered some of the free-swell displacement as evidenced by the void ratio approaching the normal compression line (Figure A15). Further loading to a stress of 4 MPa approaches the HCB1 line where HCB1, in turn, approaches the normal compression line. This indicates that the free-swell disturbance to HCB5 is fully recovered and does not appear to have adversely affected the test.

The loss of pressure has a positive serendipitous result. The free-swell disturbance demonstrates that any preconsolidation effects due to unsaturated specimen compaction (i.e., specimen preparation to a prescribed initial dry density) can be completely undone by free-swell (unconfined) displacements. Free swell can produce, in effect, a remoulded material at substantially lower dry density. In fresh water, restructuring of the montmorillonite particles is fully recoverable at higher stresses. This implies that the soil structure in fresh water is unstable under changing stresses.

A.5.2 Calcium-Chloride Solution Specimens

The 'as prepared' dry densities and loading schedules for the three saline-water specimens, like the fresh-water specimens, are quite different (Figure A17). The first two specimens with identical initial dry densities but very different loading paths (i.e., HCB3 and HCB4) produced almost identical results in terms of compression (C_c) and rebound (C_s) indices (Table A20) and void ratios (Figure A17).
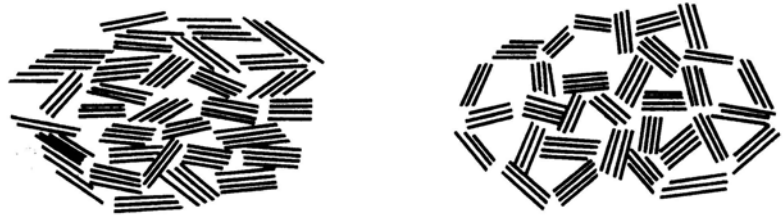
Face-to-face   (a)   Edge-to-face
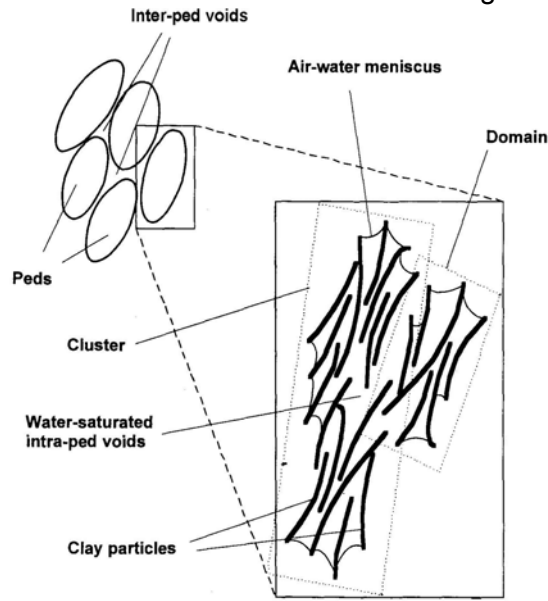
(b)
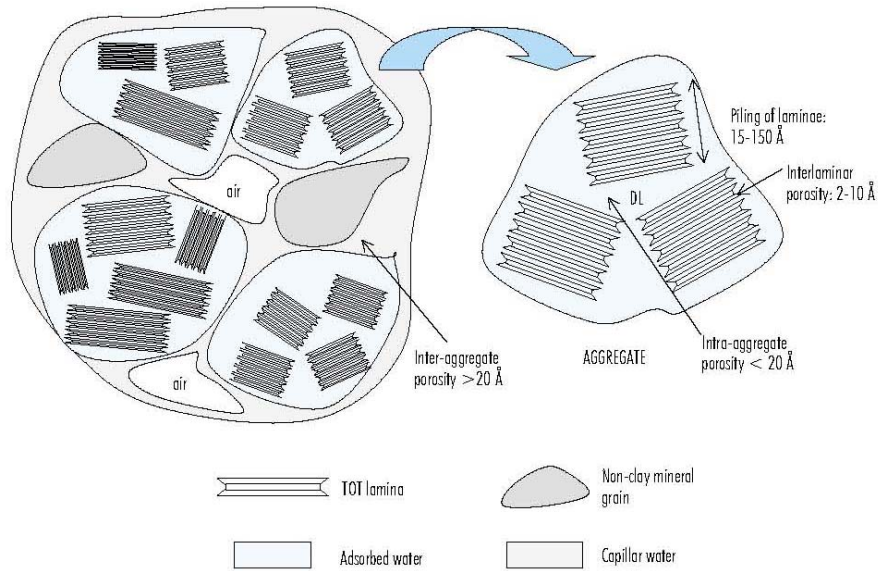
(c)

Figure A16:Simplified Representations of Complex Clay-Soil Structures (a) by Collins and McGown (1974), (b) by Wan (1996) and (c) by Villar (2002)
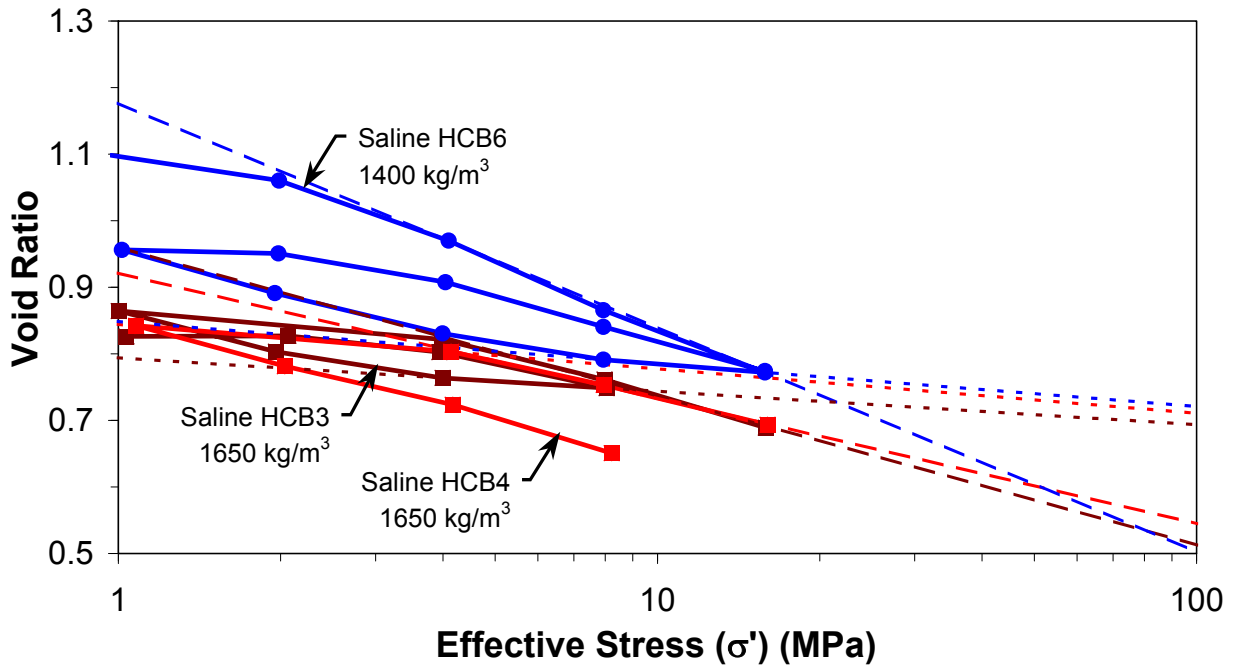
Figure A17: Void Ratio of Saline-Consolidation Specimens. Notes: The initial dry densities of the specimens are noted in the labels. The compression lines (long dashes) and rebound lines (short dashes) are also plotted.

HCB6, with a lesser initial dry density (i.e., ~1400 kg/m^3) than the other two specimens (i.e., ~1650 kg/m^3) in the saline solution, also experienced a stress reduction from 1 MPa to 0.33 MPa over a two-day period during the first load increment since both load frames were connected to the same pressure source. It produced the highest initial swelling strain for all the saline specimens probably due to the reduced compaction pressure to produce the specimen (i.e., dry density ~1400 Mg/m^3) as compared to the other two saline specimens (i.e., dry densities ~1650 Mg/m^3). Although all three specimens are permitted to swell at a confining pressure of 1 MPa, HCB6 swells more than both HCB3 and HCB4 at the same confining pressure.

The starting void ratio for HCB6 of 0.859 (ρ_d = 1474 kg/m^3) is significantly higher than those of the other two saline-solution specimens HCB3 (e = 0.701 and ρ_d = 1611 kg/m^3) and HCB4 (e = 0.560 and ρ_d = 1757 kg/m^3) (Figure A17). At no time did the void ratio reduce by the end of the two loading cycles at 16 MPa to that of the other two specimens. This response implies that whatever soil-fabric restructuring occurred, the structure was largely stable in the electrolyte to at least 16 MPa. In addition, the first load cycle followed a different path than that of the second load cycle and this second load cycle has a similar shape to that of the load cycles for HCB3 and HCB4 albeit at higher void ratios. Following loading of HCB6 to a maximum of 16 MPa in the first load cycle, the unloading and reloading cycles mimic that for HCB3 and HCB4 but offset by a void-ratio difference (Δe) of ~0.1. Two possible reasons for this void-ratio difference are a systematic measurement error or a difference in the soil-fabric state of the montmorillonite particles caused by the reduced compaction energy for HCB6. Unlike the fresh-water specimen

(HCB5), the swelling had not stabilized prior to the two-day pressure drop and the subsequent loading induced displacements could not return the specimen to a "near-normal" condition.

This response implies that part of the low-pressure swelling (i.e., at 0.33 MPa) effect is recovered and that a larger fraction of the specimen has managed to restructure itself than the more confined (i.e., at 1 MPa) saline-solution specimens HCB3 and HCB4, producing a higher void ratio. The similar compressibility for the unloading and reloading of HCB6, the loading of HCB3 and the unloading and loading of HCB4 specimens, but very different void ratios, suggests that system stiffness is largely dependent on the nature of the soil structure regardless of what fraction of the specimen is in the edge-to-plate state (i.e., some independence of void ratio or, correspondingly, dry density). An alternate cause for the offset difference in void ratio may be measurement error since the thickness of the specimen is small (i.e., ~10 mm) and initial measurements are difficult to take. If it is a systemic measurement error that produced the offset, then only the void ratios are in error, not the slopes from which stiffness is calculated.

The compression index (C_c) for HCB6 is somewhat greater than those for the two previous specimens HCB3 and HCB4. The last load increment of the second load cycle (i.e., specimen stress from 8 MPa to 16 MPa) for HCB6 produces a slope very similar to the compression indices of the two previous specimens. The rebound indices for all three saline specimens are nearly identical (i.e., C_s from 0.05 to 0.07).

Notably, the compression indices (i.e., C_c between 0.19 to 0.34) and the rebound indices (i.e., C_s between 0.05 to 0.07) for the saline-solution specimens (Table A20) are about half the values corresponding to the fresh-water specimens reflecting an approximate doubling of their stiffness (i.e., the 1-D constrained moduli). These reductions are likely due to a reduction in the thickness of the double-layer surrounding the clay particles and a potential increase in structural stiffness by any increase in edge-to-plate clay-particle realignments due to the calcium-chloride solution (an electrolyte).

A.5.3 COMPARISON OF INITIAL CONDITIONS

Three types of loading conditions were attempted on specimens with two different target initial dry densities (i.e., 1650 kg/m^3 and 1400 kg/m^3): constant volume on initial loading (HCB2), confined swelling at low load (i.e., at 1 MPa) (HCB1, HCB3, HCB5 and HCB6) and instantaneous loading (i.e., at 8 MPa) (HCB4).

A.5.3.1 Constant Volume

Applying an initial constant-volume condition requires that pressure be constantly increased to prevent swelling-induced strains (i.e., less than 0.005 mm (ASTM 2003)). This was attempted on HCB2 (Table A1) by rigidly maintaining the hydraulic ram in a fixed position but leakage in the loading system prevented this. The test continued as a confined swell test at a vertical stress of 1.3 MPa.

A.5.3.2 Confined Swell

To measure the swell potential of a soil, a "nominal" load is applied to a specimen and swell is observed under that constant load. The "nominal" vertical stress selected for specimens of highly compacted Wyoming bentonite (MX80) is about 1 MPa due to the expectation that significant swelling would occur at this confining pressure (Dixon et al. 2002). Large initial swelling strains are noted in the first load increment for each specimen (i.e., 15%, 9%, 7%, 18%

and 13% for HCB1, HCB2, HCB3, HCB5 and HCB6, respectively, in Tables A3, A6, A9, A15 and A18). The swelling strains are consistently greater for the fresh-water specimens than for the specimens in the saline solution since salts notably reduce the swelling potential.

Specimens HCB1, HCB3, HCB4 and HCB6 all show some preconsolidation effects due to the compaction used to prepare the specimens as shown by their higher stiffness before reaching the compression line (C_c) (Figures A15 and A17). This could not be observed for specimen HCB2 by the jump in the load path from a specimen stress of 1.3 MPa to 16 MPa but some preconsolidation effect is implied by the slightly greater stiffness over this range than for HCB1 and HCB5. The free swell of specimen HCB5 appears to have removed all preconsolidation effects.

A.5.3.3 Instant Loading

HCB4 underwent an initial condition of instant loading to a stress of 8 MPa and then was unloaded in increments to a stress of 1 MPa (Figure A16). Thereafter, the specimen was loaded in increments to a stress of 16 MPa. The swelling strain (i.e., ~6%) at the initial specimen stress of 8 MPa was unexpectedly high. The estimated swelling pressure for a specimen at a dry density of 1650 kg/m^3 (i.e., EMDD of ~1470 kg/m^3) in a 100 g/L NaCl solution is 8 MPa or less depending on the fitting technique used for the swelling data (Baumgartner 2006).

Swelling continued with incremental specimen unloading, converging to the unloading curve of HCB3 (Figure A16). On reloading, the response continued to replicate that of HCB3 to a maximum specimen stress of 16 MPa. Clay-particle restructuring (Figure A17) appears to have occurred as the specimen swelled during the unloading stage because the specimen did not recover its initial void ratio under the first load increment at a specimen stress of 8 MPa. An increase of stress to 16 MPa did not collapse this stable structure.

A.6 SUMMARY

Six consolidation tests are performed on highly compacted bentonite (HCB) using a hydraulic load frame and a reduced diameter one-dimensional oedometer apparatus. The initial dry densities (i.e., 1650 and 1400 kg/m^3), the pore-fluid chemistry (i.e., fresh water and 75 g/L CaCl$_2$ solution) and specimen loading paths are altered to explore the effects of swelling and pore-fluid chemistry on the compression and swelling behaviour of the HCB. The results are the compression (C_c) and rebound (C_s) indices and the derived non-linear specimen stiffness (i.e., 1-D constrained moduli) as a function of applied stress. These data can be used for modelling purposes and can provide a comparison to other test materials.

The HCB specimens compacted with distilled water (i.e., also called fresh water in this report) and exposed to additional distilled water in the oedometer reservoir during testing displayed a strong swelling response as expected. The derived compression (C_c) and rebound (C_s) indices of HCB are about twice that of other remoulded clays (Bardet 1997) with much lower plasticity indices. The compression (C_c) and rebound (C_s) indices for fresh-water specimens appear almost independent of the initial dry densities and stress paths (Figure A15).

The differences in the fresh-water compression and rebound lines may be due to differences in experimental technique and in measurement error. HCB experiences significant creep (i.e., secondary consolidation) after the primary consolidation stage is complete (i.e., the end of excess pore-pressure relief). The durations of the load increments in the first two tests (i.e.,

HCB1 and HCB2) should have been longer, similar to that of the last test (i.e., HCB5), to more fully explore this creep stage.

The loss of pressure during the testing of specimen HCB5 (i.e., 0 MPa) permitted free swell to occur for two days, demonstrating that any preconsolidation effects can be obliterated (i.e., self-remoulding of the material). If any edge-to-plate restructuring had occurred, subsequent repressurization to higher pressures appeared to collapse the soil-fabric structure to permit return to the compression line (C_c), demonstrating that edge-to-plate structures are unstable under the fresh-water condition.

The specimens compacted and consolidated in saline solution (Figure A17) show less compressibility than the fresh-water specimens (Figure A15). The compression indices (C_c) for the saline specimens are 25% to 45% less than those for the fresh-water specimens. The rebound indices (C_s) are about half of the fresh-water values.

Similar to specimen HCB5, the reduction of pressure during the testing of specimen HCB6 (i.e., 0.33 MPa) permitted a more limited swell for two days. This too demonstrates that some, if not all, preconsolidation effects can be reduced or obliterated, respectively.

Clay-particle restructuring (Figure A16) appears to have occurred in the saline specimens, both during unsaturated specimen preparation and compaction and with swelling in the oedometer reservoir. The amount of initial edge-to-plate alignment during the specimen preparation may be small due to the very small quantity of saline solution used in the preparation and the very high loads used to compress the specimens to their initial dry densities. The amount of edge-to-plate structures, as a fraction of the whole specimen appears dependent on the confining pressure during unloading stage. Specimen HCB4 did not return to its original void-ratio (e) value of 0.651 at the end of the first load increment at a specimen stress of 8 MPa when reloaded not only to 8 MPa (i.e., e = 0.753) but also to 16 MPa (i.e., e = 0.693). Specimen HCB6 behaved in an identical manner to that of the other two saline specimens at relatively fixed offset void ratios. Both HCB4 and HCB6 demonstrated that a very stable edge-to-plate structure may have formed, which could not be collapsed to the maximum stress (i.e., 16 MPa) of the test series.

Corrosion of the oedometer cells is clearly apparent in these long-duration tests, beginning with the first saline-solution specimens (HCB3 and HCB4) and continuing with the last fresh-water (HCB5) and saline-solution (HCB6) specimens. The effect of iron cations in solution on specimen response is unclear in these tests.

A.7   CONCLUSION

The consolidation results demonstrate the influence of pore-fluid chemistry on the mechanical performance and swelling characteristics of HCB. The presence of the calcium chloride reduces the swelling potential likely due to the reduction in the double-layer effect of the bound water. The reduction of both the compression and rebound indices with the corresponding increase in the 1-D constrained moduli under saline conditions show that a stable soil-fabric structure has likely formed contributing to a less compliant (i.e., stiffer) structure as compared to fresh-water specimens. The reduction is 25% to 45% in the compression index and about 50% in the rebound index. The results provide a valuable set of experimental data for numerical modelling purposes.

A.8   RECOMMENDATIONS

The Nuclear Waste Management Organization (NWMO) has identified Ordovician sediments as potential geologic media to host a deep geologic repository for used nuclear fuel (NWMO 2005). Mazurek (2004) in his geoscientific review of the sedimentary sequence in southern Ontario indicates the presence of highly saline groundwaters (i.e., 30- to 35-g/L Ca, 40- to 60-g/L Na and 150- to 180-g/L Cl) in the Ordovician sediments, much higher salinities than the 75-g/L $CaCl_2$ tested in these consolidation tests. Consolidation testing of HCB should be extended to these high salinity levels, both on individual NaCl and $CaCl_2$ solutions and on their mixtures to measure individual effects based on salt speciation and on their combined effect to note any unique differences.

The consolidation cells should be fabricated from more corrosion-resistant materials due to these high salinities and the long durations of each test (e.g., minimum of six months per specimen for a load, unload and reload cycle over a 1 MPa to 16 MPa range). If swelling pressure measurements are to be made during consolidation, then consideration should be given to fabricating a servo-actuated loading system to increase load while maintaining less than 0.005 mm of displacement (i.e., a constant volume swelling test (ASTM 2003)).

One design decision for the engineering of a sealing system that should be considered is the preference for preparing the sealing materials with either fresh or saline water. Consolidation tests should include the preparation of specimens of HCB with fresh water and placement of the specimens in a reservoir of saline water to measure differences in response. This should be coupled with long-duration static testing, in terms of years, of single- and multiple-sealing materials in constant-volume pressure vessels immersed in both fresh- and saline-water reservoirs to measure long-term responses. Unlike consolidation tests, which provide short-term transient-response data, the static constant-volume pressure-vessel tests provide only end-of-test results. The advantage of the static constant-volume pressure-vessel tests is their simplicity, low cost and their ability to provide long-term data that includes creep effects. Their main disadvantage is the lack of mechanical data including any compliance effects.

ACKNOWLEDGEMENTS

REFERENCES

ASTM (ASTM International). 2004. Standard test methods for one-dimensional consolidation properties of soils using incremental loading. Standard D2435-04, ASTM International, West Conshohocken, Pennsylvania, USA.

ASTM (ASTM International). 2003. Standard test methods for one-dimensional swell or settlement potential of cohesive soils. Standard D4546-03, ASTM International, West Conshohocken, Pennsylvania, USA.

Bardet, J.-P. 1997. Experimental Soil Mechanics. Prentice Hall Inc., Upper Saddle River, N.J.

Baumgartner, P. 2006. Generic thermal-mechanical-hydraulic (THM) data for sealing materials - Volume 1: Soil – water relationships. Ontario Power Generation, Nuclear Waste Management Division Report 06819-REP-01300-10122-R00.

Collins, K., and A. McGown. 1974. The form and function of microfabric features in a variety of natural soils. Geotechnique, Vol. 24, No. 2, pp. 223–254.

Dixon, D.A., N.A. Chandler and P. Baumgartner. 2002. The influence of groundwater salinity and interfaces on the performance of potential backfilling materials. In Trans. 6th International Workshop on Design and Construction of Final Repositories: Backfilling in Radioactive Waste Disposal. ONDRAF/NIRAS, Brussels, Belgium, 2002 March 11-13.

Maak, P. and G.R. Simmons. 2005. Deep geologic repository concepts for isolation of used fuel in Canada. In Proc. Canadian Nuclear Society conference "Waste Management, Decommissioning and Environmental Restoration for Canada's Nuclear Activities: Current Practices and Future Needs". 2005 May 8-11, Ottawa.

Mazurek, M. 2004. Long-term used nuclear fuel waste management – Geoscientific review of the sedimentary sequence in southern Ontario. Institute of Geological Sciences, Univ. of Bern, Technical Report TR 04-01, Bern, Switzerland.

Mitchell, J.K. 1976. Fundamentals Of Soil Behaviour. John Wiley And Sons, Toronto.

NWMO (Nuclear Waste Management Organization). 2005. Choosing a way forward: The future management of Canada's used nuclear fuel, final study. Nuclear Waste Management Organization, Toronto, Canada (www.nwmo.ca).

Russell, S.B. and G.R. Simmons. 2003. Engineered barrier system for a deep geologic Repository. In Proc. 2003 International High-Level Radioactive Waste Management Conference, Las Vegas, USA, 2003 March 30 – April 02.

Villar, M.V. 2002. Thermo-hydro-mechanical characterization of a bentonite from Cabo de Gata. A study applied to the use of bentonite as sealing material in high level radioactive waste repositories. Publicación Técnica ENRESA 01/2002, p. 258. Madrid.

Wan, A.W.L. 1996. The Use of Thermocouple Psychrometers to Measure In Situ Suctions and Water Contents in Compacted Clays. Ph.D. Thesis. Dept. of Civil and Geological Engineering, Univ. of Manitoba.

Yong, R.N. and B.P. Warkentin. 1975. Developments in Geotechnical Engineering. 5: Soil Properties and Behaviour. Elsevier, Amsterdam.

APPENDIX B: DENSE BACKFILL (DBF)

J.R. Baldwin and J.A. Blatz
Department of Civil Engineering
University of Manitoba

CONTENTS

B.1   DBF

Dense backfill is a clay-based sealing-system component proposed for use in a nuclear fuel waste repository (Maak and Simmons 2005). The DBF proposed for repository use is composed of 5% bentonite, 25% glacial clay and 70% crushed granite aggregate by mass (Russell and Simmons 2003), compacted to a dry density of 2120 kg/m^3 at a water content of 8.5% producing an initial degree of saturation of ~80%. For the consolidation tests, a DBF, composed of 75% crushed granite, 18.75% crushed illite clay (i.e., Sealbond) and 6.25% Avonlea bentonite, from a previous experiment in the URL was supplied to the University of Manitoba's Geotechnical Laboratory by Atomic Energy of Canada Limited. This previously prepared material is used because no source of glacial-lake clay is currently available and the test results can be compared to previously performed tests on this specific mixture, if needed.

B.2   DBF OEDOMETER TESTING

B.2.1 DBF TEST DESCRIPTION

Standard ASTM procedures cannot be followed due to the nature of the DBF (i.e., crushed granite aggregate) and the proposed initial conditions to be imposed on specimens. Large oedometer cells are used in this testing program to accommodate the large size of the aggregate (i.e., up to 35-mm granite chips) in the DBF. The cells are manufactured at the University of Manitoba from type-316 stainless steel to provide corrosion resistance against the concentrated salt solutions. The 101-mm-diameter cells are 101-mm high. Six specimens are tested at the AECL-specified initial conditions (Table B1). The testing includes a defined loading and unloading schedule for all stages of each test. This report summarizes the procedures used in all of the testing, the detailed measurements taken during the tests and comparisons of the test results in light of the initial conditions.

Specimens are prepared from reconstituted specimens from previously completed triaxial tests. The specimens are oven dried and wetted to a water content of 10.6%. Oedometer specimens are prepared by manually compacting the material inside the oedometer specimen ring using a specified mass of material and compaction volume (strain-based measurement in the static mould) to ensure an optimal bulk density of 2324 kg/m^3. After a specimen is compacted to the target conditions, the filled specimen ring is placed in the oedometer cell and specified initial consolidation conditions are applied as defined by the planned testing matrix (Table B1).

As noted in Table B1, two broadly different initial conditions for the specimens are examined, constant volume conditions during water uptake and limited swelling conditions to a target maximum. Two types of load application schedules are specified by AECL (Table B2). The first load schedule (i.e., Type 1) follows a relatively standard incremental load and unload pattern for oedometer tests. The second load schedule includes an unload-re-load loop to better identify the elastic and plastic behaviour of the material under the load conditions. This second load schedule (i.e., Type 2) is derived from a review of the results from the first four tests and requires sufficient time for total swell to be measured during the unloading stages.

Table B1: Planned 1-D Consolidation Testing Matrix for DBF Specimens

Test No.	Mixing Water	Reservoir Water	Swelling on Initial Water Uptake	Loading Path
1	Distilled	Distilled	20% at Low Load*	Load to 3900 kPa after initial swelling
2	Distilled	Distilled	Rigidly Confined**	Load to 3900 kPa
3	100 g/L CaCl$_2$	100 g/L CaCl$_2$	20% at Low Load	Load to 3900 kPa after initial swelling
4	100 g/L CaCl$_2$	100 g/L CaCl$_2$	Rigidly Confined	Load to 3900 kPa
5	Distilled	Distilled	N.A.†	Load to 4000 kPa
6	100 g/L CaCl$_2$	100 g/L CaCl$_2$	N.A.	Load to 4000 kPa

*   Low Load is the oedometer top-head seating load (see first load increment in test results).
** Rigidly Confined – Constant volume by means of increasing load with zero displacement.
†   N.A. (not applicable) – Specimen immediately loaded to 1 MPa.

Table B2: Specified Loading Schedules for all DBF Specimens

Stage	Load Schedule Type 1	Load Schedule Type 2
Step 1	Load to 1 MPa	Load to 1 MPa
Step 2	Load to 2 MPa	Load to 2 MPa
Step 3	Load to 4 MPa	Load to 4 MPa
Step 4	Load to 8 MPa	Unload to 2 MPa
Step 5	Load to 16 MPa	Unload to 1 MPa
Step 6	Unload to 8 MPa	Unload to 0.5 MPa
Step 7	Unload to 4 MPa	Load to 1 MPa
Step 8	Unload to 2 MPa	Load to 2 MPa
Step 9	Unload to 1 MPa	Load to 4 MPa

B.2.2 DBF TEST PROCEDURE

DBF specimens are compacted to a bulk density of ~2300 kg/m^3 at an initial water content of ~10.6%. Oven dry specimens are wetted with either distilled water or a 100 g/L CaCl$_2$ solution (see Table B1) and equilibrate for a minimum of two days in an environmental chamber. Specimens are compacted in five, 189-g, 10.15-mm-high lifts, to a planned specimen height of ~50.8 mm. The reservoir solution in the oedometer is identical to that of the mixing solution. Upon assembling the oedometers, tests either begin under constant-strain, free-swell or instantaneous-loading conditions according to the testing matrix.

The load is changed (i.e., increased or decreased increments) only when no significant change occurs in the void ratio (i.e., in the third decimal place) over a twenty-four hour period. The total times to complete primary consolidation were calculated for Tests 1 and 2 for each load and unload increment. The consolidation times were used to aid in predicting load times and total test times for the remaining tests.

B.3   DBF TEST RESULTS

The results of the DBF consolidation tests are presented as individual test results; comparisons between tests based on pore-fluid solutions; and comparisons between tests based on initial conditions.

B.3.1   INDIVIDUAL TEST RESULTS

Test results of the six individual specimens are plotted (Figures B1 through B6) showing the stress-dependent void ratio at the end of each load step and the time-dependent displacements occurring in each load step. For the consolidation of test specimen 1, Figures B1a and B1b show the final void ratio vs. applied pressure and displacement vs. the square root of time, respectively. The water uptake during swell is the process of specimen saturation as it approaches equilibrium under the imposed initial and boundary conditions. Equilibrium is not reached in test 1 (see Figure B1b) and so subsequent loads are applied during unsaturated conditions; this could interfere with the true behaviour of the specimen and yield inferior data. Fully saturated conditions are reached in Test 2, 3 and 4 by allowing the specimens to equilibrate before applying subsequent loads. This allows for more accurate specimen behaviour with respect to conventional consolidation theory; larger vertical stresses result in larger vertical strains.

The compression (c_c) and swelling (c_s) indices are calculated from the slopes of the void-ratio curves (i.e., Figures B1a, B2a, B3a, B4a, B5a and B6a). The indices are dimensionless with c_c > c_s. These indices are typically established from standard consolidation tests and are used to assess the constrained compressibility for normally and overconsolidated soil conditions. The test indices are summarized in Table B3.

Table B3: Compression and Swelling Indices

Test	C_c	C_s	
		Min	Max
Test 1 – Distilled, Unconfined Swell	0.051	0.007	
Test 2 – Distilled, No Swell	0.049	0.006	
Test 3 – 100 g/L $CaCl_2$, Unconfined Swell	0.039	0.003	
Test 4 – 100 g/L $CaCl_3$, No Swell	0.042	0.005	
Test 5 – Distilled	0.050	0.005	0.007
Test 6 – 100 g/L $CaCl_2$	0.040	0.001	0.005

B.3.2   COMPARISON OF MIXING AND RESERVOIR CONDITIONS

B.3.2.1 Distilled Water

The 'as prepared' void ratios for the three distilled-water specimens are similar, yet as initial conditions differ, resulting void ratios under identical loading conditions vary significantly (Figure B7). The compression index varies considerably until a pressure of 1 MPa is reached. Thereafter, the slopes stabilize to a consistent value. The compression index ranges between

0.049 and 0.051, demonstrating a log-linear behaviour of the material in the stress range between 1 and 4 MPa. The lack of linearity in the lower stress range could be attributed to particle realignment of the bentonite-aggregate matrix, secondary compression (creep).
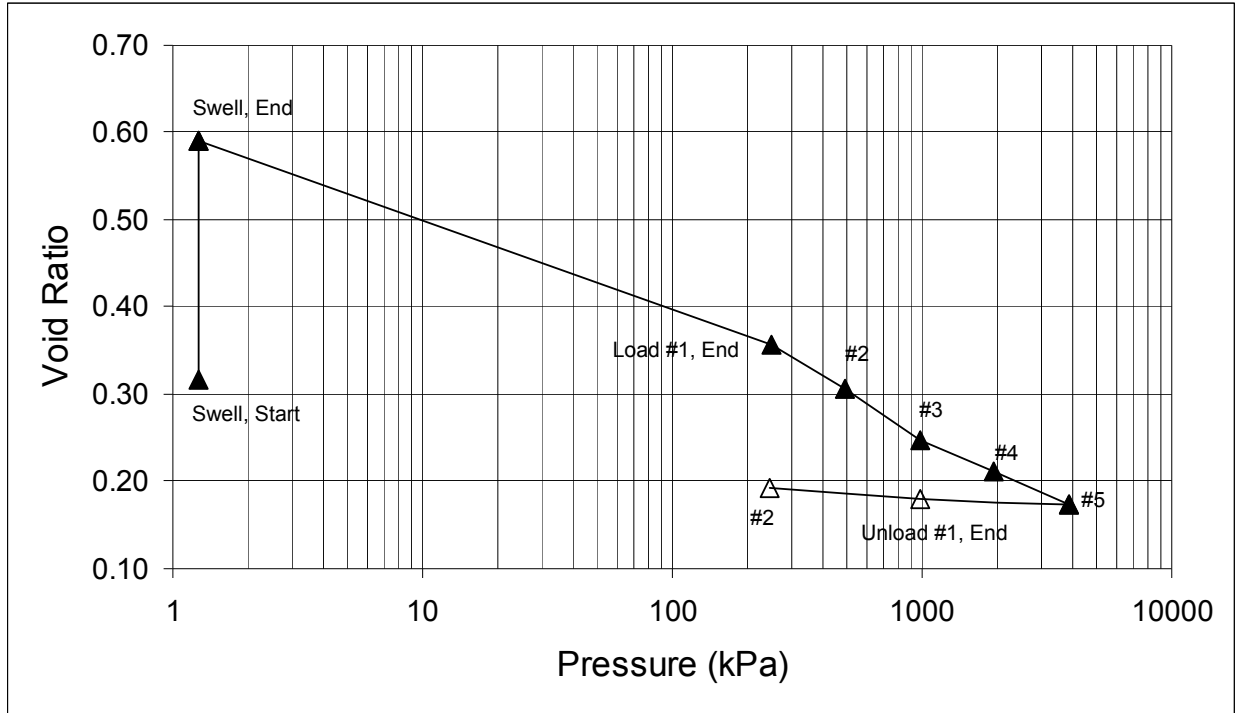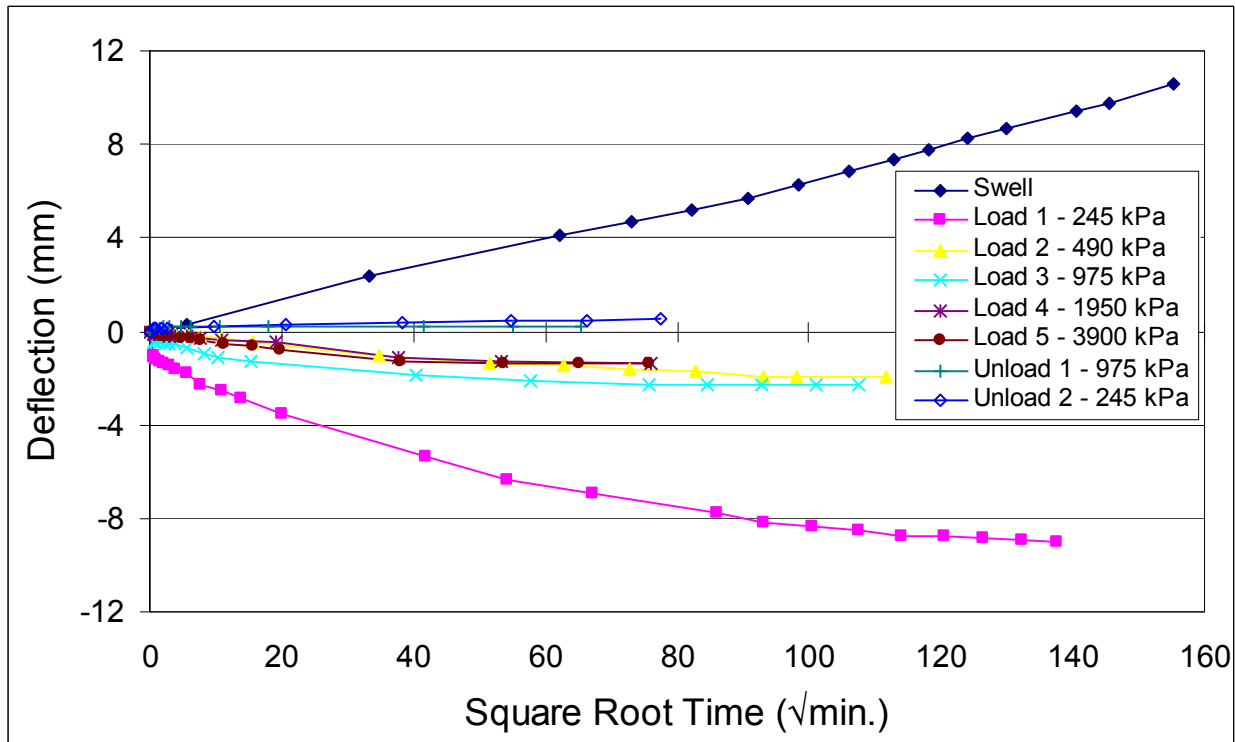
Figure B1: Test 1 – a) Change in Final Void Ratio as a Function of Applied Stress b) Specimen Displacement as a Function of the Square Root of Time
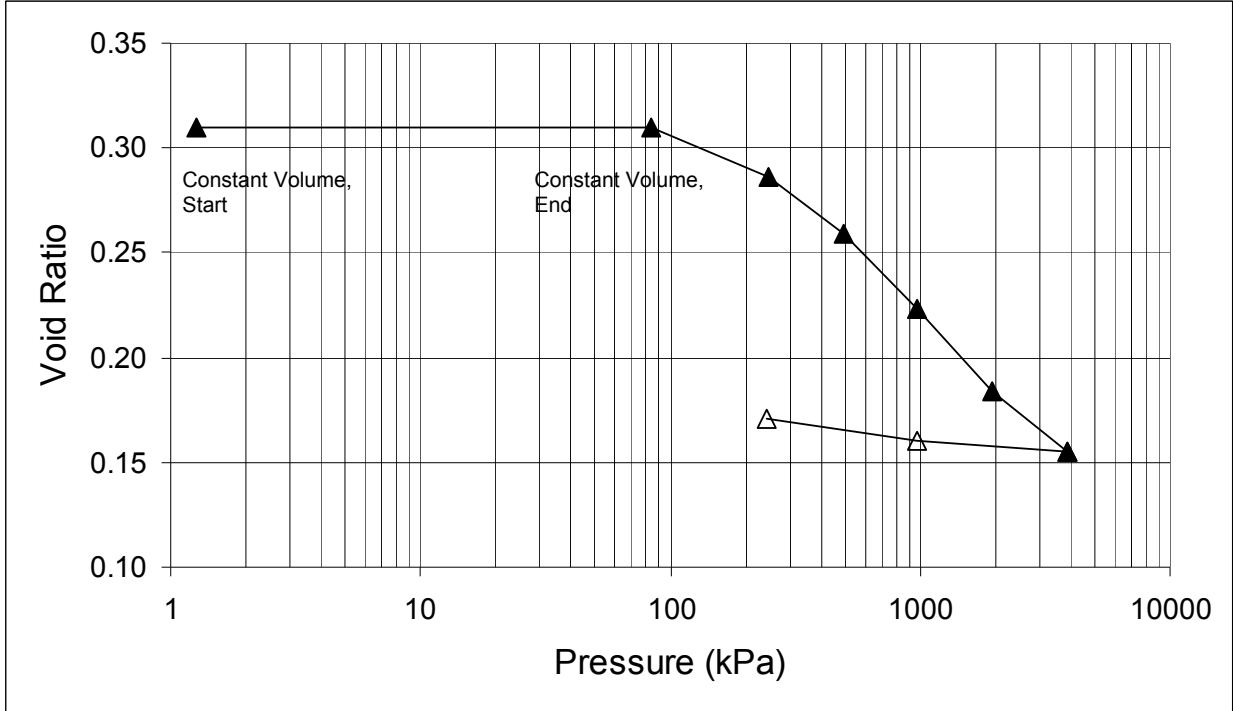
a)
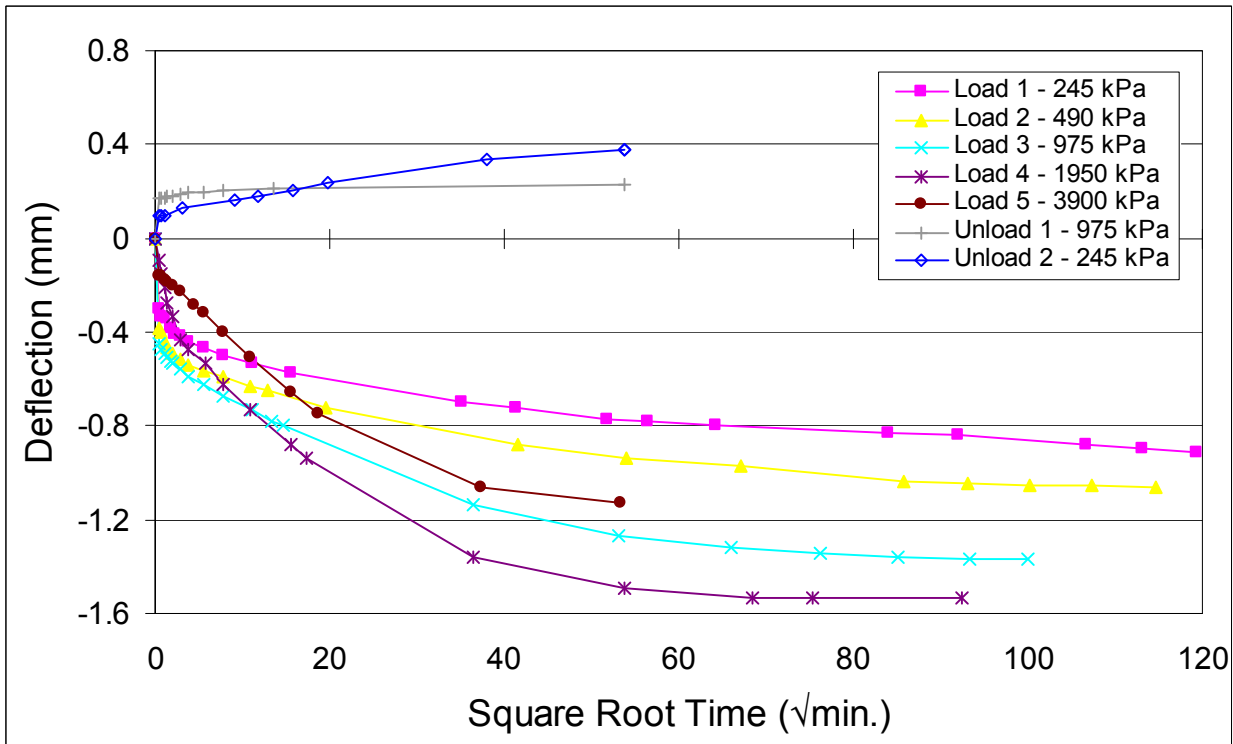
b)

**Figure B2: Test 2 – a) Change in Final Void Ratio as a Function of Applied Stress
b) Specimen Displacement as a Function of the Square Root of Time**
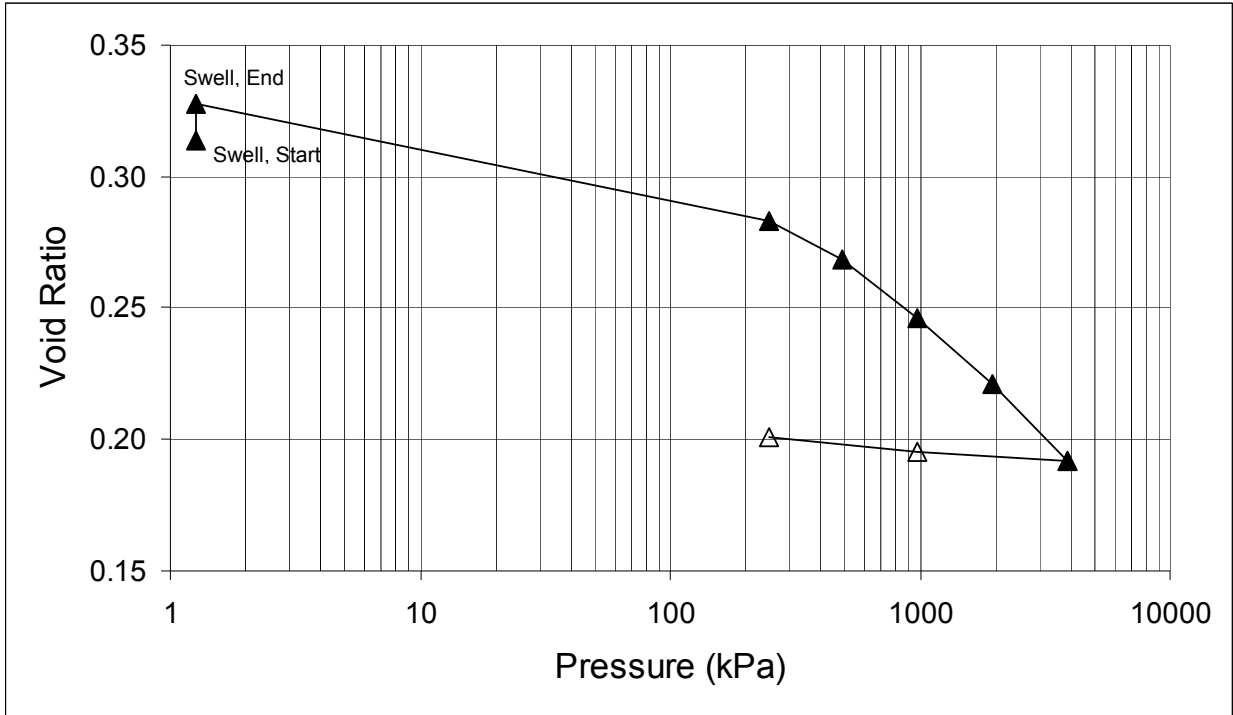
a)
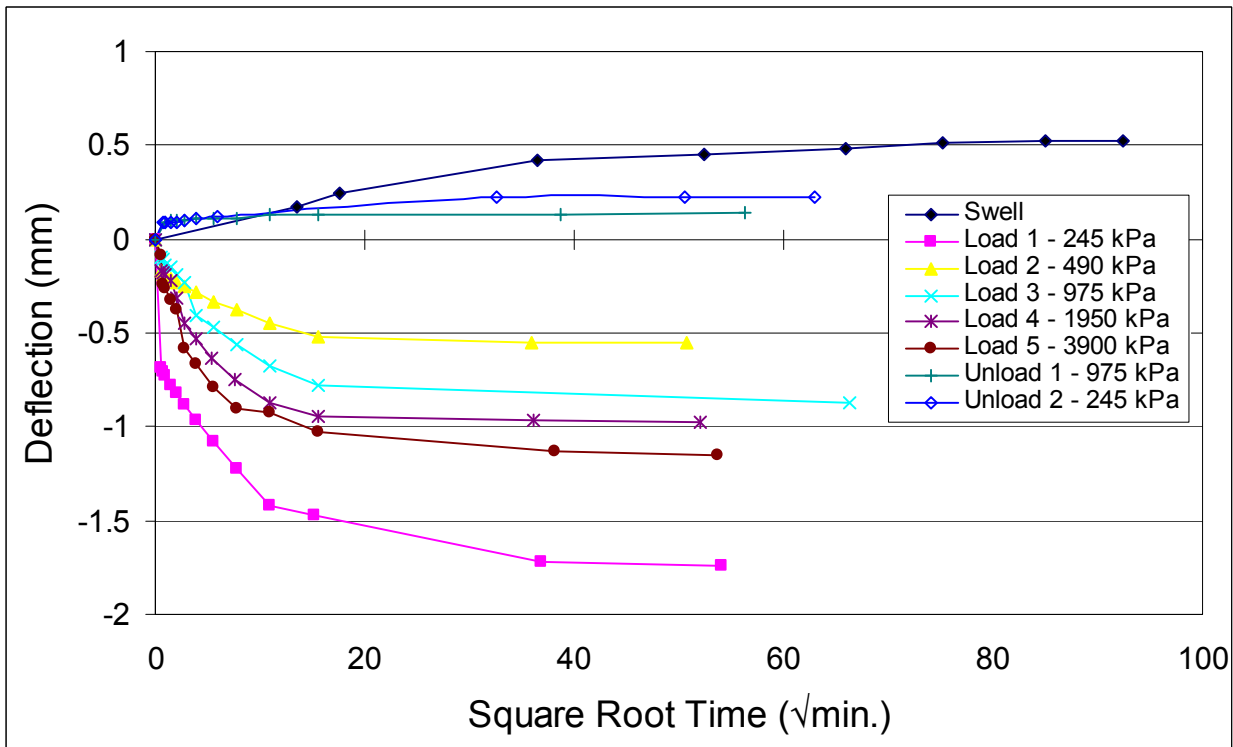
b)

**Figure B3: Test 3 – a) Change in Final Void Ratio as a Function of Applied Stress
b) Specimen Displacement as a Function of the Square Root of Time**
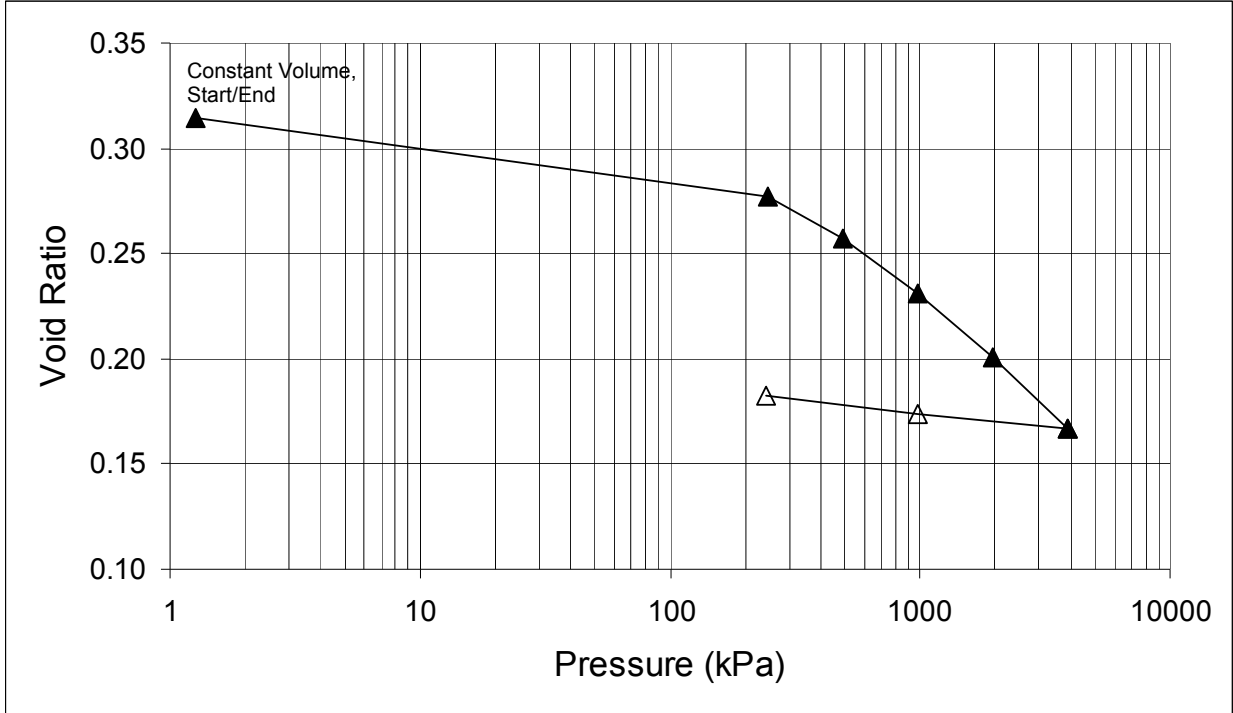
a)
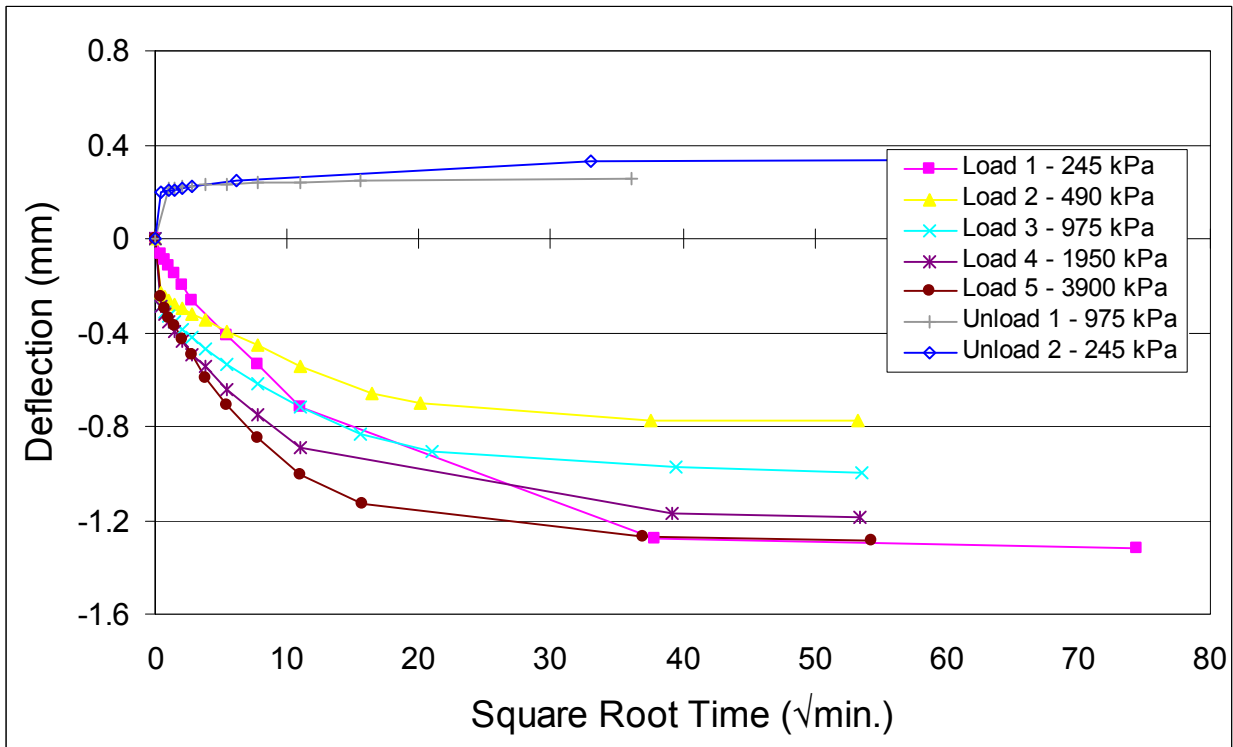
b)

**Figure B4: Test 4 – a) Change in Final Void Ratio as a Function of Applied Stress
b) Specimen Displacement as a Function of the Square Root of Time**
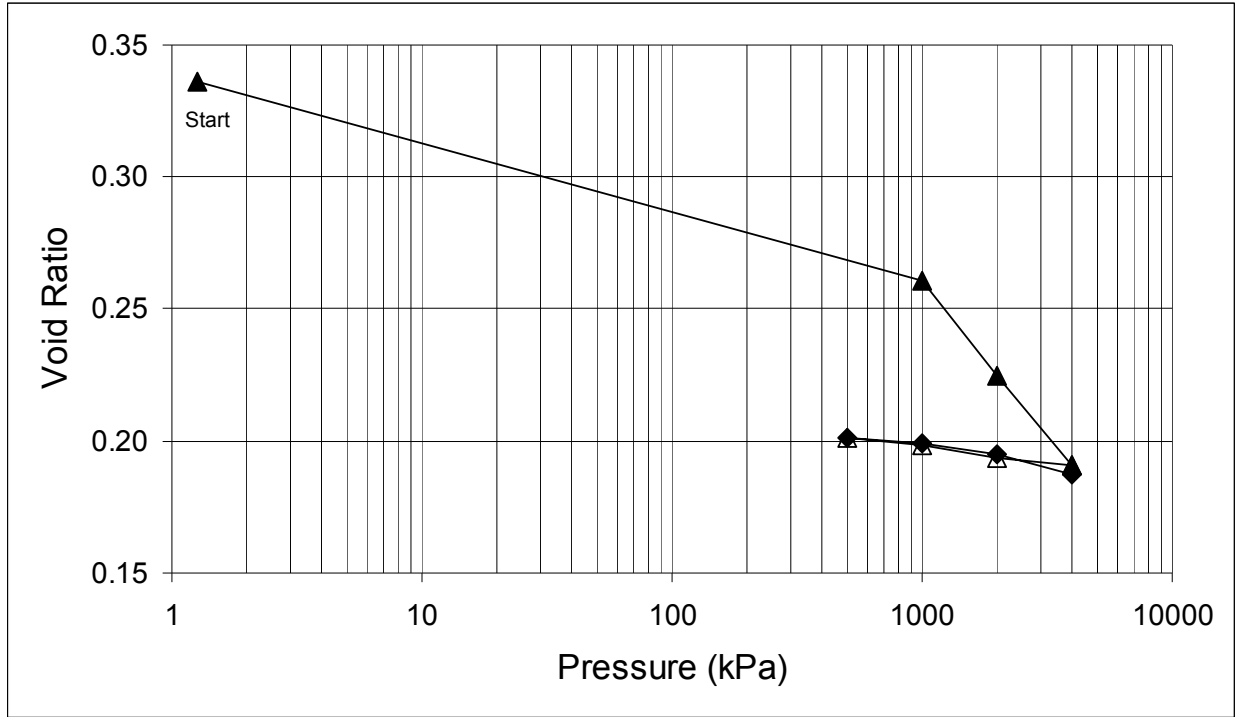
a)
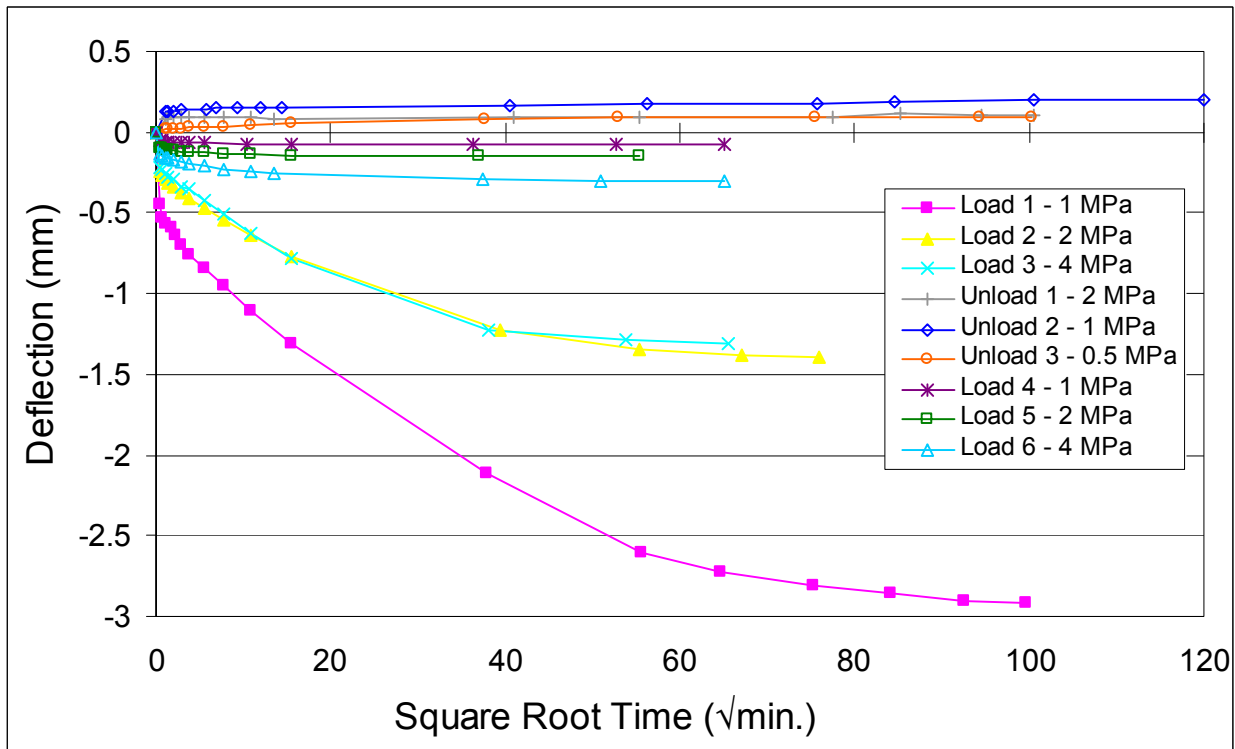
b)

**Figure B5: Test 5 – a) Change in Final Void Ratio as a Function of Applied Stress
b) Specimen Displacement as a Function of the Square Root of Time**
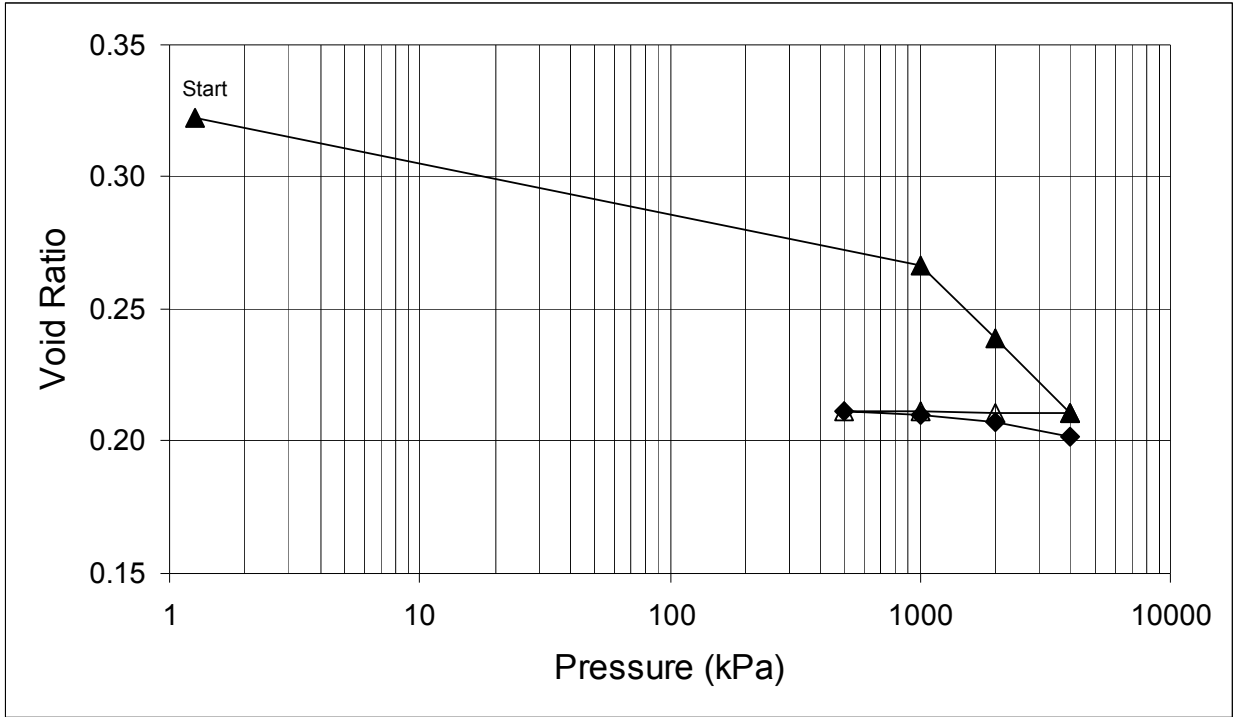
a)
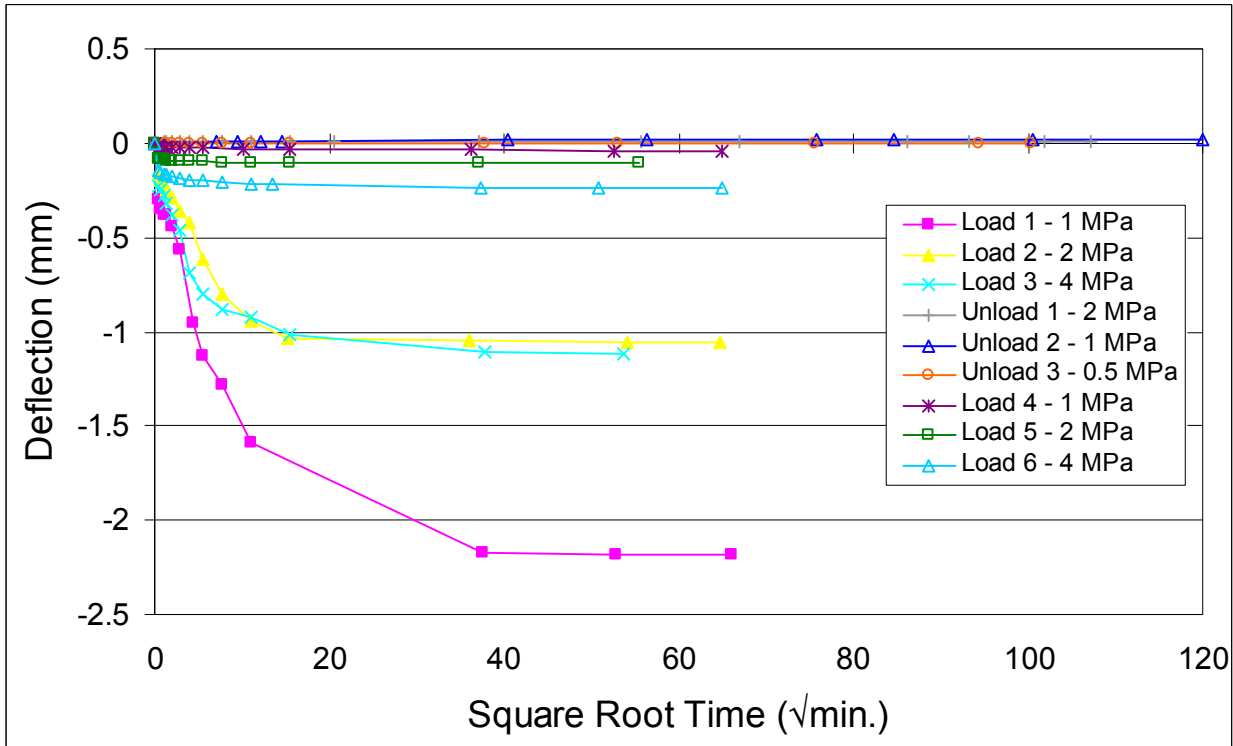
b)

**Figure B6: Test 6 – a) Change in Final Void Ratio as a Function of Applied Stress
b) Specimen Displacement as a Function of the Square Root of Time**
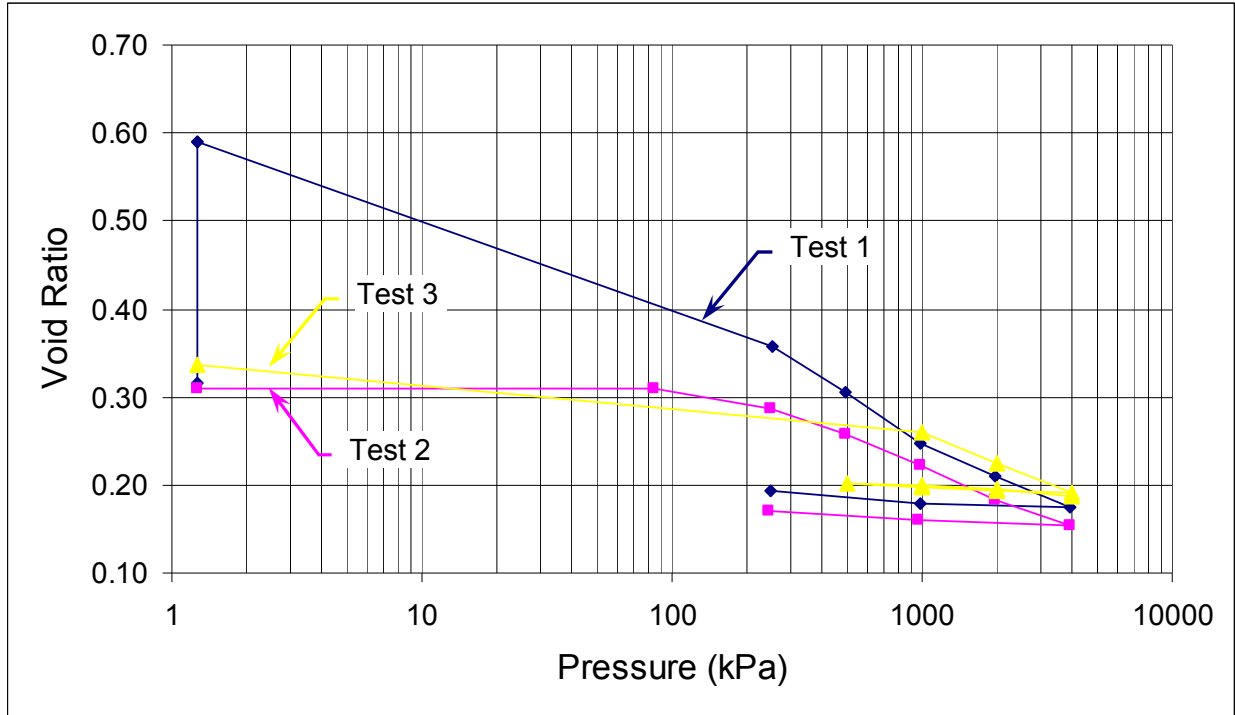
Figure B7: Void-Ratio Comparison for Specimens in Distilled Water

Swelling indices ranges between 0.005 and 0.007 over a wider stress range of 250 kPa to 4 MPa. Strong hysteresis is present in these curves, evident during unloading of each specimen, where a slight upward concavity rests in the void ratio vs. log pressure plots. Insufficient unloading steps yield an inability to accurately extrapolate back to a vertical stress of 1 kPa; though in speculation, void ratio may potentially converge to that of the initial unconfined increment.

B.3.2.2 Calcium Chloride Solution

Similar to the distilled-water specimens, the 'as prepared' void ratios for the saline-solution specimens are consistent (Figure B8). The compression indices differ considerably until ~500 kPa, where the slopes approach similar values ranging between 0.039 and 0.042. Lack of consistency over the lower stress range can be also attributed to secondary compression. This act of soil reconfiguration has been present during all tests, occurring more significantly in lower vertical stress ranges. Notably, the upper limit is smaller for the $CaCl_2$ solution then that of distilled water. The unconfined swell and constant volume specimens show similar swelling index values, 0.003 to 0.005, though the final test series (i.e., specimens 5 and 6) suggest differently. In defence, hysteresis present in previous tests suggest that if an additional unload increment took place, the specimen could experience a similar change in void ratio as measured in Tests 3 and 4 for the same change in vertical stress, resulting in improved conformity.

The compression and swelling indices for specimens prepared and submersed in the saline solution are notably less than those specimens in distilled water. The time plots (Figures B1b, B2b, B3b, B4b, B5b and B6b) also show that the time to complete primary consolidation is

decreased for saline conditions (i.e., inferring an increased hydraulic conductivity). These reductions are likely due to a reduction in thickness of the double-layer surrounding the clay particles caused by the calcium-chloride solution.
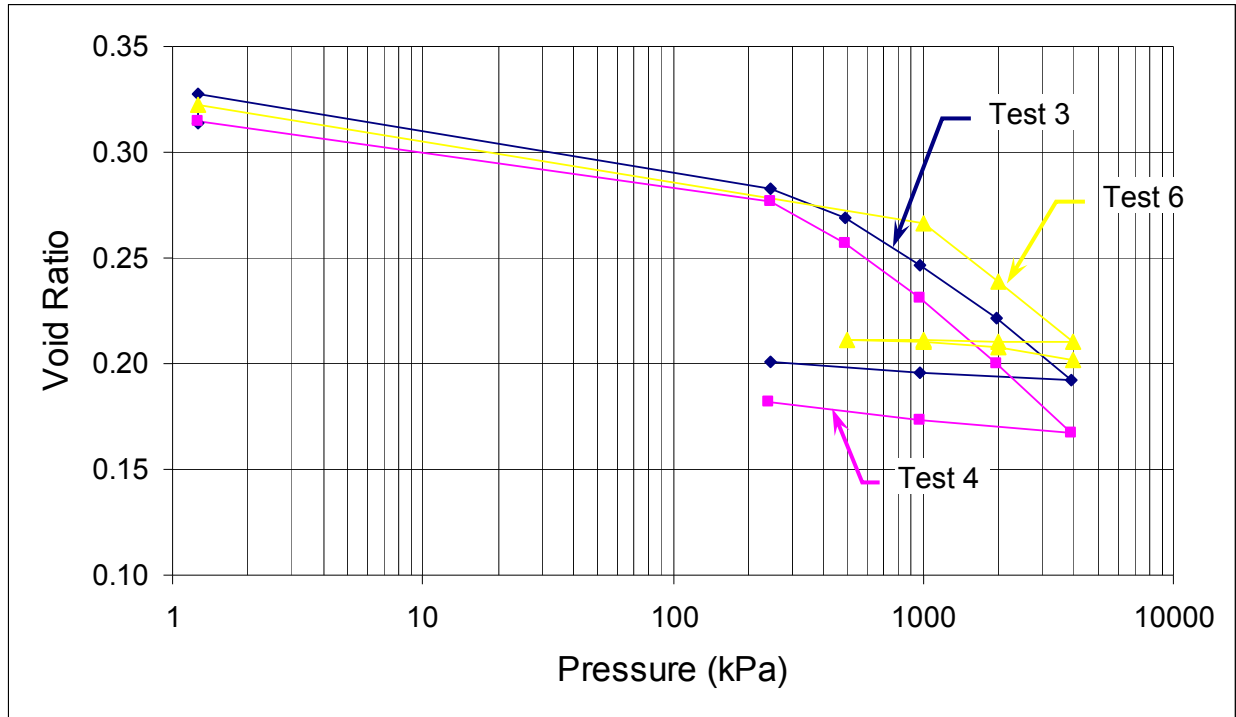
Figure B8: Void-Ratio Comparison for Specimens in CaCl₂ Solution

B.3.3   COMPARISON OF INITIAL CONDITIONS

B.3.3.1 Unconfined Swell

To measure the swell potential of a soil, a nominal load is applied to a specimen and swell under that constant load is observed. The swell behaviour of the specimens tested is examined under a load of 1.27 kPa, the pressure applied by the top cap alone. Specimens are allowed to swell under adsorption of water to a maximum swelling strain (total vertical swell) of 20% (Table B1). This strain criterion was arbitrarily chosen to reduce test time. Comparing the void ratio vs. pressure curves (i.e., Figure B9) for the unconfined swell specimens in distilled water and saline solution suggests that the presence of calcium chloride notably reduces free-swell potential. Swell has a significant effect on time for total consolidation of subsequent loads, that is, the length of time for a consolidation step before application of the next step is a function of the amount of swelling that has previously occurred.

B.3.3.2 Constant Volume

Ensuring an initial constant-volume condition requires that pressure be increased such that specimen volume is held constant until static equilibrium is reached. Essentially, this is identical to the unconfined swell case where the nominal static equilibrium pressure is 1.27 kPa. A final

pressure of 84 kPa was required to maintain constant volume in the distilled specimen whereas only 1.27 kPa (i.e., the top cap) prevents swelling of the saline-solution specimen (Figure B10). This confirms the work by Dixon et al. (2002) that the swelling potential of bentonite is a function of salinity, with diminishing swelling pressure as a function of increasing salt concentration.
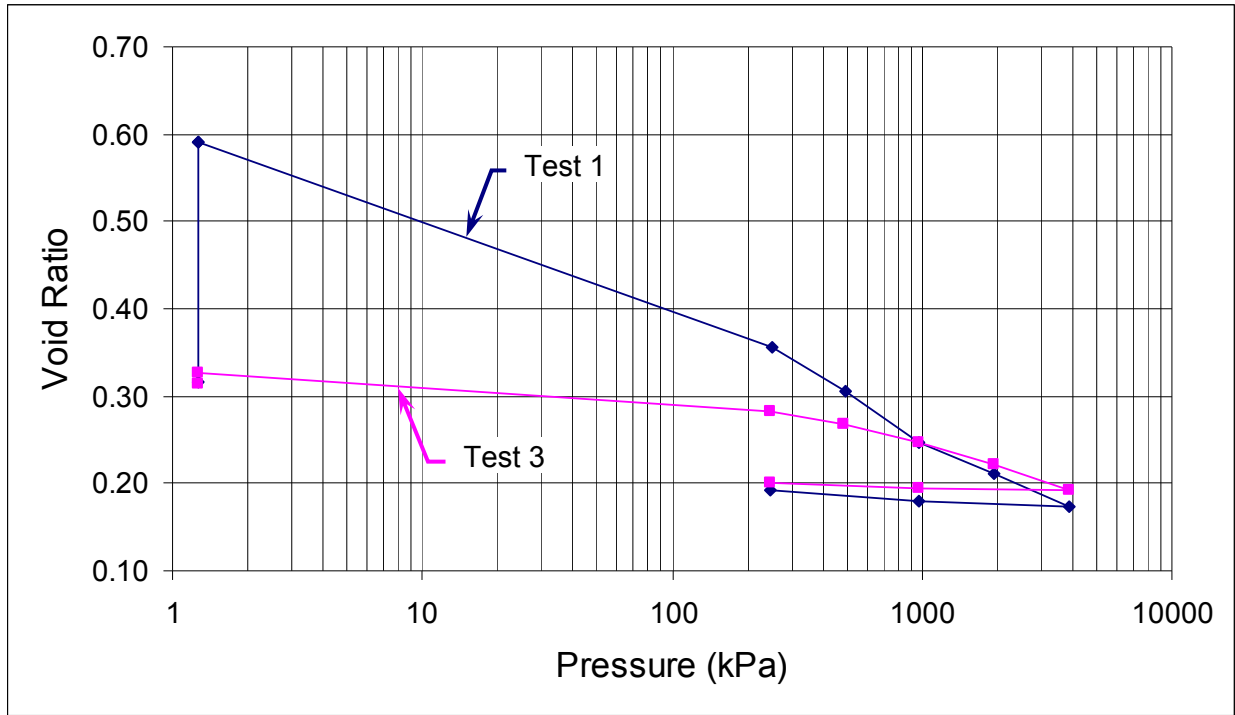
Figure B9: Void-Ratio Comparison for Specimens under Unconfined Swelling
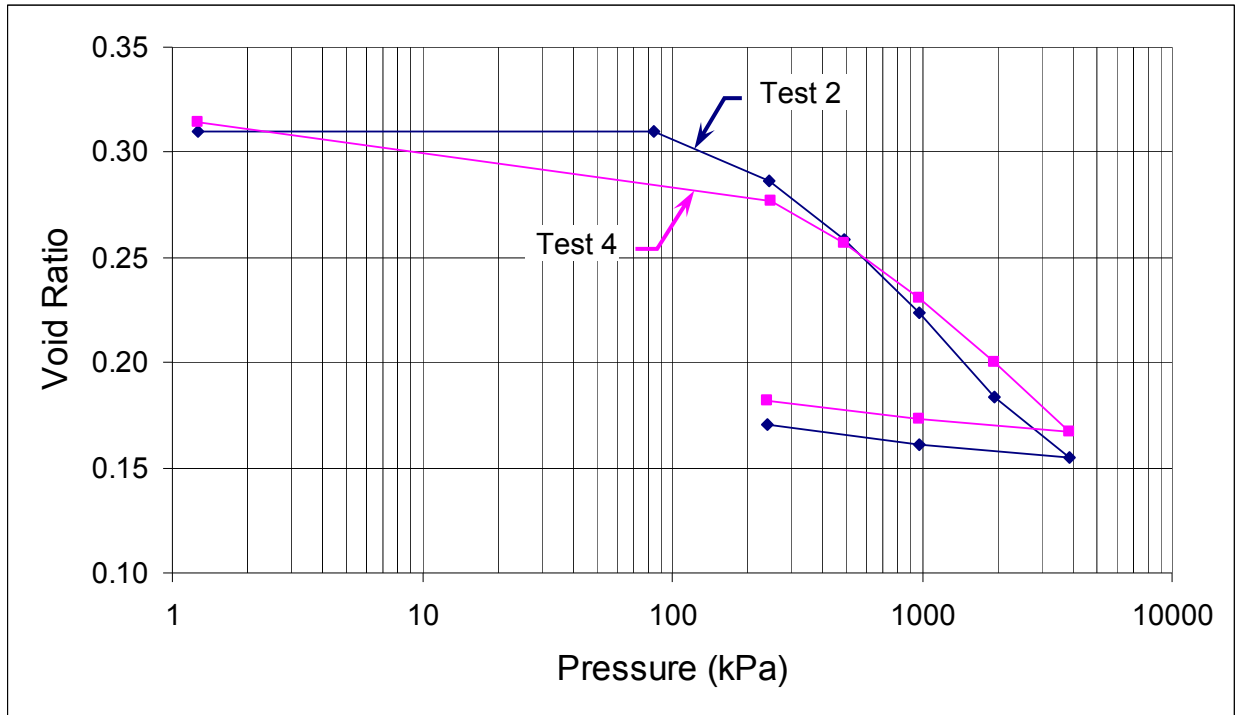
Figure B10: Void-Ratio Comparison for Specimens under Constant Volume

As mentioned previously, swelling has an effect on total consolidation of subsequent loads. This case shows that volumetric confinement reduces time for total consolidation significantly for both solution types. A lower slope in both the compression and swelling paths suggest that the presence of calcium chloride in solution decreases swelling and compressibility, though the difference is not considerable.

B.3.3.3 Instantaneous Loading

Tests 5 and 6 are performed under instant-loading initial conditions, as specified by AECL following review of the first four draft results. The specimens are instantaneously loaded to a pressure of 1 MPa. This load was chosen because it is the pressure where linearity[B1] begins in the previous tests (Figures B1a, B2a, B3a, and B4a). The unloading phase included extra unloading steps down to 500 kPa, following a peak pressure of 4 MPa. Additional time is used to enhance the monitoring of volume changes. A re-loading phase from 500 kPa to 4 MPa is used to further investigate the reloading behaviour. As with the unconfined-swell and constant-volume initial conditions, the specimen compacted in saline solution showed less compressibility than its distilled-water counterpart (Figure B11). The compression index for the saline case is 20% less than those for distilled water. The difference in swelling indices between the two is more difficult to interpret given the incompleteness of the swelling steps.

[B1] linearity from the log-normal perspective for the commonly termed normal consolidation line (NCL).
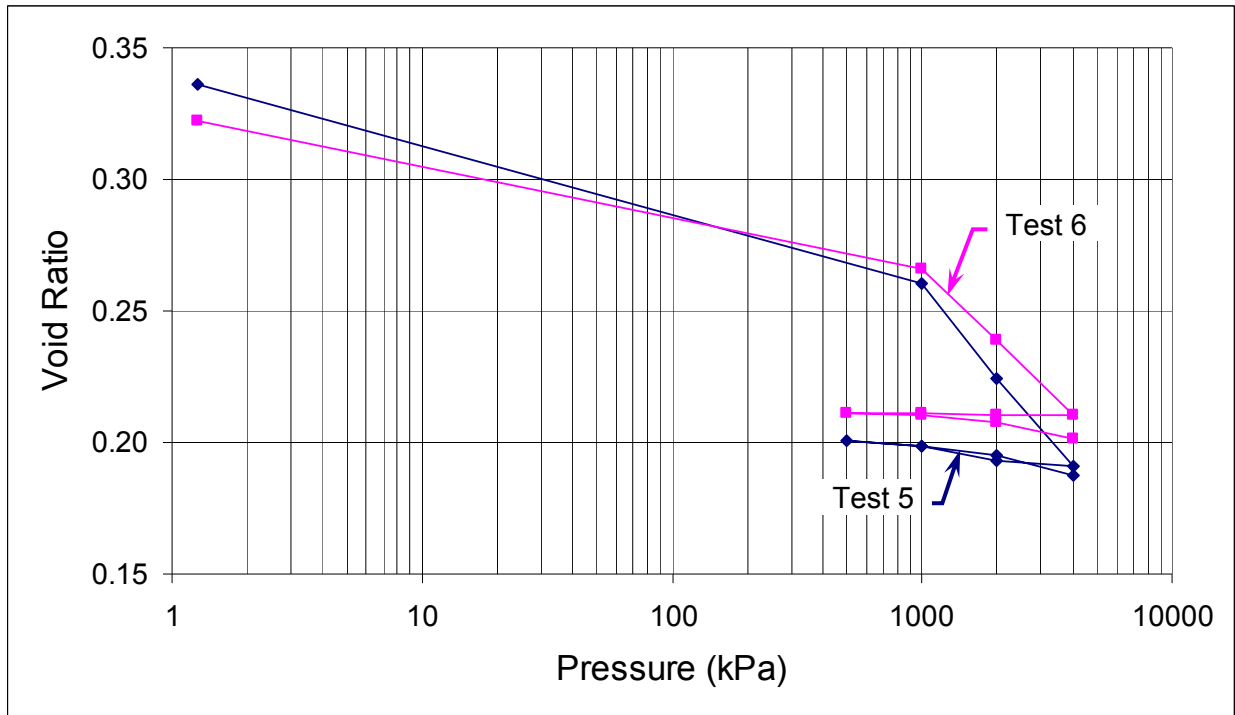
Figure B11: Void-Ratio Comparison for Specimens under Instantaneous Load

B.4   SUMMARY

Six consolidation tests are performed on dense backfill (DBF) using a modified one-dimensional oedometer apparatus developed at the University of Manitoba. The initial conditions and pore-fluid chemistry are altered to explore the effects of swelling and pore-fluid chemistry on the compression and swelling behaviour of this material. The results are the compression and swelling indices, which can be used for modelling exercises and can provide a comparison to other test materials. As a result of compacting the specimen to a predetermined density before testing, preconsolidation pressure is an irrelevant characteristic of the specimen.

B.5   CONCLUSION AND RECOMMENDATIONS

The results demonstrate the influence of pore-fluid chemistry on the mechanical performance and swelling characteristics of dense backfill materials. The presence of the calcium chloride reduces the swelling potential, likely due to the reduction in the double layer effects. Both the compression and swelling indices show a reduction for specimens prepared or subjected to the saline solution during loading. This reduction is up to 20% in the compression index.
The unloading behaviour shows slightly non-linear behaviour in log space that may in part be due to the swelling behaviour being inhibited to the external applied stress. More loading points and further unloading would help demonstrate this effect and help better define the hysteretic behaviour of the material. The results provide a valuable set of experimental data to be used to establish material-behavioural parameters for input into numerical models.

ACKNOWLEDGEMENTS

REFERENCES

Dixon, D.A., N.A. Chandler and P. Baumgartner. 2002. The influence of groundwater salinity and interfaces on the performance of potential backfilling materials. In Trans. 6th International Workshop on Design and Construction of Final Repositories: Backfilling in Radioactive Waste Disposal. ONDRAF/NIRAS, Brussels, Belgium, 2002 March 11-13.

Maak, P. and G.R. Simmons. 2005. Deep geologic repository concepts for isolation of used fuel in Canada. In Proc. Canadian Nuclear Society conference Waste Management, Decommissioning and Environmental Restoration for Canada's Nuclear Activities: Current Practices and Future Needs. 2005 May 8-11, Ottawa.

Russell, S.B. and G.R. Simmons. 2003. Engineered barrier system for a deep geologic repository. Presented at the 2003 International High-Level Radioactive Waste Management Conference. 2003 March 30-April 2, Las Vegas, NV.

APPENDIX C: LIGHT BACKFILL (LBF)

B.H. Kjartanson and H. Batenipour
Department of Civil Engineering
Lakehead University

CONTENTS

C.1   MATERIALS AND METHODS

C.1.1 LBF MATERIAL

The 50/50 bentonite/sand mixture in gravimetric proportions used as the LBF in these tests was obtained from a stock of material prepared and used for both the URL Buffer/Container Experiment (BCE) and the Isothermal Test (ITT). The bentonite clay component was batched and reblended Saskatchewan bentonite with the properties listed in Table C1. The montmorillonite content used for EMDD calculations is 80%. The 50/50 bentonite/sand mixture was prepared to a gravimetric water content of approximately 18% using groundwater recovered from Fracture Zone 2 (FZ2). This groundwater was recovered from approximately 20 m below the floor of Room 213 and was quite low in total dissolved minerals (Graham et al. 1997). The water content of the 50/50 bentonite/sand mixture used in these tests was in the range of about 20% to 21%, a little higher than the original target water content of 18%. This is likely due to some temperature-gradient-driven water redistribution within the barrels during storage.

Table C1: Properties of the Bentonite Component of LBF (after Graham et al. 1997)

Property	Value
Montmorillonite Content, %	80
Liquid Limit, %	214 ± 6
Plasticity Index	182 ± 5
Cation Exchange Capacity, meq/100g	88
Specific Surface area, m^2/g	520-630

Table C2 shows the results of wet sieve tests carried out to characterize the 50/50 bentonite/sand mixture used in the ITT (Dixon et al. 1994). These sieve results indicate a maximum particle size of about 2 mm, with about 90% of the particles less than 0.85 mm in size.

C.1.2 CONSOLIDATION TEST EQUIPMENT

Two Wykeham Farrance model 24251 front-loading and two Wykeham Farrance model 24001 rear-loading consolidation frames were used in this test program. The consolidation frames are pictured in Figure C1. Conventional 50-mm-diameter consolidation rings that allow 19-mm-high specimens were used in all four consolidation frames. The load hangers for all four frames were positioned to a give lever arm (load) ratio of 11.04:1. Given this load ratio, the stress applied to the specimen can be calculated with the following relationship:

$$[Load\ on\ hanger\ (kg)/0.0181] = Applied\ Pressure\ (kPa) \qquad (C1)$$

These specimens could be subjected to a maximum stress of about 4000 kPa using this equipment and load ratio.

Table C2: Particle Size Distribution of the 50/50 Bentonite/Sand LBF Mixture
(Dixon et al. 1994)

Sieve	Opening Size (mm)	% Passing
#8	2.36	100
#12	1.7	95.8-96.5
#20	0.85	89.5-90.5
#40	0.425	74.0-76.0
#70	0.212	64.3-66.0
#140	0.106	48.8-50.2
#200	0.075	48.2-49.8

(a)   (b)

Figure C1: Wykeham Farrance (a) Model 24251 Front-Loading and (b) Model 24001 Rear-Loading Consolidation Frames

C.1.3   SPECIMEN PREPARATION AND TEST SET UP

Table C3 shows the target water content and density specifications for preparation of LBF specimens. While the current OPG specification for LBF indicates that the material should be placed at a water content of 15%, it was agreed with AECL to test the material at its as-delivered water content of about 20% to 21%. Two specimens were tested using a 100 g/L $CaCl_2$ solution as the mixing water. These specimens were first air-dried and then mixed to a water content of about 21% using 100 g/L $CaCl_2$ solution. The mass of the $CaCl_2$ in the mixing solution was accounted for in the calculations of the water content and densities.

Table C3: Physical Characteristics of Engineering Barriers System Components
(after Russell and Simmons 2003)

Property	HCB	BSB	GF	DBF	LBF
Composition (dry mass %)	100% bentonite	50% bentonite 50% sand	100% bentonite	5% bentonite 25% glacial lake clay 70% crushed granite	50% bentonite 50% sand
Initial Gravimetric Water Content (%)	17	18.5	2	8.5	15
As-Placed Saturation (%)	65	80	6	80	33
Dry Density (Mg/m^3)	1.61	1.69	1.40	2.12	1.24
EMDD (Mg/m^3)$^+$	1.50	1.15	1.25	0.8	0.66

[+]   EMDD (Effective Montmorillonite Dry Density) = (mass of bentonite *montmorillonite fraction) / (volume of voids + volume of montmorillonite minerals)
– assumes that bentonite is 75% montmorillonite content

It was decided to use an initial, as-placed target specimen thickness of 10 mm. The rationale for this selection is as follows. Given that the consolidation time is proportional to the length of the longest drainage path squared (i.e., half the specimen thickness), the thinner the specimen, the shorter the testing time. Conversely, the specimen cannot be made too thin. The LBF mixture contains about 4% sand-sized particles coarser than 1.7-mm in size (see Table C2). Specimens at least 10-mm thick are required to minimize the effect that the larger sand particles may have on the compression behaviour of the specimen. Moreover, the 10-mm-thick specimen gives a diameter-height ratio of five, which tends to minimize consolidation ring wall friction effects and also allows for up to 90% swelling inside the 19-mm-high consolidation ring. The initial water content, height, dry density and EMDD of the LBF specimens prepared and tested in this program are listed in Table C4. These calculations use a specific gravity of soil solids of 2.70 for the LBF and an 80% montmorillonite content for the Saskatchewan bentonite used to make the 50/50 mix. The average initial water content, height, dry density and EMDD were 20.59%, 9.61 mm, 1.36 Mg/m^3 and 0.79 Mg/m^3, respectively.

The steps in the specimen preparation and test setup procedure are as follows:

Weigh 30.9 g of moist, as-delivered LBF mixture and place it loosely into the consolidation ring, on top of a piece of Whatman 40 Ashless filter paper. An example of a specimen of LBF placed loosely into the consolidation ring is shown in Figure C2a.

Weigh about the same amount of LBF from the same batch used to prepare the specimen and place it into the oven for initial water content determination.

Compress the specimen to a height of about 10 mm using a suitably-sized steel ram, as shown in Figure C2b. Because of the relatively low density of LBF, this compression could be carried out with hand pressure alone. The prepared specimen is shown in Figure C2c.

Using an electronic calliper, take measurements from the top of the consolidation ring to the top of the specimen to calculate an initial height of specimen. Typically about 12 measurements are taken and averaged to calculate an initial specimen thickness.

Table C4: Initial Properties of LBF Specimens

Test	Water Content (%)	Height (mm)	Dry Density (Mg/m^3)	EMDD (Mg/m^3)
HB2	21.19	10.29	1.26	0.71
HB3	21.19	10.40	1.25	0.70
HB4	19.63	10.10	1.30	0.74
HB6	21.23	9.90	1.31	0.75
HB7	21.03	9.61	1.35	0.78
HB8	20.70	8.88	1.47	0.88
HB9	20.67	10.01	1.30	0.74
HB11	20.04	9.28	1.41	0.83
HB12	20.27	9.45	1.39	0.81
HB13	20.88	9.53	1.37	0.79
HB14	20.04	9.49	1.38	0.80
HB15	20.95	9.33	1.40	0.82
HB16	20.43	8.65	1.51	0.92
HB19	20.03	9.67	1.36	0.78
Averages	20.59	9.61	1.36	0.79

(a)   (b)   (c)

Figure C2: Preparation of LBF Specimens: a) Loose LBF placed in the consolidation ring
b) Compression of the LBF specimen to the target height with a steel ram
c) Final prepared specimen before placement of the upper filter paper and loading cap.

Place a piece of Whatman 40 Ashless filter paper on the top of the specimen, install the consolidation ring and restraining ring into the consolidation cell, with the lower filter stone in place, and place the load cap with filter stone on top of the upper filter paper.
Place the assembled consolidation cell into the consolidation frame, set the dial gauge in place and, at the start of the test, apply the appropriate cell fluid (either distilled water or $CaCl_2$ solution) and weights to the lever-arm hanger system.

C.1.4   TEST MATRIX AND TEST PROCEDURES

The matrix of tests listed in Table C5 was carried out to meet the program objectives outlined in the main report. Six loading/wetting paths using the mixing and consolidation cell reservoir water as listed in Table C5 were followed.

The objectives of the LBF 1-D compression testing program were to:

Examine and compare the 1-D swelling/compression response under different loading/wetting paths. Three loading/wetting paths were examined:

compression/swelling behaviour of the LBF after 20% initial swelling during water uptake

compression/swelling behaviour of the LBF after water uptake under confined conditions followed by 20% swelling

compression/swelling behaviour of the LBF after water uptake under confined conditions

These loading/wetting boundary conditions are meant to encompass and bound those expected in the repository setting.

Examine and compare the 1-D swelling/compression response with distilled reservoir water, 100 g/L $CaCl_2$ and 200 g/L $CaCl_2$ reservoir solutions.

Examine and compare the 1-D swelling/compression response of LBF mixed with fresh water with LBF mixed with 100 g/L $CaCl_2$.

For path 1, the LBF was allowed to swell to a target value of 20% strain during initial distilled water uptake from the reservoir. Specimen swelling was closely monitored after the cell reservoir was filled and the loads on the hanger were adjusted accordingly to allow the specimen to swell to the target value. It was not necessary to let the specimen equilibrate under each of these loads as the 20% expansion was approached, but rather to get as close as possible to the target 20% expansion and then let the specimen equilibrate under the final applied load in this sequence. Table C5 indicates that the actual initial swelling strains achieved for the tests carried out for path 1 ranged from 19.5% to 22.4%.

Once equilibrium between the applied stress and specimen swelling was achieved, the loads on the specimens were increased using a load increment ratio of about 1 (i.e. doubling of the applied load with each increment). Following loading to the maximum stresses indicated in Table C5, the specimens were unloaded in stages. Each load and unload increment was generally applied until the vertical deformation rate was less than about 0.02 mm/day.

Path 2a and 2b differed from path 1 in that the specimens for path 2a were rigidly confined during water uptake and then loaded and the specimens for path 2b were rigidly confined during

water uptake, allowed to swell to about 20% strain and then loaded. The load and unload increments were applied in the same manner as for path 1 and distilled water was used in the reservoir.

Path 3 was intended to be the same as path 1 except that 100 g/L $CaCl_2$ solution was used as the reservoir water rather than distilled water. The intent was to allow these specimens to swell to a target value of 20% strain during initial solution uptake followed by loading of the specimens. As indicated in Table C5, however, the specimens only swelled to between about 6% and 10% strain, and this was under unloaded (unrestrained) conditions. For these specimens, once the maximum amount of swelling was achieved and the specimens came to equilibrium, they were loaded and unloaded in the same manner as the specimens for paths 1, 2a and 2b.

Table C5: Test Matrix and Loading/Wetting Paths

Path	Test	Mixing Water	Reservoir Water	Swell on Initial Water Uptake (%)	Loading Sequence
1	HB3	As supplied by AECL	Distilled	19.5	Load to 1326 kPa after initial swelling
	HB5[+]				
	HB6			20.8	Load to 3987 kPa after initial swelling
	HB8			22.4	Load to 2652 kPa after initial swelling
2a	HB1[+]	As supplied by AECL	Distilled		
	HB2			Rigidly confined	Load to 2651 kPa
	HB4				Load to 2654 kPa
2b	HB7	As supplied by AECL	Distilled	Rigidly confined	Unload, let swell to 21.2%, load to 3986 kPa
	HB9				Unload, let swell to 21.4%, load to 2659 kPa
3	HB11	As supplied by AECL	100 g/L $CaCl_2$	10.4	Load to 3990 kPa after initial swelling
	HB12			7.5	Load to 2675 kPa after initial swelling
	HB17 & HB 18[+]				
	HB19			6.3	Load to 2660 kPa after initial swelling
4	HB10*	As supplied by AECL	100 g/L $CaCl_2$		
	HB14			Rigidly confined	Unload, let swell to 3.6%, load to 4000 kPa
5	HB13	100 g/L $CaCl_2$	100 g/L $CaCl_2$	6.4	Load to 2650 kPa after initial swelling
	HB15			7.1	Load to 3985 kPa after initial swelling
6	HB16	As supplied by AECL	200 g/L $CaCl_2$	6.1	Load to 2650 kPa after initial swelling

[+] Tests discontinued prematurely due to equipment problems
*   HB10 - initial trial to test the unrestrained swelling ability of the LBF with 100 g/L $CaCl_2$ reservoir fluid

Path 4 was intended to be the same as path 2b except that 100 g/L CaCl$_2$ solution was used as the reservoir water rather than distilled water. After initial solution uptake with the specimen rigidly confined, the intent was to allow this specimen to swell to a target value of 20% strain, followed by loading of the specimen. As shown in Table C5, however, the specimen only swelled to 3.6% strain, and this was under essentially unloaded conditions. Once the maximum amount of swelling was achieved and the specimen came to equilibrium, the specimen was loaded and unloaded in the same manner as the specimens for the other paths.

Path 5 was set up to examine the effect of using 100 g/L CaCl$_2$ solution as both the LBF mixing water and reservoir water. The response of the specimens in this path could then be directly compared with the response of the path 3 specimens, which used 100 g/L CaCl$_2$ solution as the reservoir water only. The intent, as with path 3, was to allow these specimens to swell to a target value of 20% strain during initial solution uptake followed by loading of the specimens. As shown in Table C5, however, the specimens only swelled to between about 6% and 7% strain, and this was under essentially unloaded conditions. For these specimens, once the maximum amount of swelling was achieved and the specimens came to equilibrium, they were loaded and unloaded in the same manner as the specimens for the other paths.

Path 6 was set up to examine the effect of using a reservoir CaCl$_2$ solution concentration of 200 g/L. The response of the specimens in this path could then be directly compared with the response of the path 3 specimens, which used a reservoir CaCl$_2$ solution concentration of 100 g/L. The intent, as with path 3, was to allow these specimens to swell to a target value of 20% strain during initial solution uptake followed by loading of the specimens. As shown in Table C5, however, the specimens only swelled to about 6% strain, and this was under essentially unloaded conditions. For these specimens, once the maximum amount of swelling was achieved and the specimens came to equilibrium, they were loaded and unloaded in the same manner as the specimens for the other paths.

Once equilibrium was achieved under the last unloading increment of the test, the cell was quickly disassembled and the final height of the specimen was measured using an electronic calliper. As with the initial height, typically about 12 measurements were made and averaged to obtain the final specimen height. Next, the consolidation ring containing the specimen and the top and bottom filter papers was weighed and then placed in the oven for drying. The next day the consolidation ring containing the oven-dry specimen and filter papers was weighed. These weights were used to calculate the specimen mass, final water content, void ratio, degree of saturation and dry density.

Calibration tests were carried out to determine the dry and wet masses and dry and wet thickness of the filter paper used in these tests. Repeat calibration tests showed excellent reproducibility of the filter paper masses and thickness, and these masses and thickness were used in calculating the specimen heights and masses for all stages of the test.

Masses to determine the mass of solids for the specimens using CaCl$_2$ solution for mixing and reservoir water were corrected for the mass of CaCl$_2$ in the pore fluid.

C.2 RESULTS

The specimen height versus time graphs for all of the loading and unloading increments for the tests are included in Addendum I. The applied stress for each of the loading and unloading increments is indicated. These graphs show that there is significant hysteresis in the specimen height when comparing the loading/compression with the unloading/swelling responses. This

hysteresis is much more pronounced in the tests using $CaCl_2$ as the reservoir fluid as opposed to the tests using distilled water as the reservoir fluid. For example, compare the response of test HB9, which used distilled water (Figure CI-7 in Addendum I), with the response of test HB11, which used 100 g/L $CaCl_2$ as the reservoir fluid (Figure CI-8 in Addendum I). In addition, several loading and unloading increments were left on for extended time periods to examine the potential for longer term creep. The 663 kPa loading increment of test HB9, the 2660 kPa loading increment of test HB11, the 336 kPa loading increment of test HB12, the 663 kPa loading increment of test HB9, the 1326 kPa unloading increment of test HB13 and the 165 kPa loading increment of test HB15 indicate that long term creep is negligible for this material under these test conditions.

Values of vertical strain, void ratio, dry density, coefficient of volume compressibility (m_v), hydraulic conductivity (k) and EMDD for the loading and unloading increments of the tests are tabulated in Addendum II. The equilibrium height for each loading and unloading increment was used to calculate the vertical strain, void ratio, dry density and EMDD for the increment.
The coefficient of volume compressibility (m_v) was calculated for a loading increment using the equation:

$$m_v = \frac{1}{1 + e_0}\left(\frac{e_0 - e_1}{\sigma_1' - \sigma_0'}\right)$$
(C2)

where e_0 is the void ratio corresponding to σ_0', the initial effective stress for the increment, and e_1 is the void ratio corresponding to σ_1', the final effective stress for the increment.

The t_{90} values (time to 90% consolidation) used for calculating the c_v (coefficient of consolidation) values for the increments were determined using the square root of time graphical construction method (ASTM 1998). Hydraulic conductivity values were calculated for the increments using the equation:

$$k = c_v\,(m_v)\,\gamma_w$$
(C3)

where c_v and m_v are as defined previously and γ_w is the unit weight of water. For some of the square root of time versus compression graphs t_{90} values could not be properly identified. The m_v and k values are not given for those increments. Figure C3 shows an example of a specimen height versus square root of time graph.
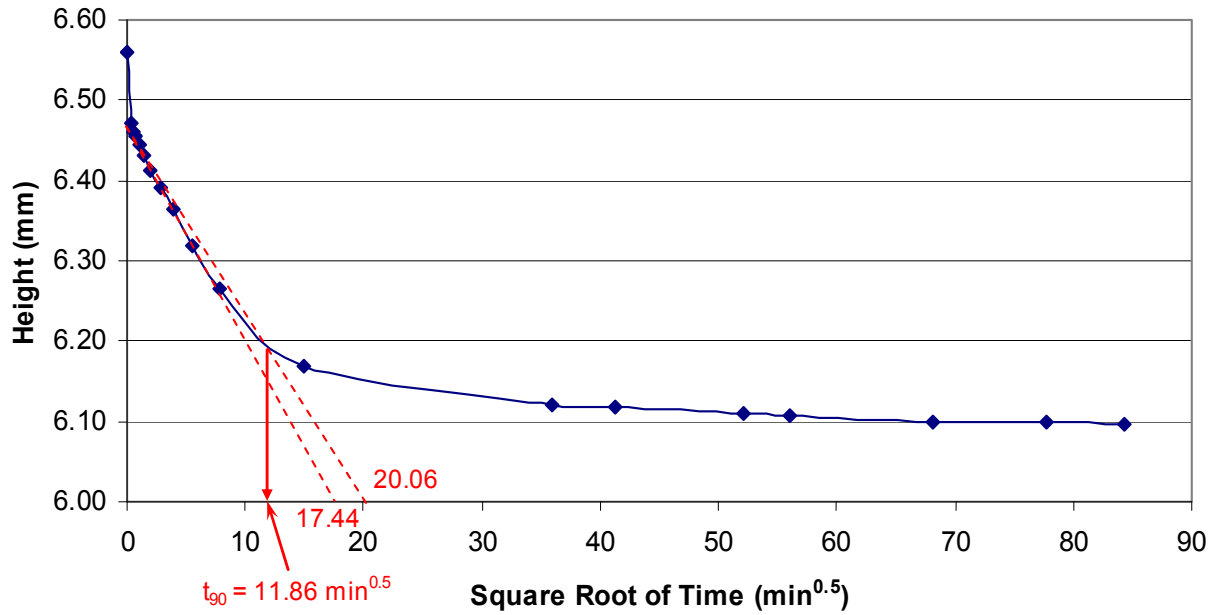
Figure C3: Example Height Versus Square Root of Time Graph This load increment is from Test HB 14 with an applied stress of 2673 kPa on the loading path.

Relationships between EMDD and swelling pressure (Figure C4) and between EMDD and hydraulic conductivity (Figure C5) for bentonite clays with permeants of varying salinity have been included for comparison with the data generated in this project. These relationships are from Dixon et al. (2002). It is important to note that solutions of NaCl were used as the saline permeant rather than $CaCl_2$.
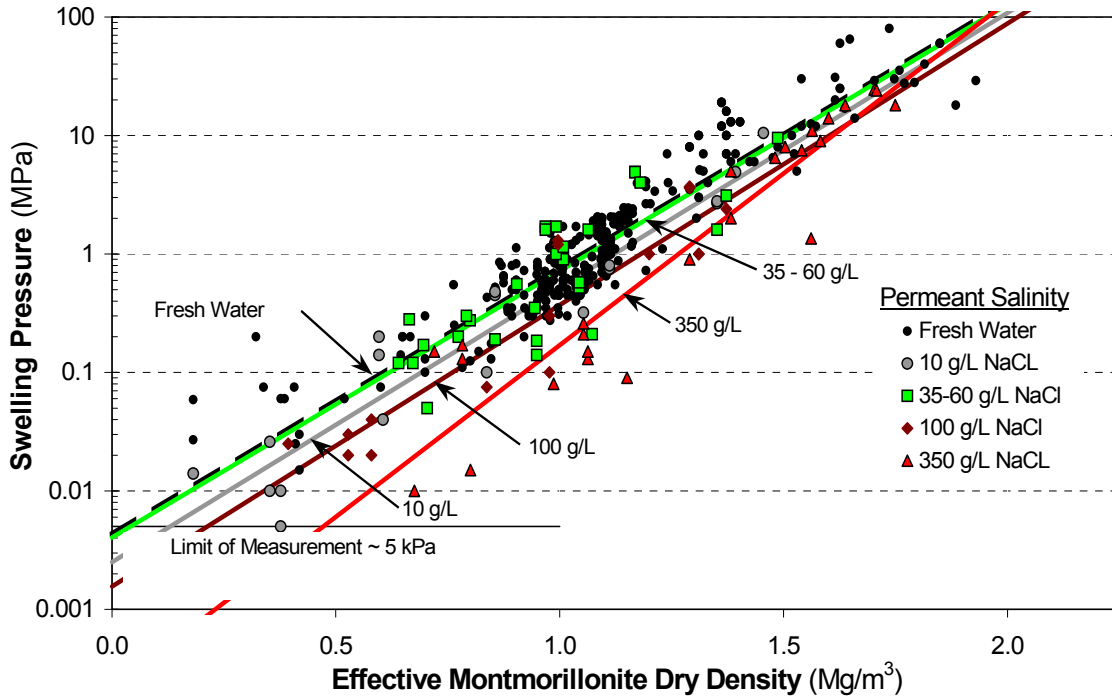
Figure C4: Relationship between Swelling Pressure and EMDD for Bentonite Clays with Varying Salinities (Dixon et al. 2002)
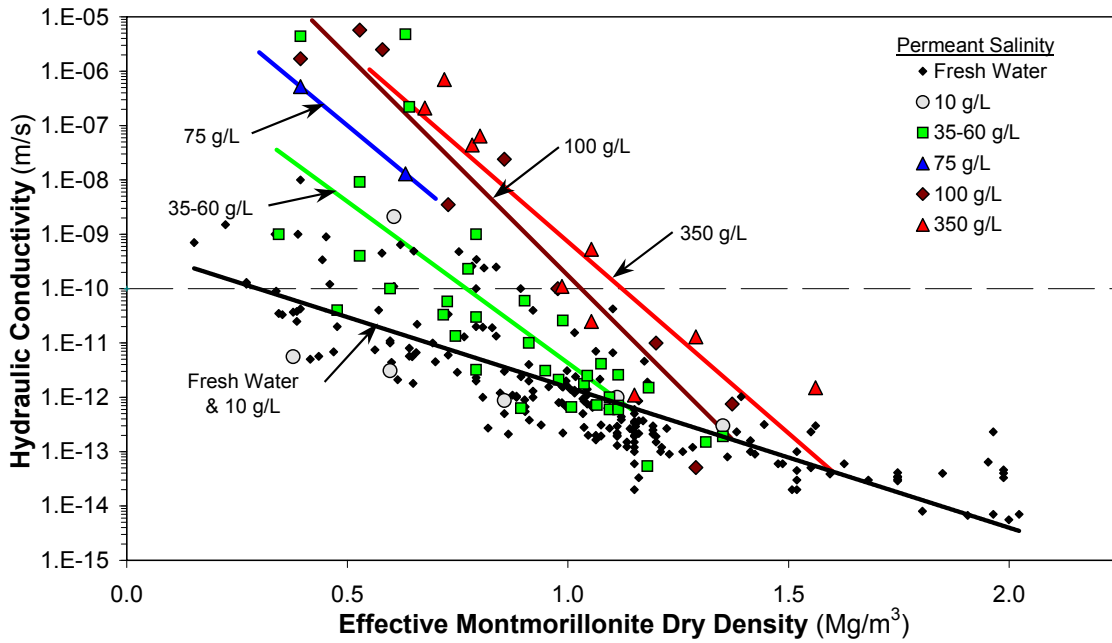
Figure C5: Relationship between EMDD and Hydraulic Conductivity in Bentonite-Based Materials with Varying Salinity (Dixon et al. 2002)

C.2.1   EMDD VERSUS APPLIED PRESSURE

Figure C6 shows the loading/compression and unloading/swelling responses for tests conducted following paths 1, 2a and 2b. All tests used fresh water as the reservoir fluid. The Dixon et al. (2002) trend lines for fresh water and 100 g/L NaCl from Figure C4 have been superimposed on this figure. The figure shows that the trend-line fit of the loading/compression data for paths 1, 2a and 2b tend to follow the trend of the Dixon et al. (2002) trend line for fresh water. Trend lines for paths 1 and 2b, which allowed about 20% swelling prior to loading/compression, are virtually identical while the trend line for path 2a, which did not allow swelling prior to loading/compression, trends above the other two paths. The unloading/swelling trend lines for paths 1 and 2b have about the same slope as the loading compression path trend lines, but the vertical pressures for the same EMDD value are significantly lower. This indicates that there is significant hysteresis in the loading/compression and unloading/swelling paths, as discussed previously. Insufficient unloading/swelling data were collected for path 2a to make a definitive conclusion regarding this response.
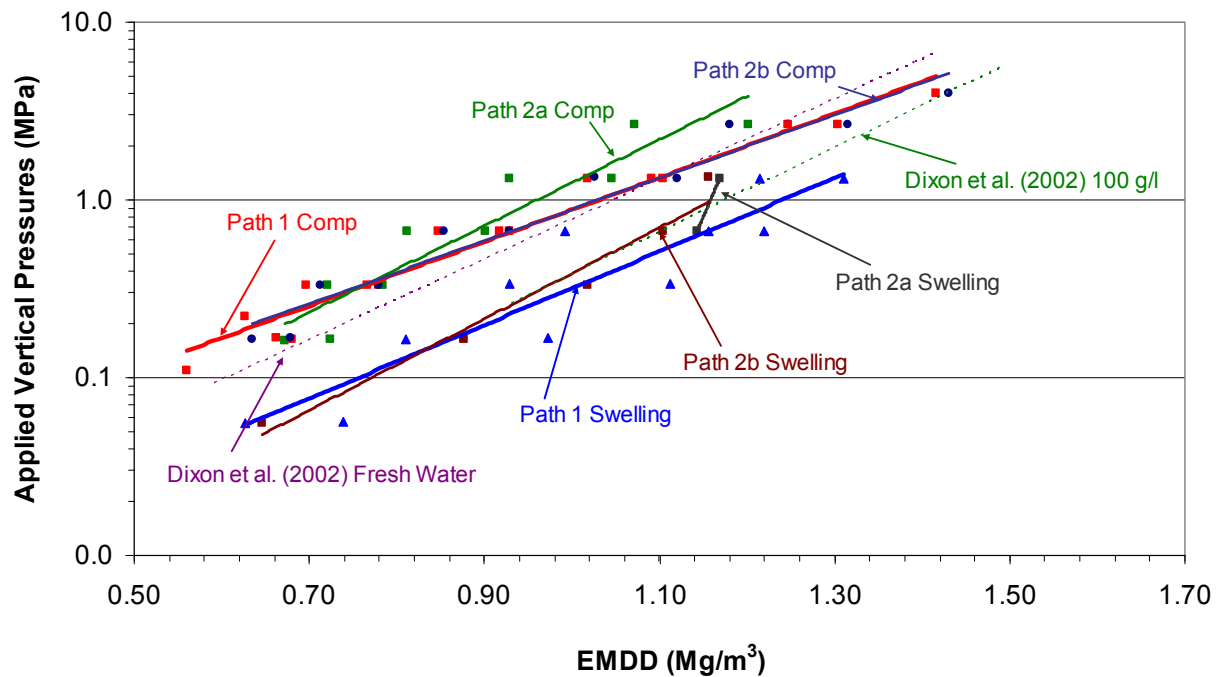
Figure C6: EMDD versus Applied Vertical Pressure for Paths 1, 2a and 2b

Figure C7 compares the loading/compression and unloading/swelling responses for paths 1 and 3. Path 1 used fresh water as the reservoir fluid while path 3 used 100 g/L $CaCl_2$ solution as the reservoir fluid. Figure C7 illustrates the distinct behaviour in both the loading/compression and unloading/swelling responses when 100 g/L $CaCl_2$ solution is used as the reservoir fluid as opposed to fresh water. The path 3 vertical pressures for the same EMDD value are substantially lower than the path 1 pressures and lower than the Dixon et al. (2002) trend line for 100 g/L NaCl. Conversely, the LBF specimens exposed to 100 g/L $CaCl_2$ solution undergo significantly more compression, with significantly higher EMDD values for the same applied vertical pressures. The swelling or recovery to lower EMDD values on the unloading/swelling

path is also significantly suppressed by the 100 g/L $CaCl_2$ solution. Very significant hysteresis is apparent in loading/compression and unloading/swelling responses for path 3. It is important to note that the path 3 loading/compression and unloading/swelling trend lines were fit to the results of tests HB11, HB12 and HB19. The loading/compression trend line has a correlation coefficient (r^2) value of 0.98 and the unloading/swelling trend line has a correlation coefficient (r^2) value of 0.93, indicating strong correlation of the results of the three tests and excellent repeatability of the response.
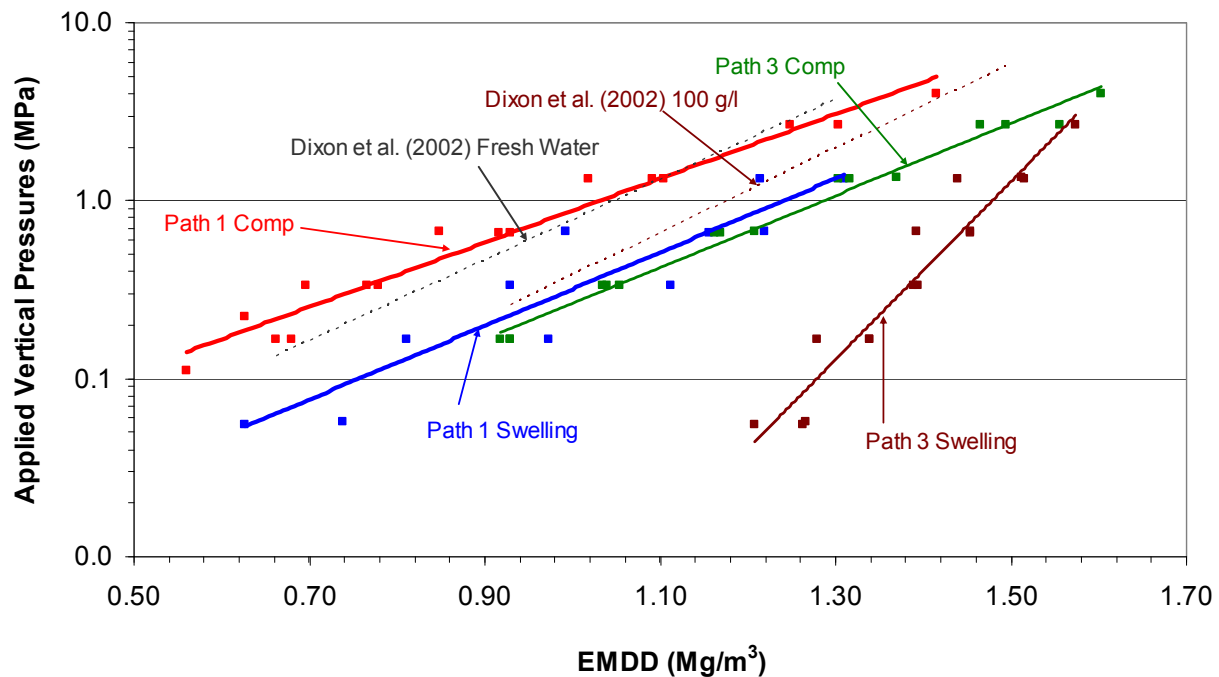
Figure C7: EMDD versus Applied Vertical Pressure for Paths 1 and 3

Figure C8 shows the loading/compression and unloading/swelling responses for paths 3, 4 and 5. Paths 3, 4 and 5 used 100 g/L $CaCl_2$ solution as the reservoir fluid. Path 5 also used 100 g/L $CaCl_2$ solution as the mixing fluid. Paths 3 and 5 allowed for swelling on fluid uptake while for path 4 the specimen was kept rigidly confined during fluid uptake.

Figure C8 shows that while the general trends of behaviour for paths 3, 4 and 5 are similar and deviate significantly from the responses that used fresh water as the reservoir fluid, the use of 100 g/L $CaCl_2$ solution as the mixing fluid (path 5) tended to decrease the amount of compression for the loading/compression path, with correspondingly higher EMDD values on the unloading/swelling path. Conversely, path 5 gave higher applied vertical pressures at a given EMDD than path 3 for both the loading/compression and unloading/swelling paths. This indicates that the effects of the 100 g/L $CaCl_2$ reservoir solution were somewhat suppressed by preconditioning (i.e., mixing) the LBF mixture with the same solution. The initially restrained path 4 specimen showed the largest compression on the loading/compression path, with the correspondingly lowest vertical pressures for the same values of EMDD.

Figure C9 shows the loading/compression and unloading/swelling responses for paths 3 and 6. Path 3 used 100 g/L $CaCl_2$ solution as the reservoir fluid while path 6 used 200 g/L $CaCl_2$

solution as the reservoir fluid. Figure C9 shows that increasing the $CaCl_2$ concentration in the reservoir fluid from 100 g/L to 200 g/L does not have a significant effect on the loading/compression and unloading/swelling responses of the LBF.
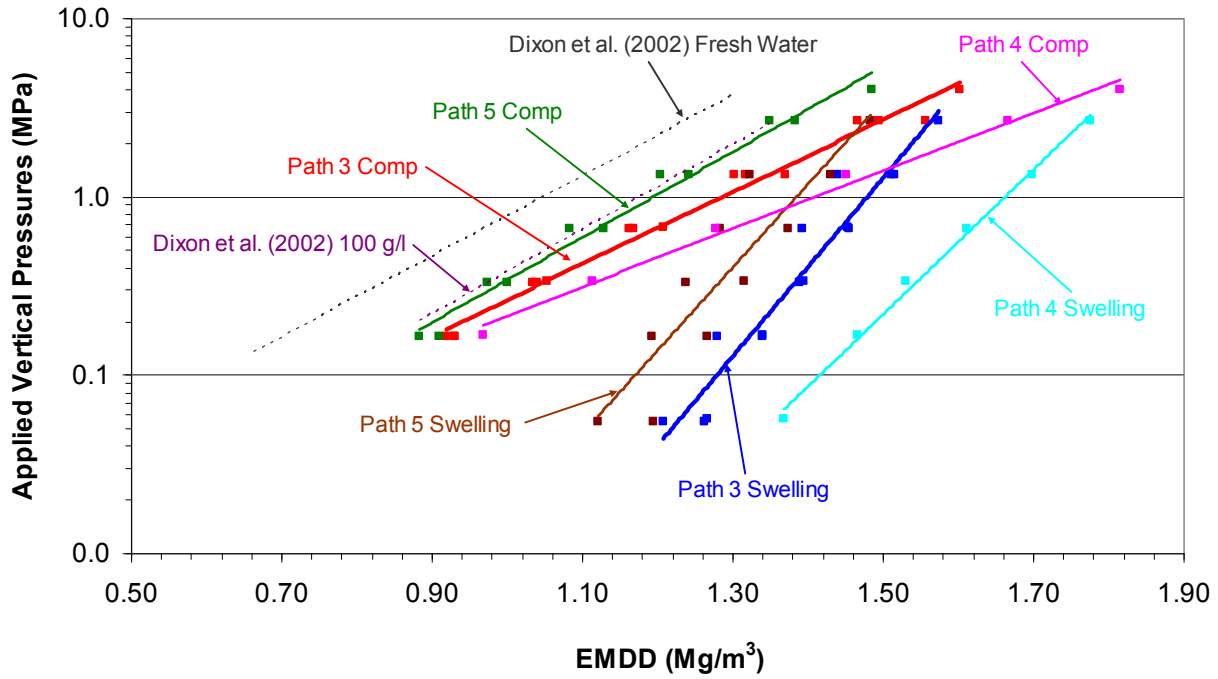
Figure C8: EMDD versus Applied Vertical Pressure for Paths 3, 4 and 5
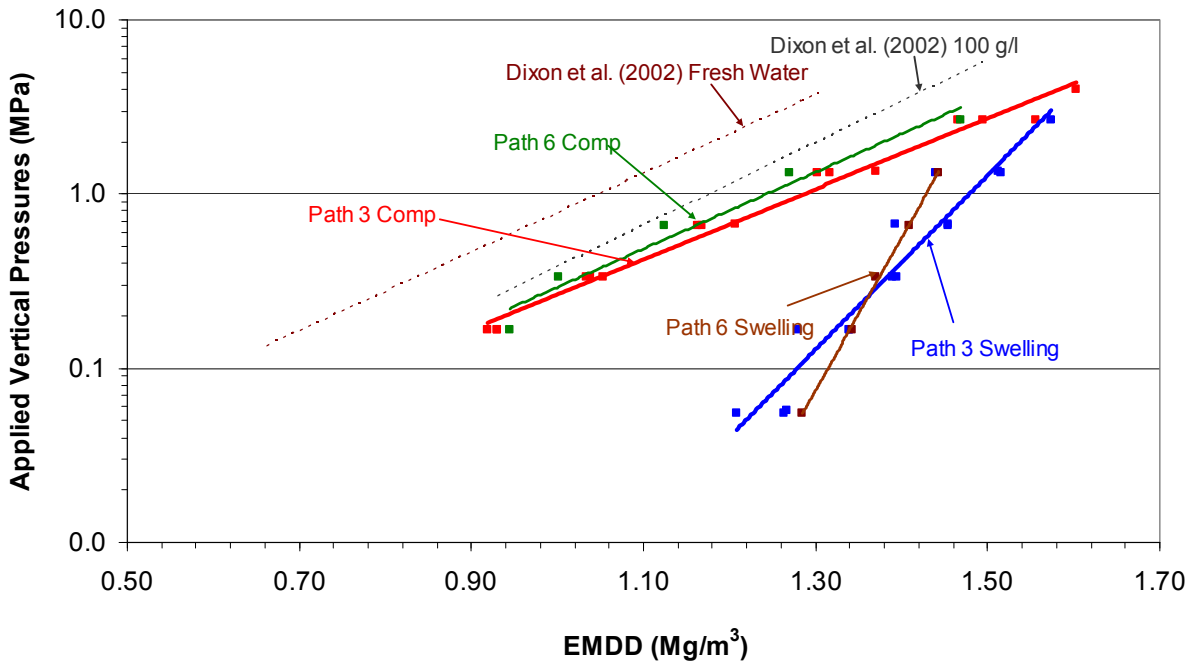
Figure C9: EMDD versus Applied Vertical Pressure for Paths 3 and 6

The loading/compression and unloading/swelling data for all paths are summarized on Figures C10 and C11, respectively.
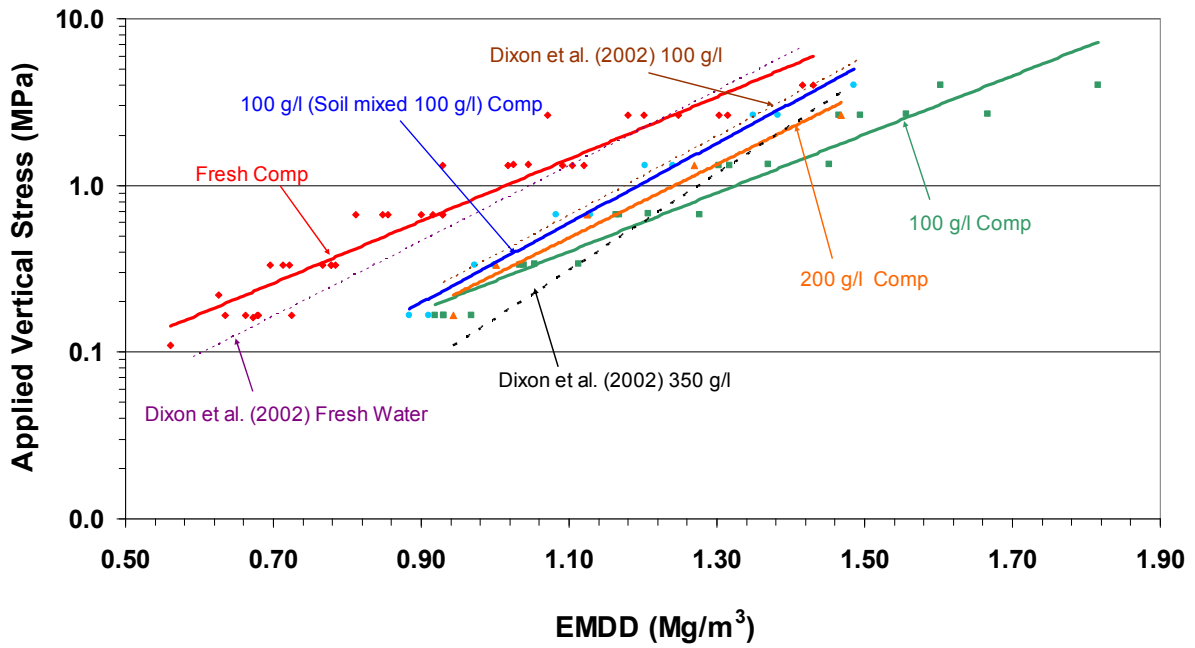
Figure C10: EMDD versus Applied Vertical Pressure for all Loading Path Data
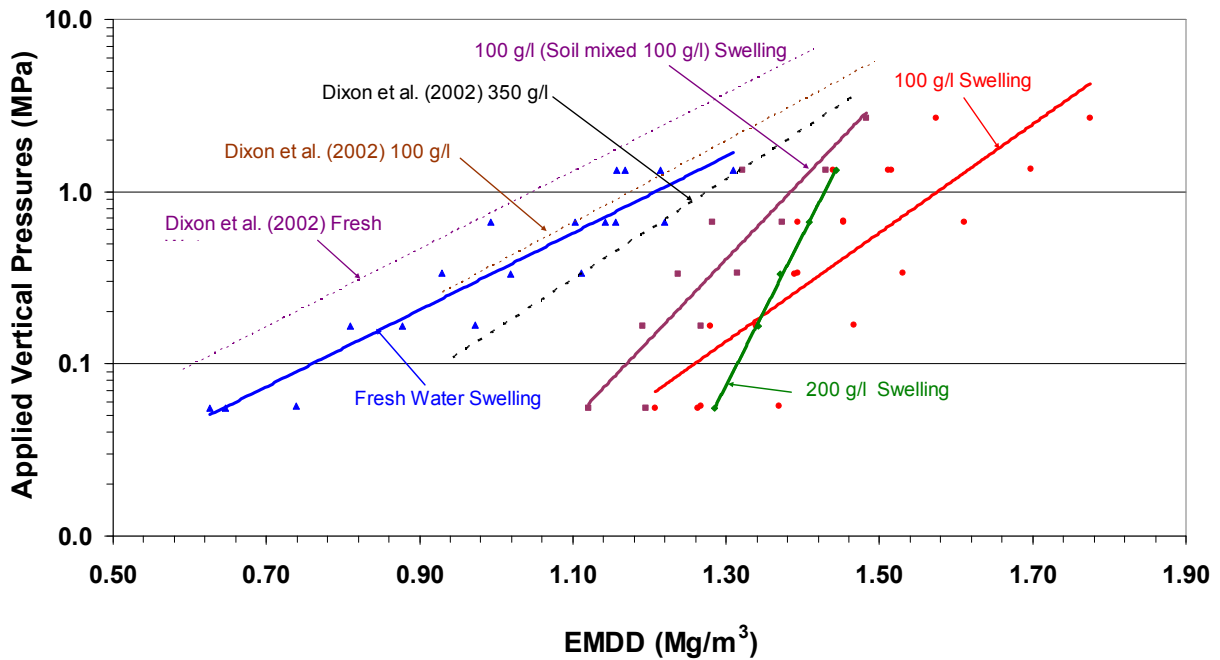
Figure C11: EMDD versus Applied Vertical Pressure for all Unloading Path Data

C.2.2 EMDD VERSUS HYDRAULIC CONDUCTIVITY

Figure C12 shows the hydraulic conductivity values for loading/compression and unloading/swelling for paths 1, 2a and 2b. All tests used fresh water as the reservoir fluid. The Dixon et al. (2002) trend lines for fresh water (including 10 g/L) and 100 g/L NaCl from Figure C5 have been superimposed on this figure. The figure shows that the trend lines for the loading/compression hydraulic conductivity data for paths 1 and 2b tend to follow the trend of the Dixon et al. (2002) trend line for fresh water. Path 2a, which did not allow swelling prior to loading/compression, trends below the other two paths with lower hydraulic conductivity values. The unloading/swelling hydraulic conductivity data for paths 1 and 2b have about the same slope as the loading compression hydraulic conductivity data, but the hydraulic conductivity values for the same EMDD value are generally lower.
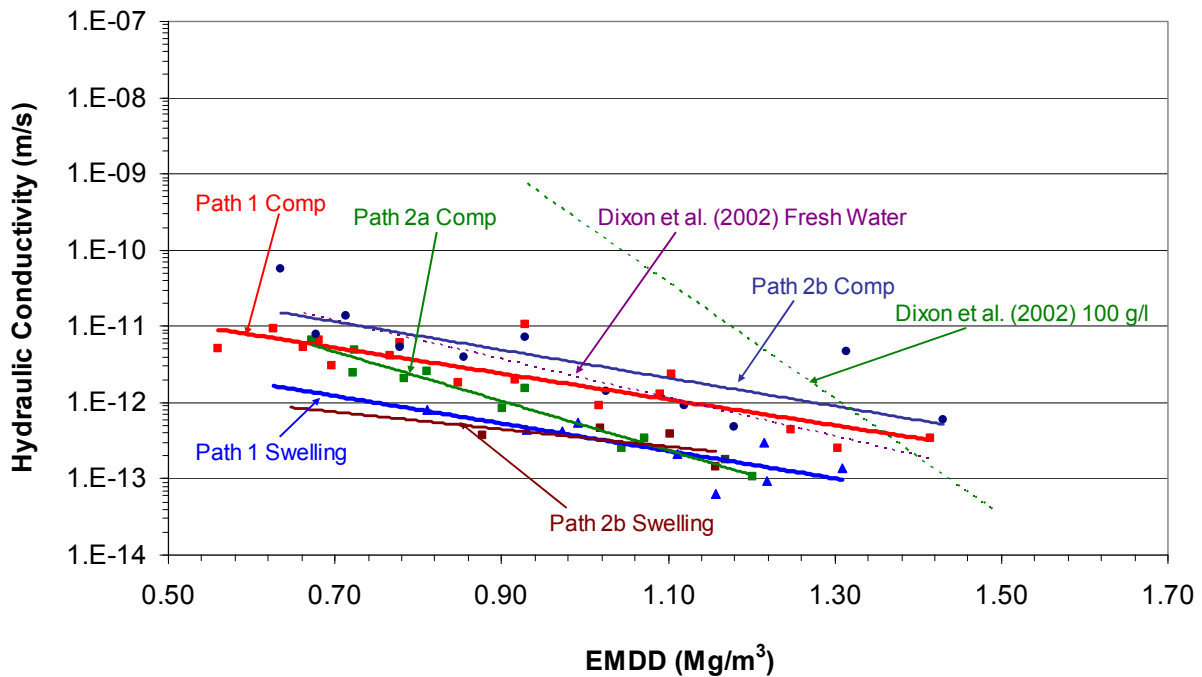
Figure C12: EMDD versus Hydraulic Conductivity for Paths 1, 2 and 2a

Figure C13 shows the hydraulic conductivity values for loading/compression and unloading/swelling for paths 1 and 3. Path 1 used fresh water as the reservoir fluid while path 3 used 100 g/L $CaCl_2$ solution as the reservoir fluid.

The path 3 loading/compression hydraulic conductivity values in Figure C13 are substantially higher than the path 1 hydraulic conductivity values for the same EMDD and are generally higher than the Dixon et al. (2002) trend line for 100 g/L NaCl. Hydraulic conductivity values for unloading/swelling for path 3 have about the same trend as the trend lines for path 1.

Figure C14 shows the hydraulic conductivity values for loading/compression and unloading/swelling for paths 3, 4 and 5. The trends in hydraulic conductivity for loading/compression and unloading/swelling for paths 4 and 5 are very similar to the trends already described for path 3. Path 5, for which 100 g/L $CaCl_2$ solution was used as the mixing

fluid, has slightly lower hydraulic conductivity values for loading/compression than paths 3 and 4, particularly at the higher range of EMDD.
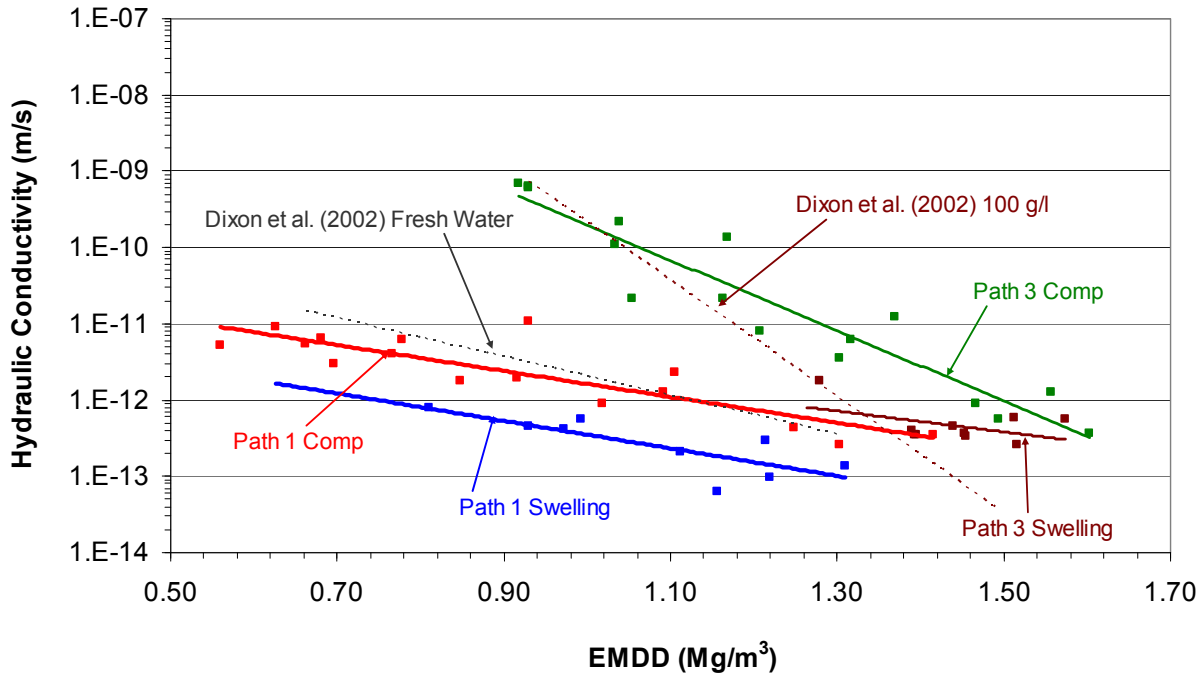
Figure C13: EMDD versus Hydraulic Conductivity for Paths 1 and 3
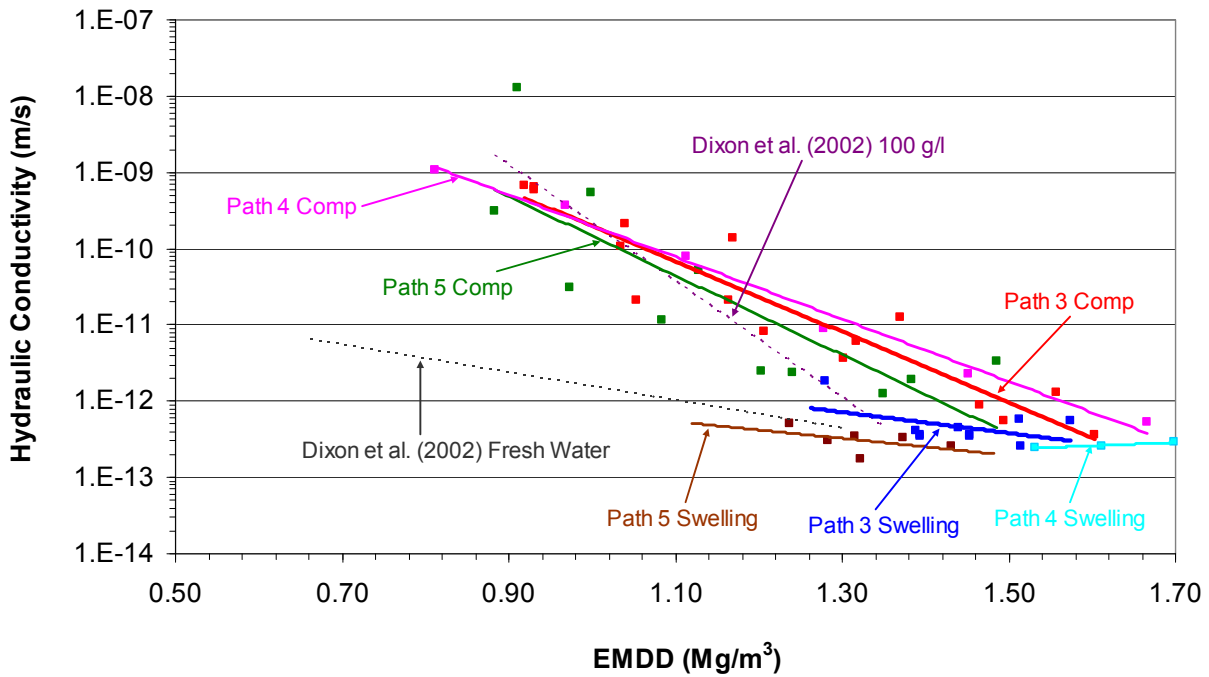
Figure C14: EMDD versus Hydraulic Conductivity for Paths 3, 4 and 5

Figure C15 shows the hydraulic conductivity values for loading/compression and unloading/swelling for paths 3 and 6. Trends in hydraulic conductivity for loading/compression and unloading/swelling for path 6, for which 200 g/L $CaCl_2$ solution was used as the reservoir fluid, do not differ significantly from the path 3 trends. This tends to follow the trends of Figure C5 where there is not a significant difference in the hydraulic conductivity data for 100 and 350 g/L NaCl.

EMDD versus hydraulic conductivity data for all loading/compression and unloading/swelling paths are given in Figures C16 and C17, respectively.
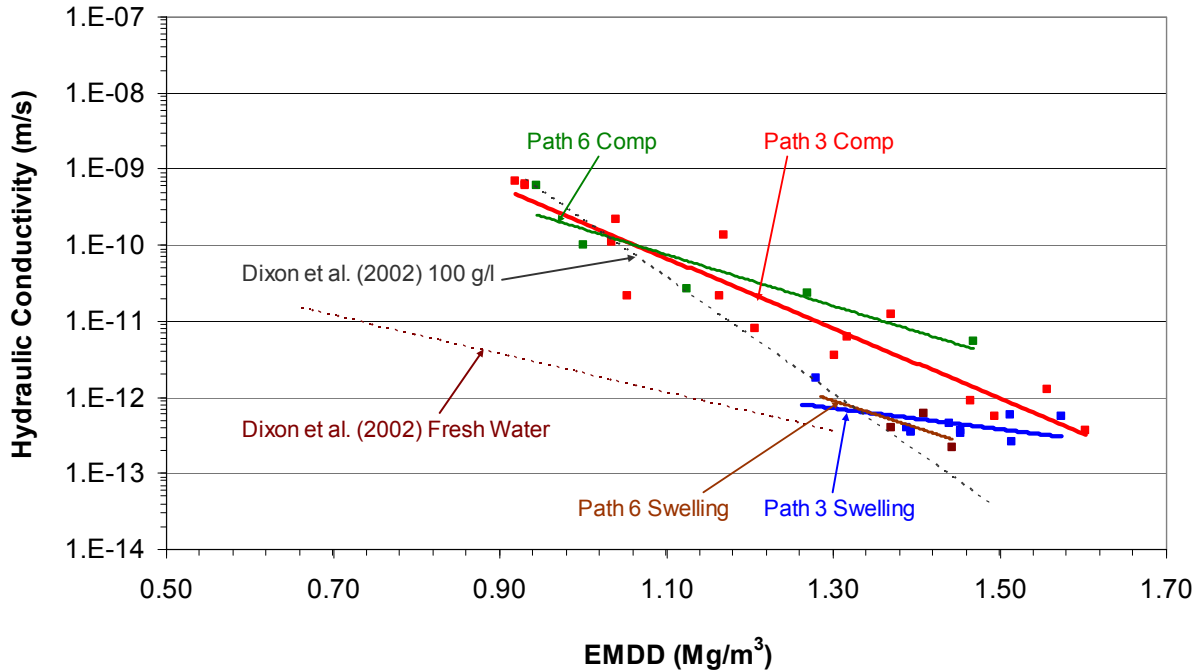
Figure C15: EMDD versus Hydraulic Conductivity for Paths 3 and 6
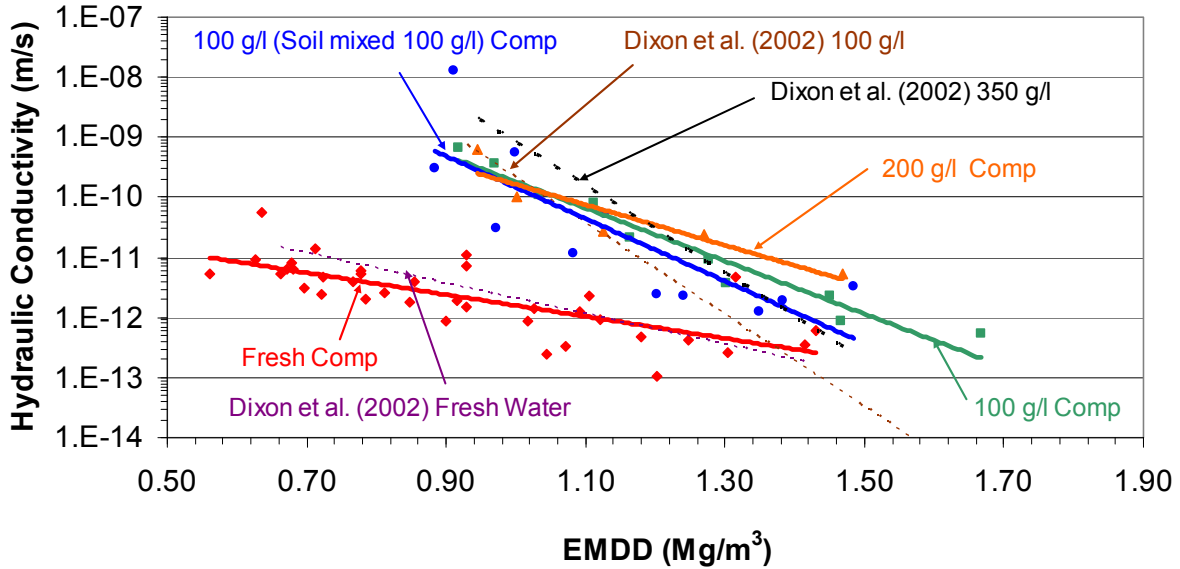
Figure C16: EMDD versus Hydraulic Conductivity for all Loading Path Data
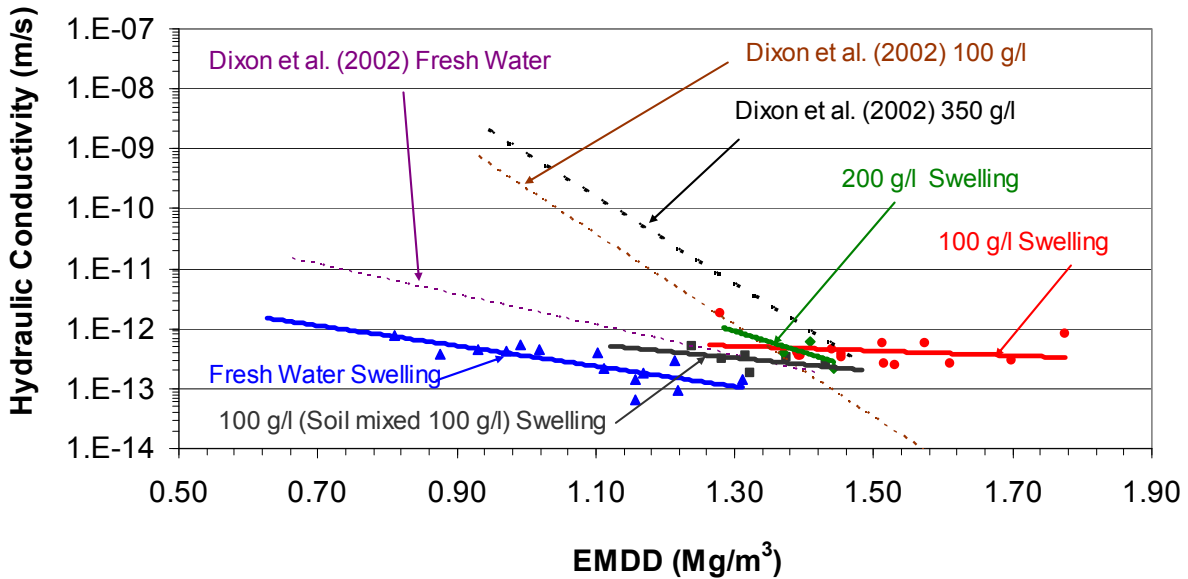
Figure C17: EMDD versus Hydraulic Conductivity for all Unloading Path Data

C.2.3   SWELLING CAPACITY OF LBF

Figure C18 illustrates the distinctly different swelling response of the LBF specimens with fresh water in the reservoir versus either 100 g/L or 200 g/L $CaCl_2$ solution in the reservoir. The specimens with fresh water in the reservoir achieved swelling strains of about 20% under applied vertical stresses of 55 kPa while the specimens with 100 g/L or 200 g/L $CaCl_2$ solution in the reservoir achieved only about 6% to 10% swelling strain under essentially unrestrained

conditions. Also note that the swelling occurred rapidly in the specimens with CaCl$_2$ solution in the reservoir as opposed to the specimens with fresh water in the reservoir. Comparison of the HB15 and HB16 graphs shows that there is not a significant difference in swelling behaviour between the specimens with 100 g/L and 200 g/L CaCl$_2$ solution in the reservoir. This follows what is shown in Figures C9 and C15 and the discussion in Section C2.2.

C.2.4 VOID RATIO VERSUS APPLIED PRESSURE

Graphs of void ratio versus applied vertical pressure (with pressure plotted to a logarithmic scale) for Paths 1 through 6 are shown in Figures C19 through C24, respectively. These graphs show similar trends in behaviour to the EMDD versus applied pressure graphs described in Section C2.1. In particular, the tests with distilled water in the consolidation cell reservoir (Paths 1 and 2 – Figures C19 and C20) show distinctly different behaviour than the tests with CaCl$_2$ in the cell reservoir (Paths 3, 4, 5 and 6 – Figures C21, C22, C23 and C24). Tests with distilled water in the reservoir have higher void ratios at the same stress levels and have less pronounced hysteresis, particularly at lower stress levels on the unloading/swelling path, than tests with CaCl$_2$ in the cell reservoir. Figure C25 illustrates this point with a direct comparison between Path 1 (Test HB6) and Path 3 (Test HB19). Figures C21 and C23 for Paths 3 and 5, respectively, also illustrate the high level of repeatability of loading/compression and unloading/swelling responses of the LBF with CaCl$_2$ in the cell reservoir.
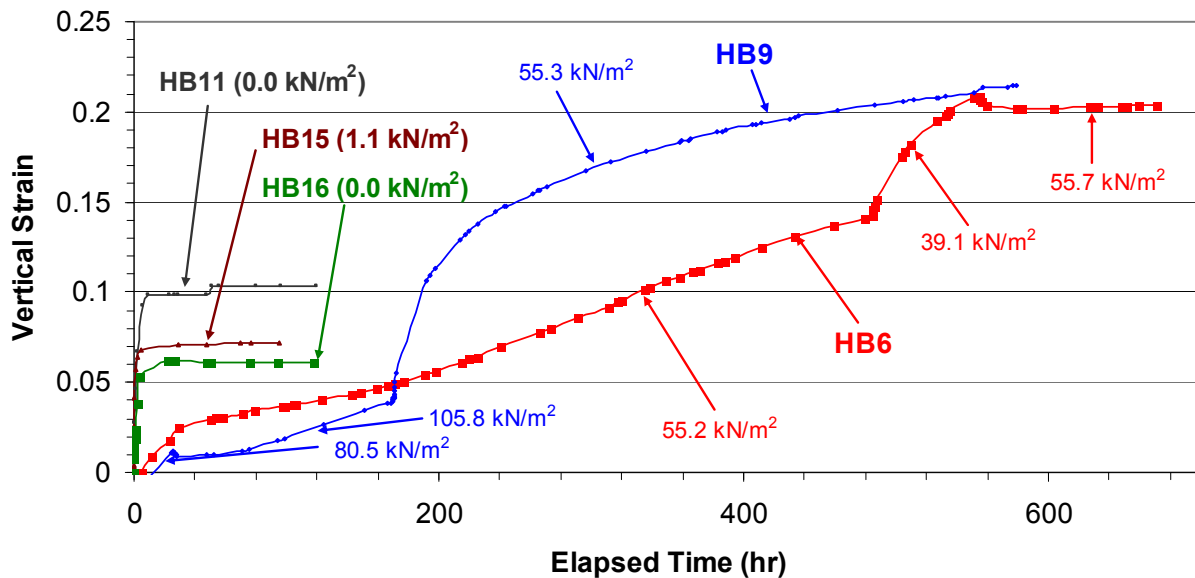
Figure C18: Strain versus Time for Tests with Fresh Reservoir Water (HB6 and HB9), with 100g/L CaCl$_2$ Reservoir Solution (HB11 and HB15) and with 200g/L CaCl$_2$ Reservoir Solution (HB16)
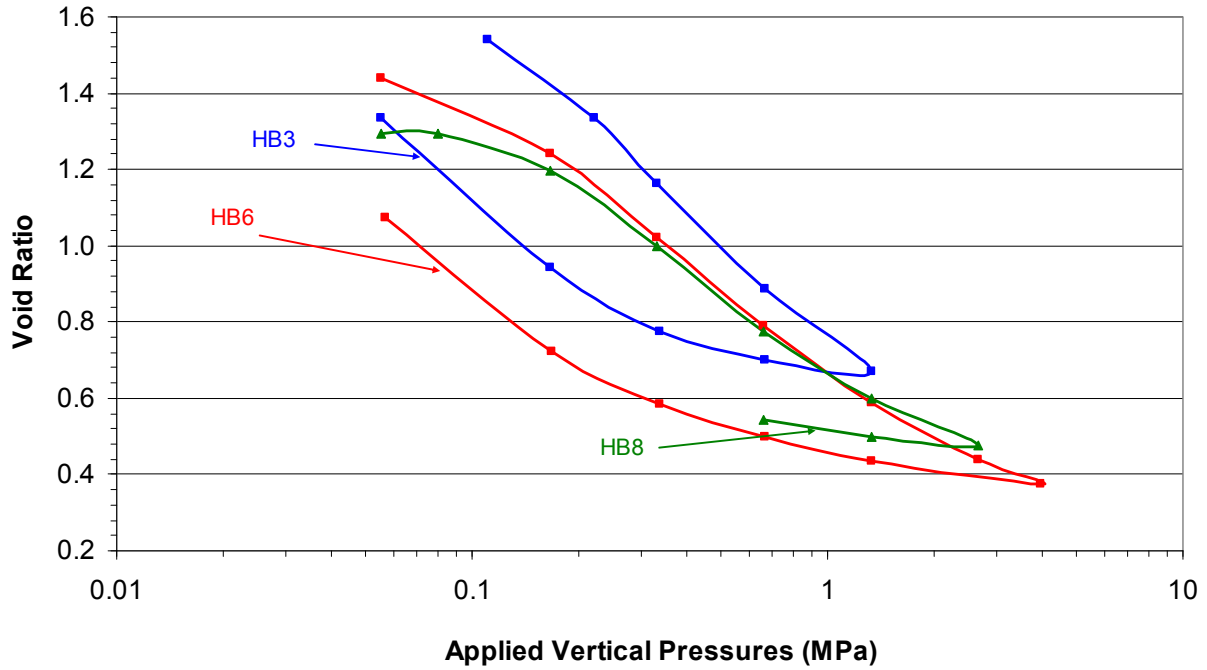
Figure C19: Applied Vertical Pressure versus Void Ratio for Path 1 Tests
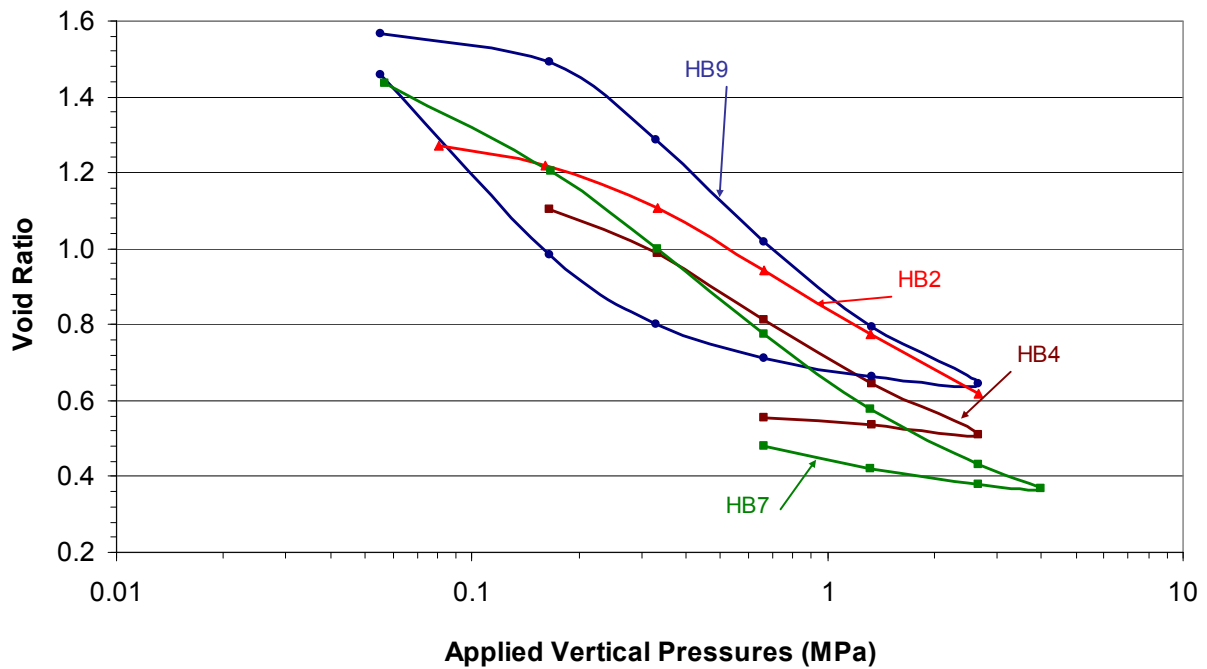
Figure C20: Applied Vertical Pressure versus Void Ratio for Path 2 Tests
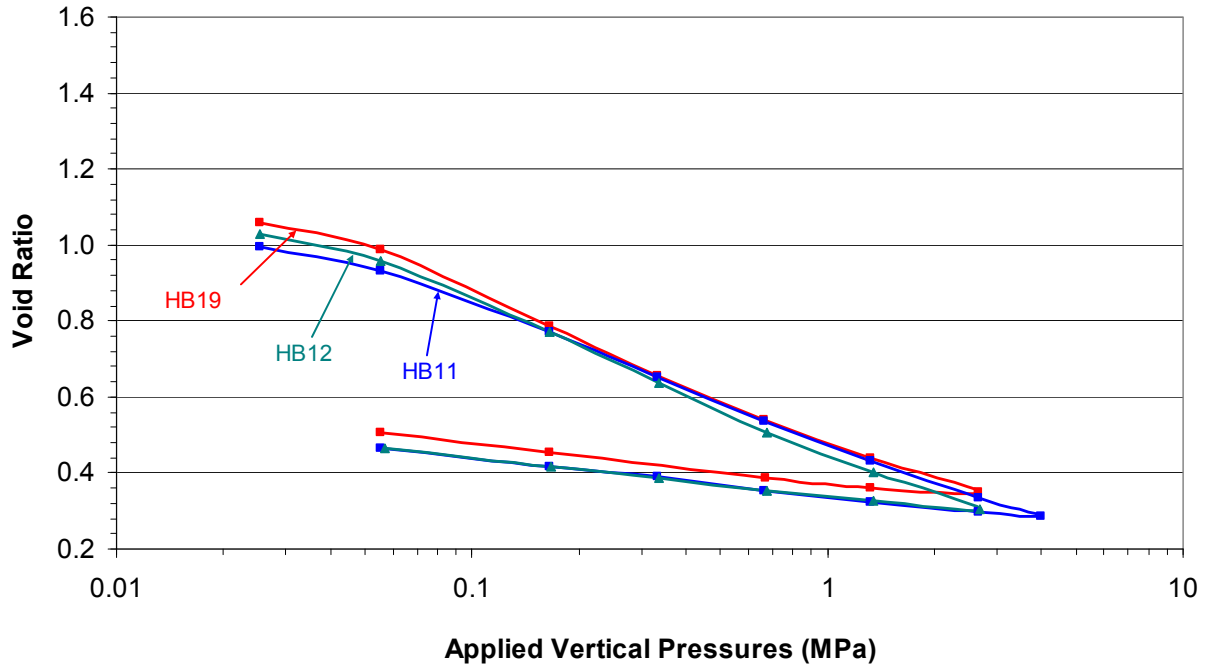
Figure C21: Applied Vertical Pressure versus Void Ratio for Path 3 Tests
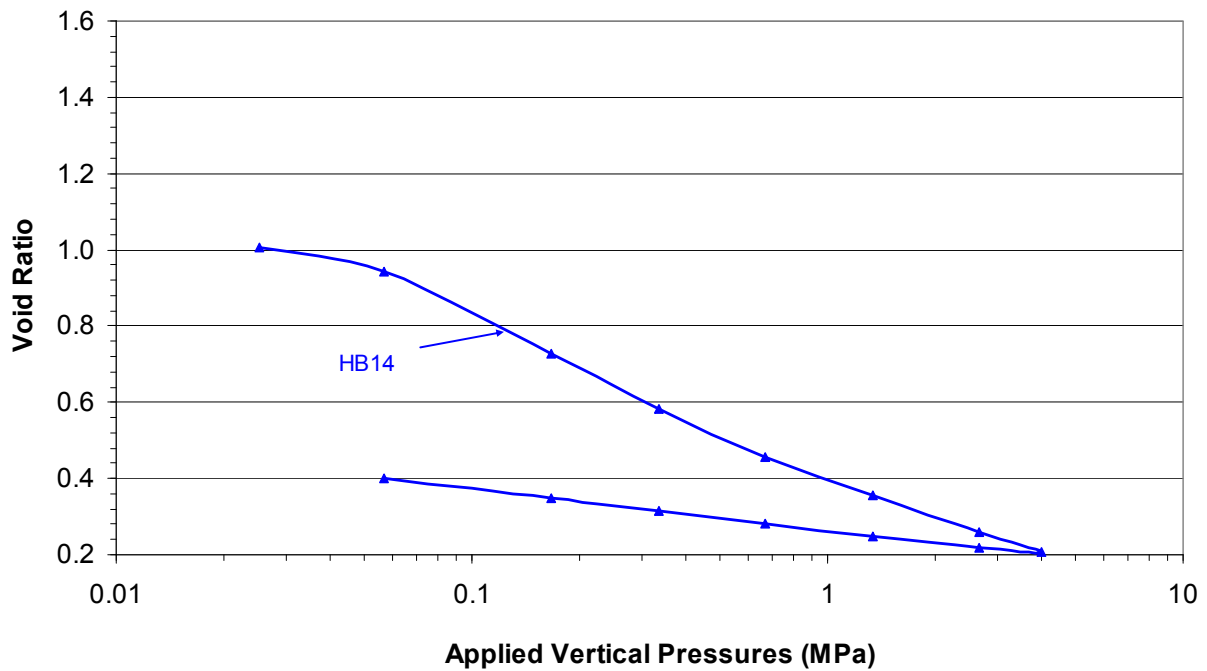
Figure C22: Applied Vertical Pressure versus Void Ratio for Path 4 Test
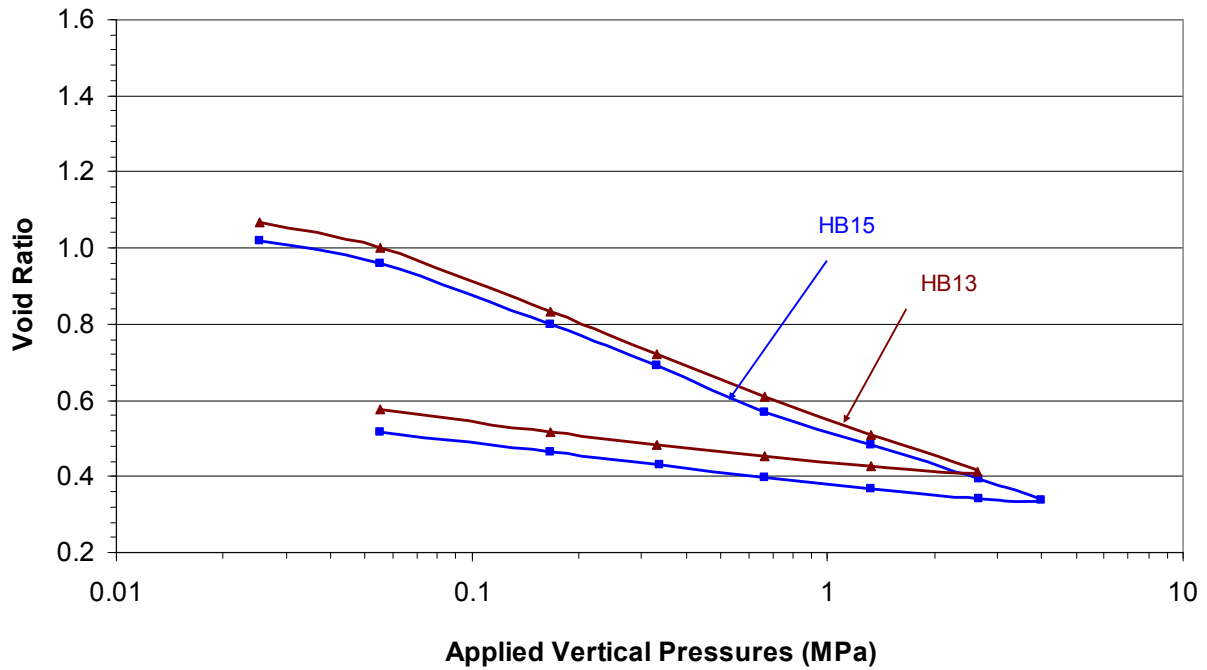
Figure C23: Applied Vertical Pressure versus Void Ratio for Path 5 Tests
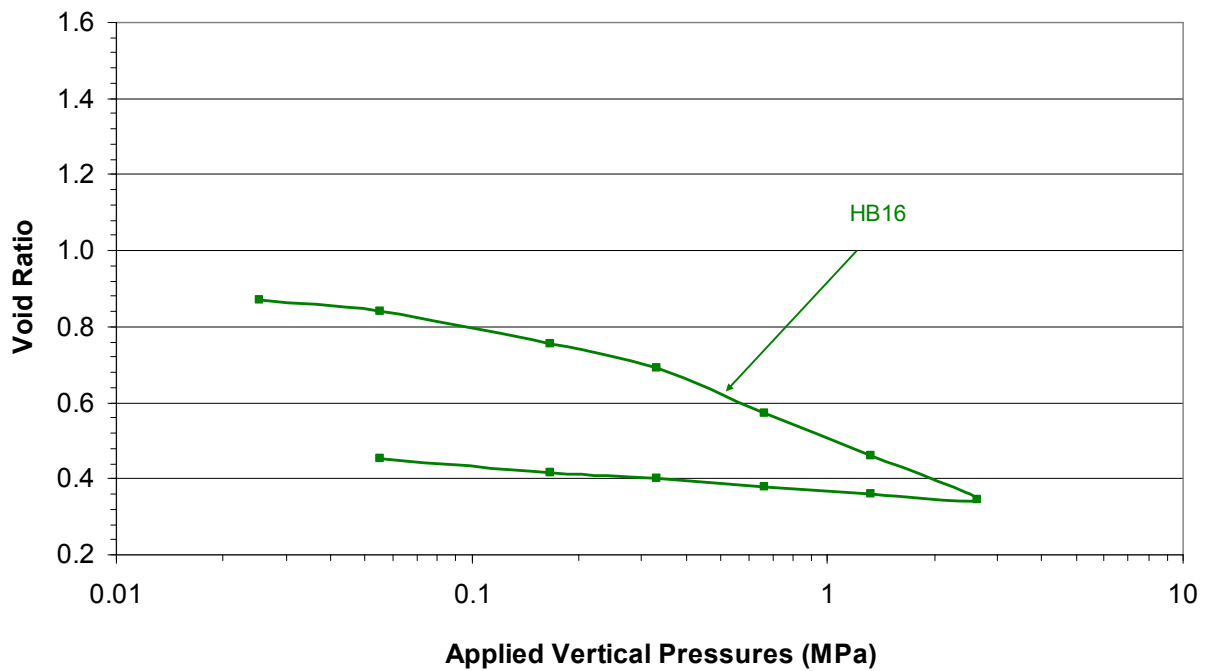
Figure C24: Applied Vertical Pressure versus Void Ratio for Path 6 Test
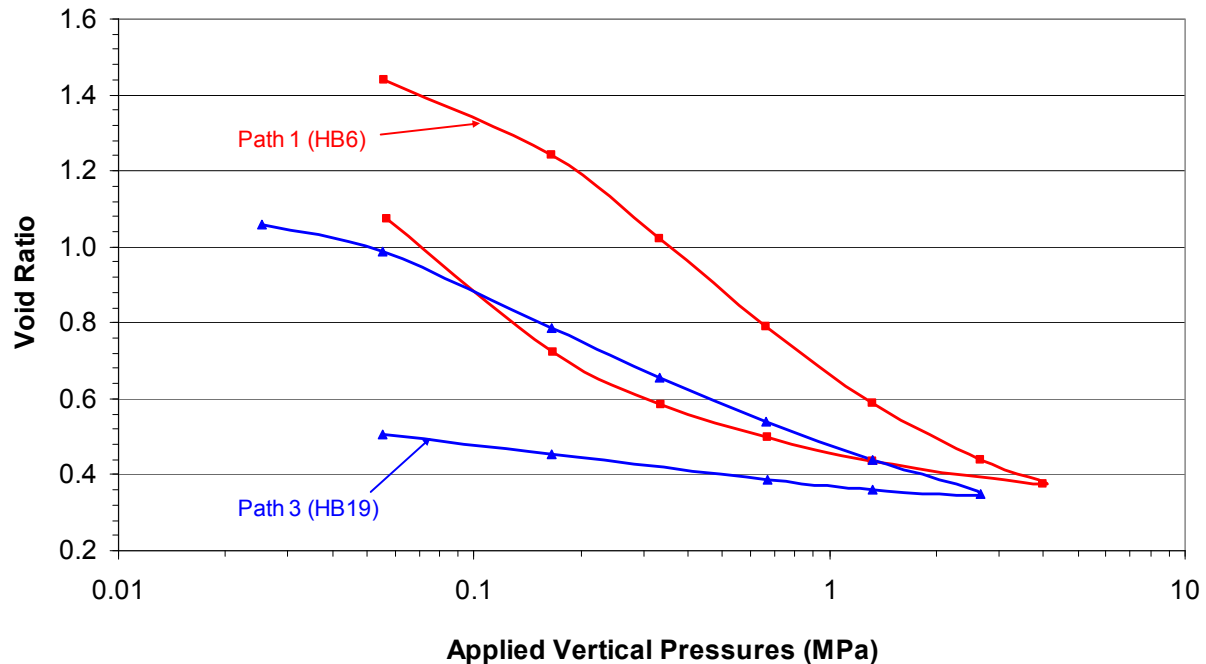
Figure C25: Applied Vertical Pressure versus Void Ratio for Path 1 Test HB6 and Path 3 Test HB19

C.3   SUMMARY

This series of tests examined the 1-D compression and swelling behaviour of LBF material under different loading and wetting paths and using different mixing and consolidation cell reservoir fluids. Following are key results and observations of this test program.

1. The test results show linear relationships between the logarithm of vertical applied pressure and EMDD and the logarithm of hydraulic conductivity and EMDD, both for loading/compression and unloading/swelling paths. The relationships between vertical applied pressure and EMDD and hydraulic conductivity and EMDD follow the form presented by Dixon et al. (2002).

2. The tests show that the relationship between vertical applied pressure and EMDD and the hydraulic conductivity and EMDD are non-unique for a given permeant salinity. These relationships also depend on loading path and stress and strain history. All of the tests showed significant hysteresis between the loading/compression and unloading/swelling paths. The hysteresis was more pronounced in the tests that used $CaCl_2$ in the consolidation cell reservoir.

3. The compression, swelling and hydraulic behaviour of LBF with 100 g/L or 200 g/L $CaCl_2$ cell reservoir solution is distinctly different than the behaviour of LBF with distilled water in the cell reservoir. The LBF is much more compressible with 100 g/L or 200 g/L $CaCl_2$ cell reservoir solution and its swelling capability and hydraulic performance are adversely affected. Graphs of void ratio versus the logarithm of applied vertical pressure show that tests with distilled water in the reservoir have higher void ratios at the same stress levels and

have less pronounced hysteresis, particularly at lower stress levels on the unloading/swelling path, than tests with $CaCl_2$ in the cell reservoir. Based on comparisons with the Dixon et al. (2002) data, the effects appear more pronounced than with NaCl used as the permeant. While it could be argued that this difference may be somewhat due to the difference between the tests used to generate the data presented in Dixon et al. (2002) and the tests used for this study, the potential impact of high salinity, Ca-rich solutions on the hydraulic and mechanical performance of LBF needs further study.

4. Increasing the cell reservoir $CaCl_2$ solution concentration from 100 g/L to 200 g/L does not create a significant difference in the compression, swelling and hydraulic response of LBF. The change in compression, swelling and hydraulic response is much more pronounced in the change from distilled water to 100 g/L cell reservoir fluid.

5. Preconditioning (i.e. mixing) the LBF mixture with the same $CaCl_2$ solution as contained in the cell reservoir, in this case with a $CaCl_2$ concentration of 100 g/L, somewhat suppresses the compression, swelling and hydraulic behaviour of LBF. This should be studied further.

ACKNOWLEDGEMENTS

REFERENCES

ASTM. 1998. Standard Test Method for One-Dimensional Consolidation Properties of Soils – D 2435-90. Annual Book of ASTM Standards, Vol. 04.08, American Society for Testing and Materials, Philadelphia.

Dixon, D.A., S.L. Campbell and D.S. Hnatiw. 1994. Pre-placement quality control and as-placed properties of the buffer materials used in the URL Isothermal Buffer Experiment. Atomic Energy of Canada Limited Technical Record, TR-612, COG-94-35.*

Dixon, D.A., N.A. Chandler and P. Baumgartner. 2002. The influence of groundwater salinity and interfaces on the performance of potential backfilling materials. Proc. 6th Intl. Workshop on Design and Construction of Final Repositories, Brussels, Belgium, Mar. 2002.

Graham, J., N.C. Chandler, D.A. Dixon, P.J. Roach, T. To and A.W.L. Wan. 1997. The Buffer Container Experiment: Results, Synthesis, Issues. Atomic Energy of Canada Limited Report, AECL-11746, COG-97-46-I.*

Russell, S.B. and G.R. Simmons. 2003. Engineered barrier system for a deep geologic Repository. In Proc. 2003 International High-Level Radioactive Waste Management Conference, Las Vegas, USA, 2003 March 30 – April 02.

* Available from SDDO, Atomic Energy of Canada Limited, Chalk River Laboratories, Chalk River, Ontario K0J 1J0.

ADDENDUM I:
SPECIMEN HEIGHT VERSUS TIME GRAPHS
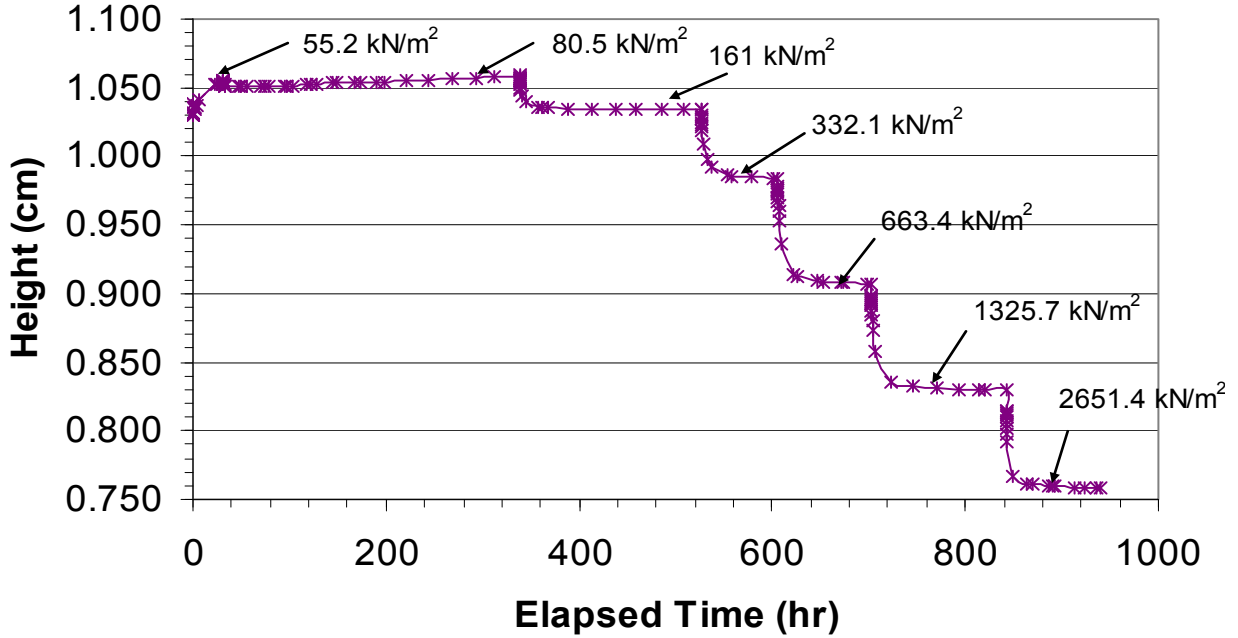
Figure CI-1: Test HB2 Specimen Height vs. Time (stress increments are labelled)
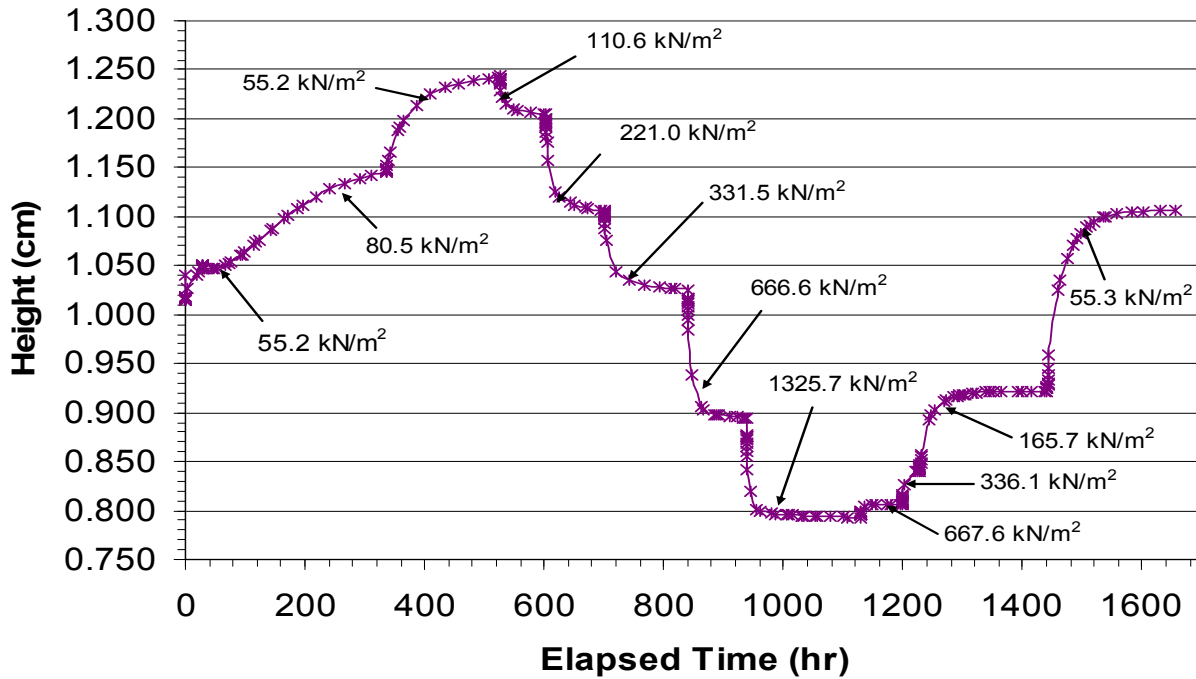
Figure CI-2: Test HB3 Specimen Height vs. Time (stress increments are labelled)
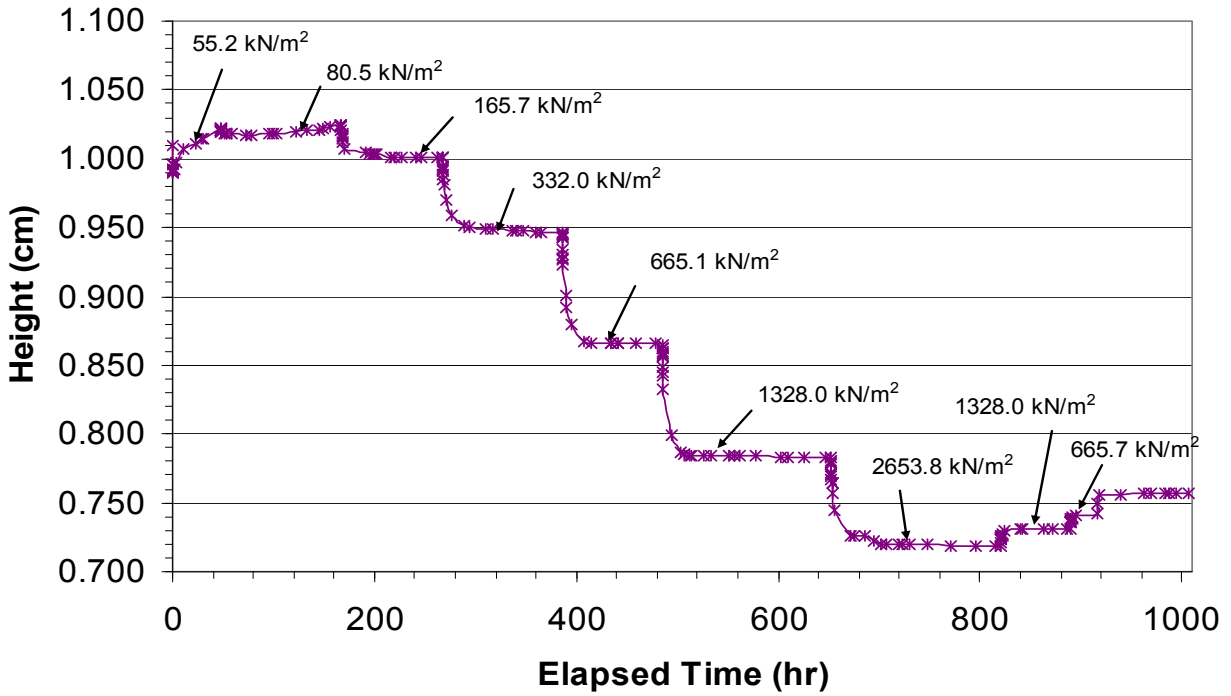
Figure CI-3: Test HB4 Specimen Height vs. Time (stress increments are shown)
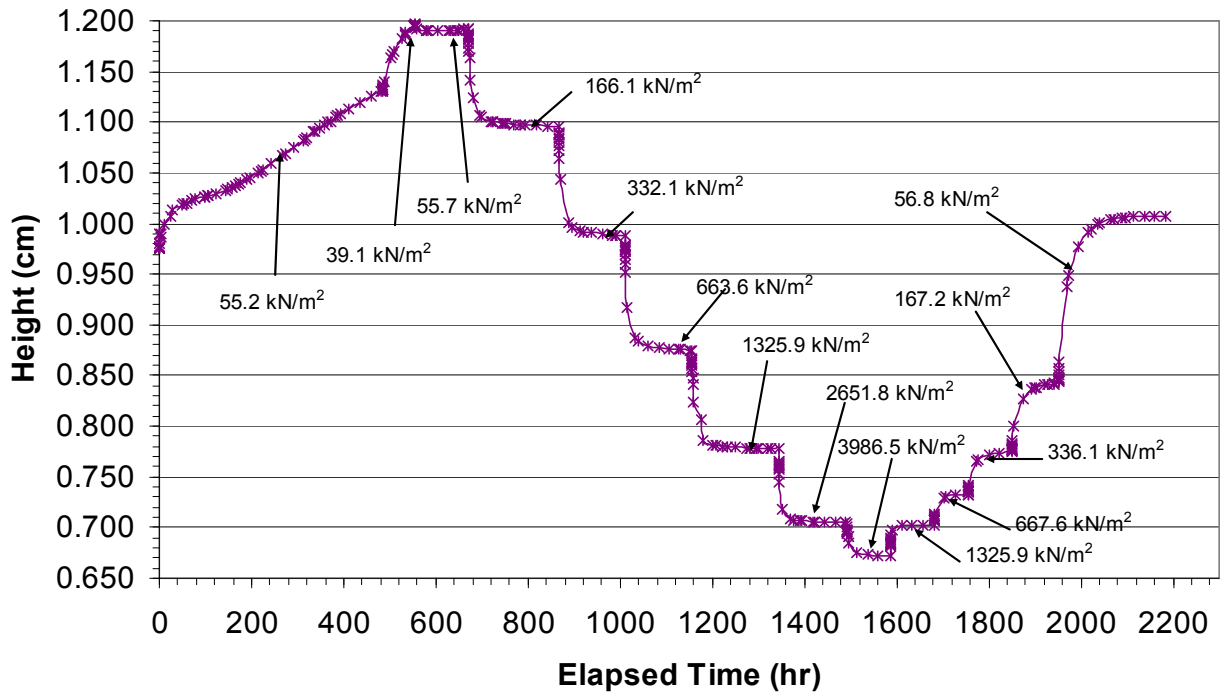
Figure CI-4: Test HB6 Specimen Height vs. Time (stress increments are labelled)
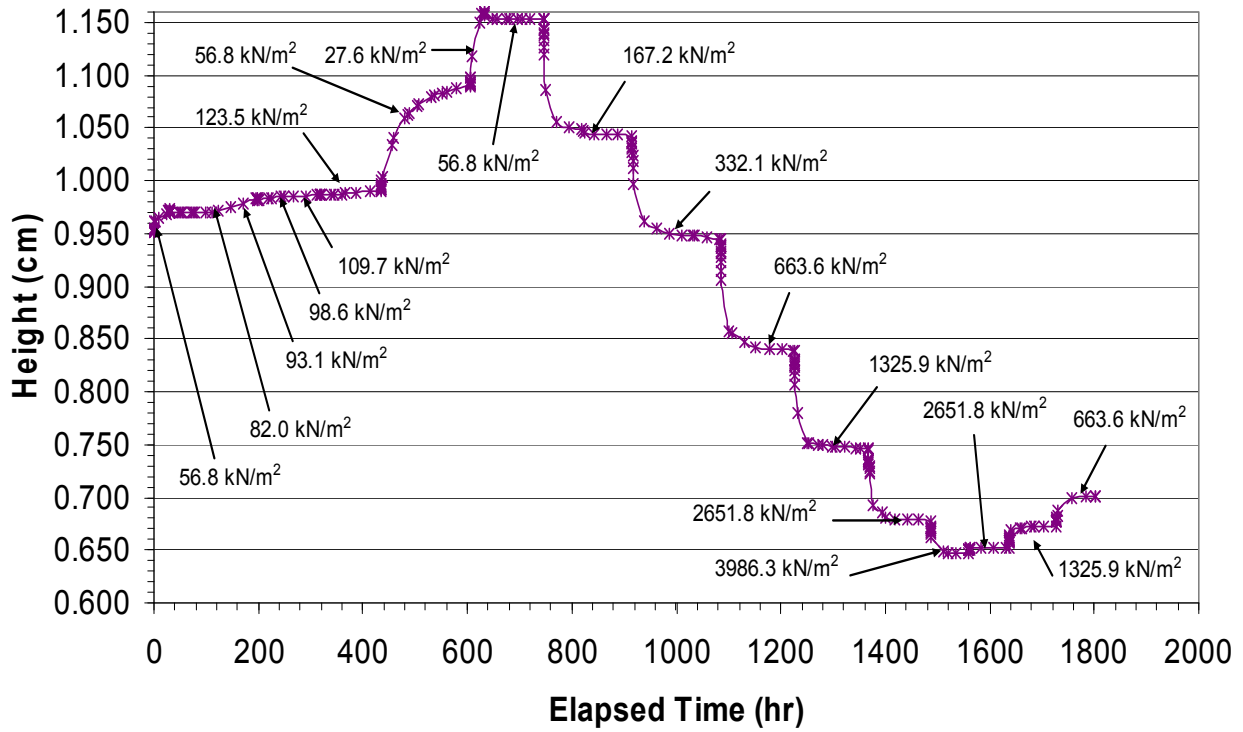
Figure CI-5: Test HB7 Specimen Height vs. Time (stress increments are labelled)
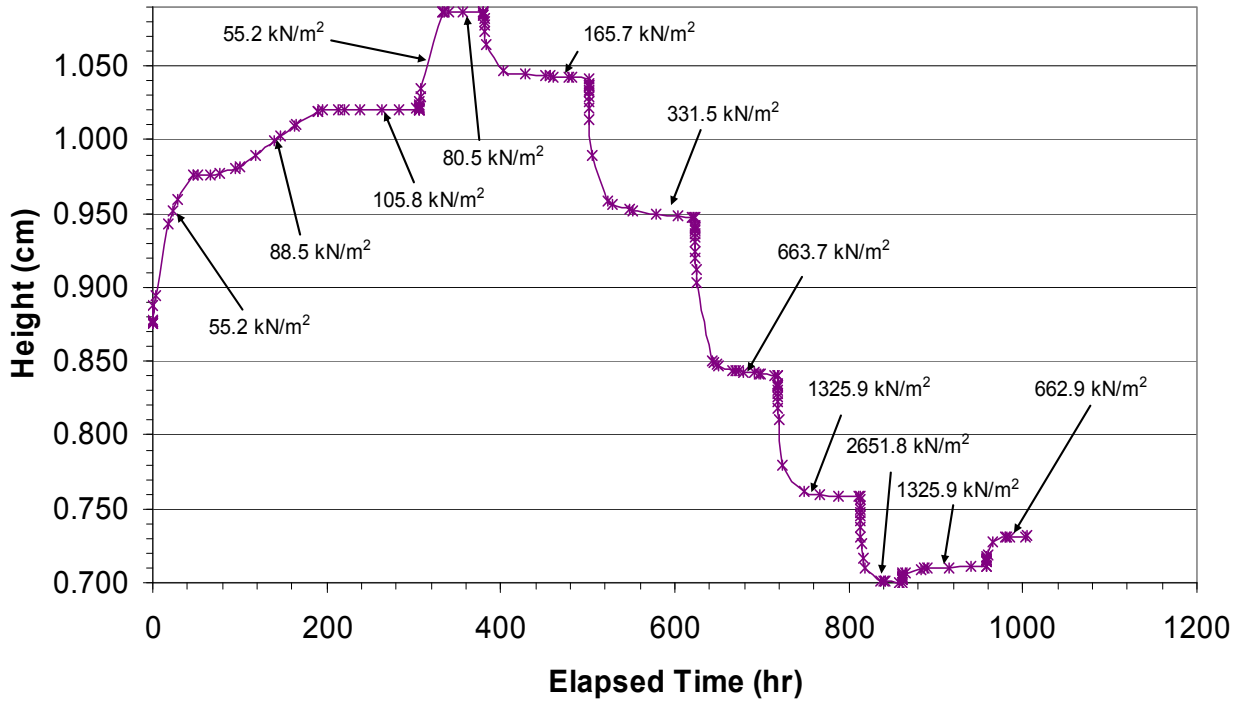
Figure CI-6: Test HB8 Specimen Height vs. Time (stress increments are labelled)
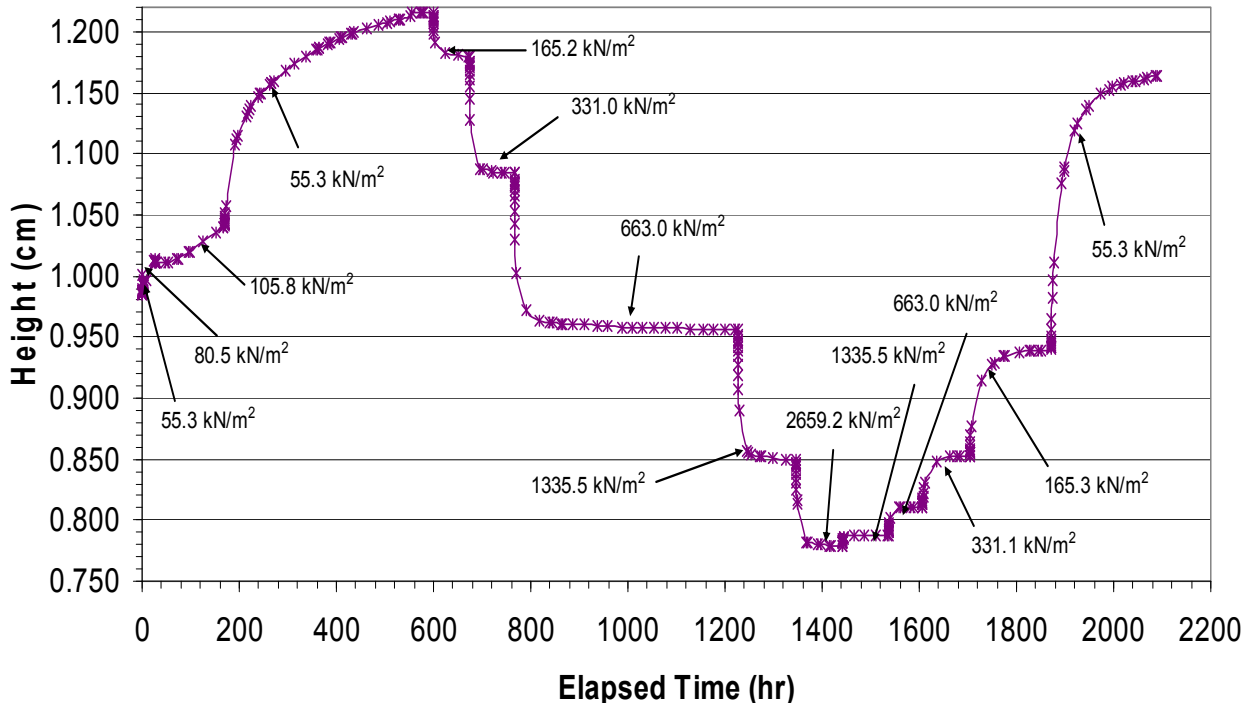
Figure CI-7: Test HB9 Specimen Height vs. Time (stress increments are labelled)
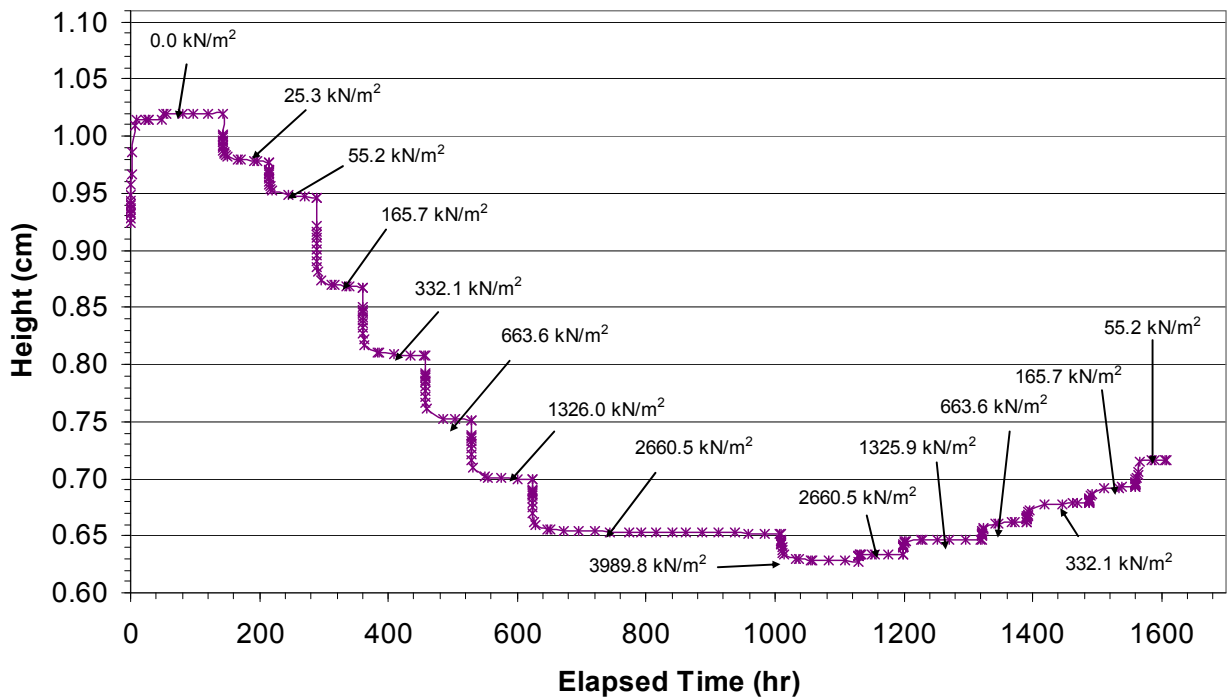
Figure CI-8: Test HB11 Specimen Height vs. Time (stress increments are labelled)
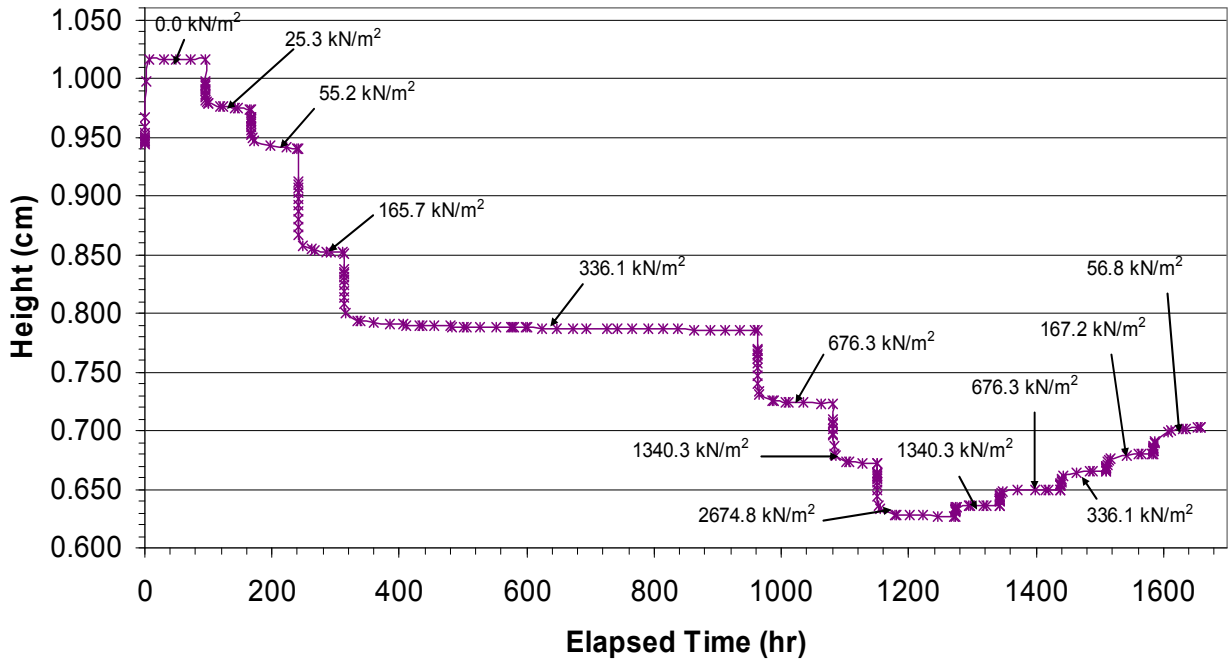
Figure CI-9: Test HB12 Specimen Height vs. Time (stress increments are labelled)
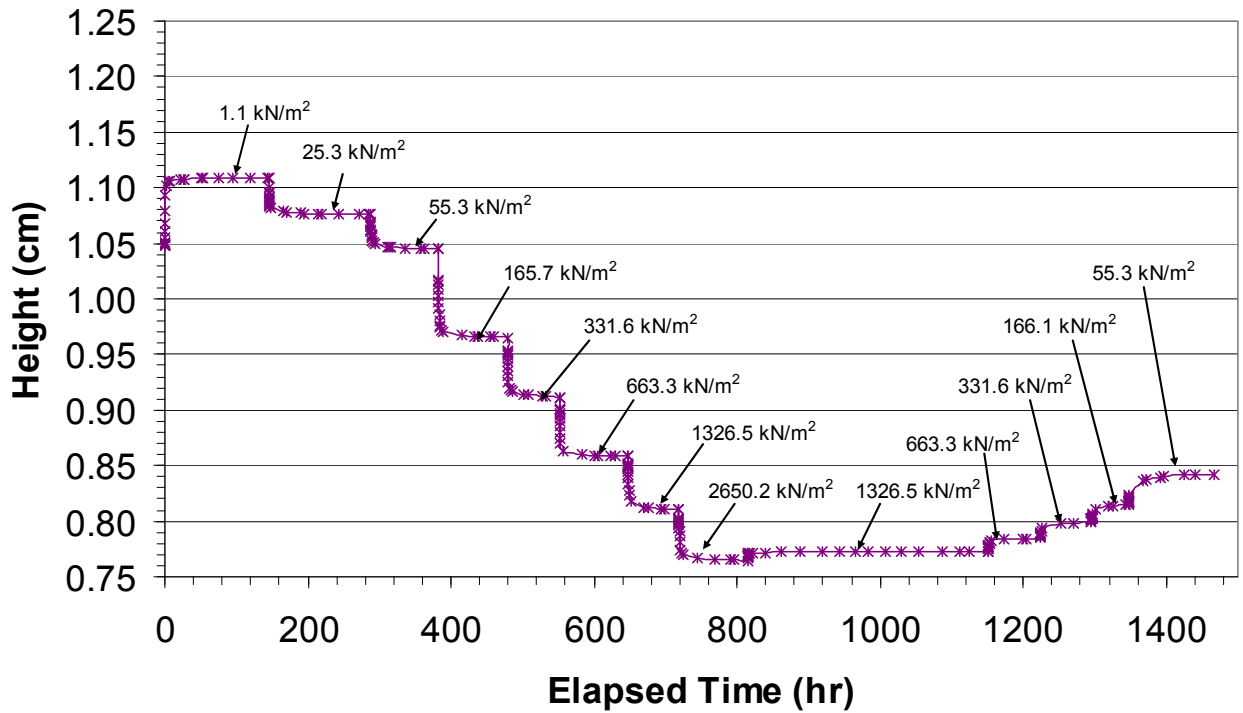
Figure CI-10: Test HB13 Specimen Height vs. Time (stress increments are labelled)
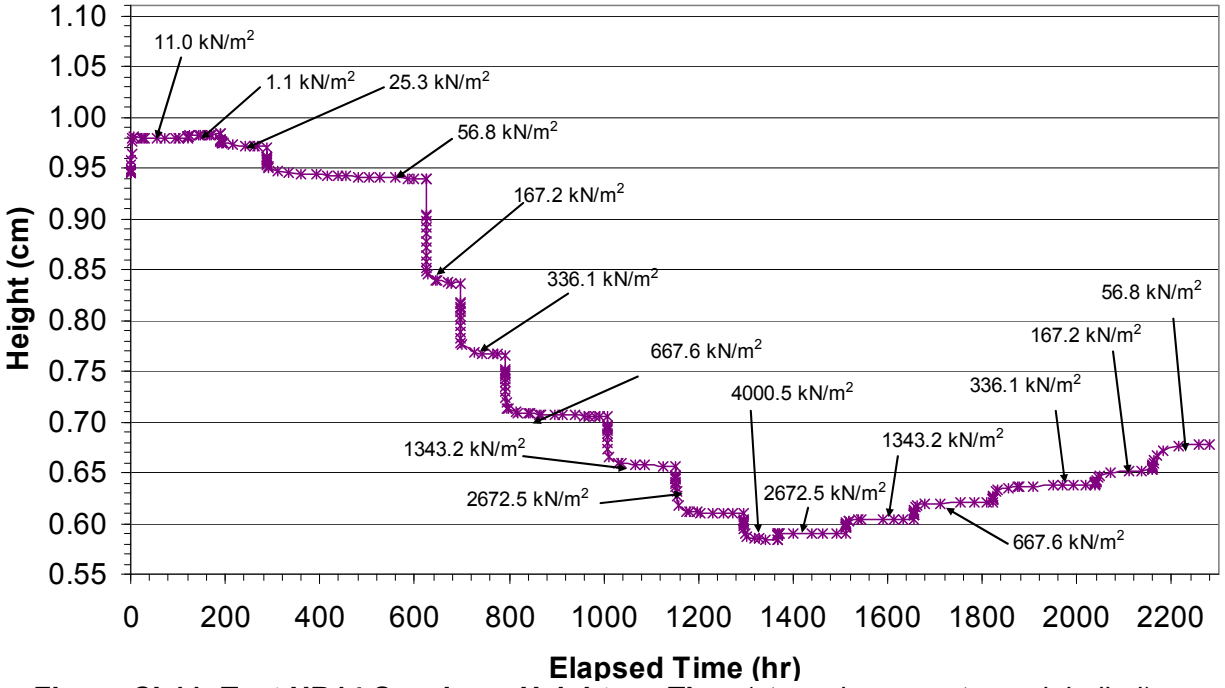
Figure CI-11: Test HB14 Specimen Height vs. Time (stress increments are labelled)
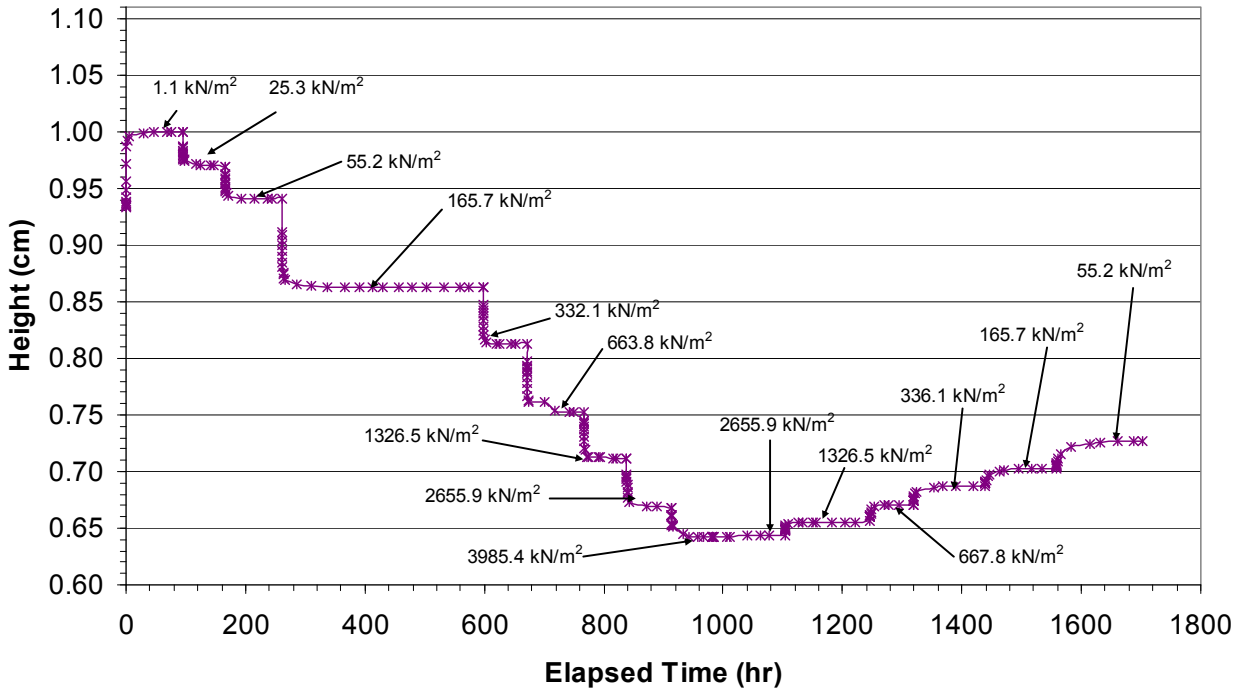
Figure CI-12: Test HB15 Specimen Height vs. Time (stress increments are labelled)
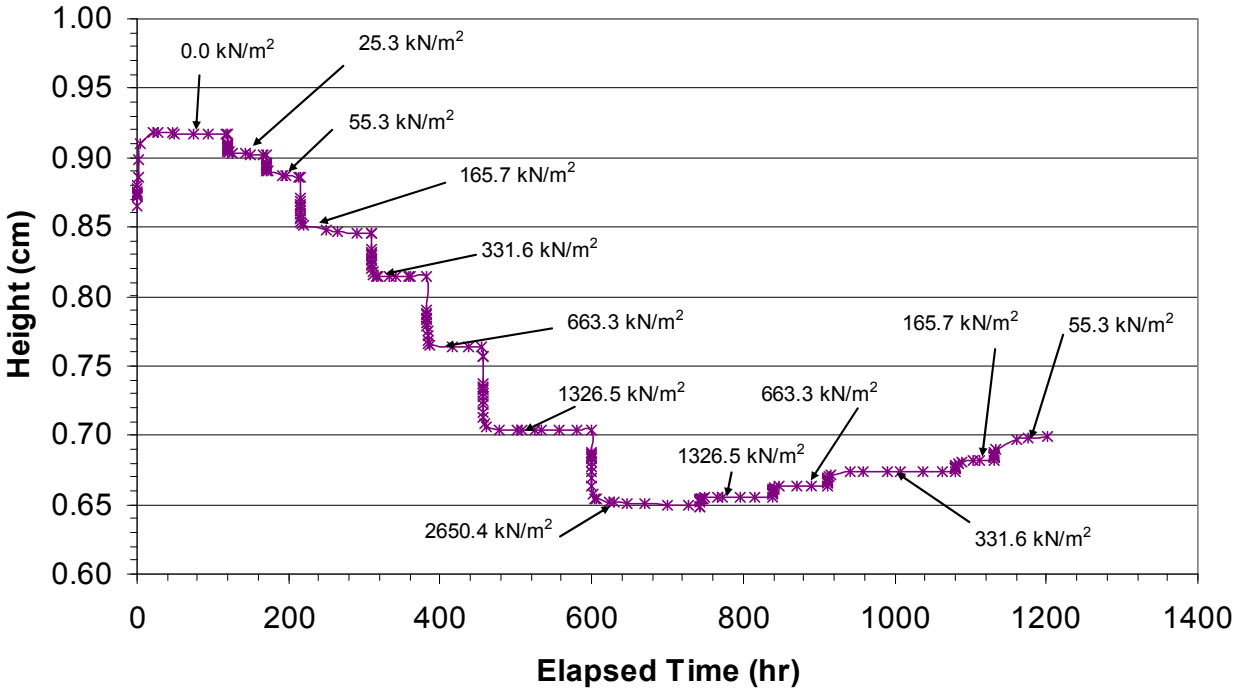
Figure CI-13: Test HB16 Specimen Height vs. Time (stress increments are labelled)
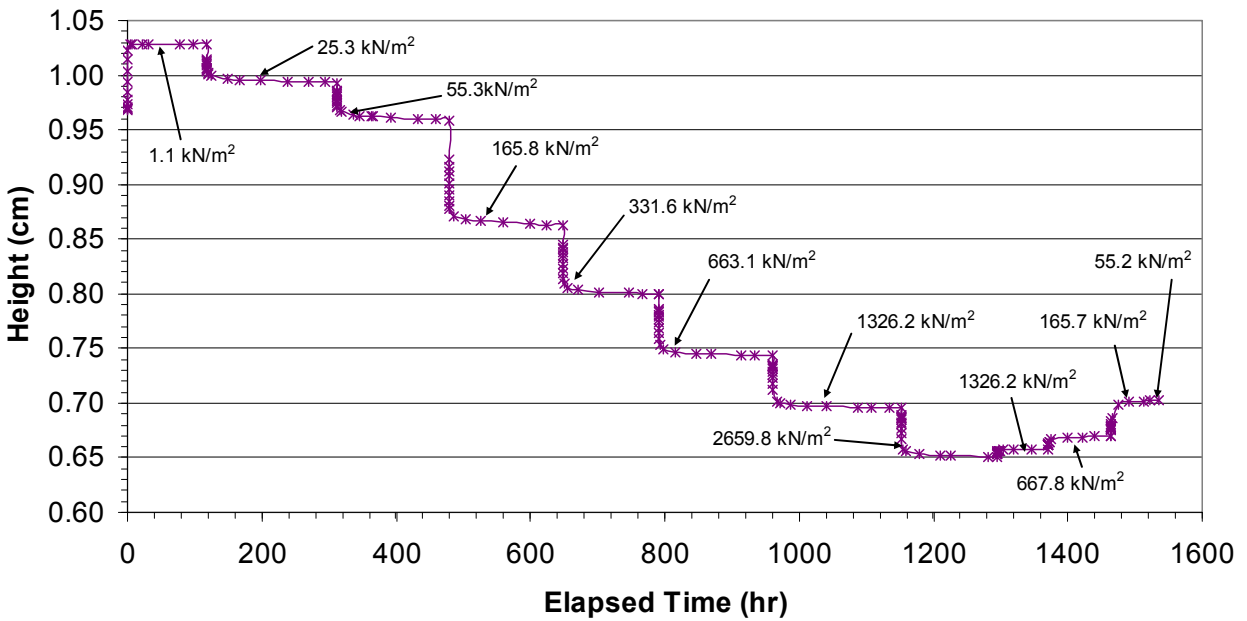
Figure CI-14: Test HB19 Specimen Height vs. Time (stress increments are labelled)

ADDENDUM II:
DATA FOR TEST LOAD AND UNLOAD INCREMENTS

Test	Applied Pressure (kPa)	Log Applied Stress	Equilibrium Vertical Strain	Void Ratio	Dry Density (Mg/m³)	m_v (m²/MN)	K (m/s)	EMDD (Mg/m³)
HB2	55.2	1.7	-0.016	1.264	1.193			0.65
	80.5	1.9	-0.019	1.270	1.189			0.65
	161.0	2.2	0.004	1.218	1.217	0.284	6.46E-12	0.67
	332.1	2.5	0.053	1.109	1.280	0.289	2.44E-12	0.72
	663.4	2.8	0.128	0.942	1.390	0.239	2.53E-12	0.81
	1325.7	3.1	0.203	0.774	1.522	0.131	1.54E-12	0.93
	2651.4	3.4	0.273	0.619	1.667	0.066	3.41E-13	1.07
HB3	55.2	1.7	-0.011	1.216	1.218			0.67
	80.5	1.9	-0.102	1.417	1.117			0.60
	55.2	1.7	-0.195	1.621	1.030			0.54
	110.6	2.0	-0.158	1.539	1.063	0.567	5.17E-12	0.56
	221.0	2.3	-0.064	1.334	1.157	0.730	9.24E-12	0.63
	331.5	2.5	0.013	1.164	1.248	0.662	3.05E-12	0.70
	666.6	2.8	0.140	0.885	1.432	0.381	1.81E-12	0.85
	1325.7	3.1	0.238	0.672	1.615	0.171	8.94E-13	1.02
	667.6	2.8	0.225	0.700	1.589	0.025	5.52E-13	0.99
	336.1	2.5	0.191	0.773	1.522	0.131	4.47E-13	0.93
	165.7	2.2	0.113	0.944	1.389	0.565	7.92E-13	0.81
	55.3	1.7	-0.064	1.334	1.157			0.63
HB4	55.2	1.7	-0.013	1.149	1.257			0.70
	80.5	1.9	-0.238	1.626	1.028			0.54
	165.7	2.2	0.009	1.103	1.284	0.275	4.79E-12	0.72
	332.0	2.5	0.062	0.989	1.357	0.324	2.02E-12	0.78
	665.1	2.8	0.147	0.811	1.491	0.270	8.49E-13	0.90
	1328.0	3.1	0.225	0.645	1.642	0.138	2.48E-13	1.05
	2653.8	3.4	0.288	0.510	1.788	0.062	1.06E-13	1.20
	1328.0	3.1	0.276	0.535	1.759	0.013	1.78E-13	1.17
	665.7	2.8	0.266	0.556	1.735			1.14

Test	Applied Pressure (kPa)	Log Applied Stress	Equilibrium Vertical Strain	Void Ratio	Dry Density (Mg/m³)	m_v (m²/MN)	K (m/s)	EMDD (Mg/m³)
HB6	55.2	1.7	-0.142	1.313	1.167			0.63
	39.1	1.6	-0.208	1.446	1.104			0.59
	55.7	1.7	-0.204	1.438	1.107			0.59
	166.1	2.2	-0.107	1.242	1.204	0.729	5.42E-12	0.66
	332.1	2.5	0.002	1.021	1.336	0.594	4.05E-12	0.77
	663.6	2.8	0.116	0.790	1.509	0.345	1.96E-12	0.92
	1325.9	3.1	0.215	0.589	1.699	0.169	2.32E-12	1.10
	2651.8	3.4	0.289	0.440	1.875	0.071	2.55E-13	1.30
	3986.5	3.6	0.321	0.374	1.964	0.034	3.45E-13	1.42
	1325.9	3.1	0.291	0.436	1.880	0.017	1.39E-13	1.31
	667.6	2.8	0.261	0.497	1.803	0.065	9.55E-14	1.22
	336.1	2.5	0.218	0.583	1.706	0.173	2.13E-13	1.11
	167.2	2.2	0.149	0.722	1.568	0.520	4.13E-13	0.97
	56.8	1.8	-0.024	1.074	1.302			0.74
HB7	1.8	0.2	-0.012	1.056	1.313			0.75
	1.9	0.3	-0.023	1.077	1.300			0.74
	2.0	0.3	-0.024	1.080	1.298			0.74
	2.0	0.3	-0.025	1.082	1.297			0.73
	2.0	0.3	-0.028	1.088	1.293			0.73
	2.1	0.3	-0.031	1.093	1.290			0.73
	1.8	0.2	-0.134	1.303	1.173			0.64
	1.4	0.2	-0.212	1.461	1.097			0.58
	56.8	1.8	-0.200	1.436	1.108	0.342	2.83E-11	0.59
	167.2	2.2	-0.085	1.203	1.225	0.866	7.98E-12	0.68
	332.1	2.5	0.016	0.998	1.351	0.565	5.27E-12	0.78
	663.6	2.8	0.127	0.774	1.522	0.339	7.26E-12	0.93
	1325.9	3.1	0.224	0.576	1.714	0.169	9.18E-13	1.12
	2651.8	3.4	0.295	0.433	1.885	0.068	4.60E-12	1.31
	3986.3	3.6	0.327	0.366	1.976	0.035	6.06E-13	1.43
	2651.8	3.4	0.321	0.379	1.957			1.41
	1325.9	3.1	0.301	0.420	1.901			1.34
	663.6	2.8	0.270	0.482	1.822			1.24

Test	Applied Pressure (kPa)	Log Applied Stress	Equilibrium Vertical Strain	Void Ratio	Dry Density (Mg/m³)	m_v (m²/MN)	K (m/s)	EMDD (Mg/m³)
HB8	55.2	1.7	-0.100	1.061	1.310			0.74
	80.5	1.9	-0.148	1.152	1.255			0.70
	105.8	2.0	-0.149	1.153	1.254			0.70
	55.2	1.7	-0.224	1.294	1.177			0.64
	80.5	1.9	-0.224	1.294	1.177			0.64
	165.7	2.2	-0.173	1.199	1.228	0.490	6.52E-12	0.68
	331.5	2.5	-0.066	0.999	1.351	0.549	6.14E-12	0.78
	663.7	2.8	0.053	0.774	1.522	0.338	1.08E-11	0.93
	1325.9	3.1	0.146	0.601	1.686	0.147	1.26E-12	1.09
	2651.8	3.4	0.212	0.477	1.828	0.058	4.34E-13	1.25
	1325.9	3.1	0.199	0.501	1.799	0.012	2.95E-13	1.21
	662.9	2.8	0.175	0.545	1.747	0.045	6.38E-14	1.16
HB9	55.3	1.7	0.005	1.103	1.284			0.805
	80.5	1.9	-0.012	1.138	1.263			0.785
	105.8	2.0	-0.039	1.196	1.229			0.756
	55.3	1.7	-0.214	1.566	1.052			0.609
	165.2	2.2	-0.178	1.490	1.084	0.269	5.74E-11	0.634
	331.0	2.5	-0.082	1.288	1.180	0.491	1.38E-11	0.713
	663.0	2.8	0.045	1.018	1.338	0.355	3.95E-12	0.855
	1335.5	3.1	0.152	0.792	1.507	0.167	1.43E-12	1.025
	2659.2	3.4	0.222	0.643	1.643	0.063	4.70E-13	1.180
	1335.5	3.1	0.213	0.663	1.623	0.009	1.42E-13	1.157
	663.0	2.8	0.190	0.712	1.577	0.043	3.87E-13	1.103
	331.1	2.5	0.148	0.800	1.500	0.155	4.56E-13	1.018
	165.3	2.2	0.062	0.983	1.361	0.615	3.75E-13	0.877
	55.3	1.7	-0.163	1.457	1.099			0.646
HB11	0.0		-0.104	1.081	1.297			0.73
	25.3	1.4	-0.058	0.996	1.353	1.629	8.16E-10	0.78
	55.2	1.7	-0.025	0.933	1.397	1.046	2.65E-10	0.82
	165.7	2.2	0.060	0.773	1.523	0.751	6.33E-10	0.93
	332.1	2.5	0.125	0.651	1.636	0.413	2.16E-10	1.04
	663.6	2.8	0.186	0.536	1.758	0.210	1.38E-10	1.17
	1326.0	3.1	0.241	0.431	1.886	0.103	6.16E-12	1.32
	2660.5	3.4	0.293	0.334	2.024	0.051	5.51E-13	1.49
	3989.8	3.6	0.319	0.285	2.101	0.028	3.62E-13	1.60
	2660.5	3.4	0.312	0.297	2.081	0.007	5.58E-13	1.57
	1325.9	3.1	0.298	0.324	2.039	0.015	2.62E-13	1.52
	663.6	2.8	0.282	0.354	1.994	0.034	3.41E-13	1.45
	332.1	2.5	0.264	0.389	1.944	0.077	4.05E-13	1.39
	165.7	2.2	0.248	0.418	1.904			1.34
	55.2	1.7	0.223	0.466	1.841			1.26

Test	Applied Pressure (kPa)	Log Applied Stress	Equilibrium Vertical Strain	Void Ratio	Dry Density (Mg/m³)	m_v (m²/MN)	K (m/s)	EMDD (Mg/m³)
	0.0		-0.075	1.116	1.276			0.72
	25.3	1.4	-0.031	1.029	1.331	1.628	8.32E-10	0.76
	55.2	1.7	0.005	0.959	1.378	1.151	1.07E-09	0.80
	165.7	2.2	0.099	0.773	1.523	0.861	5.98E-10	0.93
	336.1	2.5	0.169	0.637	1.650	0.451	2.14E-11	1.05
	676.3	2.8	0.235	0.506	1.793	0.234	8.08E-12	1.21
HB12	1340.3	3.1	0.289	0.400	1.929	0.106	1.25E-11	1.37
	2674.8	3.4	0.337	0.305	2.069	0.051	1.29E-12	1.56
	1340.3	3.1	0.327	0.326	2.037	0.012	5.81E-13	1.51
	676.3	2.8	0.312	0.354	1.994	0.033	3.68E-13	1.45
	336.1	2.5	0.296	0.386	1.948	0.069	3.58E-13	1.39
	167.2	2.2	0.280	0.418	1.904			1.34
	56.8	1.8	0.256	0.464	1.844			1.27
	1.1	0.0	-0.064	1.137	1.264			0.708
	25.3	1.4	-0.030	1.067	1.306	1.339	2.95E-09	0.742
	55.3	1.7	0.003	1.002	1.349	1.061	7.08E-10	0.777
	165.7	2.2	0.087	0.834	1.472	0.759	3.10E-10	0.883
	331.6	2.5	0.143	0.721	1.569	0.370	3.12E-11	0.973
	663.3	2.8	0.199	0.608	1.679	0.198	1.17E-11	1.083
HB13	1326.5	3.1	0.248	0.509	1.789	0.093	2.45E-12	1.203
	2650.2	3.4	0.297	0.412	1.913	0.049	1.27E-12	1.350
	1326.5	3.1	0.289	0.428	1.890	0.009	1.78E-13	1.322
	663.3	2.8	0.276	0.454	1.857	0.027	3.05E-13	1.282
	331.6	2.5	0.261	0.484	1.819	0.063	5.01E-13	1.238
	166.1	2.2	0.244	0.518	1.779			1.192
	55.3	1.7	0.215	0.575	1.714			1.120
	11.0	1.0	0.979	1.022	1.335			0.766
	1.1	0.0	0.983	1.032	1.329			0.760
	25.3	1.4	0.971	1.005	1.346	0.539	7.23E-10	0.775
	56.8	1.8	0.940	0.941	1.391	1.014	1.07E-09	0.812
	167.2	2.2	0.836	0.726	1.564	1.002	3.73E-10	0.969
	336.1	2.5	0.766	0.582	1.707	0.495	7.90E-11	1.112
	667.6	2.8	0.705	0.457	1.853	0.239	9.03E-12	1.277
HB14	1343.2	3.1	0.656	0.355	1.992	0.103	2.33E-12	1.452
	2672.5	3.4	0.610	0.259	2.144	0.053	5.25E-13	1.666
	4000.3	3.6	0.584	0.206	2.239	0.032	7.31E-12	1.816
	2672.5	3.4	0.590	0.220	2.214	0.009	8.30E-13	1.775
	1343.2	3.1	0.604	0.247	2.164	0.017	2.91E-13	1.698
	667.6	2.8	0.620	0.282	2.107	0.041	2.57E-13	1.611
	336.1	2.5	0.637	0.317	2.050	0.083	2.45E-13	1.531
	167.2	2.2	0.652	0.348	2.003			1.466
	56.8	1.8	0.678	0.400	1.928			1.369

Test	Applied Pressure (kPa)	Log Applied Stress	Equilibrium Vertical Strain	Void Ratio	Dry Density (Mg/m³)	m_v (m²/MN)	K (m/s)	EMDD (Mg/m³)
	1.1	0.0	-0.071	1.082	1.297			0.734
	25.3	1.4	-0.039	1.020	1.337	1.242	4.72E-09	0.767
	55.2	1.7	-0.008	0.959	1.378	1.005	1.24E-09	0.801
	165.7	2.2	0.075	0.798	1.502	0.743	1.31E-08	0.910
	332.1	2.5	0.129	0.692	1.595	0.354	5.51E-10	0.999
	663.8	2.8	0.193	0.569	1.721	0.220	5.27E-11	1.128
	1326.5	3.1	0.238	0.481	1.823	0.084	2.35E-12	1.241
HB15	2655.9	3.4	0.284	0.392	1.939	0.045	1.96E-12	1.383
	3985.4	3.6	0.311	0.338	2.017	0.029	3.35E-12	1.485
	2655.9	3.4	0.311	0.340	2.015	0.001		1.483
	1326.5	3.1	0.297	0.366	1.976	0.015	2.53E-13	1.430
	667.8	2.8	0.281	0.398	1.932	0.035	3.32E-13	1.373
	336.1	2.5	0.263	0.433	1.885	0.075	3.49E-13	1.315
	165.7	2.2	0.247	0.464	1.844			1.267
	55.2	1.7	0.220	0.515	1.782			1.195
	0.0		-0.061	0.904	1.418			0.84
	25.3	1.4	-0.043	0.872	1.443	0.681	5.03E-10	0.86
	55.3	1.7	-0.025	0.840	1.468	0.570	1.09E-10	0.88
	165.7	2.2	0.022	0.755	1.538	0.415	6.19E-10	0.94
	331.6	2.5	0.058	0.690	1.597	0.224	1.02E-10	1.00
	663.3	2.8	0.124	0.572	1.718	0.211	2.70E-11	1.12
HB16	1326.5	3.1	0.186	0.462	1.847	0.106	2.39E-11	1.27
	2650.4	3.4	0.250	0.347	2.005	0.059	5.47E-12	1.47
	1326.5	3.1	0.242	0.360	1.986	0.007	2.17E-13	1.44
	663.3	2.8	0.232	0.378	1.959	0.020	6.09E-13	1.41
	331.6	2.5	0.220	0.400	1.929	0.047	4.06E-13	1.37
	165.7	2.2	0.211	0.416	1.907			1.34
	55.3	1.7	0.191	0.452	1.860			1.28
	1.1	0.0	-0.062	1.129	1.268			0.71
	25.3	1.4	-0.027	1.057	1.313	1.393	9.16E-10	0.75
	55.3	1.7	0.009	0.986	1.359	1.148	7.90E-10	0.79
	165.8	2.2	0.108	0.787	1.511	0.906	6.85E-10	0.92
	331.6	2.5	0.173	0.656	1.631	0.443	1.08E-10	1.03
	663.1	2.8	0.231	0.540	1.753	0.211	2.15E-11	1.16
HB19	1326.2	3.1	0.281	0.440	1.874	0.097	3.61E-12	1.30
	2659.8	3.4	0.327	0.348	2.003	0.048	8.87E-13	1.47
	1326.2	3.1	0.320	0.362	1.983	0.008	4.51E-13	1.44
	667.8	2.8	0.308	0.387	1.947	0.028	3.51E-13	1.39
	165.7	2.2	0.274	0.455	1.855	0.099	1.81E-12	1.28
	55.2	1.7	0.249	0.506	1.793			1.21

APPENDIX D: VOLUME-MASS RELATIONSHIPS OF SOIL WITH FRESH-WATER AND SALINE SOLUTIONS

D.G. Priyanto and P. Baumgartner
Waste Technology Division
Atomic Energy of Canada Limited

CONTENTS

D.1   INTRODUCTION

The soil volume-mass relationships are essential in the interpretation of geotechnical tests. General volume-mass relationships presented in the geotechnical textbooks (e.g., Craig 1992, Das 1998, Budhu 2000) are limited to soil with fresh water as the liquid phase. Neglecting the salinity is insignificant in the analysis of volume-mass relationship when the salt concentrations are low. This is not the case for high salt concentrations. The conventional volume-mass relationship for soil with fresh water should be modified to consider salinity effects. Soils testing at AECL include both distilled water (also called fresh water in this report) and saline solutions (e.g., $CaCl_2$, NaCl).

The analysis of volume-mass parameters at pre- and post-tests conditions is important in the interpretation of the test. The process for measuring water content in soil specimens requires an oven-drying and weighing process for the specimen. If the pore fluid is saline, solute (e.g., salt) from the solution is retained with the soil solids in dry specimen. This mass of solute affects the volume-mass relationships for soil with a high-salinity solution.

The following analysis extends the 'conventional' volume-mass relationships providing volume-mass relationships for soil with various solutions. Two new volume-mass parameters (e.g., gravimetric solution content (w_l) and degree of solution saturation (S_l)) are introduced in these new volume-mass relationships. These new relationships return to the 'conventional' volume-mass relationships when the total dissolved solids (TDS) in the solution is zero.

D.2   THREE-PHASE, FOUR-COMPONENT SYSTEM

Soil is divided into a three-phase, four-component system (Figure D1) to develop the volume-mass relationships for saline-pore fluids. The phases consist of a solid (e.g., soil minerals), a liquid (e.g., fresh water or a solution) and a gas (e.g., air). For soil with a saline solution as its pore fluid, the liquid phase is comprised of a solute and a solvent (Streitwieser et al. 1992). Consequently, the system consists of four components: solid, gas, solvent and solute. The solute and solvent are salt and water, respectively. The volume-mass relationships discussed below are applicable to soils with any pore-fluid solution.

The total volume of the soil specimen is (Figure D1):

$$V = V_s + V_g + V_l \qquad (D1)$$

where V =   total volume;
$\quad\quad V_s$ =   volume of solid;
$\quad\quad V_g$ =   volume of gas; and
$\quad\quad V_l$ =   volume of liquid.

and

$$V_l = V_w + V_{salt} \qquad (D2)$$

where V_w =   volume of water (solvent); and
$\quad\quad V_{salt}$ =   volume of salt (solute).
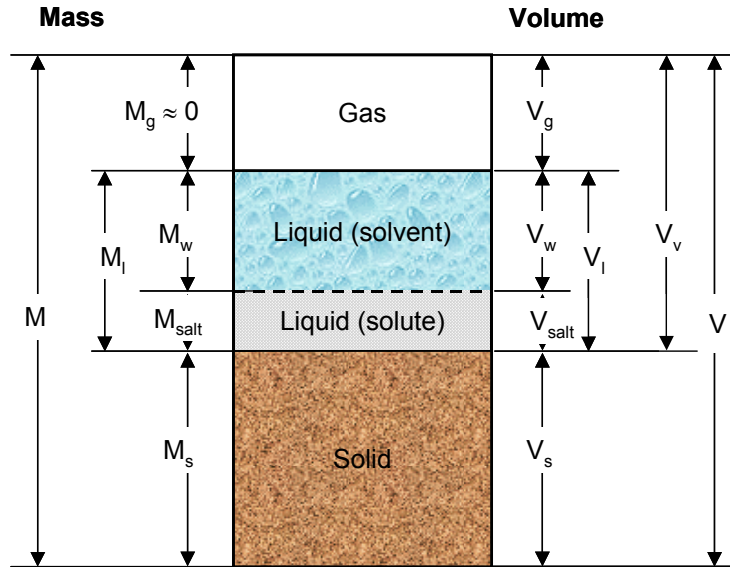
Figure D1: Three-Phase, Four-Component Soil System

Assuming that the mass of the air is negligible, the total mass of the specimen (M) is:

$$M = M_s + M_l \tag{D3}$$

where M   = total mass;
        M_s = mass of solid; and
        M_l = mass of liquid.

and

$$M_l = M_w + M_{salt} \tag{D4}$$

where M_w = mass of water (solvent); and
        M_{salt} = mass of salt (solute).

When the liquid phase within the system is fresh water, the volume and mass of salt are equal to zero, so that the volume-mass relationships revert to that of soil with fresh water as the pore fluid.

D.3   DENSITY OF THE PHASES

The density of each component in the soil system (Figure D1) is required to derive the volume-mass relationships. The gas density is very small compared to the other component system and is neglected. The densities of other components (e.g. water, salt and soil solid) are discussed below.

D.3.1 WATER DENSITY

Water density (ρ_w) is dependent on the temperature (Table D1) (Lide 2006). The derived empirical relationship of the water density (ρ_w) to temperature (T) for the range of 0°C to 100°C is the following (Figure D2):

$$\rho_w = 1.7381 \text{x} 10^{-8} T^3 - 6.1130 \text{x} 10^{-6} T^2 + 2.3538 \text{x} 10^{-5} T + 1.0000 \qquad \text{(D5)}$$

where T   =   temperature (°C)
       ρ_w =   water density (Mg/m^3).

Table D1: Water Density as a Function of Temperature (after Lide 2006)

Temperature (°C)	Density (Mg/m^3)
0	0.99984
10	0.99970
20	0.99821
30	0.99565
40	0.99222
50	0.98804
60	0.98320
70	0.97776
80	0.97179
90	0.96531
100	0.95837

D.3.2 SOLUTION AND SOLUTE DENSITIES

The solution and solute densities are required to calculate the volume-mass relationships of soil with saline pore fluids. A solution is a homogeneous mixture composed of one or more substances, known as solutes, dissolved in a solvent (Streitwieser et al. 1992). The normal solvent in soil is water. Concentration (c, in units of mol/L of solution), molality (m_b, in units of mol/kg of solution) and total dissolved solids (TDS, in units of g/L of solution) are various expressions that define the salinity of a solution. The density of the solution (ρ_l) is dependent on the type of the solution, solution concentration and temperature.
The relationships of the solution densities and concentrations for common saline solutions (e.g., calcium chloride ($CaCl_2$), sodium chloride (NaCl) and sodium carbonate (Na_2CO_3)) are illustrated in Figure D3 (after Lide 2006). The empirical equations describing the TDS-density relationships for the three solutions are presented in the figure. The summary of the molecular mass, density of solute, and other properties at specific concentrations (i.e., TDS) is presented in Table D2. The conversion from concentration (c) to TDS for a solute X is:

$$TDS = c \times M(X) \tag{D6}$$

where TDS = total dissolved solids (g/L);
       c   = concentration (mol/L of solution; and
       M(X) = molar mass of solute X (g/mol).

$$y = 1.7381E\text{-}08x^3 - 6.1130E\text{-}06x^2 + 2.3538E\text{-}05x + 1.0000E\text{+}00$$
$$R^2 = 9.9995E\text{-}01$$
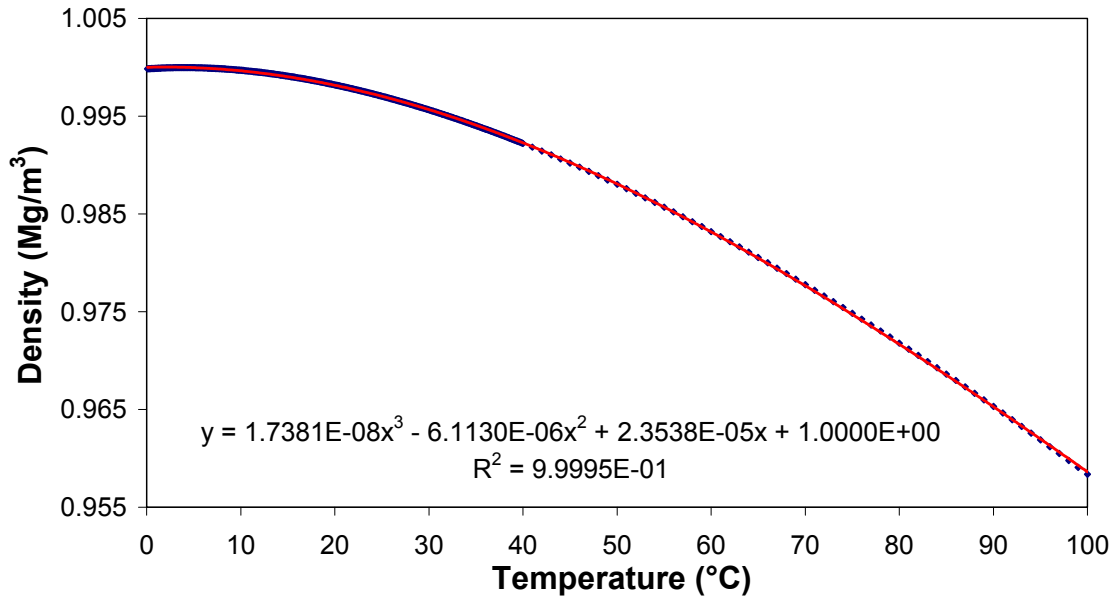
Figure D2: Water Density Dependence to Temperature (after Lide 2006)

$$y = 2.217E\text{-}10x^3 - 3.442E\text{-}07x^2 + 8.410E\text{-}04x + 9.982E\text{-}01$$

CaCl$_2$

$$y = 4.966E\text{-}09x^3 - 1.942E\text{-}06x^2 + 1.119E\text{-}03x + 9.982E\text{-}01$$

Na$_2$CO$_3$

NaCl

$$y = 1.224E\text{-}09x^3 - 7.534E\text{-}07x^2 + 7.656E\text{-}04x + 9.982E\text{-}01$$

Note: Densities at room temperature (i.e., 20°C)
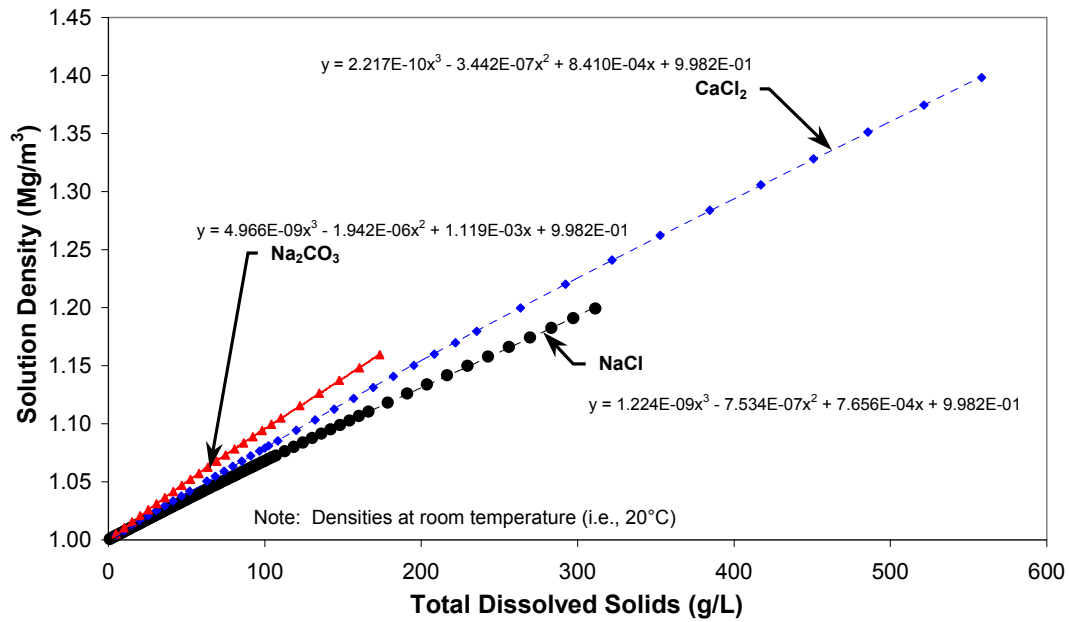
Figure D3: Common Solution Densities as a Function of Concentration (after Lide 2006)

The solution concentration can also be presented as the mass fraction of solute dissolved in the solution. The relationship between TDS and mass fraction of solute in solution (C_m) is:

$$C_m = \frac{TDS}{\rho_l}$$

(D7)

where C_m = mass fraction of the solute to the solution;
TDS = total dissolved solids (g/L); and
ρ_l = solution density (g/L).

Table D2: Properties of Solute and Solution for Selected TDS

Solute	Molar Mass (g/mol)	Solute density (Mg/m^3)	TDS (g/L)	Mass Fraction C_m	Molality m_b (mol/kg)	Concentration c (mol/L)	Solution Density ρ_l (g/L)
CaCl$_2$	110.98	2.17	75.6	0.0714	0.6929	0.6812	1058.4
NaCl	58.44	2.15	100	0.0938	1.7714	1.7111	1066.1
Na$_2$CO$_3$	105.99	2.54	100	0.0914	0.9496	0.9435	1093.7

D.3.3 RELATIVE DENSITY

Relative density is the replacement term for specific gravity and specific weight (CSA 1989) that relates the density of solid phase to the density of the liquid phase (i.e., conventionally water), as follows:

$$G_s = \frac{\rho_s}{\rho_w}$$

(D8a)

where ρ_s = density of solid phase; and
ρ_w = density of water.

With a saline solution as the pore fluid, the relative density of the soil solid to the solution (G'_s) is:

$$G'_s = \frac{\rho_s}{\rho_l}$$

(D8b)

where ρ_l = density of liquid phase (i.e., the saline solution).

The relationship between the relative density of the solid in water (G_s) to the relative density of the solid in a saline solution (G'_s) is:

$$G_s{}' = \frac{\rho_s}{\rho_l} = \frac{\rho_s}{\rho_w} \cdot \frac{\rho_w}{\rho_l} = G_s \times \frac{\rho_w}{\rho_l} \tag{D8c}$$

For example, the relative densities of the HCB to selected solutions are summarized in Table D3.

Table D3: Relative Densities of HCB in Selected Solutions

Selected Solute	Molecular Mass (g/mol)	Solute Density (Mg/m³)	TDS (g/L)	Solution Density ρ_l (Mg/m³)	Relative Density of Solids to Water G_s	Relative Density of Solids to Solution $G_s{}'$
$CaCl_2$	110.98	2.17	75.6	1.058	2.745	2.589
NaCl	58.44	2.15	100	1.066	2.745	2.570
Na_2CO_3	105.99	2.54	100	1.094	2.745	2.505

D.4 VOLUME-MASS RELATIONSHIPS FOR A THREE-PHASE SYSTEM

The volume-mass relationships commonly used in three-phase system are: void ratio, porosity, degree of saturation, gravimetric water content, dry density, bulk density and saturated density.

D.4.1 VOID RATIO AND POROSITY

Void ratio (e) is defined as the ratio of the volume of voids (V_v) to the volume of solid (V_s) (Figure D1):

$$e = \frac{V_v}{V_s} \tag{D9}$$

where the volume of void (V_v) is:

$$V_v = V - V_s \tag{D10}$$

Porosity (n) is the ratio of the volume of void (V_v) to the total volume (V):

$$n = \frac{V_v}{V} \tag{D11}$$

The relationship between porosity (n) and void ratio (e) is:

$$n = \frac{e}{1+e} \tag{D12a}$$

and conversely:

$$e = \frac{n}{1-n} \tag{D12b}$$

D.4.2 WATER CONTENT

The measurement of the water content is the most fundamental laboratory test performed on soils. The procedure is to measure the mass of soil specimen (M), oven dry the specimen for 24 hrs at 105°C to 110°C and then measure the mass of the dried specimen (M_s) (ASTM 2002). The difference in mass between the two measurements is the mass of the evaporated water (M_w). Assuming that the mass of gas (M_g) is negligible, the gravimetric water content (w_w) is defined as follows (Figure D1):

$$w_w = \frac{M_w}{M_s} \tag{D13}$$

When the contained liquid is a saline solution, oven drying only removes the water (solvent) leaving the salts (solute) behind, yielding the bulk water content (w) as:

$$w = \frac{M_w}{M_s + M_{salt}} \tag{D14}$$

Whereas the actual gravimetric water content is:

$$w_w = \frac{M_w}{M_s} = \frac{M_l - M_{salt}}{M_s} \tag{D15}$$

To determine the mass of dry soil and that for salt, we define the gravimetric liquid (or solution) content (w_l) as:

$$w_l = \frac{M_l}{M_s} = \frac{M_w + M_{salt}}{M_s} \tag{D16}$$

The mass of soil solid (M_s) is:

$$M_s = G'_s \cdot \rho_l \cdot V_s = G_s \cdot \rho_w \cdot V_s \tag{D17}$$

The mass of solution (M_l) is (Eqns. D8 and D16):

$$M_l = M_w + M_{salt} = w_l \cdot G'_s \cdot \rho_l \cdot V_s = w_l \cdot G_s \cdot \rho_w \cdot V_s \tag{D18}$$

The mass of salt (M_{salt}) is:

$$M_{salt} = C_m \cdot M_l = C_m \cdot w_l \cdot G'_s \cdot \rho_l \cdot V_s = C_m \cdot w_l \cdot G_s \cdot \rho_w \cdot V_s \tag{D19}$$

Substituting Eqns. D16, D18 and D19 into Eqn. D15 results in:

$$w_w = w_l(1 - C_m)$$ (D20)

Eqn. D20 shows that $w_l = w_w$ when C_m is zero (i.e., TDS = 0). The assumption is made that the solution concentration remains constant throughout any test except for the conditions of drying (i.e., desaturation) or other processes resulting in preferential salt retention (e.g., osmosis). Based on Eqns. D15 and D16, the mass of salt (M_{salt}) is:

$$M_{salt} = M_l - M_w = M_s(w_l - w_w)$$ (D21)

Substituting Eqns D15 and D21 into Eqn D14 results in the following relationship:

$$w = \frac{w_w}{1 + w_l - w_w}$$ (D22)

Substituting Eqn D20 for w_l in Eqn. D22 and solving for w_w produces:

$$w_w = \frac{w(1 - C_m)}{1 - C_m(1 + w)}$$ (D23)

or for w_l:

$$w_l = \frac{w}{1 - C_m(1 + w)}$$ (D24)

D.4.3   DEGREE OF SATURATION

The degree of saturation (S) is defined as the ratio of the volume of liquid to the volume of void (Figure D1), which is commonly expressed as a percentage:

$$S = \frac{V_l}{V_v}$$ (D25)

In the case of soil with a fresh-water pore fluid (i.e., $V_{salt} = 0$ and $V_l = V_w$), the degree of saturation (S) is:

$$S = \frac{V_w}{V_v}$$ (D26)

In the case of soil with saline pore fluid, the volume of void (V_v) is:

$$V_v = V - V_s = V_w + V_{salt} + V_g = V_l + V_g$$ (D27)

Two forms of the degree of saturation can be defined: the degree of liquid saturation (S_l) and the degree of water saturation (S_w), as follows:

$$S_l = \frac{V_l}{V_v} \tag{D28}$$

$$S_w = \frac{V_w}{V_w + V_g} = \frac{V_w}{V_v - V_{salt}} \tag{D29}$$

The relationship of the degree of solution saturation (S_l) and gravimetric solution content (w_l) is:

$$S_l = \frac{w_l \cdot G'_s}{e} \tag{D30}$$

Based on Eqns. D28 and D29, the definitions of the degrees of water and solution saturation $(S_w$ and $S_l)$, the following conditions are achieved:

At the condition of full saturation, the volume of void is filled with the liquid and the gas phase is no longer present in the system. The degrees of water and solution saturation are equal to 100% $(S_w = S_l = 100\%)$;

When the pore fluid is fresh water and volume of salt is zero, the degrees of water and solution saturation are equal $(S_w = S_l)$; and

The degree of water saturation (S_w) is not equal to the degree of solution saturation (S_l) for unsaturated soil with a saline pore fluid present $(S_w \neq S_l)$.

The relationship between degree of water saturation (S_w) and degree of solution saturation (S_l) is:

$$S_w = \frac{S_l(1-A)}{1 - S_l \cdot A} \tag{D31}$$

where:

$$A = \frac{C_m \cdot \rho_l}{\rho_{salt}} \tag{D32}$$

D.4.4 BULK DENSITY, SATURATED DENSITY AND DRY DENSITY

The bulk density of the soil specimen can be calculated as:

$$\rho = \frac{M}{V} = \frac{M_s + M_l}{V} = \frac{(1 + w_l)G'_s \cdot \rho_l}{1 + e} \tag{D33}$$

Substituting w_l from Eqn. D30 into Eqn. D33 produces:

$$\rho = \frac{(G'_s + S_l e)\rho_l}{1 + e} \tag{D34}$$

When $S_l = 1$ (i.e., fully saturated), the saturated density (ρ_{sat}) is determined as:

$$\rho_{sat} = \frac{(G'_s + e) \cdot \rho_l}{1 + e} \tag{D35}$$

Dry density (ρ_d) is defined as:

$$\rho_d = \frac{M_s}{V} \tag{D36}$$

Using dry density (ρ_d) in Eqn. D36, the void ratio (e) is:

$$e = \frac{G'_s \cdot \rho_l}{\rho_d} - 1 \tag{D37}$$

D.5   CONCLUDING REMARKS

1. The assumption of soil as three-phase, four-component system can be used to derive the volume-mass relationships of soil with a saline pore fluid.

2. The calculation of the volume-mass properties of soil with a saline pore fluid requires additional information, as follows:

   - Total Dissolved Solids (TDS);
   - Density of solution (ρ_l); and
   - Density of dry solute (ρ_{salt}).

3. Additional volume-mass relationships introduced are:

   - Relative density of soil solid to the solution (G_s')
   - Degree of solution (liquid) saturation (S_l);
   - Degree of water saturation (S_w);
   - Gravimetric water content (w_w) relative to the mass of soil solid;
   - Gravimetric solution (liquid) content (w_l) relative to mass of soil solid; and
   - Bulk water content (w) relative to the combined mass of soil solid and any salts remaining after the oven-drying process.

4. The derived relationships are based on the assumption that the solution concentration remains constant throughout any test and do not hold for the conditions of drying (i.e., desaturation) or other processes resulting in preferential salt retention (e.g., osmosis) in bentonite clay.

REFERENCES

ASTM (American Society for Testing and Materials). 2002. Standard D2216-98. Standard method for laboratory determination of water (moisture) content of soil and rock by mass. <u>In</u> 2002 Annual Book of ASTM Standards, Volume 4.08, Soil and Rock; Building Stones. ASTM, Philadelphia, PA.

Budhu, M. 2000. Soil Mechanics and Foundations. John Wiley and Sons.

Craig, R.F. 1992. Soil Mechanics, 5th Edition. Chapman and Hall, London.

CSA (Canadian Standards Association). 1989. Canadian Metric Practice Guide. National Standard of Canada CAN/CSA-Z234.1-89 (Reaffirmed 1995). Canadian Standards Association, Rexdale (Toronto), Ontario.

Das, B.M. 1998. Principles of Geotechnical Engineering, 4th Edition. PWS Publishing Company, Boston, MA.

Lide, D.R., ed. 2006. CRC Handbook of Chemistry and Physics, Internet Version 2006-2007, (87th Edition), http://www.hbcpnetbase.com

Streitwieser, A., C.H. Heathcock and E.M. Kosower. 1992. Introduction to Organic Chemistry, 4th ed. Macmillan Publishing Company, New York.